Modeling and Analysis for Electro-osmotic Peristaltic Flows

By

Sadaqut Hussain

Reg. # 55-FBAS/PHDMA/F15

Department of Mathematics and Statistics

Faculty of Basic and Applied Sciences

International Islamic University, Islamabad

Pakistan

2020

Numerical Analysis

Mathematics

Modeling and Analysis for Electro-osmotic Peristaltic Flows

By

Sadaqut Hussain
Reg. # 55-FBAS/PHDMA/F15

Supervised by

Dr. Nasir Ali

Department of Mathematics and Statistics
Faculty of Basic and Applied Sciences
International Islamic University, Islamabad
Pakistan

2020

Modeling and Analysis for Electro-osmotic Peristaltic Flows

By

Sadaqut Hussain
Reg. # 55-FBAS/PHDMA/F15

A DISSERTATION SUBMITTED IN THE PARTIAL FULFILLMENT
OF THE REQUIREMENTS FOR THE DEGREE OF

DOCTOR OF PHILOSOPHY
IN
MATHEMATICS

Supervised by

Dr. Nasir Ali

Department of Mathematics and Statistics
Faculty of Basic and Applied Sciences
International Islamic University, Islamabad
Pakistan
2020

Author's Declaration

I, **Sadaqut Hussain** Reg. No. **55-FBAS/PHDMA/F15** hereby state that my Ph.D. thesis titled: **Modeling and Analysis for Electro-osmotic Peristaltic Flows** is my own work and has not been submitted previously by me for taking any degree from this university, **International Islamic University, Sector H-10, Islamabad, Pakistan** or anywhere else in the country/world.

At any time if my statement is found to be incorrect even after my Graduation the university has the right to withdraw my Ph.D. degree.

Name of Student: *(Sadaqut Hussain)*
Reg. No. **55-FBAS/PHDMA/F15**
Dated: **24/12/2020**

Plagiarism Undertaking

I solemnly declare that research work presented in the thesis titled: **Modeling and Analysis for Electro-osmotic Peristaltic Flows** is solely my research work with no significant contribution from any other person. Small contribution/help wherever taken has been duly acknowledged and that complete thesis has been written by me.

I understand the zero tolerance policy of the HEC and University, **International Islamic University, Sector H-10, Islamabad, Pakistan** towards plagiarism. Therefore, I as an Author of the above titled thesis declare that no portion of my thesis has been plagiarized and any material used as reference is properly referred/cited.

I undertake that if I am found guilty of any formal plagiarism in the above titled thesis even after award of Ph.D. degree, the university reserves the rights to withdraw/revoke my Ph.D. degree and that HEC and the University has the right to publish my name on the HEC/University Website on which names of students are placed who submitted plagiarized thesis.

Student/Author Signature: Sadaqat

Name: **(Sadaqut Hussain)**

Certificate of Approval

This is to certify that the research work presented in this thesis, entitled: **Modeling and Analysis for Electro-osmotic Peristaltic Flows** was conducted by **Mr. Sadaqut Hussain,** Reg. No. **55-FBAS/PHDMA/F15** under the supervision of **Dr. Nasir Ali** no part of this thesis has been submitted anywhere else for any other degree. This thesis is submitted to the **Department of Mathematics & Statistics, FBAS, IIU, Islamabad** in partial fulfillment of the requirements for the degree of **Doctor of Philosophy in Mathematics, Department of Mathematics & Statistics, Faculty of Basic & Applied Science, International Islamic University, Sector H-10, Islamabad, Pakistan.**

Student Name: Sadaqut Hussain **Signature:** _____

Examination Committee:

a) **External Examiner 1:**
(Name/Designation/Office Address) **Signature:** _____

Prof. Dr. Tasawar Hayat
Professor of Mathematics,
Department of Mathematics,
QAU, Islamabad

b) **External Examiner 2:**
(Name/Designation/Office Address) **Signature:** _____

Prof. Dr. Muhammad Ayub
Professor of Mathematics,
Faculty of Basic Sciences
HITEC University, Taxila, Pakistan.

c) **Internal Examiner:**
(Name/Designation/Office Address) **Signature:** _____

Dr. Tariq Javed
Associate Professor

Supervisor Name:
Dr. Nasir Ali **Signature:** _____

Name of Chairman:
Dr. Tariq Javed **Signature:** _____

Name of Dean:
Prof. Dr. Muhammad Irfan Khan **Signature:** _____

Acknowledgements

First of all, I pay special thanks to Almighty Allah, Who assisted me in all walks of life and also assisted and guided me throughout my PhD work and in the accomplishment of this thesis too. Many Salat-o-Salam on our Holy Prophet Hazrat Muhammad (PBUH) who is a source of knowledge and blessings for the entire creations.

I would like to acknowledge the worth mentioning supervision of **Dr. Nasir Ali** who guided me and supported me during my whole research work. Moreover, his supervision enabled me to develop an understanding of the field. Without his sincere efforts I was unable to complete this hard task of my life. Really I am thankful to **Dr. Nasir Ali** for his inspiration and encouragement in every field of life especially in education and teaching. **Almighty Allah** may bless him with long life, health, happiness and knowledge. Moreover, I would like to express my sincere thanks to all faculty members of Department of Mathematics and Statistics IIU Islamabad especially to Dr. Tariq Javed (Chairman). I would also like to thank all other faculty member of my university for their sincere appreciation, comments and suggestions. I express my thanks to all staff of Mathematics and Statistics Department, IIU, for their various services. I am thankful to my all friends and would like to mention the names of some friends, Dr. Zeeshan Asghar, Dr. Zaheer Asghar, Mr. Kaleem Ullah, Mr. Waris Saeed khan, Noveel Sadiq, Waqar Mahmood, Qammar Zaman, Abrar Ahmed khan and Muhammad Mughees for their moral support. They always remain ready to assist me when I was needed.

I especially want to acknowledge efforts and prayers of my grandparents, father, uncles, brothers, sisters, cousin's, nephews, nieces and constant financial support of my brothers during my PhD studies, for their love, care and support in my life, which has been directly encouraging me for my study.

I would consider this acknowledgement incomplete without giving my wholesome attention to my late mom whose prayers were heavier than anything else to carry me through thorny paths of my life safe and protected.

Mr. **Sadaqut Hussain**

Preface

In recent years, peristaltic transport mechanism has received a considerable attention due to its extensive relevance to medical science and engineering. The peristaltic transport is involved in the blood flow in capillaries, arteries and venules, spermatozoa transport, swallowing of food through the esophagus, transportation of lymph from lymphatic vessels and movement of the chyme in the gastrointestinal tract. Many modern bio-medical devices and chemical pumps have been designed by exploiting the peristaltic mechanism. Examples include heart-lung machines, diabetic pumps, waste migration control pumps, roller and finger pumps and pharmacological drug delivery systems. These applications and new emerging ones have mobilized significant activity in theoretical studies of peristaltic fluid dynamics. In the most of physiological ducts such as esophagus, gastrointestinal tract, lymphatic vessels and small blood vessels, it is observed that the wall pumping fluid is coated with a fluid of different characteristics than the fluid being pumped out. In order to properly recognize the influence of coated fluid on transport properties, the concept of the single-layered transport phenomenon has been extended to two-layered and three-layered phenomena by considering different viscosities layered in the flow domain. Several mathematical models of the peristaltic mechanism have been employed in the literature to recognize the proper effects different viscosity layers in the flow domain. It is important to mention that studies carried out for multi-layered peristaltic transport are valid under the constraints of "the long wavelength and low Reynolds number". An important aspect highlighted in these studies is that for prescribed wall movement, a larger viscosity fluid in the peripheral layer dramatically increases the pumped volume flow rate compared with the single-fluid pump for a fixed pressure head. Thus, the presence of a greater viscosity peripheral layer could lead to amplification in the peristaltic flow. This observation gives further motivation to identify alternative means that could results in the augmentation of peristaltic flow. One such mechanism is the electro-osmotic mechanism. Several researchers developed theoretical models of electro-osmotic flows based on Newtonian and non-Newtonian constitutive equations that are relevant to physiological mechanisms and design of accurate bio-devices. In the recent years, electro-osmotic and peristaltic phenomena have been exploited in industrial technologies, bio-medical engineering, toxic waste conveyance in chemical development engineering and biological micro-electromechanical

devices. Continuous improvements in designs require gradually more refined models for electro-osmotic peristaltic transports, employing complex working fluids (.non-Newtonian and nano-technological). The studies available on transport processes due to peristalsis and electro-osmotic phenomena analyze different flow features such as velocity profile, pressure gradient, trapping and reflux phenomena. However, such studies are limited in number and do not include important aspects arising due to the inclusion of complex non-Newtonian fluid models. Motivated by the these facts, the aim of present thesis is to study the flow generated due to combined influence of both electro-osmotic and peristaltic activity for complex non-Newtonian fluids through different geometries. The thesis is composed of seven chapters. A brief description of each chapter is given below:

Chapter 1 is the introductory chapter in which a detail explanations of peristaltic and electro-osmotic phenomena are provided. Comprehensive review of the available literature on peristaltic and electro-osmotic flows is also included at the end.

Chapter 2 presents the theoretical study of electro-osmotic peristaltic flow of third order fluid in an asymmetric microchannel. The governing equations are simplified by using the approximations of "long wavelength and low Reynolds number". **Mathematica 8.1** is used to solve these equations numerically. The influences of the emerging parameters are thoroughly studied. It is noted that the trapping is completely controlled by proper tuning of embedded parameters. The results of this chapter are submitted for publication.

Chapter 3 explores analytically the dynamics of two-fluid electro-osmotic peristaltic flow through a cylindrical tube. The rheology of the fluid in the central core (inner region or core region) is captured through the Ellis equation. The region adjacent to the wall (outer region or peripheral region) is occupied by a Newtonian fluid. The equations governing the flow in each region are modeled by using the appropriate suppositions of "long wavelength and low Reynolds number". The closed form expressions for stream function corresponding to each region are obtained and utilized to determine the axial pressure gradient and the interface between the inner and the outer regions. The pumping characteristics, trapping and reflux phenomena are investigated in detail with reference to the Ellis model parameters and the electro-kinetic slip velocity. The present model also generalizes earlier studies from the

literature which can be retrieved as special cases. The results of this chapter are published in **The European Physical Journal Plus (2019) 134: 141**

Chapter 4 investigates the effects of peripheral layer and electro-osmotic force for the peristaltic flow of Phan-Thien-Tanner fluid. The core (inner) layer fluid satisfies the constitutive equation of PTT fluid model and peripheral (outer) layer is characterized as a Newtonian fluid. The governing equations in each region are simplified by invoking the constraints of "long wavelength and low Reynolds number". Closed form expressions for velocity and stream function are derived and then employed to investigate the pressure variations, trapping, interface region and reflux for a variety of the involved parameters. The influences of the emerging parameters are thoroughly studied. It is noted that the trapping and reflux are completely controlled by proper tuning the fluid model parameters and electro-osmotic slip velocity. The results of this chapter are published **Rheologica Acta (2019) 58 603–618.**

Chapter 5 explores two-dimensional peristaltic motion of two-fluids in a flexible tube under the influence of electro-osmotic force. The flow domain is composed of two regions, namely, the core region and the peripheral region. The Newtonian and the FENE-P models are used to describe the rheology of fluids in the peripheral and the core regions, respectively. Governing flow equations corresponding to each region are established under the approximation of "long wavelength and low-Reynolds number". The interface between the two regions is computed numerically by employing a system of non-linear algebraic equations. Influence of relevant controlling parameters on pressure gradient, interface, trapping and reflux are highlighted graphically and explained in detail. Special, attention is given to estimate the influences of viscoelastic parameter of the core region fluid in the presence of electro-osmotic environment. Our investigation indicates an augmentation in the pressure drop at zero volumetric flow rate with growing the viscoelastic and occlusion parameters. Moreover, trapping, reflux and pumping efficiency are found to increase with raising the electro-osmotic and viscoelastic parameters. The results of this chapter are published **Physics of Fluid 32 023105 (2020).**

Chapter 6 aims to analyze peristaltic movement of Rabinowitsch fluid in a cylindrical tube under the effect of external electric field. We highlight the

characteristics of the two-layered fluid by considering the Newtonian fluid in the peripheral layer while the non-Newtonian (Rabinowitsch) fluid in the core layer. Some physical restrictions such as "long wavelength and low Reynolds number" have been adopted to simplify the governing flow equations in each region. The stream function expression for peripheral and core are obtained. Numerical computations are carried out using Mathematica 8.1. This study is focused on determining the phenomena of trapping, pressure rise, velocity, pumping efficiency and reflux. The computational results have also been interpreted by graphical visualization along with a detailed discussion. The results of this chapter are submitted for publication.

Chapter 7 investigates three-layered flow of power-law fluid driven by peristaltic activity and electro-osmotic phenomenon. The flow problem is modeled by invoking "long wavelength and low Reynolds number constraints". Closed form expressions of stream function are obtained for each region. The interfaces between core and intermediate and intermediate and peripheral regions are computed by solving a system of nonlinear equations numerically. Pressure rise, mechanical efficiency and trapping phenomena are also evaluated by varying the involved parameters. The present study generalizes many of the available studies on multi-phase peristaltic transport. The results of this chapter are published in **The European Physical Journal Plus (2020) 135:348.**

Contents

1 Introduction **15**

1.1 Brief introduction of peristaltic and electro-osmotic flow phenomena 15

1.1.1 Peristaltic flow 15

1.1.2 Electro-osmotic flow 18

1.1.3 Electric double layer 19

1.2 Some basic definitions related to peristaltic transport 20

1.2.1 Fluid dynamics 20

1.2.2 Newtonian fluids 21

1.2.3 Non-Newtonian fluids 21

1.2.4 Volumetric flow rate 21

1.2.5 Streamlines 22

1.2.6 Bolus 22

1.2.7 Trapping 22

1.3 Dimensionless numbers 22

1.3.1 Reynolds number 22

1.3.2 Wave number 23

1.3.3 Amplitude ratio 23

1.3.4 Weissenberg number 23

1.4 Governing equations for fluid motion 23

1.4.1 Law of conservation of mass (continuity equation) 23

1.4.2 Law of conservation of momentum (momentum equation) 24

1.5 Literature survey 24

1.5.1 Peristaltic transport of Newtonian and non-Newtonian fluids 25

1.5.2 Peristaltic transport of two-layered fluids 26

1.5.3 Peristaltic transport of multi-layered fluids 27

1.5.4 Electro-osmotic transport of Newtonian and non-Newtonian fluids 27

1.5.5 Electro-osmotic peristaltic flows 30

2 Theoretical study of electro-osmotic peristaltic flow of third order fluid in an asymmetric in microchannel **32**

2.1 Mathematical formulation of the problem 33

2.2 Mathematical formulation 33

2.2.1 Volumetric flow rate 37

2.3 Results and discussion 38

2.3.1 Velocity profile 38
2.3.2 Pressure distribution 39
2.3.3 Trapping phenomenon 39
2.4 Conclusion 40
3 Mathematical modelling of two-fluid electro-osmotic peristaltic pumping of Ellis fluid in an axisymmetric tube 49
3.1 Geometric model of the physical problem 49
3.2 Mathematical model 50
3.3 Velocity components in term of stream function 55
3.4 Graphical results and interpretations 57
3.4.1 The interface region 57
3.4.2 Pressure and volume flux variation 59
3.4.3 Mechanical efficiency 60
3.4.4 Trapping phenomenon 61
3.4.5 Reflux 62
3.5 Conclusions 63
4 Peristaltic flow of Phan-Thien-Tanner fluid: Effects of peripheral layer and electro-osmotic force 80
4.1 Basic equations 80
4.2 Problem formulation and its solution 81
4.3 Results and discussions 90
4.3.1 Analysis of interface region 90
4.3.2 Pressure expression and graphical discussion 91
4.3.3 Trapping phenomenon 92
4.3.4 Reflux 92
4.4 Deductions 93
5 An analysis of two-layered electro-osmotic peristaltic flow of FENE-P fluid in an axisymmetric tube 105
5.1 Problem description 105
5.2 Mathematical formulation 106
5.3 Results and graphical discussions 112
5.3.1 Analysis of interface 112
5.3.2 Pressure expression and results discussion 114
5.3.3 Velocity profile 115
5.3.4 Mechanical efficiency 116

5.3.5 Trapping phenomenon 116
5.3.6 Reflux 117
5.4 Deductions 118
6 Peristaltic flow of Rabinowitsch fluid in an axisymmetric tube under the influence of electro-osmotic force 131
6.1 Mathematical treatment of the flow problem 131
6.2 Governing equations and its solution 132
6.3 Results and discussions 137
6.4 Conclusion 139
7 Electro-kinetically modulated peristaltic transport of multi-layered power-law fluid in an axisymmetric tube 149
7.1 Mathematical formulation and solution of the problem 149
7.2 Problem description 154
7.2.1 Determinations fluid-fluid interface 156
7.2.2 Pumping characteristics 158
7.2.3 Pumping efficiency 160
7.2.4 Trapping phenomenon 160
7.3 Conclusion 162
Summary and future research directions 176
References 177

Nomenclature

E_z	external electric field
u, w	velocity components in tube
u, v	velocity components in channel
u_c, w_c	velocity components in core region
u_N, w_N	velocity components in peripheral region
S	shear stress
λ	wavelength
μ_1	viscosity in the core region
μ_2	viscosity in the peripheral region
ζ_1	electric potential, at lower wall of the channel
ζ_2	electric potential, at upper wall of the channel
μ_r	viscosity ratio between two regions
f	linear function for PTT fluid
Y_1	linear function for FENE-P fluid
L	extensibility parameter of the model
a	physical parameter of the FENE-P fluid
λ_d	Debye length
Q	time averaged volumetric flow rate
P_0	pressure gradient at $z = 0$
R_1	interface of the two fluid
R_0	boundary of the tube wall
q_1	flow rate in outer boundary
q	flow rate in inner boundary
ϵ_c	dielectric constant in inner region
ϵ_N	dielectric constant in outer region
De	Deborah number
κ	relaxation time
U	velocity of the tube wall
c	velocity of the channel wall
Re	Reynolds number
$1 - k$	peripheral thickness at $z = 0$
ϕ_{oc}	occlusion parameter

ψ^* stream function in fixed frame

ψ stream function in wave frame

ρ_{cN} concentration total charge density

r_0 characteristics radius of the tube

δ small parameter. (It is the ratio of the characteristics radial length to the characteristics axial length scale.)

ρ_e total ionic charge density

e elementary charge

z charge valance

n^+ number density of cations

n^- number density of anions

ε permittivity of the fluid

T temperature

k_B Boltzmann constant

D_0 diffusivity of the chemical species

n_0 ionic concentration at the bulk

ΔP_1 pressure rise per wavelength at (Q=0)

Subscripts:

c core region

N peripheral region

Chapter 1

Introduction

In this chapter, we highlight the fundamental concepts of the fluid dynamics such as Newtonian fluids, non-Newtonian fluids, peristalsis and electro-osmotic phenomena. The fundamental laws based on conservation of mass and momentum are briefly discussed. The dimensionless numbers related to the research topic are defined. A brief review of available literature on the topic under consideration is also provided.

1.1 Brief introduction of peristaltic and electro-osmotic flow phenomena

1.1.1 Peristaltic flow

The analysis of peristaltic flow has established significant attention in the last four decades because of its several biological and industrial applications. Peristaltic flow is a form of fluid flow from a region of lower to higher pressure due to progressive waves propagating along the length of the flexible confinement. Mechanism of peristaltic wave is naturally generated resulting in the motion of the physiological fluid from one part of the body to the other. This phenomenon is observed in esophagus, the ductus efferentes of male reproductive tract Batra (1974) and also in small blood vessels, small and large intestines Macagno and Christensen (1980), bile duct, urine transport through ureter Roshani et al. (1999). The said phenomenon has been also utilized in the design of heart-lung machines Taber et al. (2006), pharmacological drug delivery system Tripathi and Beg (2014), dialysis and diabetes pumps Jackman et al. (1980) and waste migration control pump. In general the most of physiological ducts such as esophagus, gastrointestinal tract Pandey et al. (2015), embryo transport Elshehawey and Gharseldien (2004), and blood transport in the small vessels Tripathi (2012), it is observed that the structure of the wall pumping the fluid is coated with a fluid of different characteristics than the fluid being pumped out. In order to properly recognize the influence of coated fluid on transport properties, the concept of the single-layered transport phenomenon should be extended to two-layered and three-layered phenomena by considering different viscosities layered in

the flow domain. Several theoretical mathematical models of the peristaltic mechanism have been employed in the literature to recognize the proper effects of the two-layered and three-layered viscosities.

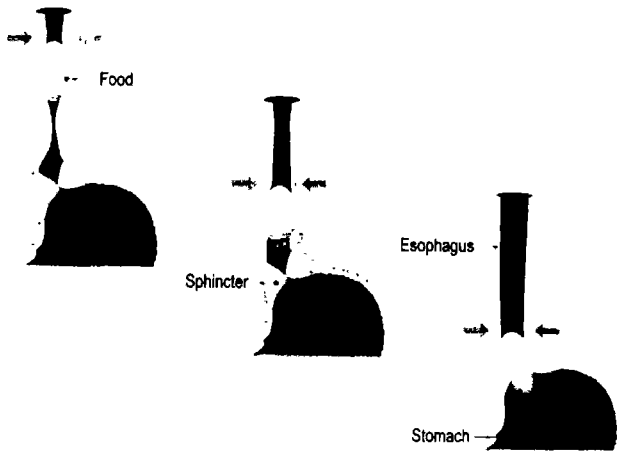

Fig. 1.1: Peristalsis phenomenon

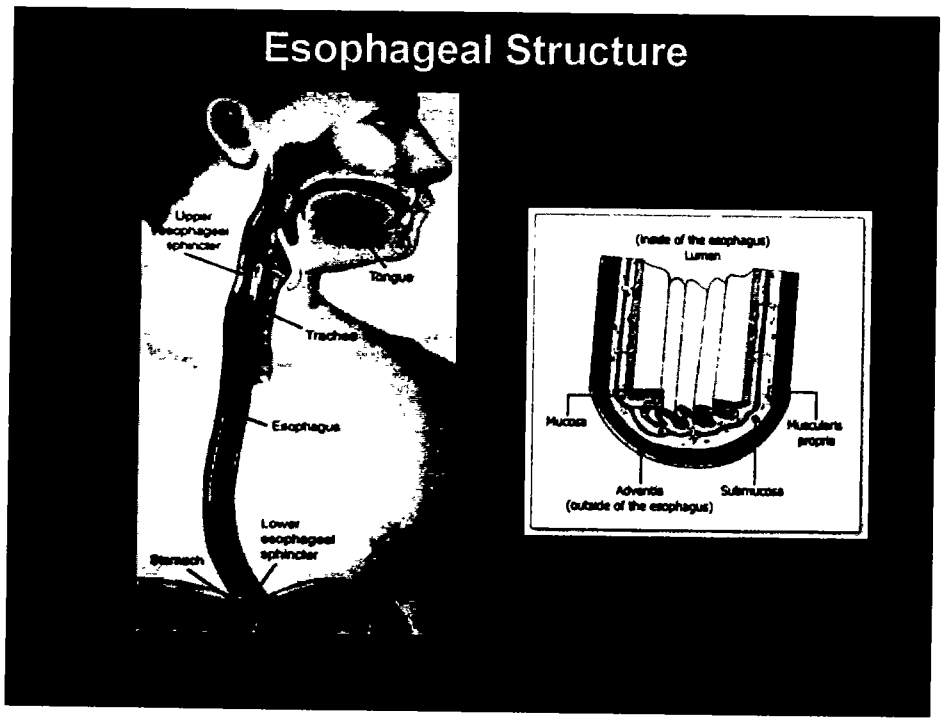

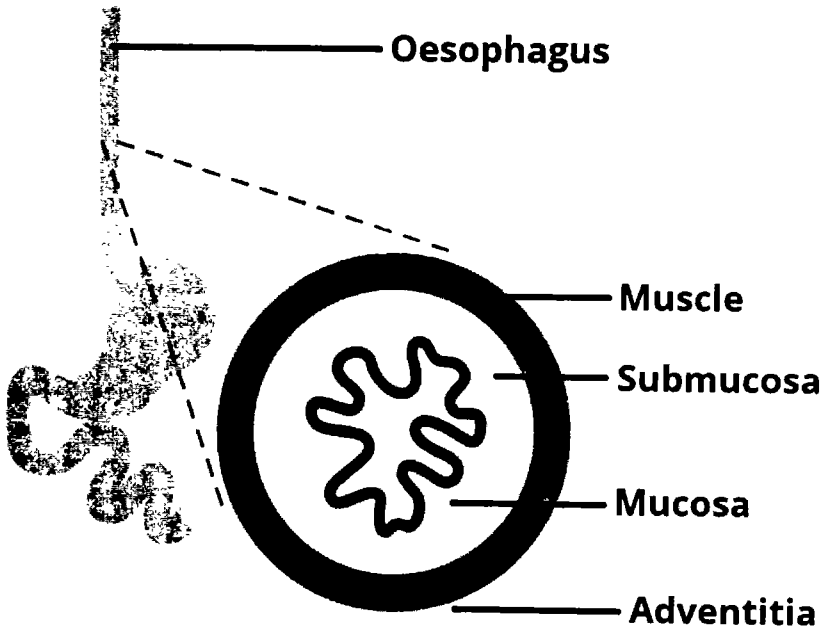

Fig. 1.2: Peristalsis flow in the esophagus in different layers

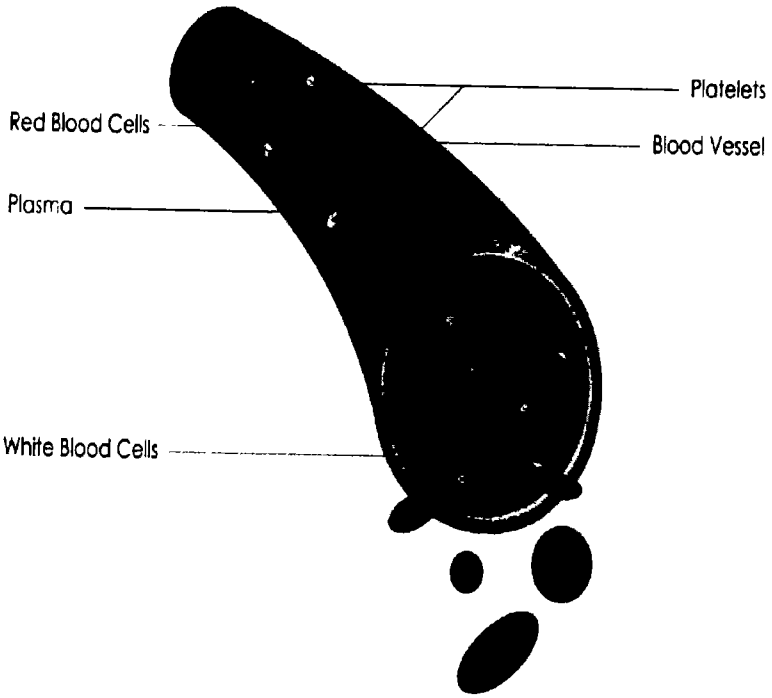

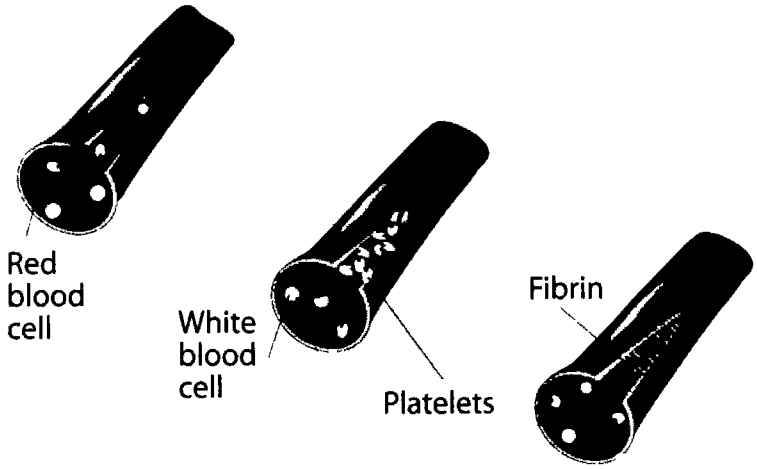

Fig. 1.3: Blood flow in the capillary with different layers

1.1.2 Electro-osmotic flow

Electro-osmotic transport flow is a process in which motion in an ionized solution (electrolyte) confined in a micro-channel is generated by the application of applied electric potential. It has many emerging applications in era of bio-microfluidics. In this regard, first attempt was made by F. F. Reuss in (1809), to study the electro-kinetic flow phenomena he considered "pumping water through a porous clay plug by positioning electrodes on opposite sides of the plug and applying electrical potential, observing what we call electro-osmosis today". Basically, the electro-kinetic phenomena is a group of influence that occur either in a solution having particles or fluid filled systems e.g., porous structures or capillaries. The common phenomena in all these effects are the electrical double layer (EDL) that arises due to the solid/fluid interaction **(see Fig. (1.5)).** The negative charged surface attracts opposite ions in the ionized solution, developing a layer of positively charged fluid near the wall and at the same time repelling the counter-ions. "The thin layer of immobile counter-ions covering the inner side of the wall of the surface is known as the *Stern layer"*. A thicker layer of moving counter-ions, known as a diffuse layer, is formed next to the Stern layer. The combination of the "Stern layer and the thicker layer is known as the electric double layer (EDL)". It is hardly, to define the exact position of the EDL where the EDL ends, and bulk fluid starts. The typical thickness of the EDL is known

as Debye length (λ_D), is defined as the "distanced outside the Stern plane at which the potential has changed by a factor $1/e$ (~0.368)". The potential at EDL is called the "zeta-potential" (ξ). The electro-kinetic body force emerges due to the difference in the amount of charges from cations and anions by connecting the system to an external applied electric field. The capability to set the diffuse layer fluid in motion with an applied external electric field, which in turn sets the bulk fluid in movement **(see Fig. (1.4))** is what makes electro-osmotic pumping possible. Similarly if fluid is forced through a capillary, with an electric double layer at the fluid/solid interface, a current is moved through the capillary and a "streaming potential" can be perceived between the capillary ends. The resulting multi-physical fluid dynamic problem encompasses the computation of the flow field developed by the combined effects of the wall movement and the electro-kinetic body force

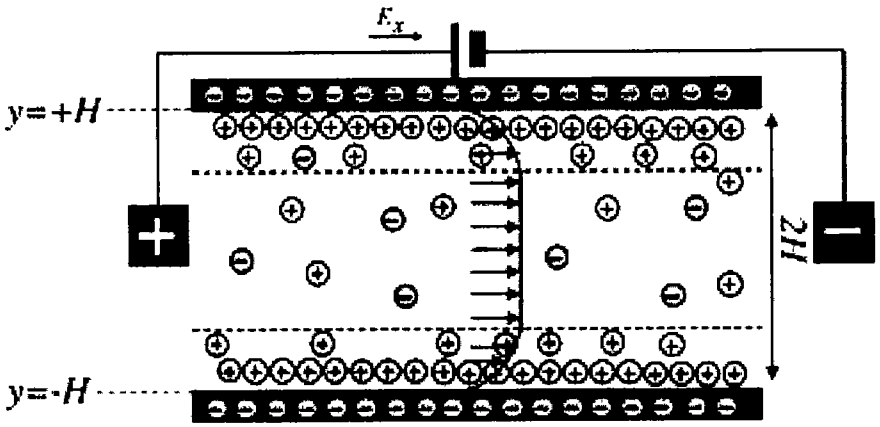

Fig. 1.4: Electroosmotic flow

1.1.3 Electric double layer

The negative charged surface attracts opposite ions in the ionized solution, developing a layer of positively charged fluid near the wall and at the same time repelling the counter-ions which shown in **Fig. (1.5)**. "The thin layer of immobile counter-ions covering the inner side of the wall is known as the *Stern layer*". A thicker layer of moving counter-ions, known as a diffuse layer, is formed next to the Stern layer. The potential at EDL is called the "zeta-potential". The combination of the "Stern layer and the thicker layer is known as the electric double layer (EDL)". When the system is connects to the external electrical potential, electro-kinetic body force emerges. The resulting multi-physical fluid dynamic problem encompasses the computation of the

flow field developed by the combined effects of the wall movement and the electro-kinetic body force.

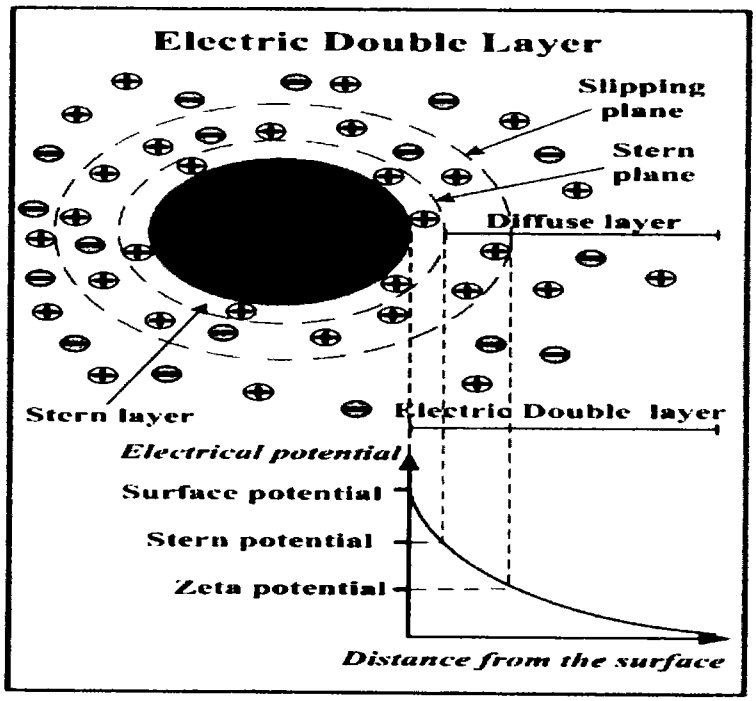

Fig. 1.5: Electric double layer

1.2 Some basic definitions related to peristaltic transport

1.2.1 Fluid dynamics

Fluid dynamics is the branch of "applied science" that describes the flow of fluids (liquid and gasses). Fluid is a substance that continually deform under an external force or shear stress. There are two types of the external forces namely; body force and surface force. The forces due to the electric field, magnetic field and gravity are the examples of body forces. The surface force is the force that acts across the external or internal surface element of the material object. Surface force can be divided into two perpendicular components as normal forces and tangential forces or shear forces. In general, the fluid behavior remains same under the action of these forces but at micro-level the fluid properties like, viscosity and density experience considerable changes. The flow of fluid in channels or tubes is due to various agents. These include pressure gradient, movement of the channel or tube wall, gravitational, electromagnetic forces etc.

1.2.2 Newtonian fluids

The most common fluids such as water, air and gasoline are Newtonian under normal condition. The Newtonian fluids follow the Newton's law of viscosity. Sir Issac Newton (1642 - 1726) was the first one who explored the flow behavior of fluids through a simple linear relation between shear stress and shear rate. This relationship is known as Newton's Law of Viscosity. The only parameter required to analyze such fluid models is the slope of the shear stress–shear rate relationship which is called viscosity. The viscosity of Newtonian fluids will remain a constant no matter how fast they are forced to flow through a duct, that is, the viscosity is independent of the shear rate.

1.2.3 Non-Newtonian fluids

A fluid which does not obey the Newton's law of viscosity is known as non-Newtonian fluid. In reality most of the fluids are non-Newtonian and the viscosity is dependent on the shear rate (shear thickening or thinning) or the deformation history (thixotropic). The non-Newtonian fluids display a non-linear relation between shear stress and shear rate. The viscosity of the shear-thinning fluids decreases with shear stress like, Ketchup, Quicksand, whole blood and many commercial house paints are the examples of the shear-thinning fluids. The viscosity of the shear-thickening fluids increases with shear stress and the synovial fluid that lubricates our joints and Cornstarch slurries are shear-thickening fluids. Fluids whose viscosities change with respect to time can also be categorized as non-Newtonian. Fluids with a viscosity that decreases over time are called thixotropic, whereas those whose viscosity increases over time are called rheopectic.

1.2.4 Volumetric flow rate

The volumetric flow rate (or volume flow rate) of a system is measure of the volume of fluid passing a point in the system per unit time.

Mathematically it is given by

$$Q = A.v. \tag{1.1}$$

Where the Q represent the volumetric flow rate, A be the cross sectional area and v be the average flow velocity.

1.2.5 Streamlines

A streamline is a curve drawn in the fluid such that tangent to it at every point is in the direction of fluid velocity at that point at the instant considered. Basically the streamlines show the path of imaginary particles suspended in it and transported along it. The streamlines in the flow can be visualized by considering the movement of a small marked element of the fluid.

1.2.6 Bolus

Trapping corresponds to the formation of eddying regions in the flow domain. Such regions enclose a volume of fluid which is usually known bolus in the literature .The bolus is transported along the tube via the peristaltic activity with the speed of wave.

1.2.7 Trapping

Trapping corresponds to the flow situation when streamline splits and encloses a fluid bolus which is translated with the wave speed along the peristaltic wave. In this phenomenon, a blockage of the flow along the central line appears due to the presence of boluses on either side of the central line.

1.3 Dimensionless numbers

The important dimensionless numbers relating to the research topic are defined as

1.3.1 Reynolds number

The Reynolds number is the ratio of inertial forces to viscous forces and usually denoted by Re. Mathematically it is written by

$$Re = \frac{\rho v L}{\mu}, \tag{1.2}$$

where v is the flow velocity, L is the length of duct and μ represents the dynamic viscosity of the fluid. It is an appropriate parameter to predict whether the flow condition will be laminar or turbulent. It can be interpreted that when the viscous forces are dominant (slow flow, low Reynolds number) they are appropriate enough to keep all the fluid particles in line, then the flow is laminar. Even very low Reynolds number specifies viscous creeping movement, where inertia influence are negligible. When the inertial forces dominate over the viscous forces (when the fluid is flowing faster and Re is larger) then the flow is turbulent.

1.3.2 Wave number

The wave number refers to the ratio of the radius (width) of the tube (channel) to the wavelength of the wave propagating along the tube (channel) wall. Usually it is denoted by Greek symbol δ. Mathematically, it is given as

$$\delta = \frac{L}{\lambda}, \tag{1.3}$$

where L denotes the characteristic length and λ is the wavelength.

1.3.3 Amplitude ratio

It is ratio of amplitude of the peristaltic wave to the radius (width) of the tube (channel). It is usually denoted by φ.

1.3.4 Weissenberg number

The Weissenberg number is a dimensionless quantity used to describe the viscoelastic flows. It is a ratio of the elastic forces to the viscous forces. Basically, it compares the elastic forces to the viscous forces. It is usually define by the relation of stress relaxation time of the fluid and a specific process time. Weissenberg number, denoted by Wi or We, is defined as

$$We = \frac{\text{elastic forces}}{\text{viscous forces}} \tag{1.4}$$

The Weissenberg number shows the degree of orientation produced by the deformation, and is suitable to investigate flows with a constant stretch history, such as simple shear.

1.4 Governing equations for fluid motion

To study the physical behavior of fluid flow features such as: velocity profile, pressure gradient, streamline topology, efficiency and reflux, etc. We must have to use some fundamental mathematical relations including law of conservation of mass, law of conservation of momentum and law of conservation of energy. Basically, these fundamental laws provide the relations for the rate of change of mass, momentum and energy.

Now we discuss the governing equations as:

1.4.1 Law of conservation of mass (continuity equation)

According to law conservation of mass, the mass of enclosed system always remains constant with passage of time, unless mass is added or removed from the system.

The mathematical form of law of conservation of mass is given by

$$\frac{\partial \rho}{\partial t} + \nabla.(\rho \mathbf{V}) = 0, \tag{1.5}$$

is known as equation of continuity. It relates the density and velocity of the fluid. For incompressible flow it take the following form

$$\nabla.\mathbf{V} = 0. \tag{1.6}$$

1.4.2 Law of conservation of momentum (momentum equation)

The mathematical form of law of conservation of momentum is define as

$$\rho \frac{d\mathbf{V}}{dt} = -\nabla p + \nabla.\boldsymbol{\tau} + \rho \mathbf{F}, \tag{1.7}$$

where p is the pressure, $\boldsymbol{\tau}$ be the extra stress tensor defined differently for different fluid models and $\mathbf{F}$ represents the body force vector.

1.5 Literature survey

In recent years, electro-kinetically modulated peristaltic transport mechanism has received a considerable attention due to its extensive relevance to medical science and engineering. The peristaltic transport is involved in the blood flow in capillaries, arteries and venules, spermatozoa transport, swallowing of food through the esophagus, transportation of lymph from lymphatic vessels and movement of the chyme in the gastrointestinal tract. In general the most of physiological ducts such as esophagus, gastrointestinal tract, embryo transport, and blood transport in the small vessels, it is observed that the structure of the wall pumping the fluid is coated with a fluid of different characteristics than the fluid being pumped out. In order to properly recognize the influence of coated fluid on transport properties, the concept of the single-layered transport phenomenon should be extended to two-layered and three-layered phenomena by considering different viscosities layered in the flow domain. Several theoretical mathematical models of the peristaltic mechanism have been employed in the literature to recognize the proper effects of the single-layered, two-layered and three-layered viscosities. Many modern bio-medical devices and chemical pumps have been designed by exploiting the peristaltic mechanism. Examples include heart-lung machines, diabetic pumps, waste migration control pumps, roller and finger pumps and pharmacological drug delivery systems. These applications and new emerging ones have mobilized significant activity in theoretical studies of peristaltic

fluid dynamics. In the beginning all researchers were focusing on the single layered analysis. Latham (1966) was the first one who introduced the idea of peristaltic flow phenomenon. The brief review of literature on peristaltic and electro-osmotic transport of Newtonian and non-Newtonian fluids is given below.

1.5.1 Peristaltic transport of Newtonian and non-Newtonian fluids

In the beginning, Newtonian fluid models were developed to explore the peristaltic flow characteristic. These earlier research on peristalsis were restrained to study the urine transport through ureter (1964). Shapiro (1967) discussed peristaltic transport of a two-dimensional model and developed a closed form solution under small wave number and negligible inertial effects. Weinberg (1970) and Shapiro and Latham (1966) provided a comparison between the experimental and theoretical results. On the later stage a theoretical model, developed by Shapiro et al. (1969) and Fung and Yih (1968) approximated the actual situation as the flow in a flexible tube with a sinusoidally deformed boundary. They simplified the governing equations under constrains of creeping flow and long wavelength. The pumping, trapping and reflux phenomena were discussed in detail. Later studies on this topic can be considered as the extensions of the work of Shapiro et al. Barton and Raynor (1968) suggested a model of intestinal transport of peristaltic flow circular tube under the constrain of long wavelength. Raju and Devanathan (1972) discussed the peristaltic transport of a power law fluid in a circular tube, with a sinusoidal wave of small amplitude travelling down along the length of the channel wall. Bohme and Friedrich (1983) explored the peristaltic phenomenon for an incompressible linear viscoelastic fluid by taking general second order integral constitutive equation. They discussed the pumping efficiency and the pressure discharge characteristics of the peristaltic pump. Peristaltic transport of second grade fluid in circular tube and channel geometry was investigated by Siddiqui et al. (1991) and Siddiqui and Schwarz (1994).

Several important non-Newtonian effects were investigated in these extensions. For example, non-Newtonian fluid characteristics (rheology) were analyzed by Provost and Schwarz (1994), Wang et al. (2008), Rao and Mishra(2004), Hayat et al. (2008) and Hayat et al. (2007), Wang et al. (2004), Wang et al. (2011), Wang et al. (2011), inertial and streamline curvature effects were discussed by Jaffrin (1973), Rao and Mishra (2004) and Usha and Rao (2000), heat and mass transfer effects by Hayat et al. (2016), Misra et al. (2018) and Ali et al. (2010), conduit wall elastic effects by

Takagi and Balmforth (2011a, 2011b), wall curvature effects by Ali et al. (2010, 2011), Ali et al. (2015a), Ali et al. (2016) and Tanveer et al. (2017) and wave profile effects by Hayat et al. (2006) and Dobrolyubovn et al. (2002).

1.5.2 Peristaltic transport of two-layered fluids

Most of the theoretical analyses on peristaltic motion are carried out for a single layer fluid. However, in many physiological systems this assumption may not hold. For instance, the fluids flowing through the core region of the small intestine, esophagus, gastrointestinal tract, small blood vessels and cervical ducts are surrounded by a thin layer of another fluid of different viscosity. Therefore, in such ducts the flow must be considered as a two-phase flow. In order to properly recognize the influence of coated fluid on transport properties, the concept of the single-layered transport phenomenon should be extended to two-layered and three-layered phenomena by considering different viscosities layered in the flow domain. Several theoretical mathematical models of the peristaltic mechanism have been employed in the literature to recognize the proper effects of the single-layered, two-layered and three-layered viscosities. The first study in this direction was initiated by Shukla et al. (1980) in symmetric ducts for a specified interface shape between the peripheral and the core regions. Brasseur et al. (1987) revisited the same problem for the channel geometry when interface is unknown a priori and provided a detailed discussion on trapping, reflux and interface shape. Later attempts on the two-fluid peristaltic flows were made by Rao and Usha (1995) who examined the pumping of two-immiscible Newtonians fluids in circular tube geometry and emphasized the trapping under co-pumping conditions and the detachments of the trapped bolus from the centerline. The simplified model of Shukla et al. (1980) was also extended by Srivastava and Saxena (1995) by taking the Casson fluid in the center region of a cylindrical tube. Misra and Pandy (1999) followed the approach of Brasseur et al. (1987) and presented the analytical results for peristaltic flow of power-law fluid in a channel with a peripheral layer. The effects of porous medium in the model of Brasseur et al. (1987) were incorporated by Mishra and Rao (2005). Vajrarelu et al. (2006) utilized the Herschel-Bulkley constitutive equation to characterize the fluid in the central region and highlighted the influence of yields stress in peristaltic movement of two immiscible fluids through a channel. The analysis of Usha and Rao (1995) was extended by Vajravelu et al. (2009) to the flow of Casson fluid in the core region and a viscous fluid in the peripheral region in a tube

with permeable wall. Peristaltic flow of Bigham fluid in contact with viscous fluid was analyzed by Narahari and Sreendh (2010) and Prabakara et al. (2013). More recently, Kavitha et al. (2017) investigated the peristaltic flow of Jeffery fluid in an inclined channel with peripheral layer and reported the variations in the shape of interface with respect to the Jeffery parameter.

1.5.3 Peristaltic transport of multi-layered fluids

The idea of peristaltic transport of two-layered fluid system has also been extended to three-layered fluid system. In this context, Elshehawey and Gharseldien (2004) developed a theoretical model of three-layered peristaltic transport in a channel with variable viscosity. The resemblance of this flow situation is to the embryo transport mechanism where the fluid can be divided in three regions; egg and the fluid close to it occupies core region, intermediate region is filled with culture fluid and the outer peripheral layer comprises of intrauterine fluid. Tripathi (2012) studied three-layered blood flow in cylindrical tube geometry by assuming that the RBC (red blood cell) in the central (core) region, WBC (white blood cell) in the intermediate region and the plasma in the outer (peripheral) region. Later, Pandey et al. (2015a, 2015b) investigated the peristaltic transport of three-layered power-law fluid in both channel and tube geometry and developed its relevance with the intestinal flow in the gastrointestinal tract. In the gastrointestinal tract the chyme is basically a partially-digested food mixed with intestinal secrants and is usually characterized as a non-Newtonian fluid. The rheological character of chyme is much closer to the behavior of the power-law fluid. In a small intestine the mucous layer behave as a peripheral layer and plays the role of a lubricant which protect the inner part of the intestine from the raw material of the chyme and secrets enzymes to help digestion. In this way, the flow inside the small intestine may be treated as a two-layered peristaltic flow.

1.5.4 Electro-osmotic transport of Newtonian and non-Newtonian fluids

It is important to mention that all the studies mentioned above are valid under the constraints of the long wavelength and low Reynolds number. An important aspect highlighted in these studies is that for prescribed wall movement, a larger viscosity fluid in the peripheral layer dramatically increases the pumped volume flow rate compared with the single-fluid pump for a fixed pressure head. Thus, the presence of a greater viscosity peripheral layer could lead to amplification in the peristaltic flow.

This observation gives further motivation to identify alternative means that could results in the augmentation of peristaltic flow.

In all the above cited, literature the flow is solely driven by peristaltic waves as there is not any other agent of flow like, electro-osmosis, electro-phrosis etc. The electro-osmosis is a process in which the movement of the fluid in any conduit (capillary tube, microchannel) is produced under the effect of an applied external potential. In this mechanism, the solid surface remains stationary and fluid moves due the influence of electric field. This process plays a vital role in the chemical separation technique. The electro-kinetic phenomenon has been subsequently used in improving various devices in medicine (2005) and other field of technology (1994). Several researchers developed theoretical models of electro-osmotic flows based on Newtonian and non-Newtonian constitutive equations that are relevant to physiological mechanisms and design of accurate bio-devices. Recent studies regarding electro-osmotic transports of Newtonian fluids in micro-channels and capillaries have been carried out by Haywood et al. (2014), Herr et al. (2000), Kang et al. (2002) and Yang et al. (2001). In the realm of non-Newtonian electro-osmotic flows, the following studies are worth mentioning. Ng (2013) studied the electro-osmotic flow of Casson fluid in a micro-channel. Ng and Qi (2014) investigated the electro-osmotic flow of power-law fluid in a non-uniform micro-channel. Si and Jian (2015) analyzed the flow phenomena of Jeffery fluid via electro-osmotic mechanism in a corrugated microchannel. Ghosh and Chakraborty (2016) demonstrated the electro-osmotic flow over a non-homogenous charged surface in the presence of non-electrostatic ion-ion interactions. Jimenez et al. (2016) examined the flow of Maxwell fluid in an electro-osmotic environment through a rectangular microfluidic channel. Lei et al. (2017) provided an analysis of electro-osmotic flow over a slightly bumpy plate. Afonso et al. (2009) analytically studied combined influence of electro-kinetic force and pressure gradient on flow through a microchannel by invoking the Debye-Huckel approximation. Zhao and Yang (2013) described the electro-kinetic transport on nano-scale. They developed a mathematical model to study the electro-osmotic effects on flow of power-law fluid in a micro-channel. Kou and Dejam (2019) studied the electro-osmotic and pressure driven flow in a channel surrounded by a permeable porous medium. Gailwad et al. (2016) developed a model to study the electro-osmotic and pressure driven movement of immiscible binary system with a layer of non-conducting fluid under interfacial slip. They also studied the slip driven micro-

pumping of binary system with a layer of non-conducting fluid in the presence of electric double layer mechanism and applied pressure gradient (2017). On the later stage, Zhao et al. (2013) examined key properties of non-steady flow of Oldroyd-B fluid in a capillary under the effect of electro-kinetic force. Afonso et al. (2013) analytically tackled the two-fluid electro-kinetic flow of viscoelastic liquid in a cylindrical tube. Ferras et al. (2014) probed electro-kinetic effects in annular flow of viscoelastic fluid and provided both numerical and analytical illustration of the solution of the problem. Ferras et al. (2016) made another attempt to investigate the electro-osmotic and pressure driven movement in micro-channel. They provided both analytical and semi-analytical solution of the flow problem. Kaushik and Chakraborty (2017) developed a theoretical model to analysis the electro-osmotic transport of Oldroyd-B fluid in a rectangular micro-channel with symmetric and asymmetric wall zeta potentials. It is important to mention that all the above mentioned studies were carried out without considering the interfacial transport and contact line dynamics phenomena. The two-fluid transport phenomena with interfacial transport and contact line dynamics of non-Newtonian fluids is a well-established area and interesting studies in this regard are available in the literature Yue and Feng (2012), Yue et al. (2006) and Weidner and Schwartz (1994).

Park and Lee (2008) investigated the electro-osmotic flow of Phan-Thien and Tannr in a rectangular duct under the influence of external potential and pressure gradient. They also obtain the numerical solution by using the finite volume technique. Berli and Olivares (2008) developed a theoretical model of electro-osmotic transport of power-law fluid in a cylindrical microchannel. Zhao et al. (2008) explored the electro-osmotic flow of power-law fluid in a silt channel. They also obtain the exact solution of the velocity distribution. Siddiqui and Lakhatia (2009) developed a theoretical model of electro-osmotic flow of micropolar fluid in uniform rectangular microchannel under the effect of external electric field. Vasu and De (2010) discussed the electro-osmotic flow of power law fluid in a rectangular microchannel at high zeta potential and simplify the flow problem without invoking the Debye-Huckel linear approximation. Sadeghi et al. (2011) studied the electro-osmotic flow of PTT and FENE-P fluids in slit microchannel and also obtain the analytical solutions of the transverse distribution of velocity, and thermal transport characteristics. Jian et al. (2014) present the Semi-analytical solutions for transient electro-osmotic flow of Maxwell fluid between micro-parallel plates. More recent studies dealing with the

application of electro-osmotic methods for transportation of fluid in channel or tube were carried out by Afonso et al. (2009, 2013), Dhinakaran et al. (2010), Ferras et al. (2014), Das and Chakraborty (2006).

1.5.5 Electro-osmotic peristaltic flows

Motivated by the bio-microfluidics developments of electro-kinetic flow, recently some analyses on electro-kinetically modulated physiological transport have also been presented. These investigations explored the complex flow situation including electro-kinetic and other physical effects. Chakraborty (2006) was the first one to develop a mathematical model to investigate the effects of electro-osmosis on peristaltic transport. The analysis of Chakraborty (2006) was also extended by several researchers. In this regard, Tripathi et al. (2016) extended Chakraborty's model with the inclusion of a transverse magnetic field for time-dependent peristaltic flow. Prakash and Tripathi (2018) discussed the flow of non-Newtonian ionic nano-fluid in a tapered peristaltic channel. They utilized constitutive equations of the Williamson viscoelastic model and obtained linearized solutions via perturbation and MATLAB routine bvp-4c methods. Later on Misra et al. (2014) investigated the electro-osmotic peristaltic transport of micro-polar liquid in a flexible channel. Tripathi et al. (2017) studied the electro-kinetic modulated peristaltic transport of the viscoelastic fluid in a finite length capillary. Tripathi et al. (2018a) developed a model to study the combined influence of electro-kinetically modulated peristaltic movement of nano-fluid in a micro-channel along with joule heating and buoyancy effects. Prakash et al. (2018) described the electro-kinetic peristaltic flow of nano-liquid in a micro-fluidic channel. Goswami et al. (2016) analyzed the two-layered electro-osmotic peristaltic movement of power-law fluid in a tabular geometry which closely resembles with a blood vessel. Goswami et al. (2016) explored the simultaneous effects of a thin peripheral layer and electro-osmotic body force on the peristaltic movement of power-law fluid through a circular tube. The analysis of Goswami et al. (2016) is a direct extension of the work by Usha and Rao (1995). Flow of Jeffrey fluid in an asymmetric channel induced by electro-osmosis and peristaltic activity has been investigated by Tripathi et al. (2018b). Narla and Tripathi (2019) discussed the two-layer electro-osmotic transport in a curved channel by considering the viscous fluid in both regions. Electro-osmotic peristaltic transport of a Jeffrey fluid model in a tapered channel induced by asymmetric zeta potential at the walls of the channel has been

analyzed by Narla et al. (2018). Chaube et al. (2018) investigated the inertia free peristaltic flow of a power-law aqueous solution in a mirco-channel under the influence of electro-kinetic body force. Prakash et al. (2019) examined the peristaltic transport of pseudoplastic aqueous nano-liquids in a micro-channel under the effects of electric field. The pseudoplastic aqueous liquid has been modeled by tangent hyperbolic equation. Mondal et al. (2015) developed a model to analyze the interfacial transport and contact line dynamics of two-fluid system with chemically patched walls under the electrokinetic effects. They employed the constitutive equations of the power-law to capture the behavior of the non-Newtonian fluid and employed the diffuse interface phase-field technique to investigate the interfacial transport and contact line dynamics. Recently, Tripathi et al. (2017) discussed the electro-osmotic peristaltic transport of three-layered microvascular fluid. They assumed that RBC occupies the central (core) layer, WBC the intermediate layer and plasma the outer (peripheral) region.

It is noted from the literature cited above that due attention has been given to study the dynamics of the flows generated by the combination of peristaltic and electro-osmosis for Newtonian and generalized Newtonian fluid models. However, there is hardly a study available where such flows has been analyzed for advanced non-Newtonian models like PTT and FENE-P models. Further, the models like Rabinowitsch and third grade are also not integrated in this frame work. Same is the case when it comes to multi-layered electro-osmotic peristaltic flows. Motivated by the these facts, the aim of present thesis is to study the flow generated due to combined influence of both electro-osmotic and peristaltic activities for complex non-Newtonian fluids through different geometries. The complex non-Newtonian fluids are modeled through the constitutive relations of third grade, PTT, FENE-P, Rabinowitsch and power-law models.

Chapter 2

Theoretical study of electro-osmotic peristaltic flow of third order fluid in an asymmetric in microchannel

In chapter 2, a theoretical study of electro-osmotic peristaltic transport of third order fluid in an asymmetric microchannel is presented. The equations governing the flow are modeled by using the suitable approximations of long wavelength and low Reynolds number. A numerical procedure is implemented in Mathematica 8.1 to compute velocity, pressure gradient and stream function. The computational results are presented graphically for several values of the controlling parameters. It is noted that trapping is more sensitive due to an external applied potential rather than the electro-osmotic parameter and third order fluid model parameters. The results obtained may be applicable in the modulation of peristaltic pumping in the efficient operation of various industrial and bio-medical devices.

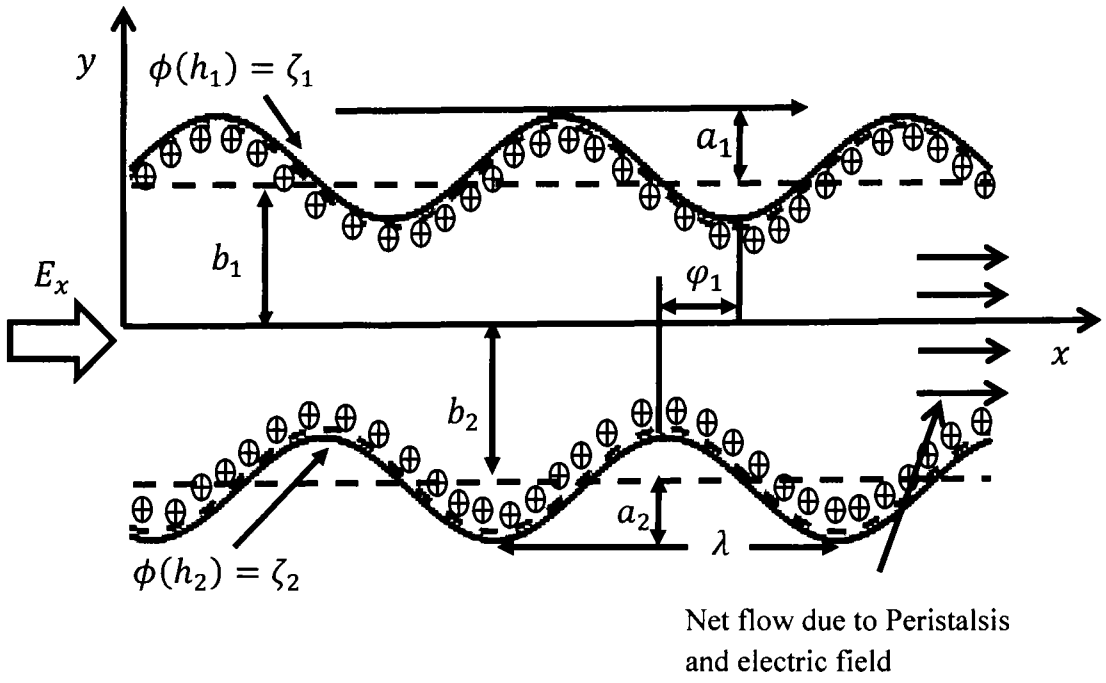

Fig. 2.1: Geometry of the flow problem

2.1 Mathematical formulation of the problem

We considered a flexible asymmetric microchannel having width $(b_1 + b_2)$ through which a bio-fluid is flowing due to peristaltic movement of microchannel walls and under the action of an electro-osmotic body force (**Fig. (2.1)**). The upper and lower walls surface satisfy:

$$H_1 = b_1 + a_1 \sin\left(\frac{2\pi}{\lambda}(x - ct)\right), \tag{2.1}$$

$$H_2 = -b_2 - a_2 \sin\left(\frac{2\pi}{\lambda}(x - ct) + \varphi_1\right). \tag{2.2}$$

In the above relations, λ is the wavelength, x is the axial coordinate and t is the time, a_1, a_2 are the waves amplitude and φ_1 is the phase difference with $0 \leq \varphi_1 \leq \pi$. $\varphi_1 = 0$ corresponds to the symmetric microchannel with waves out of phase and for $\varphi_1 = \pi$ the waves are in phase. The bio-fluid in the channel characterized by the third grade model is considered to be an ionized solution that is sensitive to an external applied potential along the length of the microchannel. When the negatively charged walls of the microchannel are in contact with the ionized solution, an electric double layer is established within the flow domain due to the solid-liquid interaction. Upon applying the external potential along the axis of the channel, an electrical field is generated, which exerts a body force on the opposite ions of the EDL, and as a result of which the EDL moves along the channel dragging the neutral liquid. Thus, the motion in the fluid is generated by a combination of peristalsis and electro-osmotic mechanisms. In subsequent parts, a mathematical model is established and later analyzed to investigate the non-Newtonian liquid movement via electro-osmosis and peristaltic activities.

2.2 Mathematical formulation

The vector form of the momentum equation for the flow under consideration **Fig. (2. 1)** is given by:

$$\rho\left(\frac{D\mathbf{V}}{Dt}\right) = -\nabla p + \nabla.\mathbf{S} + \mathbf{F}_e, \tag{2.3}$$

where ρ is the density of the fluid, $\mathbf{S}$ be the extra stress tensor, p is the pressure and $\mathbf{F}_e$ represents the electro- kinetic body force. The continuity equation is given by:

$$\left(\frac{\partial \rho}{\partial t}\right) + \nabla.(\rho\mathbf{V}) = 0. \tag{2.4}$$

The extra stress tensor **S** is defined for third order fluid as: (Hayat and Abbasi (2011), Ali et al. (2010))

$$\mathbf{S} = \left(\mu + \beta_3 tr(\mathbf{A}_1^2)\right)\mathbf{A}_1 + \alpha_1\mathbf{A}_2 + \beta_1\mathbf{A}_1 + \alpha_2\mathbf{A}_1^2 + \beta_2(\mathbf{A}_2\mathbf{A}_1 + \mathbf{A}_1\mathbf{A}_2), \quad (2.5)$$

where $\mu, \alpha_1, \alpha_2, \beta_1, \beta_2, \beta_3$ are the materials constants and $\mathbf{A_1}, \mathbf{A_2}, \mathbf{A_3}$ are the Rivlin Ericksen tensor defined through the relation: (Rivlin and Ericksen (1955))

$$\mathbf{A_1} = (\nabla\mathbf{V}) + (\nabla\mathbf{V})^T,$$

$$\mathbf{A}_n = \frac{d\mathbf{A}_{n-1}}{dt} + \mathbf{A}_{n-1}(\nabla\mathbf{V}) + (\nabla\mathbf{V})^T\mathbf{A}_{n-1}, n > 1, \quad (2.6)$$

where ∇ denotes the gradient operator, **V** be the velocity and d/dt is the material time derivative. A comprehensive thermodynamic discussion of equation (2.5) is provided by Fosdick and Rajagopal (1980). According to this study, when the fluid locally at rest then these material constants satisfy the following inequalities:

$$\mu \geq 0,\ \alpha_1 \geq 0,\ \beta_3 \geq 0, \qquad |\alpha_1 + \alpha_2| \leq \sqrt{24\mu\beta},\ \beta_1 = \beta_2 = 0. \quad (2.7)$$

In this investigation, we considered that the fluid is thermodynamically compactible then from Eq. (2.5), we get

$$\mathbf{S} = \left(\mu + \beta_3 tr(\mathbf{A}_1^2)\right)\mathbf{A}_1 + \alpha_1\mathbf{A}_2 + \alpha_2\mathbf{A}_1^2. \quad (2.8)$$

The velocity profile for an asymmetric microchannel flow is

$$\mathbf{V} = \left[u(x,y,t), v(x,y,t), 0\right]. \quad (2.9)$$

We perform our analysis in the moving frame of reference, which is related to the laboratory frame of reference via relations:

$$\bar{y} \to y, \bar{p} \to p, \bar{u} \to u - c, \bar{x} \to x - ct, \bar{v} \to v. \quad (2.10)$$

The continuity equation (2.3) and momentum equation (2.4) in moving frame of reference can be written as:

$$\frac{\partial \bar{u}}{\partial \bar{x}}+\frac{\partial \bar{v}}{\partial \bar{y}}=0, \tag{2.11}$$

$$\rho\left(\bar{u}\frac{\partial \bar{u}}{\partial \bar{x}}+\bar{v}\frac{\partial \bar{u}}{\partial \bar{y}}\right)=-\frac{\partial \bar{p}}{\partial \bar{x}}+\left[\frac{\partial\left(\bar{S}_{\bar{x}\bar{x}}\right)}{\partial \bar{x}}+\frac{\partial \bar{S}_{\bar{x}\bar{y}}}{\partial \bar{y}}\right]+\bar{F}_e, \tag{2.12}$$

$$\rho\left(\bar{u}\frac{\partial \bar{v}}{\partial \bar{x}}+\bar{v}\frac{\partial \bar{v}}{\partial \bar{y}}\right)=-\frac{\partial \bar{p}}{\partial \bar{y}}+\left[\frac{\partial\left(\bar{S}_{\bar{y}\bar{x}}\right)}{\partial \bar{x}}+\frac{\partial \bar{S}_{\bar{y}\bar{y}}}{\partial \bar{y}}\right], \tag{2.13}$$

where $\bar{S}_{\bar{x}\bar{x}}, \bar{S}_{\bar{x}\bar{y}}, \bar{S}_{\bar{y}\bar{x}}, \bar{S}_{\bar{y}\bar{y}}$ are the extra stress tensor and $\bar{u}, \bar{v}$ are the velocity components in Cartesian coordinate and E_x be the axial electric field given by

$$\bar{F}_e=\bar{\rho}_e E_x. \tag{2.14}$$

Here $\bar{\rho}_e$ be the total ionic charge density, which is associated to the electric potential $\bar{\phi}$ through the equation

$$\nabla^2\bar{\phi}=-\bar{\rho}_e/\varepsilon, \tag{2.15}$$

in which ε is the permittivity of the medium. For symmetric electrolyte solution, the total ionic distribution $\bar{\rho}_e$ is defined as $\bar{\rho}_e = ez(\bar{n}^+ - \bar{n}^-)$. The ionic number distributions of single species are obtained through Nernst-Planck equation for each species. That is,

$$\frac{\partial \bar{n}_\pm}{\partial \bar{t}}+\bar{u}\frac{\partial \bar{n}_\pm}{\partial \bar{x}}+\bar{v}\frac{\partial \bar{n}_\pm}{\partial \bar{y}}=D_0\left(\frac{\partial^2 \bar{n}_\pm}{\partial \bar{x}^2}+\frac{\partial^2 \bar{n}_\pm}{\partial \bar{y}^2}\right)\pm\frac{D_0 ze}{k_B T}\left(\frac{\partial}{\partial \bar{x}}\left(\bar{n}_\pm\frac{\partial \bar{\phi}}{\partial \bar{x}}\right)+\frac{\partial}{\partial \bar{y}}\left(\bar{n}_\pm\frac{\partial \bar{\phi}}{\partial \bar{y}}\right)\right). \tag{2.16}$$

It is assumed that coefficients of ionic diffusions for both species are equal and the transport of the species is evaluated through Einstein formula.

The appropriate dimensionless quantities are

$$\left.\begin{aligned}
&x^*=\frac{\bar{x}}{\lambda}, y^*=\frac{\bar{y}}{b_1}, v^*=\frac{\bar{v}}{\mathrm{c}}, u^*=\frac{\bar{u}}{c}, t^*=\frac{c}{\lambda}\bar{t}, \delta=\frac{b_1}{\lambda}, S^*=\frac{b_1}{\mu\lambda c}\bar{S}, p^*=\frac{b_1^2}{\mu c\lambda}\bar{p},\\
&Re=\frac{\rho c b_1}{\mu}, \phi^*=\frac{k_B T\bar{\phi}}{ez}, n^*=\frac{\bar{n}}{n_0}, \lambda_1=\frac{\alpha_1 c}{\mu b_1}, \lambda_2=\frac{\alpha_2 c}{\mu b_1}, \gamma_1=\frac{\beta_1 c^2}{\mu b_1^2}, \gamma_2=\frac{\beta_2 c^2}{\mu b_1^2}\\
&\gamma_3=\frac{\beta_3 c^2}{\mu b_1^2}, h^*{}_2=\frac{\bar{h}_2}{b_1}, h^*{}_1=\frac{\bar{h}_1}{b_1}, \rho_e^*=\frac{b_1{}^2 k_B T\bar{\rho}_e}{ez\varepsilon}, a=\frac{a_1}{b_1}, d=\frac{b_2}{b_1}, \mathrm{b}=\frac{a_2}{b_1}.
\end{aligned}\right\} \tag{2.17}$$

where Re is the Reynold number, De be the Deborah number and δ is the wave number. After applying the dimensionless quantities (2.17) and the approximations that $\delta, Pe, Re \ll 1$, where $Pe = ReSc$ and $Sc = \mu/\rho D_0$ represent the ionic Peclet

number and Schmidt number, respectively, the Poisson and Nernst Planck equations reduce to (dropping asterisk)

$$\frac{\partial^2\phi}{\partial^2 y} = -m_e 2\left(\frac{n_+ - n_-}{2}\right), \tag{2.18}$$

$$\frac{\partial^2 n_\pm}{\partial^2 y} \pm \frac{\partial}{\partial y}\left(n_\pm \frac{\partial\phi}{\partial y}\right) = 0. \tag{2.19}$$

where $m_e = b_1 ez\sqrt{2n_0/\varepsilon K_B T} = b_1/\lambda_d$, is the electro-osmotic parameter.

Now solving the Eq. (2.19) subject to the bulk condition as $n_\pm = 1$ at $\phi = 0$ and $\frac{\partial n_\pm}{\partial y} = 0$ where $\frac{\partial\phi}{\partial y} = 0$, we get

$$n_\pm = e^{\mp\phi}. \tag{2.20}$$

In view of Eq. (2. 18) and Eq. (2. 20) we obtain

$$\frac{\partial^2\phi}{\partial^2 y} = m_e{}^2 \sinh(\phi) \tag{2.21}$$

By invoking the linearization approximation, Eq. (2.21) reduces to

$$\frac{\partial^2\phi}{\partial^2 y} = m_e{}^2\phi \tag{2.22}$$

Now solving Eq. (2.22) by using the condition at $\phi\big|_{y=h_1} = \zeta_1$ and $\phi\big|_{y=h_2} = \zeta_2$ we obtain the electric potential as follow

$$\phi = C_1 e^{m_e h_1} + C_2 e^{-m_e h_2} \tag{2.23}$$

where, $C_1 = e^{h_2 m_e}\zeta_2 - e^{h_1 m_e}\zeta_1 / e^{2h_2 m_e} - e^{2h_1 m_e}$ and

$C_2 = e^{h_1 m_e + h_2 m_e}\left(e^{h_1 m_e}\zeta_2 - e^{h_2 m_e}\zeta_1\right)/e^{2h_1 m_e} - e^{2h_2 m_e}$

Applying the long wavelength ($\delta \ll 1$) and low Reynolds number ($Re \ll 1$) approximations, Eqs. (2.11) – (2.13) becomes (dropping asterisk)

$$\frac{\partial u}{\partial x} + \frac{\partial v}{\partial y} = 0, \tag{2.24}$$

$$\frac{\partial p}{\partial x} = \frac{\partial}{\partial y}\left[\frac{\partial u}{\partial y} + 2\Gamma\left(\frac{\partial u}{\partial y}\right)^3\right] + m_e{}^2 U_E \phi, \tag{2.25}$$

$$0=\frac{\partial p}{\partial y}, \tag{2.26}$$

where, $U_E = -E_x \varepsilon \zeta / \mu c$ is the electro-kinetic slip velocity and $\Gamma = \gamma_1 + \gamma_2$.

The velocity components in term of stream function are

$$u=\frac{\partial \psi}{\partial y}, v=-\frac{\partial \psi}{\partial x}. \tag{2.27}$$

Invoking relations (2.27) in above equations, the continuity equation is satisfied identically and Eq. (2.25) reads

$$\frac{\partial p}{\partial x}=\frac{\partial}{\partial y}\left[\frac{\partial^2 \psi}{\partial^2 y}+2\Gamma\left(\frac{\partial^2 \psi}{\partial^2 y}\right)^3\right]+m_e{}^2 U_E \phi. \tag{2.28}$$

The boundary condition in term of stream function are:

$$\frac{\partial \psi}{\partial y}(h_1)=-1 \quad \text{and} \quad \frac{\partial \psi}{\partial y}(h_2)=-1. \tag{2.29}$$

2.2.1 Volumetric flow rate

The volumetric flow rate in dimensional form is defined becomes

$$Q = \int_{H_2(x,t)}^{H_1(x,t)} u(x,y,t)dy. \tag{2.30}$$

The above expression in the wave frame of reference as

$$q = \int_{h_2(x)}^{h_1(x)} \bar{u}(\bar{x},\bar{y})d\bar{y} \tag{2.31}$$

using (2.32) in (2.33), we get

$$Q = q + ch_1(x) - ch_2(x) \tag{2.32}$$

The time-averaged volume flow rate over a period T in fixed frame is defined as

$$\bar{Q} = \frac{1}{T}\int_0^T Q dt \tag{2.33}$$

Invoking the equation (2.33) in (2.34) and integrating, we get

$$\bar{Q} = q + cb_1 + cb_2 \tag{2.34}$$

The dimensionless volume flow rate in

$$\Theta = F + 1 + d, \tag{2.35}$$

where Θ is the dimensionless volume flow rate in the fixed frame and F represents the dimensionless volume flow rate in the wave frame of reference. That is,

$$F = \int_{h_2}^{h_1} \frac{\partial \psi}{\partial y} dy = \psi(h_1) - \psi(h_2) \tag{2.36}$$

Eq. (2.36) suggests that

$$\psi(h_1) = F/2 \text{ and } \psi(h_2) = -F/2, \tag{2.37}$$

where

$$h_1 = 1 + asin(2\pi x), \tag{2.38}$$

$$h_2 = -d - bsin(2\pi x + \varphi_1). \tag{2.39}$$

Eq. (2.28) along with boundary conditions (2.29) and (2.37) is not amenable to analytic solution, therefore we obtain the numerical solution of the governing equations by using Mathematica 8.1 solver NDSolve. We compute the velocity distribution, pressure gradient and streamline topologies which are analyzed in subsequent sections.

2.3 Results and discussion

In this section, we will analyze the influences of the emerging parameters such as, Γ, m_e, U_E and φ_1 on velocity profile, trapping and the pressure rise. These results are shown in **Figs. (2.2 - 2.8).**

2.3.1 Velocity profile

The velocity distribution is visualized graphically for several values of the emerging parameters (Γ, m_e, U_E and phase difference φ_1) which are shown in **Fig. (2.2).** The effects of the electro-kinetic slip velocity U_E on longitudinal velocity profile are depicted in the panels **(a)** and **(b)** of **Fig. (2.2).** The amount of the applied potential on channel walls varies the nature of the velocity profile. It is observed that for $\zeta_1 > \zeta_2$ (applied potential on upper wall is greater than the applied potential on lower wall), the velocity decreases by increasing electro-kinetic slip velocity U_E while an opposite trend is noted for $\zeta_1 < \zeta_2$. **Figs. (2.2c)** explores the variation of the velocity profile for various values of the electro-osmotic parameter m_e. The velocity reduces for enormous value of electro-osmotic parameter. An asymmetric behavior of velocity

profile is also found by varying m_e. The effects of the Γ on velocity profile are shown in the **Fig. (2.2d).** It is clearly observed that the velocity profile increases for increasing of Γ. The velocity profile against different values of the phase difference is shown in the **Fig. (2.2e).** Here reduction in the magnitude of velocity is noted for higher values of φ_1.

2.3.2 Pressure distribution

The pressure rise is an important feature of the peristaltic pumping. The pumping characteristics for several values of the electro-kinetic slip velocity, electro-osmotic parameter, Deborah number and phase difference can be visualized in the **Figs. (2.3 a-d). Fig. (2.3a)** illustrates the variations in the pressure rise for different values of the electro-osmotic parameter. An increasing trend in pressure rise is noted by increasing the value of the electro-osmotic parameter. **Fig. (2.3b)** provides the variations of Δp against the flow rate $\bar{Q}$ for different Γ. A growth in pressure is observed in the pumping region $\Delta p > 0$ while an opposite trend is noted in the co-pumping region $\Delta p < 0$ for increasing values Γ. **Fig. (2.3c)** illustrates the behavior of pressure rise with respect to electro-kinetic slip parameter. Here a significant decrease in pressure rise is observed for increasing values of electro-osmotic slip velocity. The classical linear relation between pressure difference and flow rate is also validated through this figure. The influence of the phase difference on the pressure rise is shown in the **Fig. (2.3d).** Clearly, larger phase differences produces reduction in pressure rise inside the channel.

2.3.3 Trapping phenomenon

The streamline plots showing trapping inside the asymmetric microchannel are displayed in **Figs. (2.4) – (2.7).** A detailed explanation regarding the development of trapped bolus in the flow domain is provided by Tripathi *et al.* (2017). According to Tripathi *et al.* (2017), trapping is strongly dependent upon the *bulk momentum* of the flow. The greater the momentum of the fluid, the lower the probability of fluid particles being trapped in zones of re-circulation. Trapping for several values of the emerging parameters, Γ, m_e, phase difference φ_1 and the electro-osmotic slip velocity U_E is shown in the **Figs. (2.4 - 2.7). Fig. (2.4a-c)** provides the streamlines structure for different values of the electro-osmotic slip velocity. It is observed that the size of the trapped bolus reduces for higher values of the U_E. The large value of the electro-

osmotic slip velocity means that the strong potential applied to the system. The resistance within the fluid also reduces for large U_E, which indicates that the tendency of the fluid element to flow along the length of the channel increases and as a result eradication of trapping phenomenon occurs. Further, the trapped boluses enlarge by increasing the values of the Γ and m_e **(see Figs. (2.5, 2.6))** which ensures that the size of the trapped bolus is strongly affected by changing the embedded parameters. Trapping for several values of the phase difference is displayed in the **Fig. (2.7).** No significant change in bolus size is noted except the restructuring of shape from asymmetric to symmetric for decreasing values of phase difference.

2.4 Conclusion

A theoretical analysis is presented for a two-dimensional electro-osmotic flow of third order fluid due to peristaltic activity in an asymmetric microchannel. By incorporating the suitable transformations, the governing equations are transformed from fixed frame to moving frame. The well-known assumptions of long wavelength and low Reynolds number are used to simplify the flow problem. The velocity distribution, pressure gradient and stream functions are computed numerically from the simplified momentum equation by using Mathematica 8.1 software subject to the suitable boundary conditions. The main outcomes of the present investigation are:

- The area of the trapped bolus in the channel reduces by increasing the values of the electro-osmotic slip velocity.
- The size of the trapped bolus in the flow domain increases subject to the modulations in electro-osmotic parameter.
- The longitudinal flow velocity increases for higher values of the electro-osmotic slip velocity and Deborah number.
- Growth in pressure rise appears for large values of parameters Γ and m_e.
- Reduction in pressure rise is encountered for high values of the electro-osmotic slip velocity U_E.

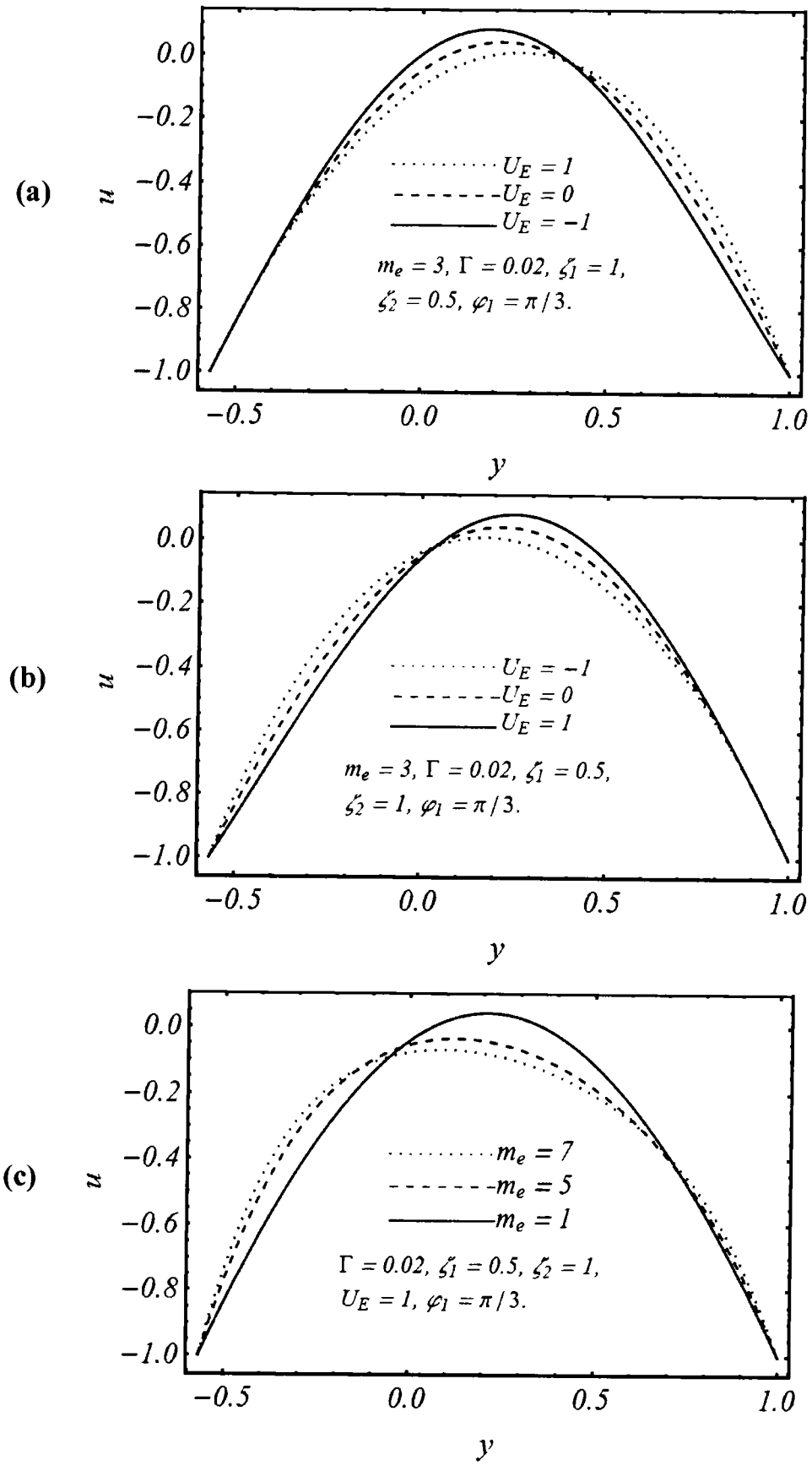

Fig. 2.2 ((a) – (c)): Velocity variations for different values of the parameters U_E and m_e.

(d)

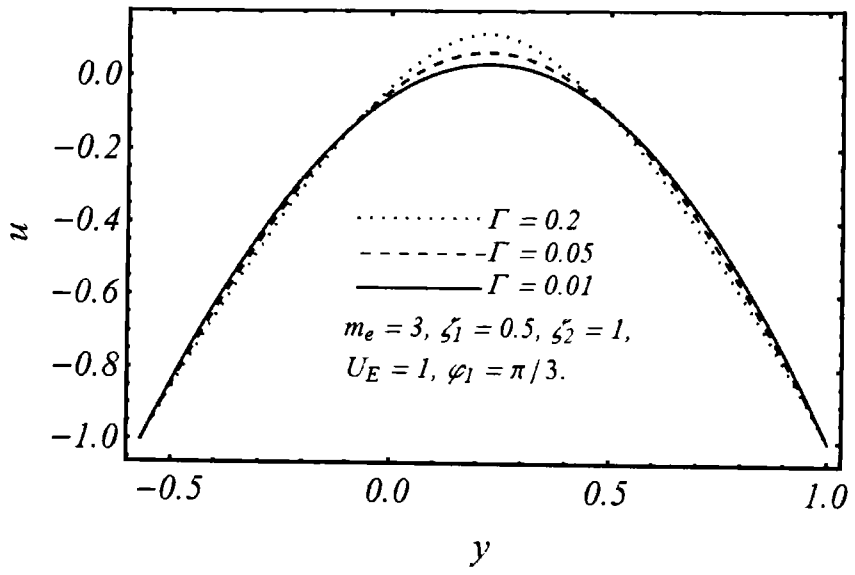

(e)

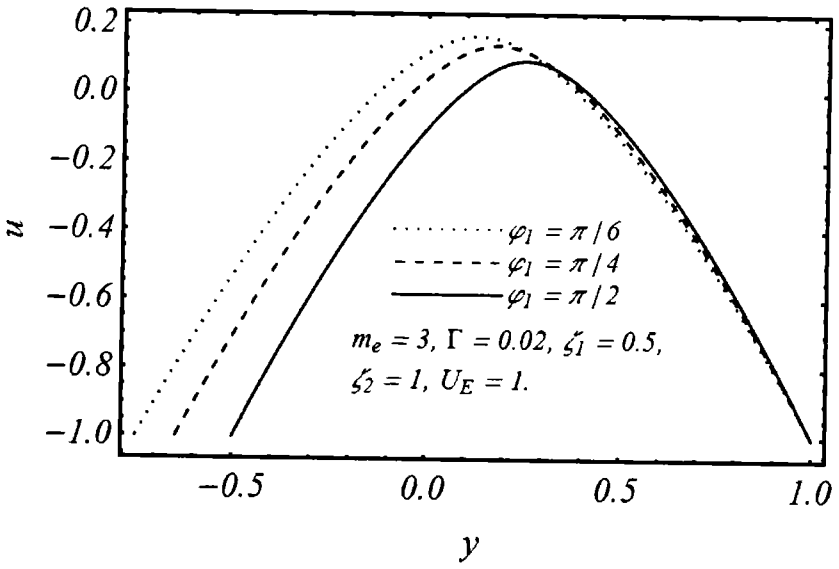

Fig. 2.2 ((d), (e)): Velocity variations for different values of the parameters Γ, φ_1 and electro-kinetic slip velocity U_E.

(a)

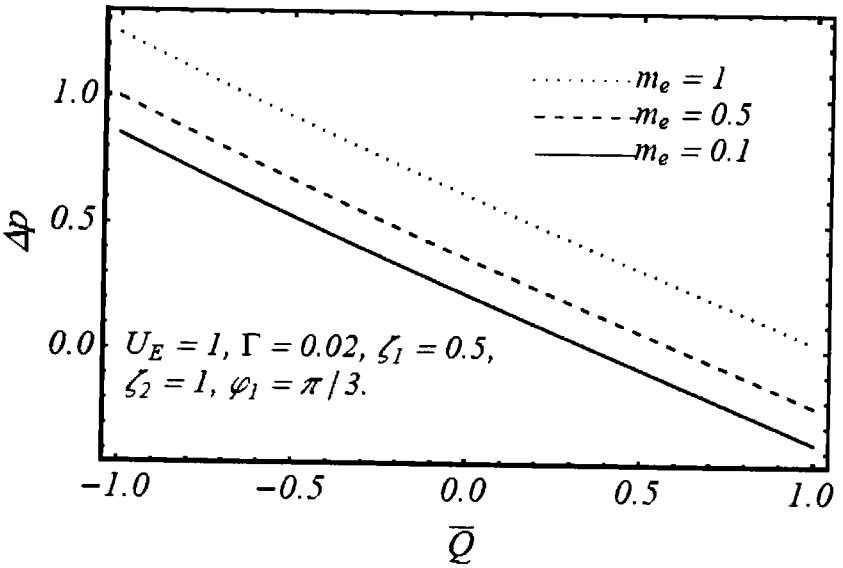

Fig. 2.3 (a): Pumping efficiency with different values of m_e.

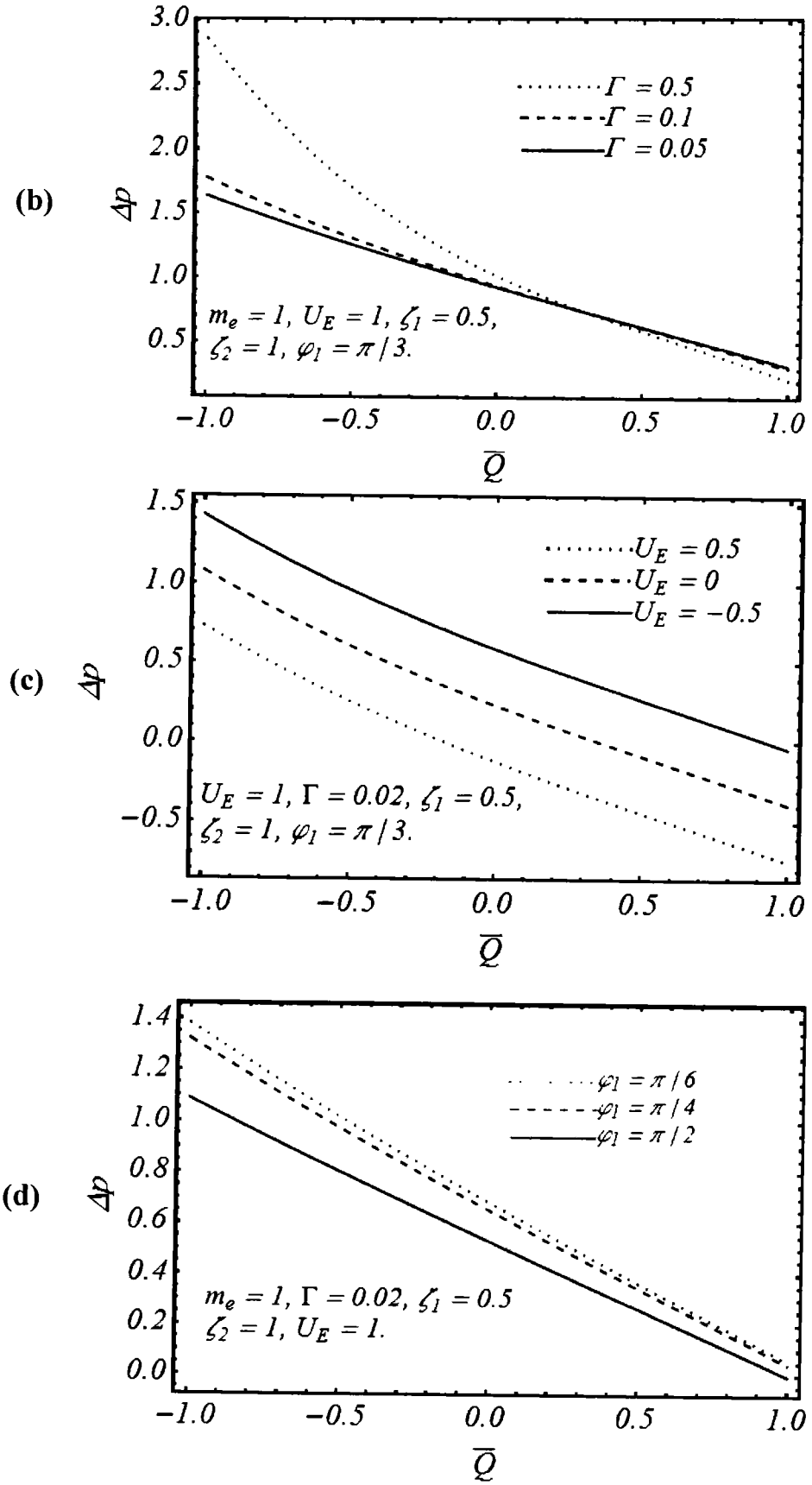

Fig. 2.3 ((b) – (d)): Pumping efficiency with respect different parameters Γ, U_E and φ_1.

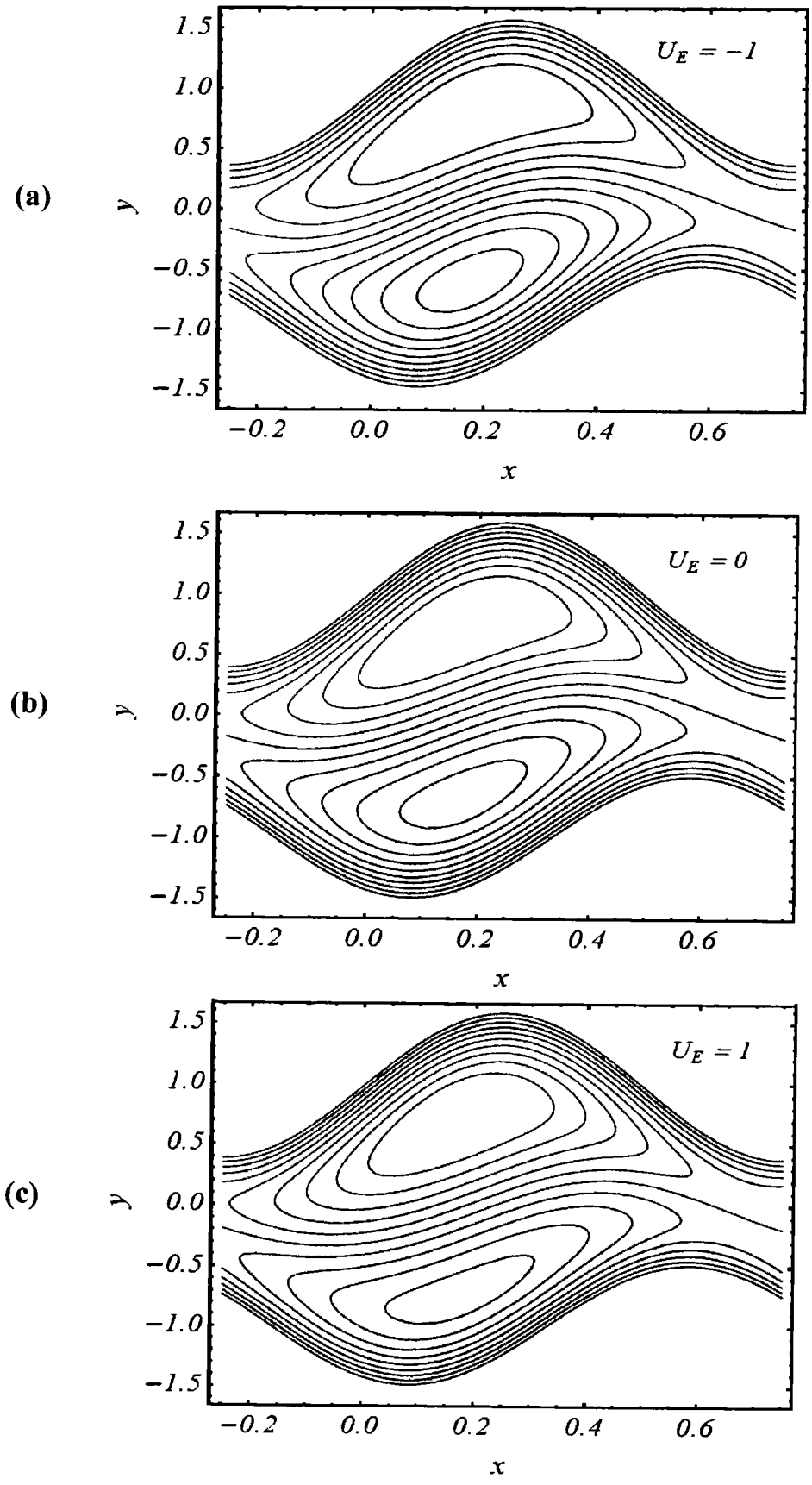

Fig. 2.4 ((a) – (c)): The streamlines variation for different values of U_E when $\Gamma = 0.02, \bar{Q} = 1.7, m_e = 1, \varphi_1 = \pi/3, \zeta_1 = 0.5, \zeta_2 = 1$.

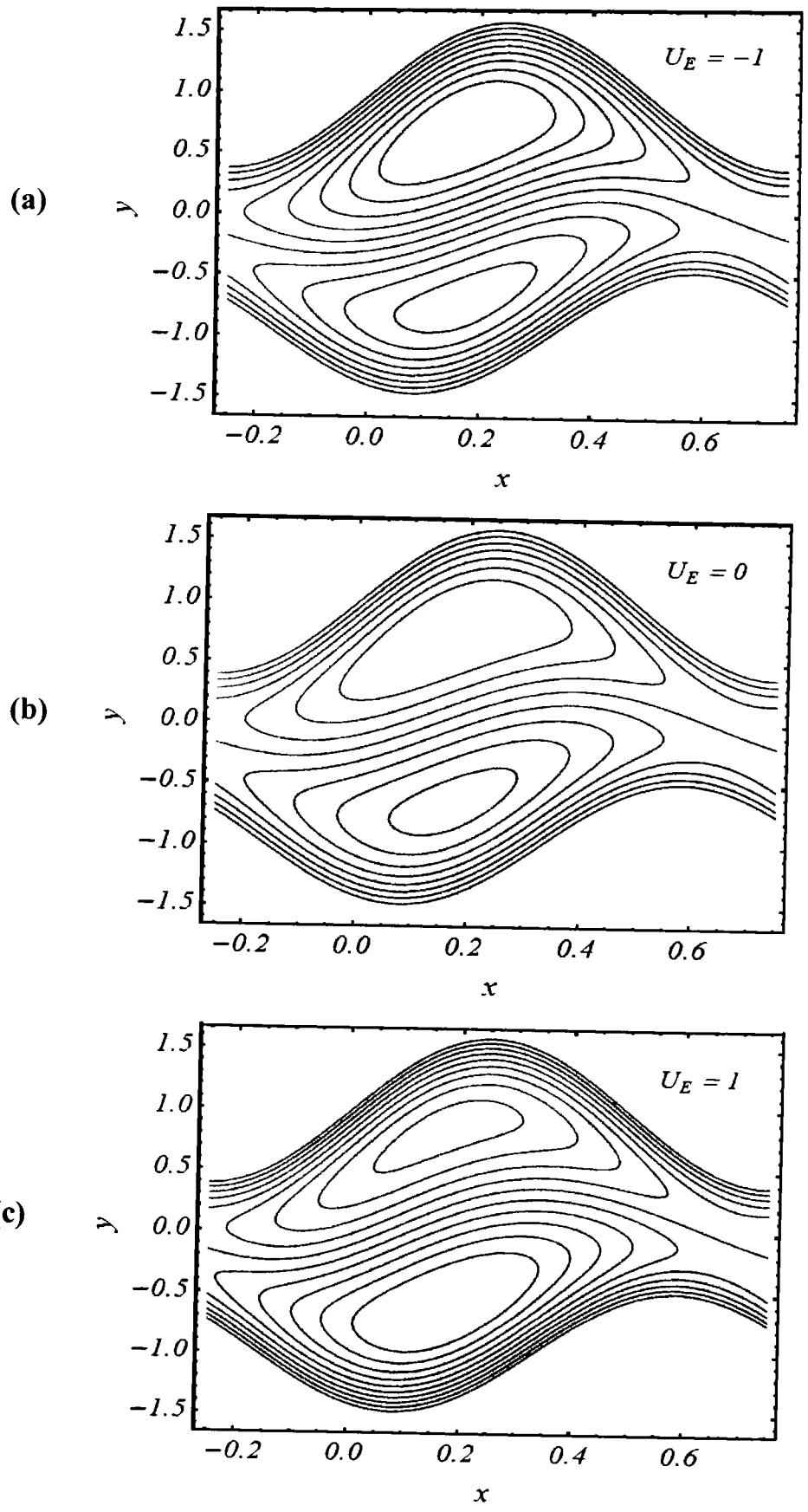

Fig. 2.4 ((a) – (c)): The streamlines variation for different values of U_E when $\Gamma = 0.02, \bar{Q} = 1.7, m_e = 1, \varphi_1 = \pi/3, \zeta_1 = 1, \zeta_2 = 0.5$.

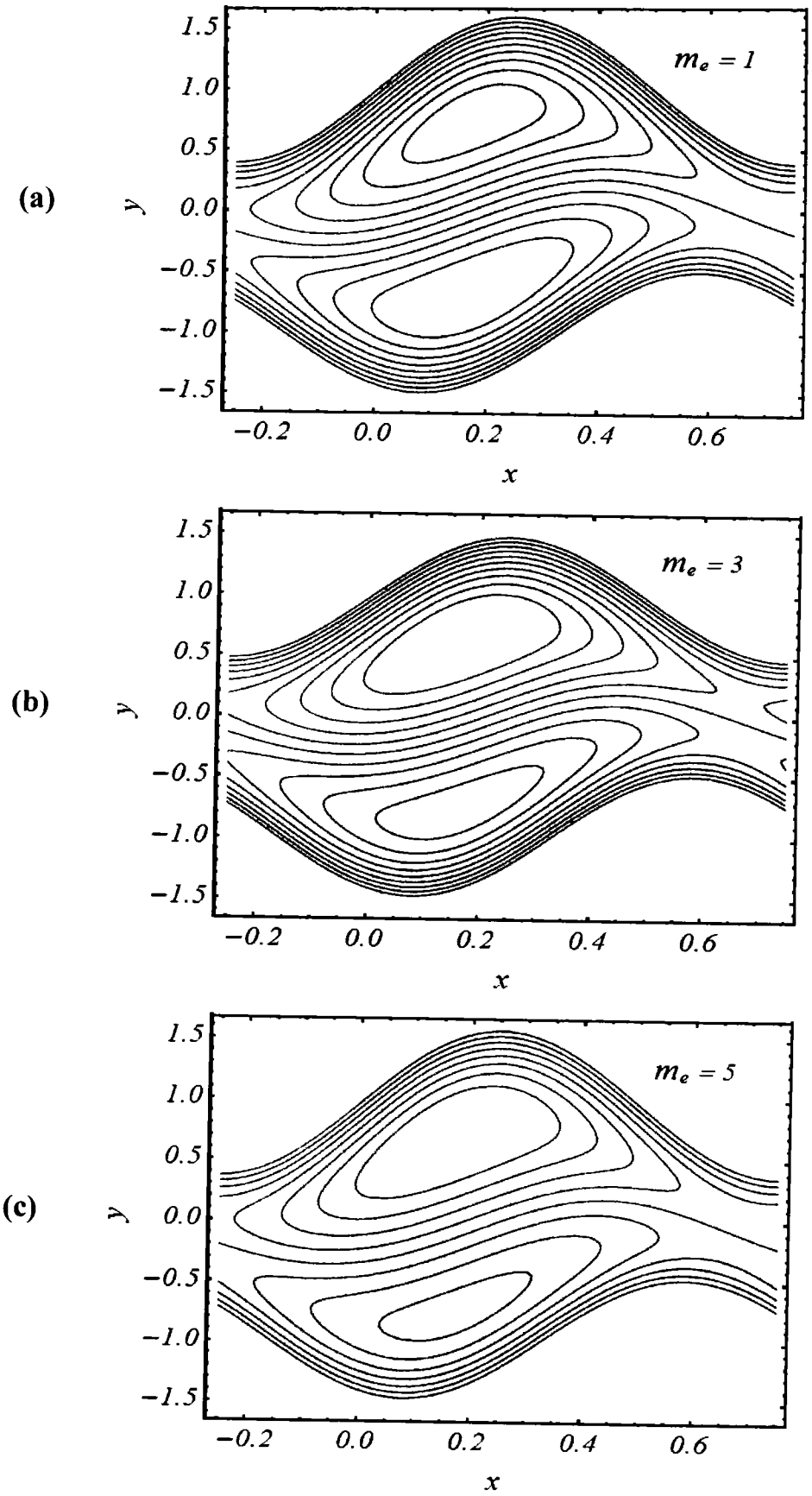

Fig. 2.5 ((a) – (c)): The streamlines variation for different parametric values of m_e when $\Gamma = 0.02, \bar{Q} = 1.7, U_E = 1,\ \varphi_1 = \pi/3\,, \zeta_1 = 0.5, \zeta_2 = 1.$

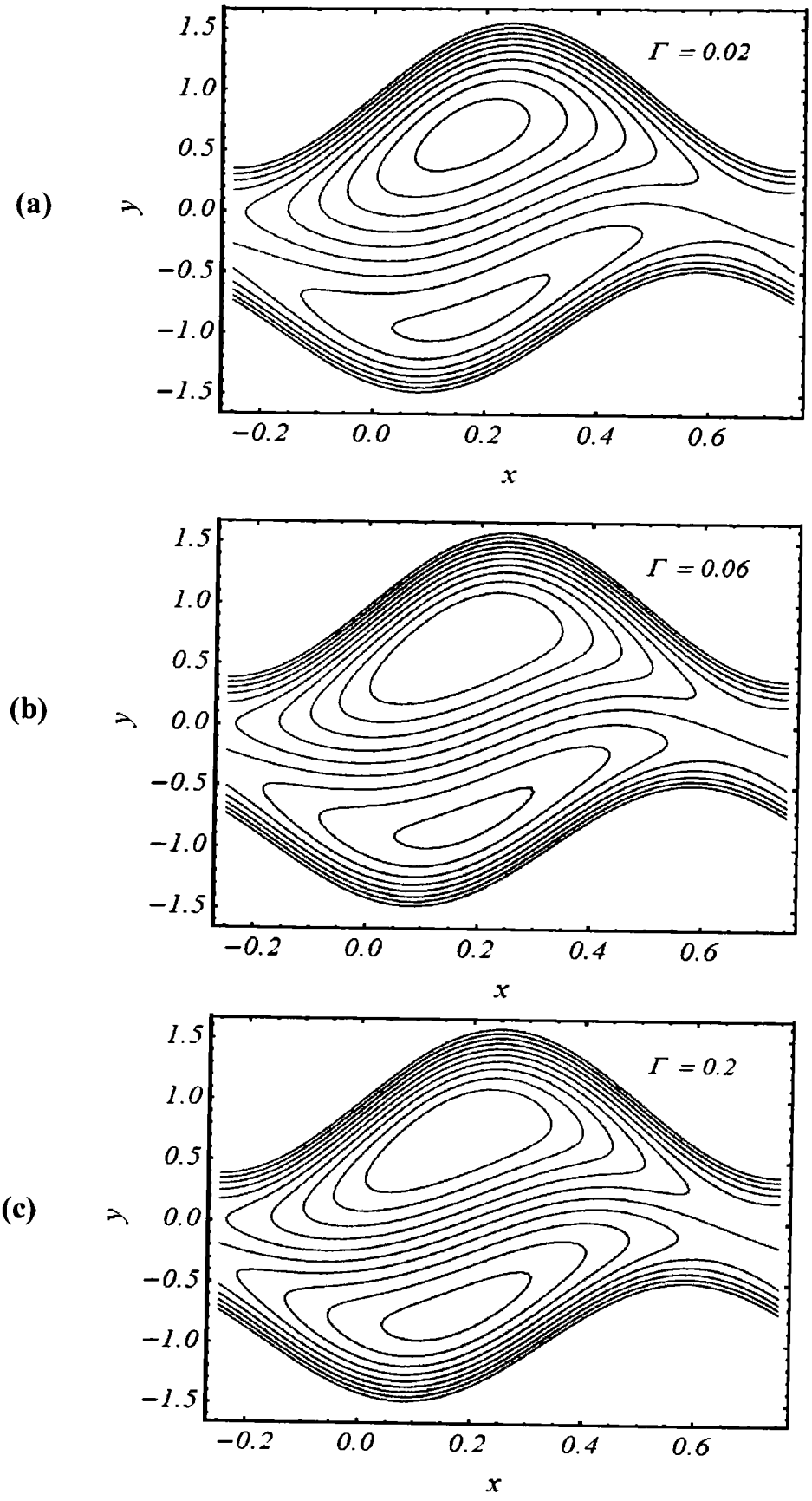

Fig. 2.6 ((a) – (c)): The streamlines variation for different values of Γ when $m_e = 1, \bar{Q} = 1.7, U_E = 1, \varphi_1 = \pi/3, \zeta_1 = 0.5, \zeta_2 = 1$.

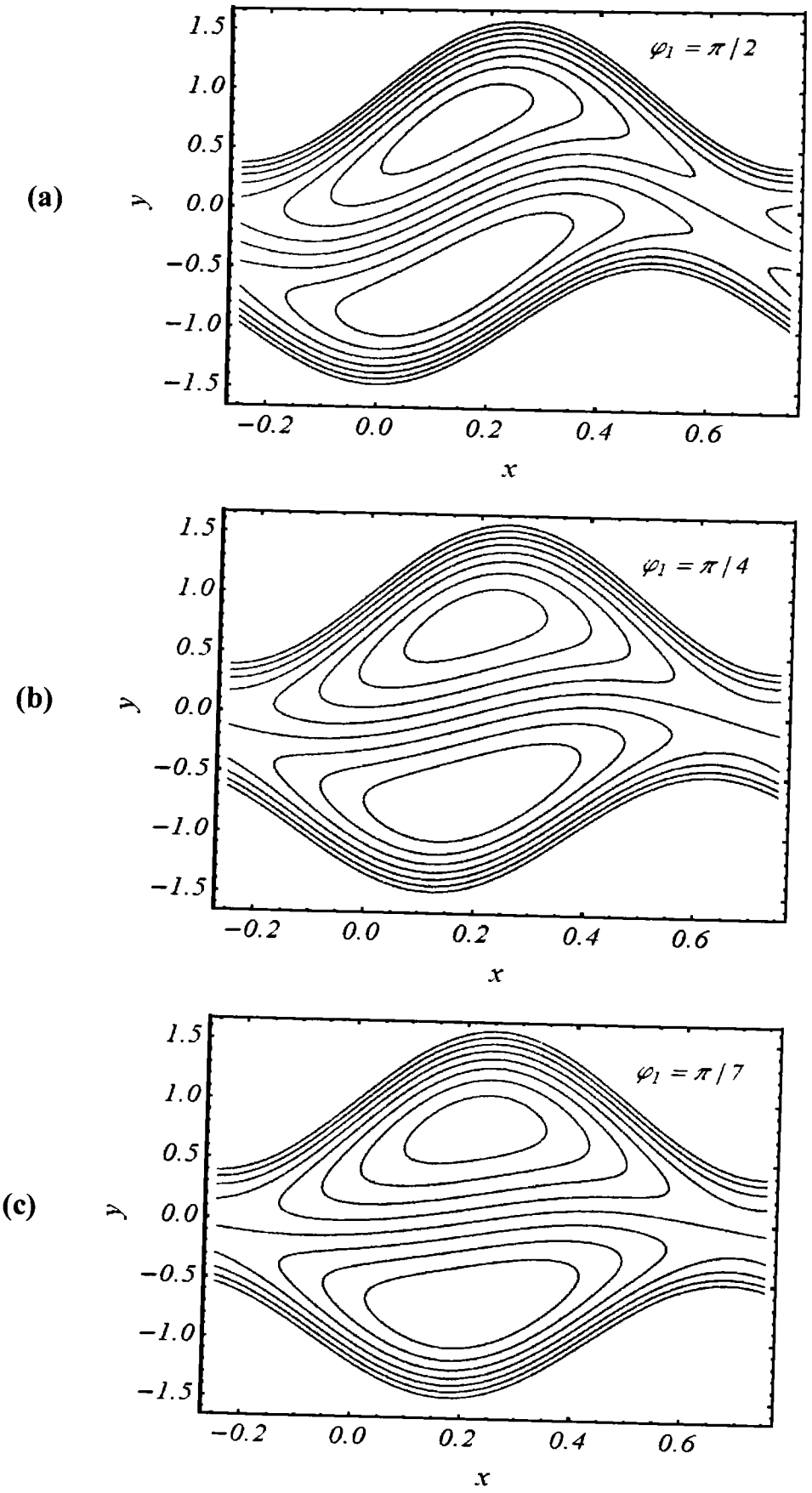

Fig. 2.7 ((a) – (c)). The streamlines variation for different values of $\varphi_1$when $\Gamma = 0.02, \bar{Q} = 1.7, m_e = 1, \zeta_1 = 0.5, \zeta_2 = 1$ and $U_E = 1$.

Chapter 3

Mathematical modelling of two-fluid electro-osmotic peristaltic pumping of Ellis fluid in an axisymmetric tube

In chapter 3, we explore analytically the dynamics of two-fluid electro-osmotic peristaltic flow through a cylindrical tube. The rheology of the fluid in the central core (inner region or core region) is captured through the Ellis equation. The region adjacent to the wall (outer region or peripheral region) is occupied by a Newtonian fluid. The equations governing the flow in each region are modeled by using the appropriate suppositions of long wavelength and low Reynolds number. Closed form expressions for stream function corresponding to each region are obtained and utilized to determine the axial pressure gradient and the interface between the inner and the outer regions. The pumping characteristics, trapping and reflux phenomena are investigated in detail with reference to the Ellis model parameters and the electro-kinetic slip velocity. The present model also generalizes earlier studies from the literature which can be retrieved as special cases. The analysis shows that pressure drop at zero volumetric flow rate is elevated with increasing occlusion parameter. Trapping and reflux phenomena are mitigated with increasing electro-osmotic slip and shear-thinning effects. At larger value of the occlusion parameter an increase in the power-law index reduces the magnitude of the pressure drop. Increasing Ellis rheological parameter reduces the pressure drop over the entire range of occlusion parameters for the case when the peripheral region fluid viscosity exceeds that of the central region fluid. The results obtained may be applicable in the modulation of peristaltic pumping in the efficient operation of various industrial and bio-medical devices.

3.1 Geometric model of the physical problem

Consider a flexible cylindrical tube of un-deformed radius r_0 through which a bio-fluid is flowing due to peristaltic movement of the tube boundary and under the action of an electro-osmotic body force as shown in **Fig. (3.1)**. The region inside the tube is

composed of the peripheral and core regions. The fluid in the core (central) region is characterized by the Ellis model whereas the fluid in the peripheral (outer) region obeys the Newtonian constitutive law.

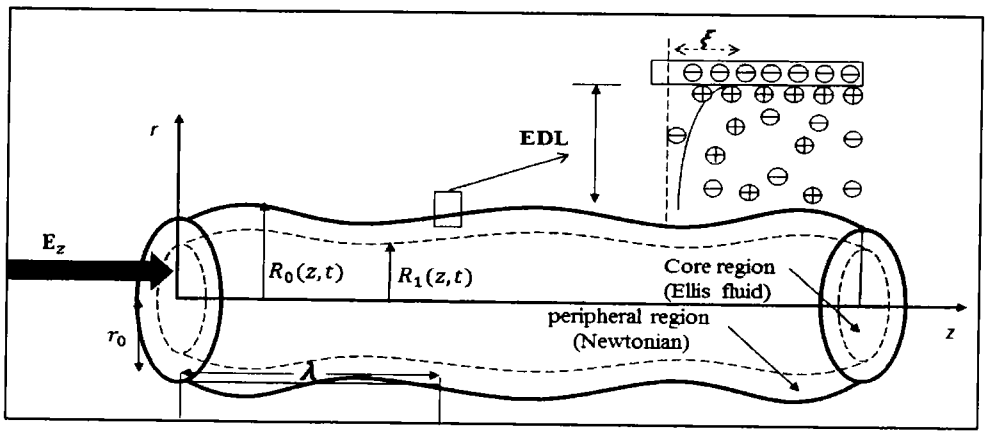

Fig. 3.1: Geometry of the flow problem.

The negative charged surface attracts opposite ions in the ionized solution, developing a layer of positively charged fluid near the wall and at the same time repelling the counter-ions. "The thin layer of immobile counter-ions covering the inner side of the wall is known as the *Stern layer*". A thicker layer of moving counter-ions, known as a diffuse layer, is formed next to the Stern layer. The combination of the "Stern layer and the thicker layer is known as the electric double layer (EDL)". When the system is connects to the external electrical potential, electro-kinetic body force emerges. The resulting multi-physical fluid dynamic problem encompasses the computation of the flow field developed by the combined effects of the wall movement and the electro-kinetic body force.

3.2 Mathematical model

The vector form of the momentum equation for the flow under consideration **(Fig. 3. 1)** is given by:

$$\rho_f \left(\frac{D\mathbf{V}}{Dt}\right) = -\nabla p + \nabla.\mathbf{S} + \mathbf{F}_e, \tag{3.1}$$

where ρ_f is the density of the fluid, $\mathbf{S}$ the extra stress tensor, p the pressure and, $\mathbf{F}_e$ is the electro- kinetic body force. The continuity equation is given by:

$$\left(\frac{\partial \rho_f}{\partial t}\right) + \nabla(\rho_f \mathbf{V}) = 0. \tag{3.2}$$

The extra stress tensor **S** is defined differently for both the core (Ellis fluid) and the peripheral (Newtonian) regions:

$$\mathbf{S} = \begin{cases} \mu_c(\gamma)\,\dot{\boldsymbol{\gamma}}, & 0 \le r < R_1(z,t), \\ \mu_N\,\dot{\boldsymbol{\gamma}}, & R_1 \le r < R_0(z,t), \end{cases} \tag{3.3}$$

where R_1 is the expression for the interface between the core and peripheral regions. Since, the core region is characterized by the Ellis model, therefore the appropriate rheological relation is:

$$\mu_c(\gamma) = \frac{\mu_0}{1+\left(\frac{\pi_s}{\tau^2_0}\right)^{\alpha-1}}, \tag{3.4}$$

Here μ_0 represents the zero-shear rate viscosity, π_s denotes the second invariant stress tensor $\dot{\boldsymbol{\gamma}}$, α is the power-law index and quantifies shear-thinning behavior ($\alpha > 1$), τ_0 is the shear stress at which the apparent viscosity becomes $\mu_0/2$, $\dot{\boldsymbol{\gamma}}$ $(= (1/2)\{\nabla\mathbf{V} - (\nabla\mathbf{V})^T\})$ is the strain-rate tensor and μ_N is the viscosity of Newtonian fluid in the peripheral region. For axisymmetric incompressible flow in the tube, it is appropriate to define the velocity vector as follows:

$$\mathbf{V} = [u(r,z,t), 0, w(r,z,t)]. \tag{3.5}$$

In view of above velocity field, the basic equations (3.1) and (3.2) the presence of the electro-kinetic force applied in the axial direction yield

$$\frac{1}{r}\frac{\partial(ru)}{\partial r} + \frac{\partial w}{\partial z} = 0, \tag{3.6}$$

$$\rho_f\left(\frac{\partial u}{\partial t} + u\frac{\partial u}{\partial r} + w\frac{\partial u}{\partial z}\right) = -\frac{\partial p}{\partial r} + \left[\frac{1}{r}\frac{\partial(rS_{rr})}{\partial r} + \frac{\partial S_{rz}}{\partial z} - \frac{S_{\theta\theta}}{r}\right], \tag{3.7}$$

$$\rho_f\left(\frac{\partial w}{\partial t} + u\frac{\partial w}{\partial r} + w\frac{\partial w}{\partial z}\right) = -\frac{\partial p}{\partial z} + \left[\frac{1}{r}\frac{\partial(rS_{rz})}{\partial r} + \frac{\partial S_{zz}}{\partial z}\right] + F_e. \tag{3.8}$$

$$w = 0, u = \frac{dR_0}{dt}, \ at\ r = R_0(z,t). \tag{3.9}$$

The Eqs. (3.6) - (3.8) are the basic equations of two-dimensional incompressible peristaltic flow in fixed frame of reference in axisymmetric tube. The body force term due to applied electric potential in the axial direction is of the form as mentioned in Hunter (1981). The continuity equation shows that the mass of the system remain conserved during the peristaltic flow and momentum equations shows that the momentum of the system remain conserved during the motion. The first boundary

condition in Eq. (3.9) represent the no-slip at the wall while the second one arise due to symmetry

It is noteworthy that:

$$(\rho_f, u, w) = \begin{cases} \rho_c, u_c, w_c \\ \rho_N, u_N, w_N \end{cases} \tag{3.10}$$

where the subscript c stands for the core region whereas N designates the peripheral region. When the external electric field E is applied, the liquid undergoes a body force which takes the form:

$$F_e = \rho_e E, \tag{3.11}$$

where ρ_e is the total ionic charge concentration which is considered as the sum of ρ_{eN} and ρ_{ec}, the ionic charge concentrations corresponding to the peripheral and the core regions, respectively. The motion of the tube is assumed to be a periodic peristaltic wave motion with wave speed U and the wavelength λ. The radius of the tube R_0 is a function of $(z - Ut)$ in the fixed frame. However, switching the analysis from the fixed frame (r, z) to the moving frame $(\bar{r}, \bar{z})$ it can be made a function of $\bar{z}$ alone. The conversion between fixed frames to wave frame is achieved via the following transformations:

$$\bar{z} \to z - Ut, \bar{r} \to r, \bar{u} \to u, \bar{w} \to w - U, \bar{p} \to p. \tag{3.12}$$

In view of Eq. (3.12) the Eqs. (3.6 -3.8) in moving frame of reference can be written as:

$$\frac{1}{\bar{r}}\frac{\partial(\bar{r}\bar{u})}{\partial \bar{r}} + \frac{\partial \bar{w}}{\partial \bar{z}} = 0, \tag{3.13}$$

$$\rho_f\left(\bar{u}\frac{\partial \bar{u}}{\partial \bar{r}} + \bar{w}\frac{\partial \bar{u}}{\partial \bar{z}}\right) = -\frac{\partial \bar{p}}{\partial \bar{r}} + \left[\frac{1}{\bar{r}}\frac{\partial(\bar{r}\bar{S}_{rr})}{\partial \bar{r}} + \frac{\partial \bar{S}_{rz}}{\partial \bar{z}} - \frac{\bar{S}_{\theta\theta}}{\bar{r}}\right], \tag{3.14}$$

$$\rho_f\left(\bar{u}\frac{\partial \bar{w}}{\partial \bar{r}} + \bar{w}\frac{\partial \bar{w}}{\partial \bar{z}}\right) = -\frac{\partial \bar{p}}{\partial \bar{z}} + \left[\frac{1}{\bar{r}}\frac{\partial(\bar{r}\bar{S}_{rz})}{\partial \bar{r}} + \frac{\partial \bar{S}_{zz}}{\partial \bar{z}}\right] + \bar{F}_e. \tag{3.15}$$

Under the action of external axial electric field $\mathbf{E} = (0, 0, E_z)$, the fluid undergoes a body force given as Hunter (1981).

$$\bar{F}_e = \bar{\rho}_e E_z \mathbf{k}, \tag{3.16}$$

where $\mathbf{k}$ is the unit vector in the axial direction and $\bar{\rho}_e$ be the total ionic charge density, which is associated to the electric potential $\bar{\phi}$ through the equation

$$\nabla^2\bar{\phi} = -\bar{\rho}_e/\varepsilon, \tag{3.17}$$

in which ε is the permittivity of the medium. For symmetric electrolyte solution, the total ionic distribution $\bar{\rho}_e$ is defined as $\bar{\rho}_e = ez(\bar{n}^+ - \bar{n}^-)$. Further, the order pairs $(\bar{\rho}_{eN}, \varepsilon_N)$ and $(\bar{\rho}_{ec}, \varepsilon_c)$ respectively denote the ionic charge density and permittivity of the fluid in peripheral and core regions. The ionic number distributions of single species are obtained through Nernst-Planck equation for each species. That is,

$$\frac{\partial\bar{n}_\pm}{\partial\bar{t}} + \bar{u}\frac{\partial\bar{n}_\pm}{\partial\bar{r}} + \bar{w}\frac{\partial\bar{n}_\pm}{\partial\bar{z}} = D_0\left(\frac{\partial^2\bar{n}_\pm}{\partial\bar{z}^2} + \frac{1}{\bar{r}}\frac{\partial}{\partial\bar{r}}\left(\bar{r}\frac{\partial\bar{n}_\pm}{\partial\bar{r}}\right)\right) \pm \frac{D_0 ze}{k_B T}\left(\frac{\partial}{\partial\bar{z}}\left(\bar{n}_\pm\frac{\partial\bar{\phi}}{\partial\bar{z}}\right) + \frac{1}{\bar{r}}\frac{\partial}{\partial\bar{r}}\left(\bar{r}\bar{n}_\pm\frac{\partial\bar{\phi}}{\partial\bar{r}}\right)\right). \tag{3.18}$$

It is assumed that coefficients of ionic diffusions for both species are equal and the transport of the species is evaluated through Einstein formula.

Now introducing the dimensionless variables

$$\left.\begin{aligned} &r^* = \frac{\bar{r}}{r_0},\ z^* = \frac{\delta\bar{z}}{r_0},\ u^* = \frac{\bar{u}}{(\delta U)},\ w^* = \frac{\bar{w}}{U},\ t^* = \frac{\delta U}{r_0}\bar{t},\ \delta = \frac{r_0}{\lambda},\\ &p^* = \frac{\delta r_0}{\mu_1 U}\bar{p},\ Re = \frac{\rho U r_0}{\mu_1},\ De = \frac{\lambda_p U}{r_0},\ \phi^* = \frac{ez\bar{\phi}}{k_B T},\ S^* = \frac{r_0}{\mu_1 U}\bar{S},\\ &n^* = \frac{\bar{n}}{n_0},\ \phi_{oc} = \frac{a_0}{r_0},\ \rho_e^* = \frac{r_0^2 k_B T\bar{\rho}_e}{ez\varepsilon_N}. \end{aligned}\right\}, \tag{3.19}$$

where Re is the Reynold number, De be the Deborah number and δ is the wave number. After applying the dimensionless quantities (3.19) and the approximations that $\delta, Pe, Re \ll 1$, where $Pe = ReSc, Sc = \mu_1/\rho D_0$ represents the ionic Peclet number and Schmidt number, respectively. Under these assumptions, the Poisson and Nernst Planck equations reduce to (dropping asterisk)

$$\frac{1}{r}\frac{\partial}{\partial r}\left(r\frac{\partial\phi}{\partial r}\right) = -m_e^2\left(\frac{n_+ - n_-}{2}\right), \tag{3.20}$$

$$0 = \frac{1}{r}\frac{\partial}{\partial r}\left(\frac{1}{r}\frac{\partial n_\pm}{\partial r}\right) \pm \frac{1}{r}\frac{\partial}{\partial r}\left(rn_\pm\frac{\partial\phi}{\partial r}\right), \tag{3.21}$$

where $m_e = r_0 ez\sqrt{2n_0/\varepsilon K_B T} = r_0/\lambda_d$, is the electro-osmotic parameter. Eqs. (3.20) and (3.21) subject to appropriate boundary conditions may give the potential distribution for both regions. Based on these potentials the explicit form of body force term corresponding to each region can be derived Tripathi et al. (2017). However, we shall

not follow this line of action in the subsequent analysis. The details about alternative course of action shall be provided in the later part of this section.

By using the approximations of long wavelength ($\delta \ll 1$) and low Reynolds number (Re) the momentum equations and the stress components in the core and peripheral regions reduce to:

The long wavelength($\delta \ll 1$) approximation means that the length of the peristaltic wave is greater than the characteristic length (width) of the channel or radius of the tube. The low Reynolds number(Re) means that the viscous forces are dominant and thus flow can be considered as inertia free. Therefore, these approximations appear to be trustable to explain biological systems (ureter and gastro-intestinal tract) and in mechanical roller pump using viscous fluid. Eqs. (3.13) – (3.15) for both regions (core and peripheral) become (dropping asterisk)

Core region:

$$0 = -\frac{\partial p}{\partial z} + \left[\left(\frac{1}{r}\frac{\partial (r\, S_{rz})}{\partial r}\right)\right] + U_E\, \frac{\mu_r}{\epsilon_r}\rho_{ec}, \tag{3.22}$$

$$0 = \frac{\partial p}{\partial r}, \tag{3.23}$$

$$S_{rr} = S_{\theta\theta} = S_{zz} = 0,\ S_{rz} = \frac{\left(\frac{\partial w}{\partial r}\right)}{1+(\beta S_{rz})^{\alpha-1}}, \tag{3.24}$$

where, $\beta = U/r_0\tau_0{}^2$

Peripheral region:

$$0 = -\frac{\partial p}{\partial z} + \mu_r\, \frac{1}{r}\left(\frac{\partial (r\, S_{rz})}{\partial r}\right) + U_E\, \mu_r\, \rho_{eN}, \quad \text{where } \mu_r = \frac{\mu_N}{\mu_c} \tag{3.25}$$

$$0 = \frac{\partial p}{\partial r}, \tag{3.26}$$

$$S_{rr} = S_{\theta\theta} = S_{zz} = 0,\ S_{rz} = \left(\frac{\partial w}{\partial r}\right). \tag{3.27}$$

The boundary conditions are:

$$\frac{\partial w_c}{\partial r} = 0, at\ r = 0;\ \text{(symmetry at the center-line)} \tag{3.28}$$

$w_c = w_N$ and $(S_{rz})_N = (S_{rz})_c$ at $r = R_1$;

(Continuity of velocity and stress at the interface) (3.29)

$w_N = -1$ at $r = R_0$; (no-slip condition at the wall). (3.30)

Following Goswami *et al.* (2016), we drop the electrokinetic body force terms from momentum equations (3.25 - 3.27) and (3.28 - 3.30) along with suitable modification of the no-slip boundary condition at the wall. In this way, the governing equations and boundary condition take the form:

Core region:

$$0 = -\frac{\partial p}{\partial z} + \left[\left(\frac{1}{r}\frac{\partial (r\, S_{rz})}{\partial r}\right)\right], \tag{3.31}$$

$$0 = \frac{\partial p}{\partial r}, \tag{3.32}$$

$$S_{rr} = S_{\theta\theta} = S_{zz} = 0,\ S_{rz} = \frac{\left(\frac{\partial w}{\partial r}\right)}{1+(\beta S_{rz})^{\alpha-1}}, \tag{3.33}$$

$$\frac{\partial w_c}{\partial r} = 0, at\ r = 0. \tag{3.34}$$

Peripheral region:

$$0 = -\frac{\partial p}{\partial z} + \mu_r \frac{1}{r}\left(\frac{\partial (r\, S_{rz})}{\partial r}\right), \tag{3.35}$$

$$0 = \frac{\partial p}{\partial r}, \tag{3.36}$$

$$S_{rr} = S_{\theta\theta} = S_{zz} = 0,\ S_{rz} = \left(\frac{\partial w}{\partial r}\right), \tag{3.37}$$

$$\frac{\partial w_c}{\partial r} = 0, at\ r = 0, \tag{3.38}$$

$$w_N = U_E - 1,\ at\ r = R_0. \tag{3.39}$$

3.3 Velocity components in term of stream function

The velocity components in term of stream function are defined by the Cauchy-Riemann equations:

$$u = -\frac{\partial \psi^*}{\partial z}, w = \frac{1}{r}\frac{\partial \psi^*}{\partial r}. \tag{3.40}$$

Here ψ^* is the stream function in the *moving* frame of reference and is related to its counterpart in the *fixed* frame via the relation $\psi = \psi^* - r^2/2$. Now introducing the stream function, the momentum equations in the core and peripheral regions become:

$$\frac{\partial}{\partial r}\left(\frac{1}{r}\frac{\partial \psi}{\partial r}\right) = \frac{r}{2}\frac{\partial p}{\partial z} + \frac{(\beta)^{\alpha-1}}{(2)^{\alpha}}\left|\frac{\partial p}{\partial r}\right|^{\alpha-1}\frac{\partial p}{\partial r} r^{\alpha}, \quad 0 \le r \le R_1 \tag{3.41}$$

$$0 = -\frac{\partial p}{\partial z} + \frac{1}{r}\frac{\partial}{\partial r}\left[\left(r\mu_r \frac{\partial}{\partial r}\left(\frac{1}{r}\frac{\partial \psi}{\partial r}\right)\right)\right]. \quad R_1 \le r \le R_0 \tag{3.42}$$

The associated boundary conditions are:

$$\psi(0) = 0,\ \frac{\partial}{\partial r}\left(\frac{1}{r}\frac{\partial \psi}{\partial r}\right)\Big|_{r=0} = 0, \tag{3.43}$$

$$\psi(R_0) = \frac{q}{2},\ \frac{\partial \psi}{\partial r} = (U_E - 1)R_0, \tag{3.44}$$

$$\psi(R_1) = \frac{q_1}{2}. \tag{3.45}$$

Here μ_r is the viscosity ratio, q_1, q are the volumetric flow rates through the inner and outer cross-sections of the tube, respectively. Now, integrating the Eqns. (3.41) and (3.41) subject to the boundary condition (3.43) and (3.44), we arrive at the following expressions for stream function in terms of R_1 for both *core* and *peripheral* regions:

$$\psi = \frac{r^2}{2}\Bigg\{(U_E - 1) + \frac{(\beta)^{\alpha-1}}{(2)^{\alpha}}\left|\frac{\partial p}{\partial z}\right|^{\alpha-1}\frac{\partial p}{\partial z}\left[\frac{2\,r^{\alpha+1}}{(\alpha+1)(\alpha+3)} - \frac{{R_1}^{\alpha+1}}{(\alpha+1)}\right] + \frac{1}{16}\frac{\partial p}{\partial z}\{r^2 - 2{R_1}^2\} + \frac{1}{4\mu_r}\frac{\partial p}{\partial z}\{{R_1}^2 - {R_0}^2\}\Bigg\}, 0 \le r < R_1 \tag{3.46}$$

$$\psi = \frac{r^2}{2}(U_E - 1) + \left(\frac{q}{2} - (U_E - 1)\frac{{R_0}^2}{2}\right) + \frac{1}{4\mu_r}\frac{\partial p}{\partial z}\left(r^2 - {R_0}^2\right)^2. R_1 \le r \le R_0 \tag{3.47}$$

From the above expressions, *axial velocity* emerges as:

$$w(r,z) = \begin{cases} (U_E - 1) + \frac{(\beta)^{\alpha-1}}{(2)^{\alpha}}\left|\frac{\partial p}{\partial z}\right|^{\alpha-1}\frac{\partial p}{\partial z}\left[\frac{2\,r^{\alpha+1}}{(\alpha+1)(\alpha+3)} - \frac{{R_1}^{\alpha+1}}{(\alpha+1)}\right] + \frac{1}{16}\frac{\partial p}{\partial z}\{r^2 - 2{R_1}^2\} \\ \qquad + \frac{1}{4\mu_r}\frac{\partial p}{\partial z}\{{R_1}^2 - {R_0}^2\},\ \ 0 \le r < R_1, \\ (U_E - 1) + \frac{1}{4\mu_r}\frac{\partial p}{\partial z}\left(r^2 - {R_0}^2\right),\ R_1 \le r \le R_0. \end{cases} \tag{3.48}$$

For the subsequent analysis, it is assumed that the shape of the outer boundary can be described by the following expression:

$$R_0(z) = 1 + \phi_{oc}\sin(2\pi z), \tag{3.49}$$

where ϕ_{oc} represents the dimensionless occlusion parameter. It is important to point that the solution to the considered problem is still not complete due to the unknowns R_1 and $\partial p/\partial z$ appearing in the expressions (3.46) and (3.47). To obtain these unknowns, the following semi-analytical approach is deployed Goswami *et al.* (2016). Using the condition (3.45), we get:

$$\frac{q_1}{2} = \frac{{R_1}^2}{2}(U_E - 1) + \left(\frac{q}{2} - (U_E - 1)\frac{{R_0}^2}{2}\right) + \frac{1}{16\mu_r}\frac{\partial p}{\partial z}\left({R_1}^2 - {R_0}^2\right)^2, \quad (3.50)$$

Here q_1 is another constant to be determined. To eliminate q_1 we set $R_0 = 1$ and $R_1 = k$ at $z = 0$ in the above equation which yields the following:

$$\frac{q_1}{2} = \frac{k^2}{2}(U_E - 1) + \left(\frac{q}{2} - (U_E - 1)\frac{1}{2}\right) + \frac{1}{16\mu_r}P_0(k^2 - 1)^2. \quad (3.51)$$

Eliminating q_1 between (3.50) and (3.51) results in the following equation:

$$\frac{k^2}{2}(U_E - 1) + \left(\frac{q}{2} - (U_E - 1)\frac{1}{2}\right) + \frac{1}{16\mu_r}P_0(k^2 - 1)^2 = \frac{{R_1}^2}{2}(U_E - 1)$$

$$+ \left(\frac{q}{2} - (U_E - 1)\frac{{R_0}^2}{2}\right) + \frac{1}{16\mu_r}\frac{\partial p}{\partial z}\left({R_1}^2 - {R_0}^2\right)^2, \quad (3.52)$$

where k is the inner layer thickness measured at $z = 0$ from the boundary wall and $P_0 = (\partial p/\partial z)|_{z=0}$. Thus we have replaced q_1 with another unknown P_0. In this way, there are three unknown to be determined to be able to close the solution i.e., P_0, R_1 and $\partial p/\partial z$. However, there is only one condition available i.e. Eqn. (3.51). The other two conditions can be furnished as follows. Since the stream function given by the Eqns. (3.46) and (3.47) must be same at the interface, therefore it follows that:

$$\frac{(\beta)^{\alpha-1}}{(2)^{\alpha+1}}\frac{\partial p}{\partial z}\left|\frac{\partial p}{\partial z}\right|^{\alpha-1}\frac{{R_1}^{\alpha+3}}{(\alpha+3)} + \frac{1}{16\mu_r}\frac{\partial p}{\partial z}\left({R_0}^4 - {R_1}^4\right) + \frac{q}{2} - (U_E - 1)\frac{{R_0}^2}{2} + \frac{{R_1}^4}{16}\frac{\partial p}{\partial z}0. \quad (3.53)$$

Proceeding with the analysis, the following equation is produced:

$$\frac{(\beta)^{\alpha-1}}{(2)^{\alpha+1}}P_0|P_0|^{\alpha-1}\frac{k^{\alpha+3}}{(\alpha+3)} + \frac{P_0}{16\mu_r}\frac{\partial p}{\partial z}(1 - k^4) + \frac{q}{2} - (U_E - 1)\frac{1}{2} + \frac{k^4}{16}P_0 = 0. \quad (3.54)$$

Effectively Eqns. (3.52) - (3.54) can be solved numerically to obtain the values of P_0, R_1 and $\partial p/\partial z$ at each axial position z. The bisection method is used for the computations. This process yields closed form expressions for stream function at each axial position z. At this point the solution to the considered problem is complete.

3.4 Graphical results and interpretations

3.4.1 The interface region

The numerical procedure based on the bisection method is implemented in the symbolic software **Mathematica 8.1** to compute the values of P_0, R_1 and $\partial p/\partial z$

corresponding to each axial position z. The plots of interface R_1 against z for different values of μ_r, α, U_E and β are displayed in **Figs. (3.2)** and **(3.3(a - d))**. It is important to remember that α and β are the material (rheological) parameters associated with the core fluid Ellis model whereas U_E is the parameter arising from the inclusion of the electro-osmotic effects. **Fig. (3.2)** illustrates the variations in the interface R_1 with respect to the parameter μ_r which is the ratio between the viscosities of the outer and inner regions.

It is observed that interface curve corresponding to $\mu_r = 1$ lies in between the corresponding curves for $\mu_r = 0.1$ and $\mu_r = 10$. In fact these curves depict the position of the interface for three situations i.e., $\mu_r < 1, \mu_r = 1$ and $\mu_r > 1$. Generally, during the flow the fluid under the crest region will experience a vertical normal force whereas the fluid in the trough region is subjected to a vertically downward force. When $\mu_r < 1$ i.e., the viscosity of the inner core exceeds the viscosity of the outer region, the fluid in the peripheral region under the wave crest will undergo a reduced vertical force in the upward direction and hence stay below the interface level for $\mu_r = 1$. At the same time, the fluid in the outer region under the wave trough will also feel a *reduced force in downward direction* and hence stay above the interface level for $\mu_r = 1$. However, a reverse trend is observed when $\mu_r > 1$. The slight shifting of the fluid in the outer region in both the crest and trough regions is of the same magnitude. However, this is not the situation when the variation is observed with respect to the other parameters such as U_E, β and α. The couple type force arrangement experienced by the peripheral fluid in the crest and trough region breaks when the core region fluid is assumed to be non-Newtonian. This is attributable to the deformation-dependent viscosity of the non-Newtonian liquid. In the crest region, the normal force acting in the upward direction is least affected with an elevation in either α, U_E and β. Significant changes in the magnitude of normal force are *only observed* in the wave trough region. Therefore, the interface in the trough region is displaced downward with increasing α and β whereas it is displaced upward with increasing U_E. Analysis of **Fig. (3.3d)** shows that the findings of present study about the interface region are consistent with the Rao and Usha (1995) study when, $\beta = 0$ and the other parameters are kept constant. By increasing the values of viscosity ratio a considerable variation occurs in the interface shape after certain values of viscosity ratio. The crest (peripheral) region viscosity becomes almost

uniform, but in trough (core) region a dramatic change occurs in the shape of interface due to a strong downward normal force.

3.4.2 Pressure and volume flux variation

The axial pressure gradient $\partial p/\partial z$ in the tube can be computed from the following equation:

$$\frac{\partial p}{\partial z} = \frac{16\mu_r}{(R_1{}^2 - R_0{}^2)^2}\left\{\frac{1}{2}(U_E - 1)\left(k^2 - R_1{}^2 + R_0{}^2\right) + \frac{1}{16\mu_r}P_0(k^2 - 1)^2\right\}. \qquad (3.55)$$

The *pressure rise over one wavelength* is obtained by integrating the above expression from the limits 0 to λ as follows:

$$\Delta P = 16\mu_r \int_0^{\lambda} \left\{\frac{\frac{1}{2}(U_E - 1)\left(k^2 - R_1{}^2 + R_0{}^2\right) + \frac{1}{16\mu_r}P_0(k^2 - 1)^2}{(R_1{}^2 - R_0{}^2)^2}\right\} dz. \qquad (3.56)$$

The *volume flux in the moving frame* q is related to its counterpart Q_S in the fixed frame of references via the relation:

$$Q_S = 2\int_0^{R_0}(w + 1)\, r\, dr = q + R_0{}^2. \qquad (3.57)$$

Averaging over a complete time-period yields:

$$Q = \frac{1}{T_P}\int_0^{T_P} Q_S\, dt = q + \left(1 + \frac{\phi^2}{2}\right), \qquad (3.58)$$

where $T_P = \lambda/U$ is a complete time-period.

The integration in Eq. (3.56) is performed numerically and the results computed which illustrate the variations in pressure rise per wavelength *at zero volumetric flow rate* $\Delta P_o = \Delta P|_{Q=0}$ against the occlusion parameter ϕ_{oc} are displayed in **Figs. (3.4(a, b))**. This figure infact provides the estimate of dimensionless pressure rise resulting from the peristaltic motion of the wall.

Fig. (3.4a) shows the results for the case when core region fluid is characterized by the Ellis model. This figure also highlights the influence of viscosity ratio on ΔP_0. Here the effects of electro-osmotic slip are not considered i.e., $U_E = 0$. It is observed that pressure drop at zero volumetric flow rate *increases with increasing occlusion parameter*. A much greater pressure drop is required to maintain zero flow rate when the *core region fluid is less viscous than the peripheral region fluid* in comparison to

the scenario where the *outer region is less viscous than the inner region fluid.* Further, the effects of the viscosity ratio are more noticeable in comparison to the effects of the power-law index, α. Infact, the effects of α are only realized at larger values of the occlusion parameter ϕ_{oc}. At larger values of the occlusion parameter a rise in the power-law index reduces the magnitude of ΔP_0. The parameter α is in fact a measure of the *shear-thinning* nature of the fluid in the core region. Larger values of α correspond to the case of fluid with pronounced share-thinning effects i.e., fluid with a significantly reduced apparent viscosity. Therefore, the depletion in pressure associated with increasing α at large occlusion is attributable to the decreased apparent viscosity of the fluid in the inner region. The effects of electro-osmotic slip velocity on ΔP_0 are shown in **Fig. (3.4b).** Here, it is evident that the presence of electro-osmotic slip velocity reduces the pressure drop only for intermediate values of the occlusion parameter. As the occlusion parameter approaches unity, the reduction is almost negligible. The effects of the Ellis parameter β on ΔP_0 are displayed in **Fig. (3.4b).** It is observed that the role of the parameter β is to decrease the pressure drop over the whole considered range of the occlusion parameter ϕ_{oc}, when the peripheral (outer) region fluid is more viscous than the core (central) region fluid. In contrast, when the core region fluid is more viscous than the peripheral region fluid the reduction in pressure drop with increasing β is only realizable at larger values of the occlusion parameter.

3.4.3 Mechanical efficiency

One of the important physical quantity known as mechanical efficiency of pumping is mathematically given as:

$$E = \frac{Q\Delta P}{\frac{1}{T}\int_0^T \int_0^{\lambda} 2R_0 p \frac{dR_0}{dt} dz dt} = \frac{Q\Delta P}{\Delta P\left(1+\frac{\phi^2}{2}\right)-I_1}, \tag{3.59}$$

where

$$I_1 = \int_0^1 \frac{dp}{dz} {R_0}^2 \, dz. \tag{3.60}$$

Basically, it is ratio between the average rate per wavelength at which work is carried out by the transport of the fluid against pressure rise and the average rate at which the peristaltic walls movement do work on the fluid. The numerical procedure based on the bisection method is implemented in the symbolic software Mathematica 8.1 to compute the value of the efficiency expression. The efficiency expression as a function of Q is illustrated in **Fig. (3.5(a - e))** for different values of the parameters. It

is observed that a considerable growth occurs in pumping efficiency by increasing the values of the parameters U_E, β and μ_r, but opposite trend is observed in case of α, because the peristaltic transport in the pumping limits depends on the viscous forces caused by the walls of the tube. For $\beta = 0$ the present analysis reduces to Newtonian case, and the efficiency expression coincide with the expression of Rao and Usha (1995) which illustrated in **Fig. (3.5e).**

3.4.4 Trapping phenomenon

The streamline plots showing trapping inside the core and peripheral regions are displayed in **Figs. (3.6(a - d)) – (3.11(a - d))**. A detailed explanation regarding the development of trapped bolus in the flow domain is provided by Goswami *et al.* (2016). According to Goswami *et al.* (2016), trapping is strongly dependent upon the *bulk momentum* of the flow. The greater the momentum of the fluid, the lower the probability of fluid particles being trapped in zones of re-circulation. **Fig. (3.6(a - d))** and **(3.7(a - d))** illustrates the effects of electro-osmotic slip velocity on the trapped bolus for the case when the inner core is less viscous than the peripheral region. It is observed that the trapped bolus, *regardless of its position*, reduces in size and finally vanishes with increasing the electro-osmotic slip velocity. For the case when viscosity of the inner core exceeds the viscosity of the peripheral region, the trapped bolus appearing either in the core or peripheral regions is *smaller* than its counterpart for the previous case. **Fig. (3.8(a - d))** shows that the effect of viscosity ratio on the trapped bolus is same as that observed for electro-osmotic slip velocity. Similarly, it is inferred from **Fig. (3.9(a - d))** that the fluid power-law index α exerts a similar effect on the trapped bolus as that observed for viscosity the ratio and the electro-osmotic slip velocity. In contrast, **Fig. (3.10(a - d))** and **(3.11(a - d))** reveals that the trapped bolus either in the core or peripheral regions increases in size with an increase in the Ellis model parameter β. However, the increase in the bolus size with increasing Ellis model parameter β is not indefinite i.e., the size of the trapped bolus increases with initial increase in β upto a certain value and thereafter it becomes independent of β. For $\mu_r = 1$, the constancy in the size of the trapped bolus is observed at values of β that are significantly larger than their counterparts for $\mu_r > 1$.

It is also of great use to determine the parametric ranges in which the trapping phenomenon occurs. In this regard, we have presented plots of $Q/Q_{\Delta p=0}$ against the occlusion parameter for several values of the key parameters such as electro-kinetic

slip velocity, viscosity ratio and material parameters of the Ellis model in **Figs. 3.12(a - d).** In fact, for each ϕ_{oc} there exists a unique value of $Q/Q_{\Delta p=0}$ and vice-versa.

The identification of plausible value of ϕ_{oc} and $Q/Q_{\Delta p=0}$ is carried out first by obtaining a trial subregion in the domain $(0 \leq Q/Q_{\Delta p=0} \leq 1);\ (0 \leq \phi_{oc} \leq 1)$ where the stream function ψ changes its sign and then employing a root-finding algorithm to exactly pinpoint the value of ϕ_{oc} and ψ at which such a transition occurs Goswami *et al.* (2016).

Two distinct regions can be readily identified for each figure. One below a specific curve and the other one above it. The region of trapping comprises of the zone that lies above a specific curve in the ϕ_{oc} - $Q/Q_{\Delta p=0}$ plane. **Figs. (3.6(a - d))** and **(3.7(a - d))** shows the effect of the electro-osmotic slip velocity on the trapping region. It is observed that trapping region reduces with increasing the electro-osmotic slip velocity, power-law index α and the viscosity ratio μ_r. In contrast, it increases with increasing the Ellis parameter β.

3.4.5 Reflux

Reflux is the process in which the fluid moves in backward direction in a complete wave cycle due to the unfavorable pressure gradient across the flow geometry or by the opposite movement of a fluid element inside the tube Goswami *et al.*(2016). It is anticipated that the reflux phenomenon in both regions depends strongly on the involved parameters. According to Shapiro *et al (1969)*, the amount of reflux can be estimated through the quantity $(Q - Q_\psi)/Q$ during one wave cycle, where Q_ψ is defined as Rao and Mishra (2004):

$$Q_\psi = 2\psi + \int_0^1 r^2\, dz. \tag{3.61}$$

The above expression emerges by transforming the following expression from the fixed frame to the wave frame and taking the average over one period of the wave:

$$Q_{\psi'} = 2\int_0^{r(\psi',z)} r\, w\, dr, \tag{3.62}$$

In (3.51) $Q_{\psi'}$ is the average volume flow rate between the axis of the tube and a streamline ψ'=constant in the fixed frame. Since the quantity Q_ψ/Q varies between 0 to 1 therefore the quantity $(Q - Q_\psi)/Q$ must vary from 1 to 0. However, under certain conditions it may happen that for some values of ψ' the quantity Q_ψ/Q

exceeds unity, or, the quantity $(Q - Q_\psi)/Q < 0$ which is an indicator that there is some sort of backward motion or reflux occurring within the flow domain. **Figs. 3.13(a-d)** shows that reflux can avoided by increasing the electro-osmotic slip velocity U_E and the fluid power-law index α. In contrast, reflux is enhanced with an increase in both the viscosity ratio μ_r and the Ellis parameter β.

Finally, we demonstrate the generality of the present analysis in comparison to the previously published results. To this end, we have shown in **Fig. (3.13(a - d))** that the results for the situation when the fluid in the core region is characterized by power-law model can be deduced from the present analysis by proper selection of the Ellis parameter α and β. Specifically, it is shown that the shape of the interface by considering the power-law fluid in the core region for $\alpha = 0.5$ can be reproduced from the present analysis by setting $\alpha = 2$ and $\beta = 20$. The other parameters which are kept same in both scenarios are $k = 0.8, \mu_r = 2, Q = 0, U_E = 0$, $\phi_{oc} = 0.6$ Similarly, it is shown that the profile of $(\Delta p)_{Q=0}$ for the case when the core region fluid is of power-law type can be deduced from our analysis by setting $\alpha = 2$, $\beta = 10$ provided that the other parameters are kept fixed in both situations to $k = 0.7, \mu_r = 0.1, Q = 0, U_E = 0$. Obviously, the present results also contract to the results for the case when the fluid in the inner region obeys the Newtonian constitutive law by setting $\alpha = 1$, $\beta = 0$.

The objective of the present study is to analyze the influence of the electro-osmotic peristaltic transport of non-Newtonian fluids. Our analysis is applicable particularly to blood flow. Our findings are more exotic than the outcomes of previous study, as it presents detailed discussion of both shear thinning and yield stress simultaneously which are essential features of blood flow. While the previous study just focused on shear thinning and ignored yield stress. So our study is more comprehensive than previous study.

3.5 Conclusions

In this chapter, an analysis is presented for peristaltic motion of two immiscible fluids in a tubular confinement under electro-osmotic body force. The core region fluid is assumed to obey the Ellis constitutive equation whereas the peripheral region fluid is characterized by the Newtonian model. The stream function for each region is derived for the case when the shape of the interface is not known a priori. The important phenomena of pumping, trapping and reflux are discussed in detail. It is found that the

maximum pressure against which peristalsis has to work as a positive displacement pump can be reduced by choosing small values of the Ellis model parameters α and β. Further, trapping and reflux phenomena can be avoided by enhancing the electro-osmotic slip and shear-thinning effects. In blood vessels, trapping is undesirable owing to its role is the formation of thrombosis of blood. Similarly, it may also trigger undesired chemical reactions in reactive fluids. Despite these disadvantages, trapping is advantageous in situations where it is desired to achieve better mixing of the contents with in the hollow structure. One such situation arises during the chyme motion in the small intestine. The reflux in the context of biological fluid transport is undesirable since it contributes to the migration of micro-organism in the opposite direction to the peristaltic wave motion. Moreover, in the magnitude of non-dimensional pressure produced by the wavy wall movement of the tube is linked with the efficiency of the pumping and therefore needs to be reduced. Our results suggest the following possible remedies to avoid trapping and reflux and to reduce the pressure evolved by the wall movement. The first option is the imposition of the electro-osmotic slip velocity which has already been proposed by previous researchers (Chakraborty (2006), Dhinkaran et al. (2010), Ferras et al. (2014), Das and Chakraborty (2006), Tripathi et al. (2016), Tripathi et al. (2018), Prakash and Tripathi (2018) and Goswami et al. (2016)). This solution is universal in the sense that it minimizes all three of the above-mentioned phenomena. The other possible way is to *enhance the shear-thinning nature* of the fluid to be transported. Similarly, the reduction in pressure and reflux can also be achieved by properly tuning the rheological characteristics of the fluid controlled by the parameter τ_0. However, this will happen at the cost of an increase in the trapping phenomenon.

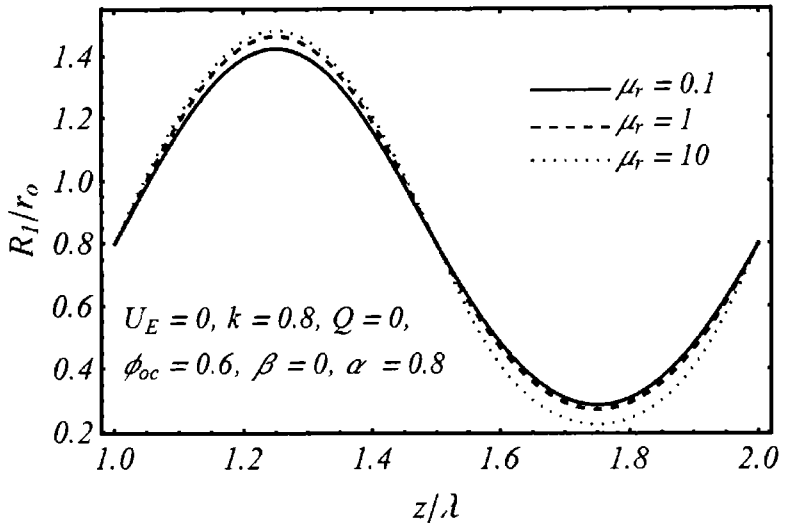

Fig. 3.2: The behavior of the interface for different values of viscosity ratio μ_r.

(a)

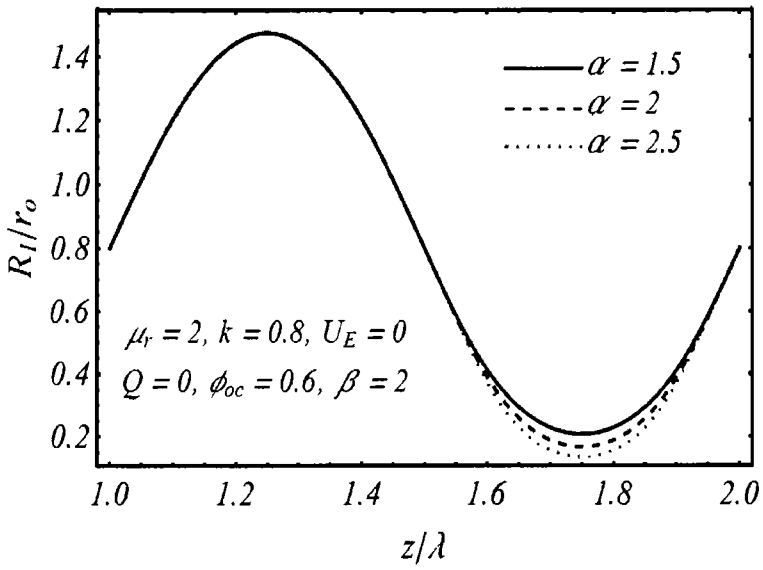

(b)

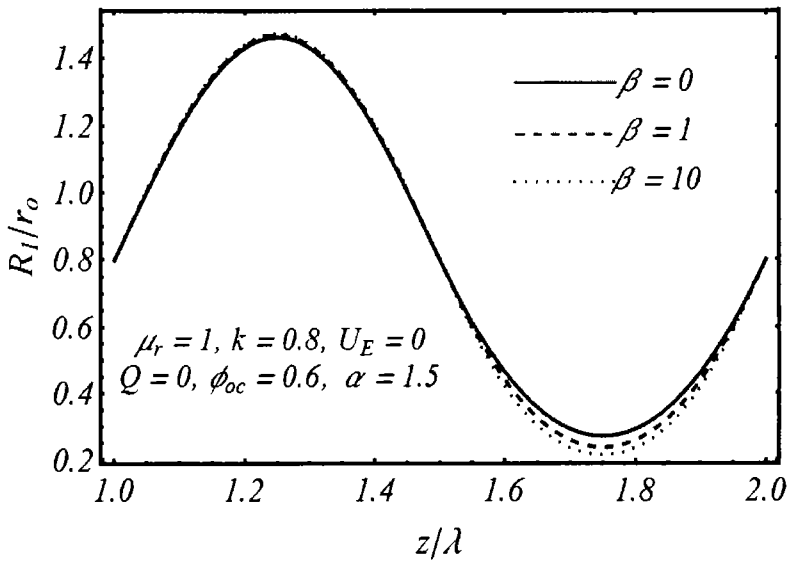

Fig. 3.3 ((a), (b)): The variations in interface with respect to Ellis model parameter α and β.

(c)

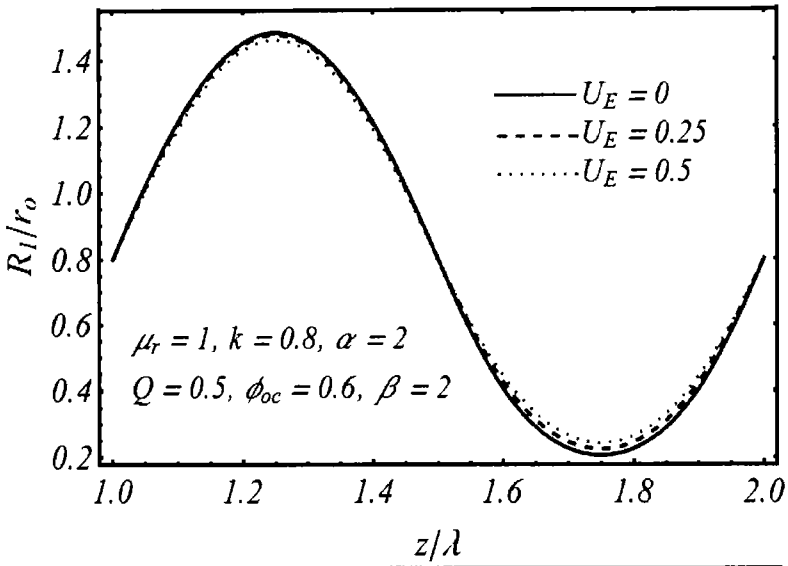

(d)

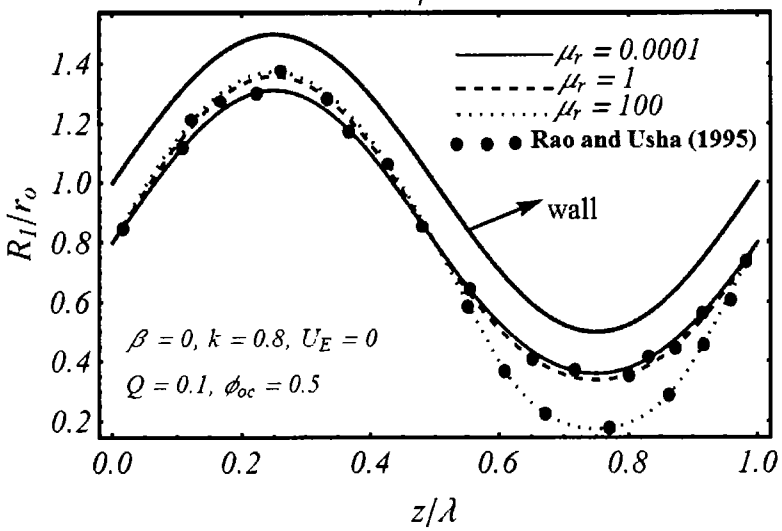

Fig. 3.3 ((c), (d)): The variations in interface with respect to electrokinetic parameter U_E and the comparison with Rao and Usha (1995) results.

(a)

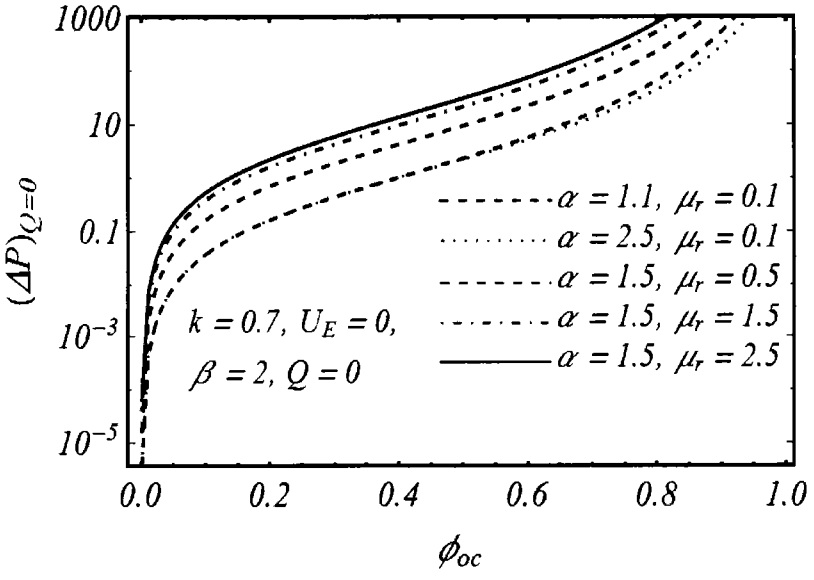

Fig. 3.4 (a): The pumping characteristics for different values of viscosity ratio and Ellis parameter α.

(b)

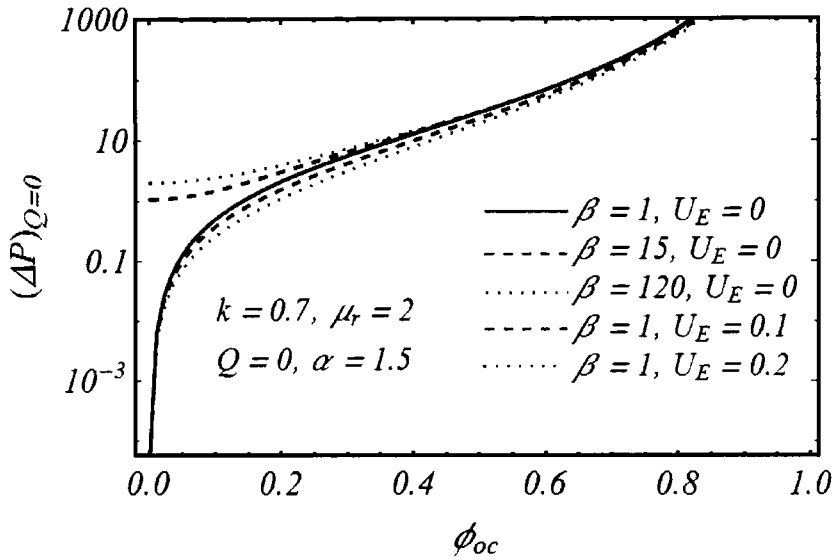

Fig. 3.4 (b): The pumping characteristics for different values of Ellis parameter β and electro-kinetic slip velocity U_E.

(a)

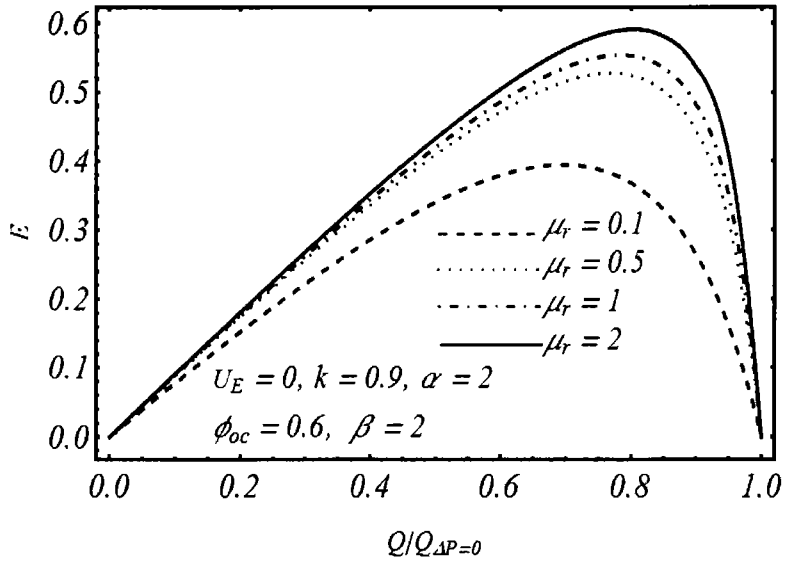

(b)

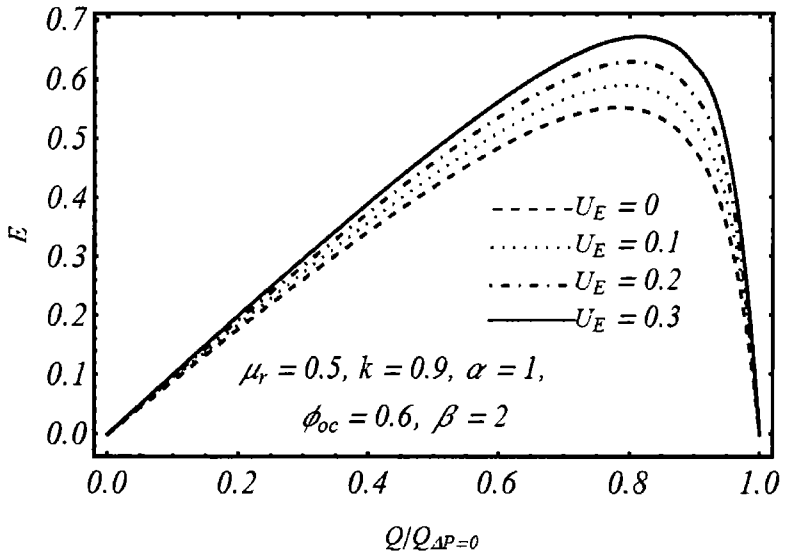

Fig. 3.5 ((a), (b)): Pumping efficiency with respect to parameters μ_r and the electro-kinetic parameter U_E.

(c)

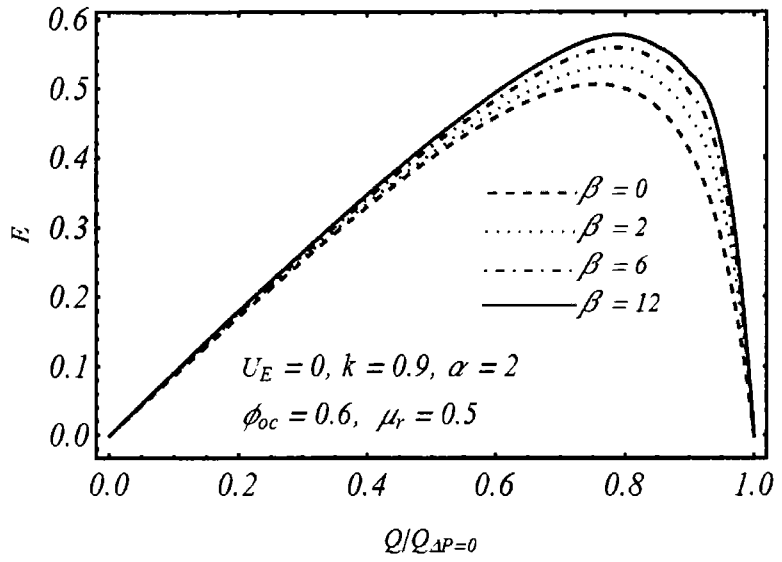

(d)

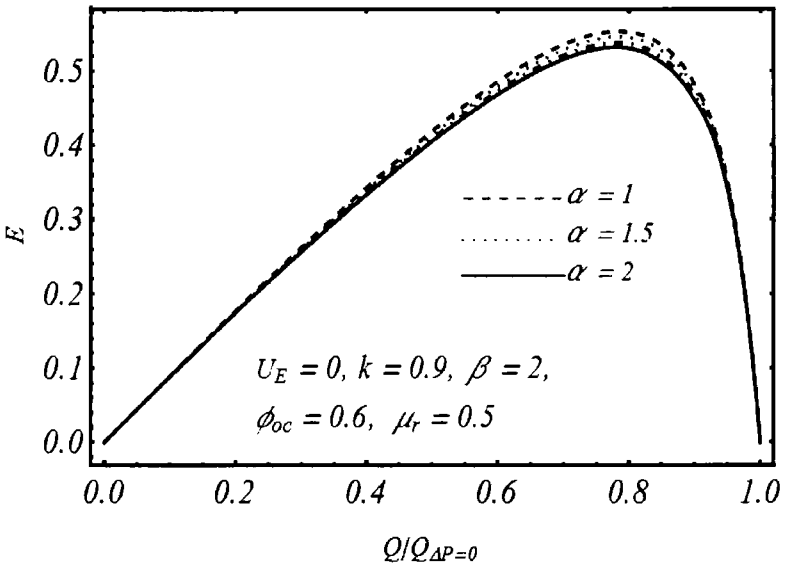

(e)

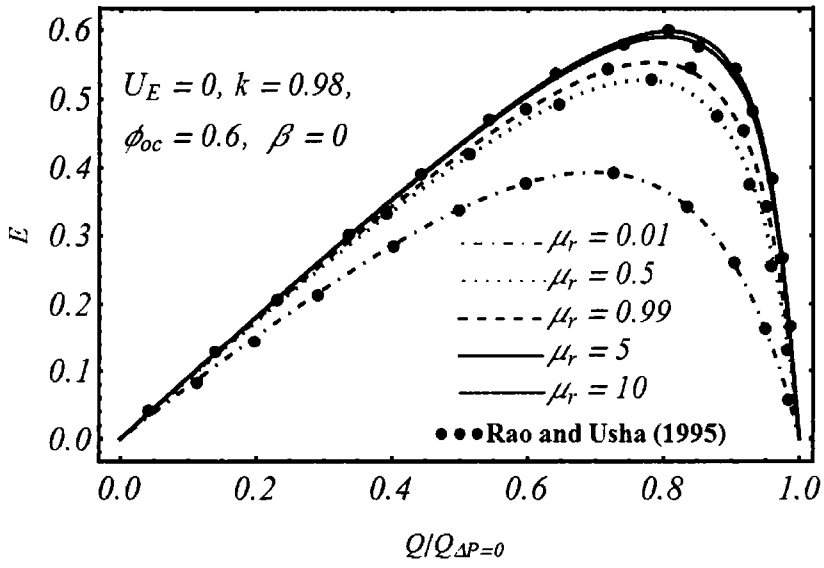

Fig. 3.5 ((c) – (e)): Pumping efficiency with respect to parameters β, α and the comparison with the Rao and Usha (1995) results.

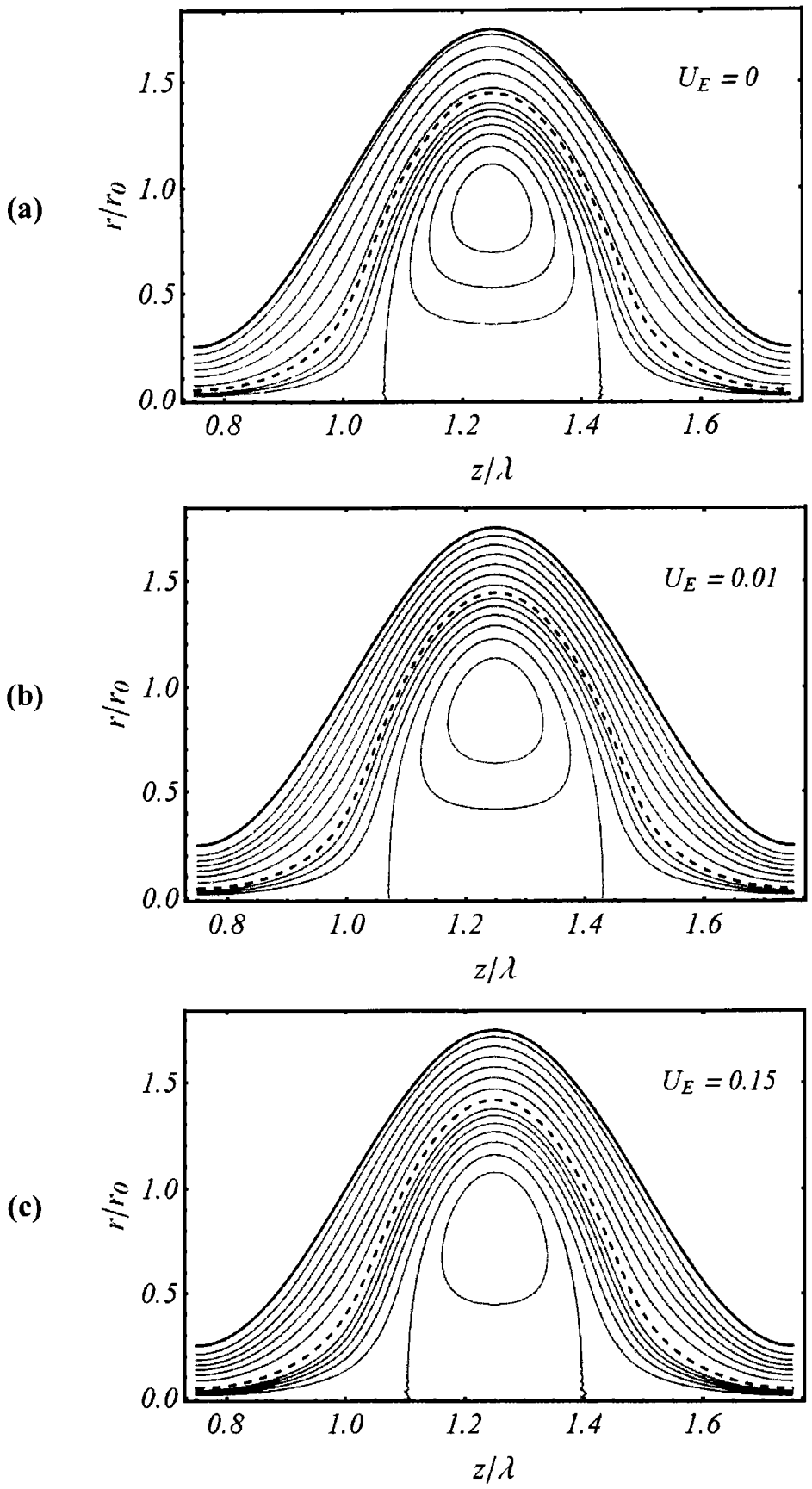

Fig. 3.6 ((a) – (c)): Streamline plots showing trapping for core region with other parameters $Q = 0$, k=0.4, $\mu_r = 10, \alpha = 1.5$, $U_E = 0$, $\phi_{oc} = 0.75, \beta = 2$.

(c)

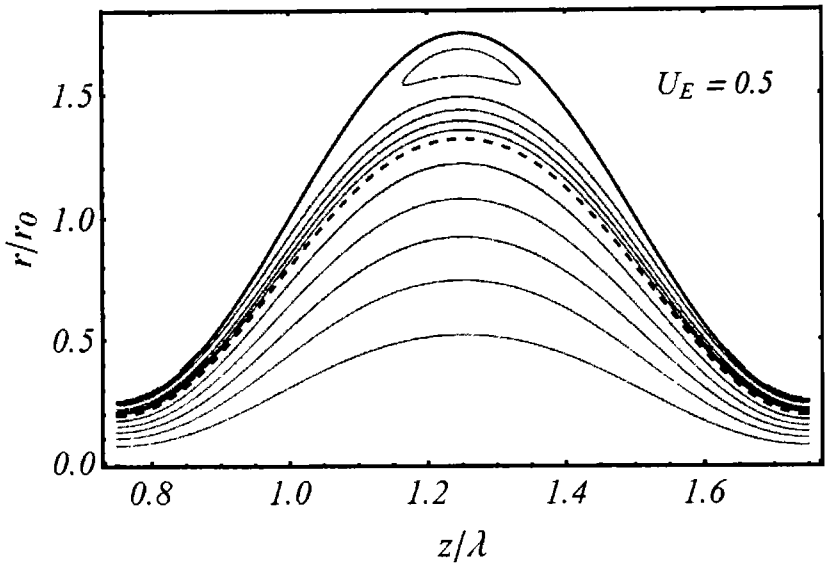

(d)

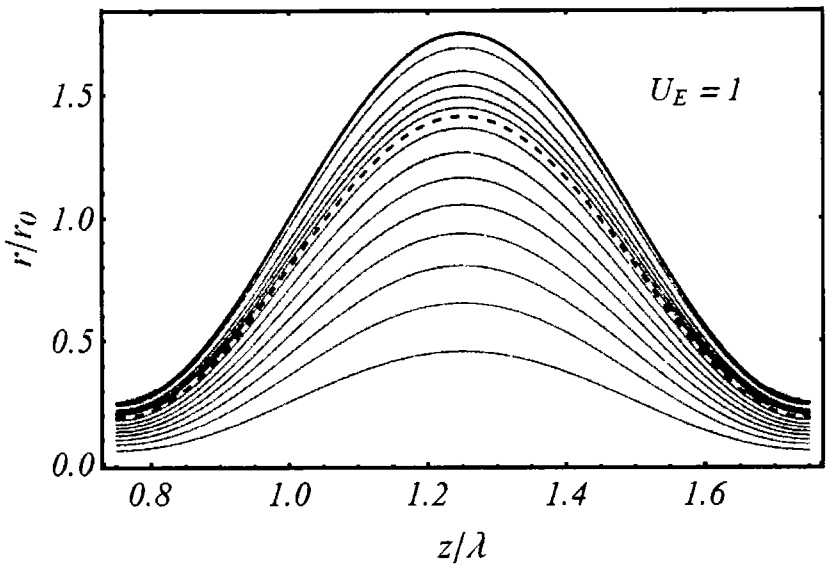

Fig. 3.7 ((c), (d)): Streamline plots showing trapping for peripheral region with other parameters $Q = 4$, k=0.8, $\mu_r = 0.1, \alpha = 1.5, \beta = 2, U_E = 0, \phi_{oc} = 0.75$.

(a)

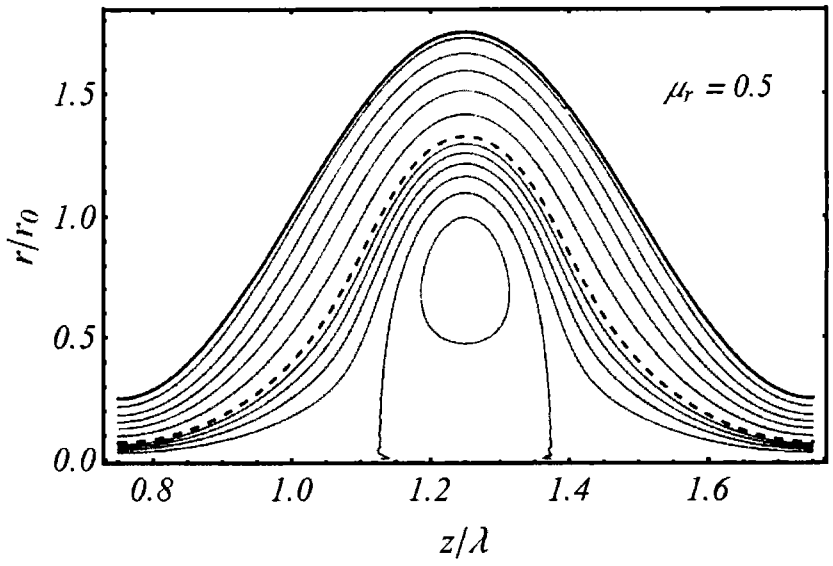

Fig. 3. 8 (a): Trapping phenomena for different values of μ_r and the values of other parameters are $Q = 0, 2, \alpha = 1.5, U_E = 0, \phi_{oc} = 0.75, \beta = 2, k = 0.4$.

(b)

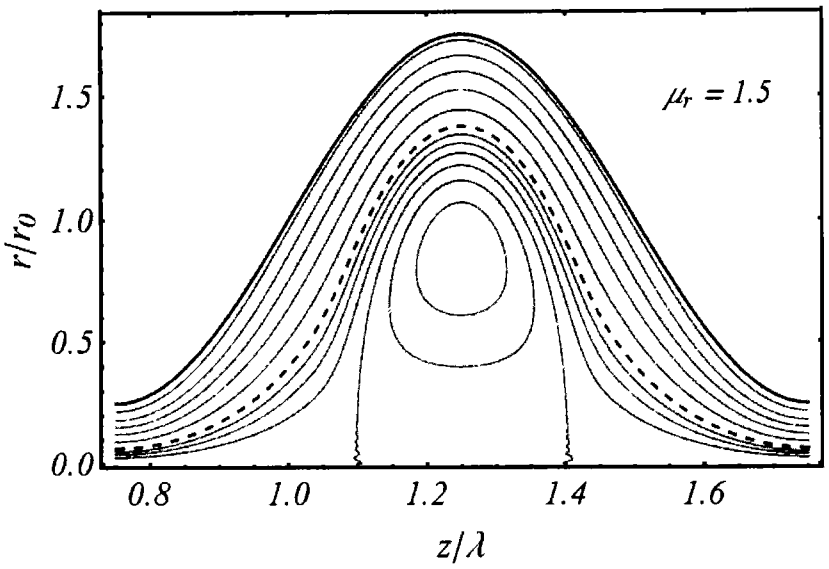

(c)

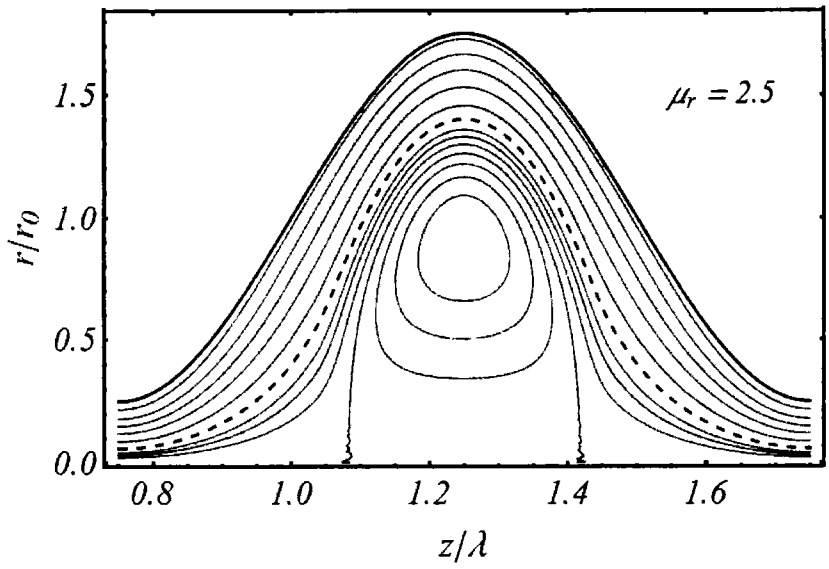

(d)

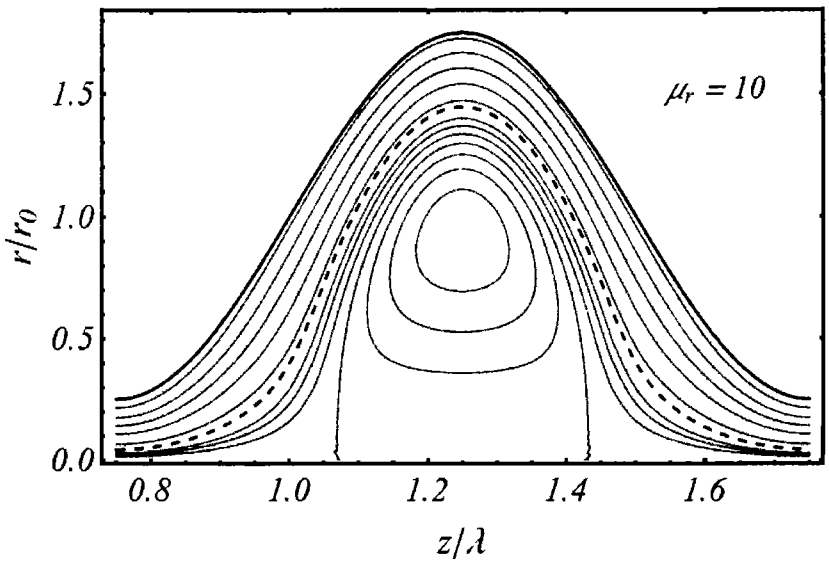

Fig. 3. 8 ((b) – (d)): Trapping phenomena for different values of μ_r and the values of other parameters are $Q = 0, 2, \alpha = 1.5, U_E = 0, \phi_{oc} = 0.75, \beta = 2, k = 0.4$.

(a)

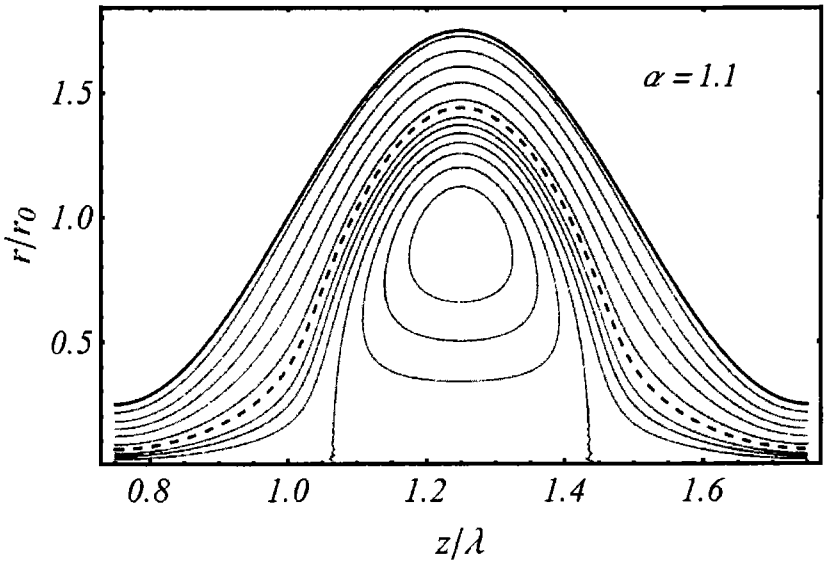

(b)

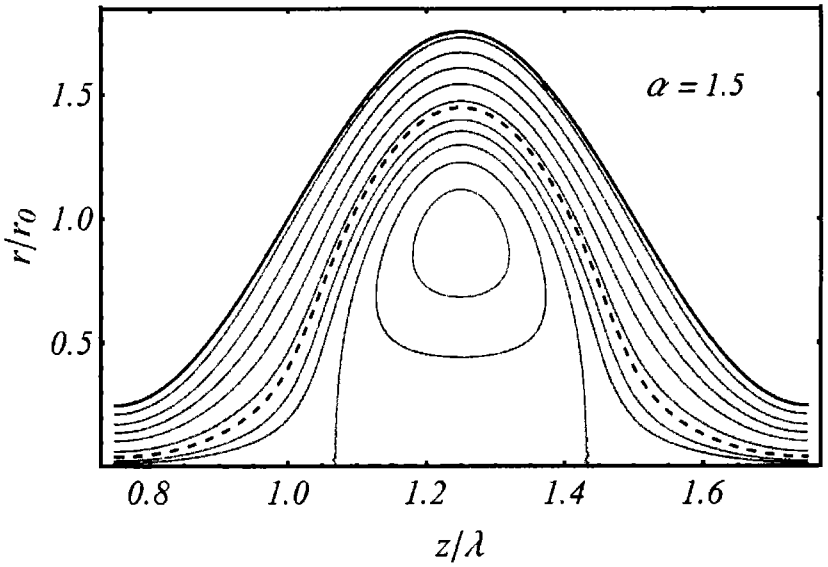

(c)

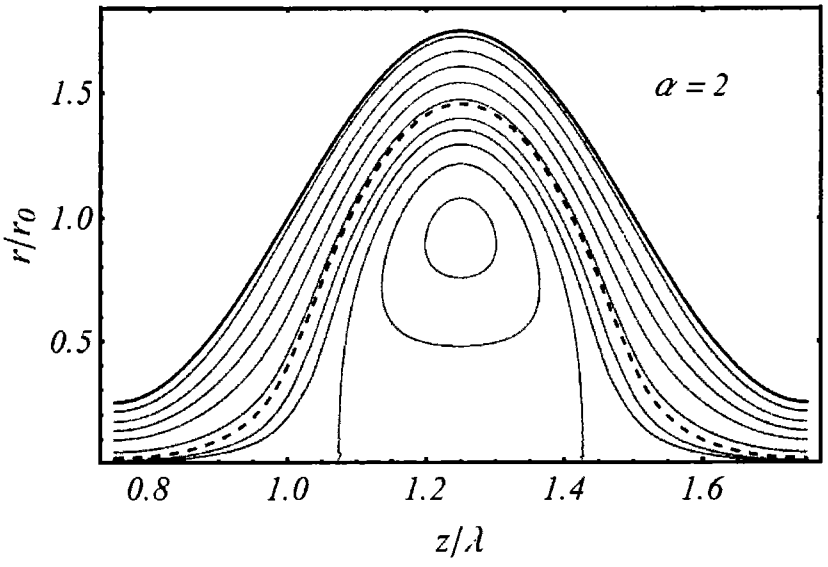

Fig. 3.9 ((a) - (c)): Trapping phenomena for different values of α when $Q = 0$, $\mu_r = 10$, $\beta = 2$, $k = 0.4, U_E = 0, \phi_{oc} = 0.75$.

(d)

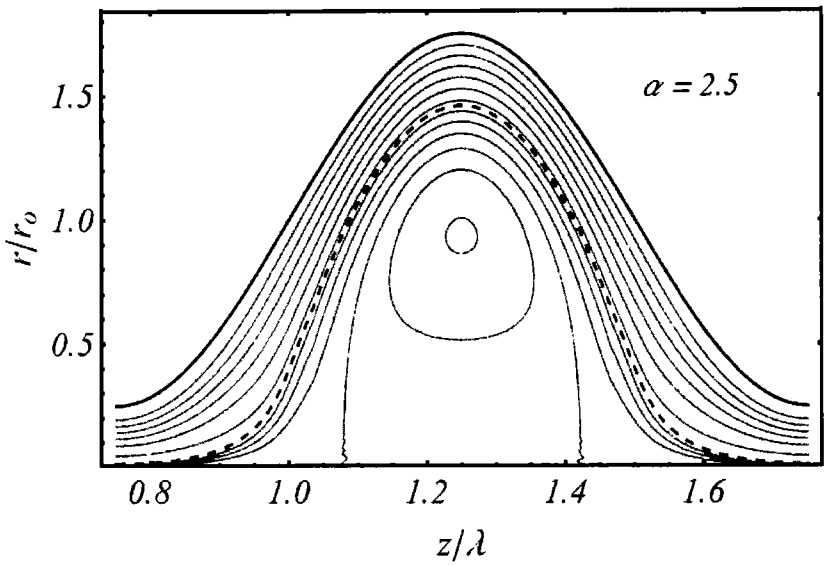

Fig. 3.9 (d): Trapping phenomena for parameter α when $Q = 0$, $\mu_r = 10, \beta = 2, k = 0.4, U_E = 0, \phi_{oc} = 0.75$.

(a)

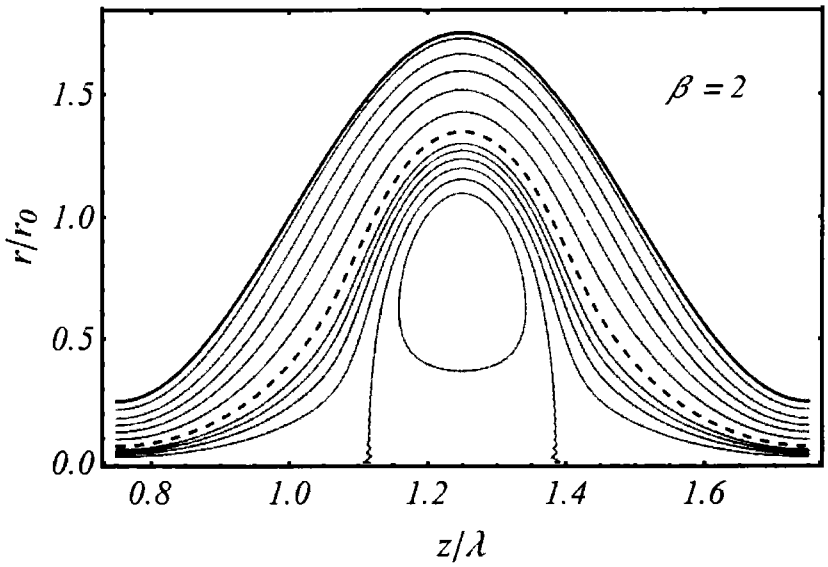

(b)

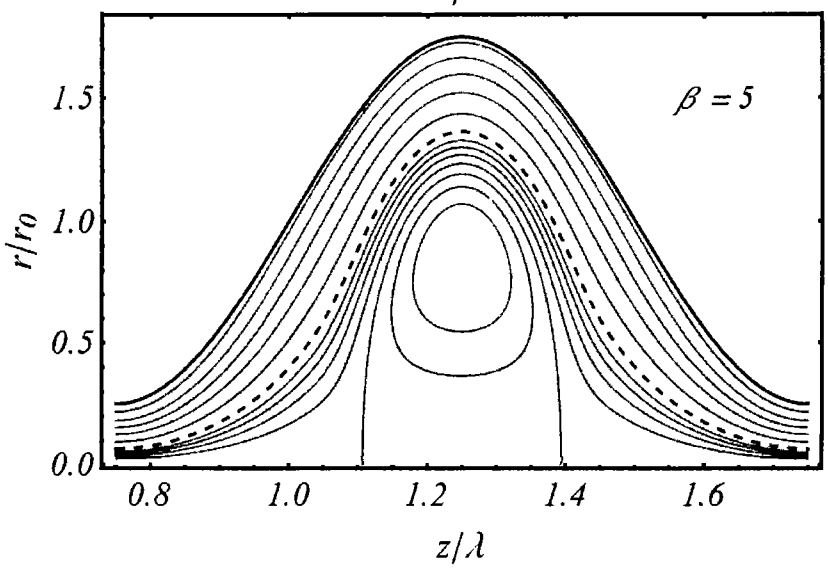

Fig. 3.10 ((a), (b)): The streamline plots showing the trapping for parameter β in core region when $Q = 0$, k=0.4, $\mu_r = 1, \alpha = 1.5, \beta = 2, \phi_{oc} = 0.75, U_E = 0$.

(c)

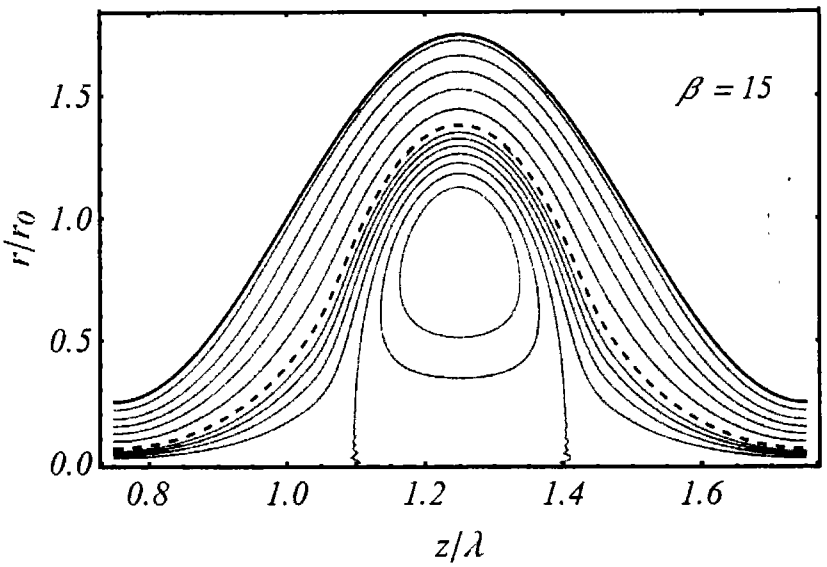

(d)

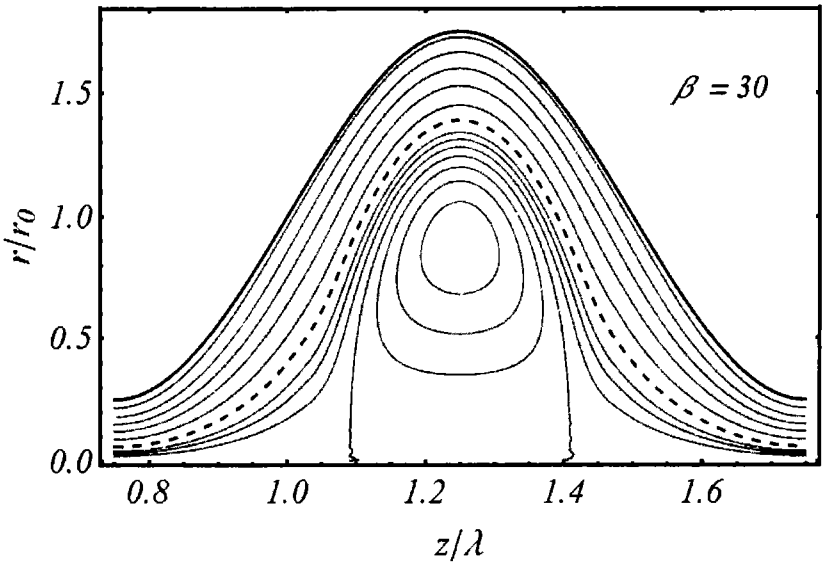

Fig. 3.10 ((c), (d)): The streamline plots showing the trapping for parameter β in core region when $Q = 0$, k=0.4, $\mu_r = 1, \alpha = 1.5, \beta = 2, \phi_{oc} = 0.75, U_E = 0$.

(a)

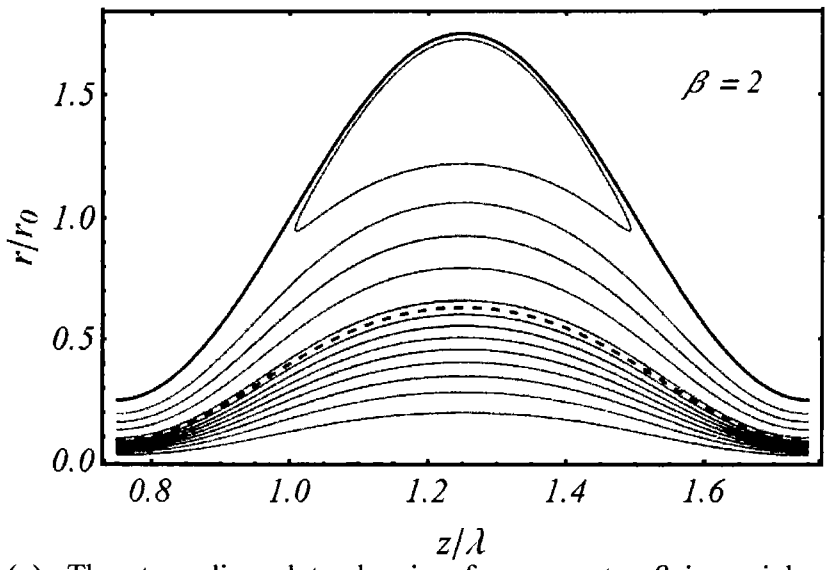

Fig. 3.11 (a): The streamline plots showing for parameter β in peripheral region when $Q = 4$, k=0.4 $\mu_r = 1, \alpha = 1.5, \beta = 2, \phi_{oc} = 0.75, U_E = 0$.

(b)

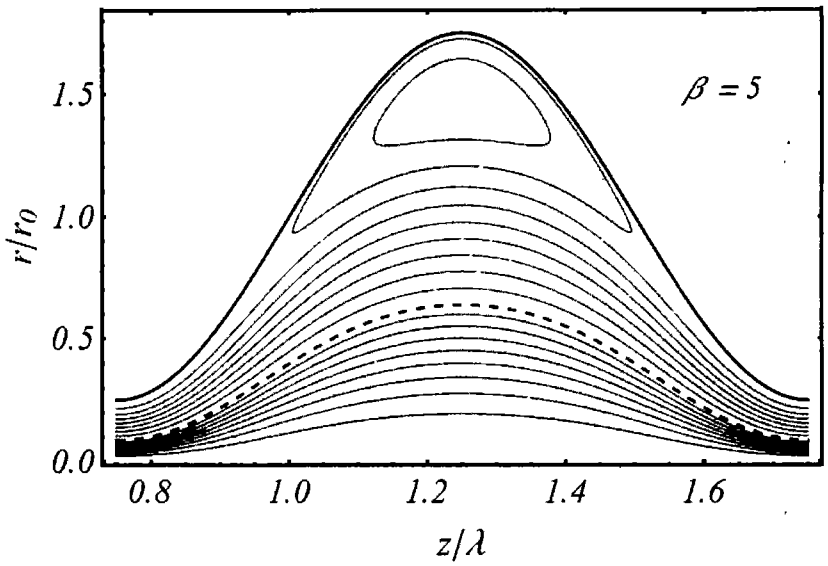

(c)

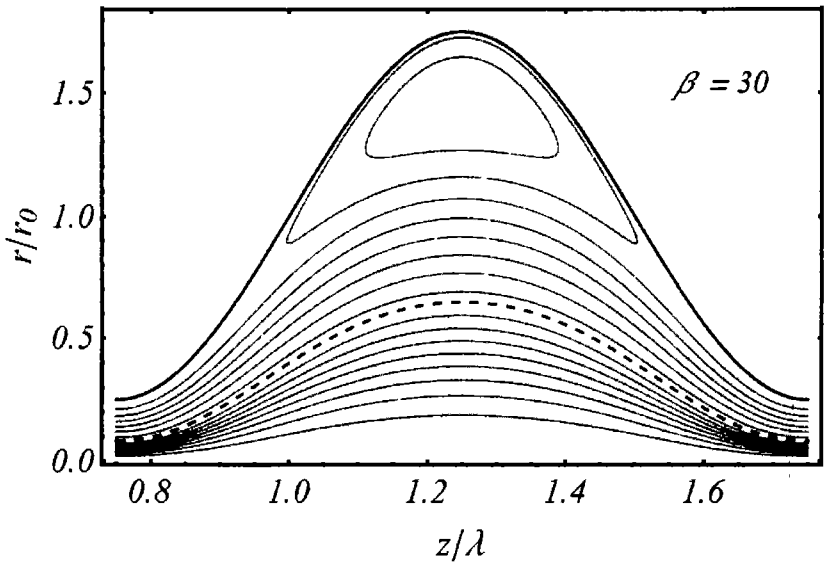

(d)

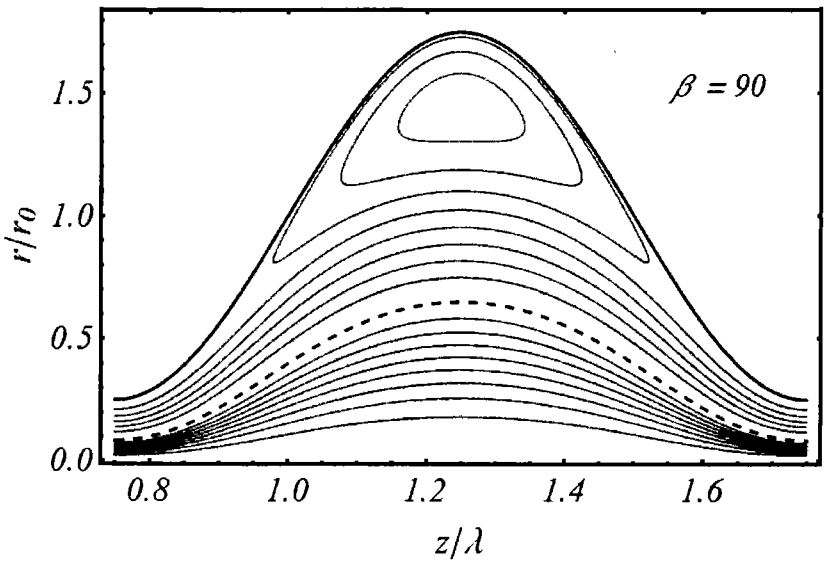

Fig. 3.11 ((b) - (d): The streamline plots showing for parameter β in peripheral region when $Q = 4$, k=0.4 $\mu_r = 1, \alpha = 1.5$, $\beta = 2, \phi_{oc} = 0.75, U_E = 0$.

(a)

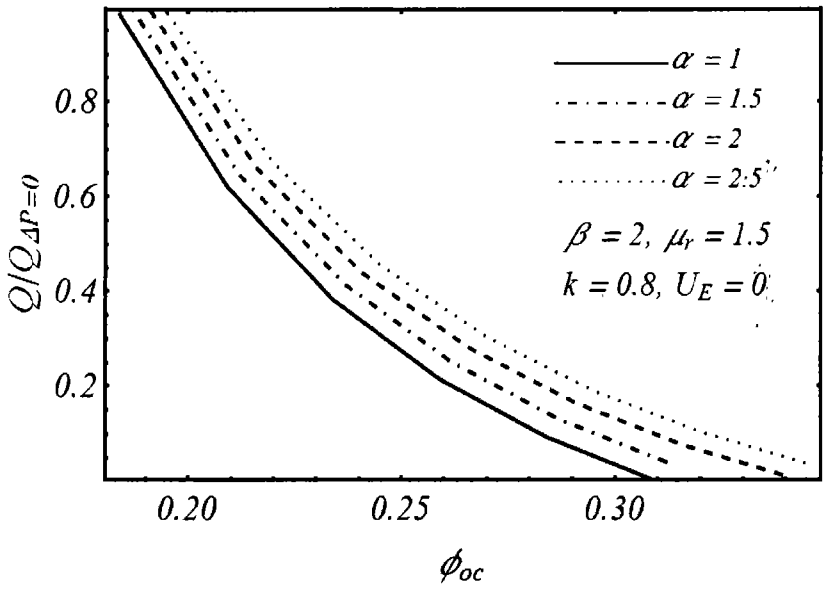

(b)

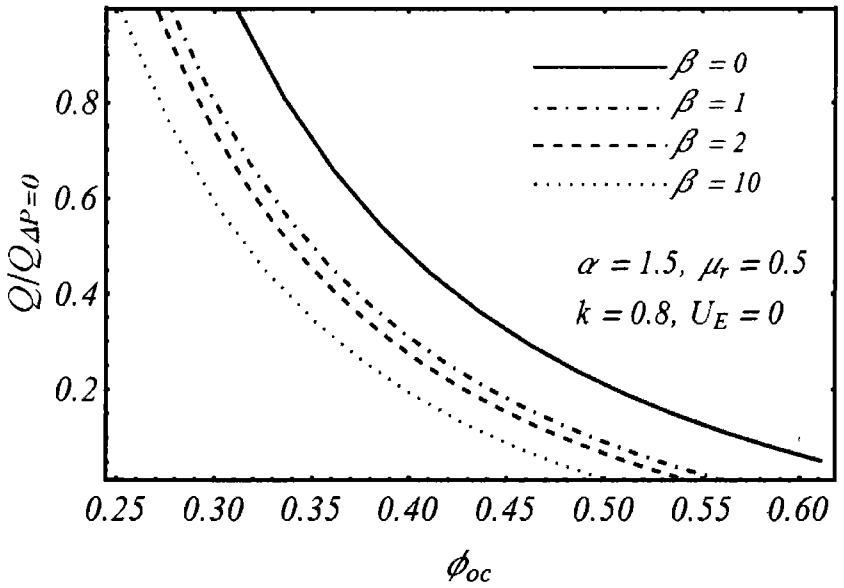

(c)

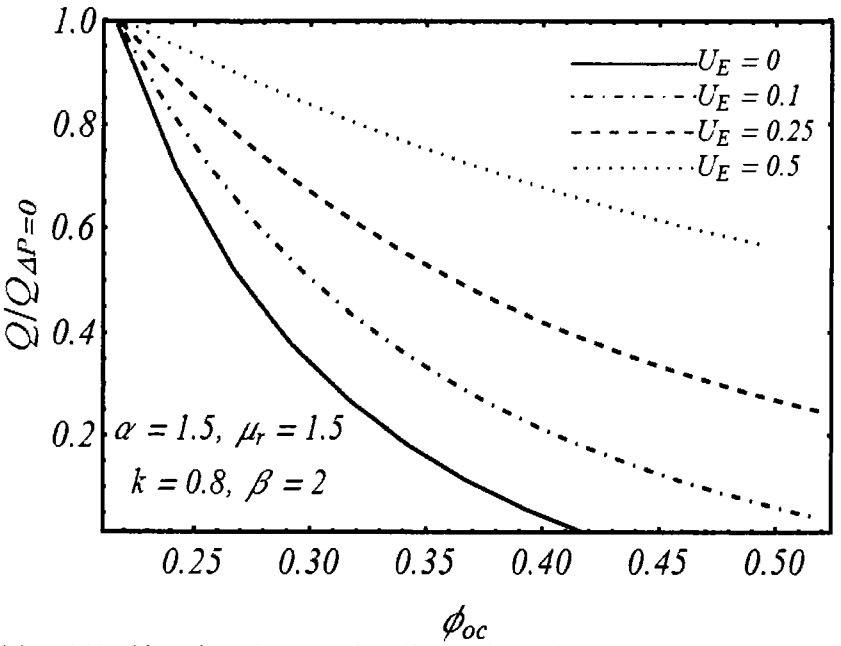

Fig. 3.12 ((a) – (c)): Showing the trapping limits for different values of parameters α, β and U_E.

(d)

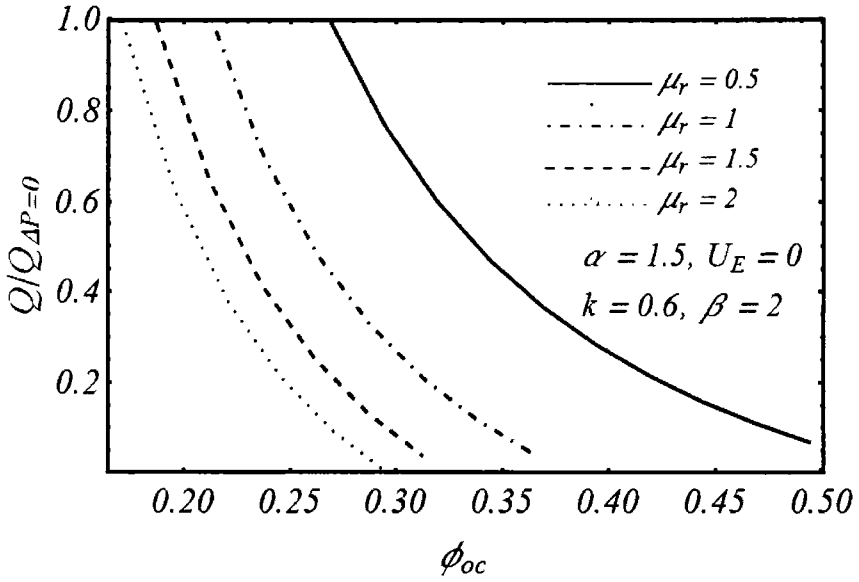

Fig. 3.12 (d): Showing the trapping limits for different values of parameter μ_r.

(a)

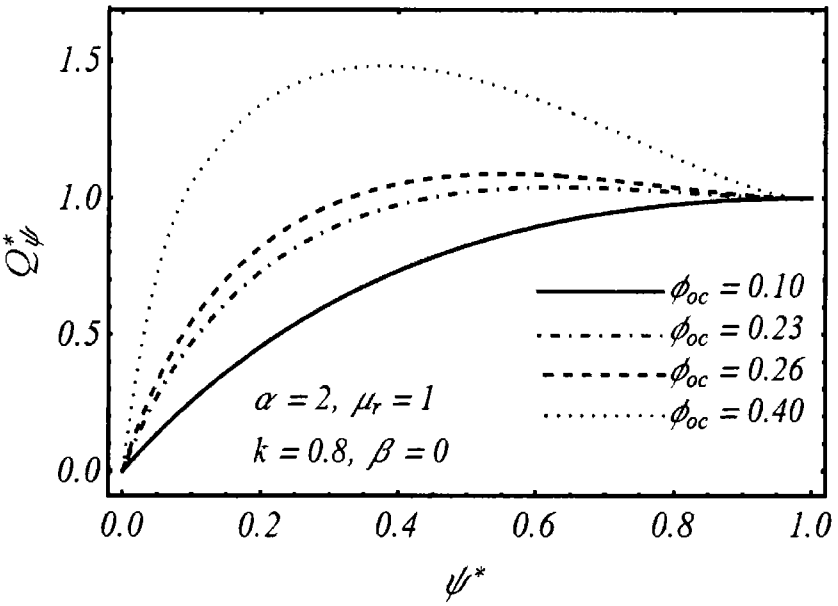

(b)

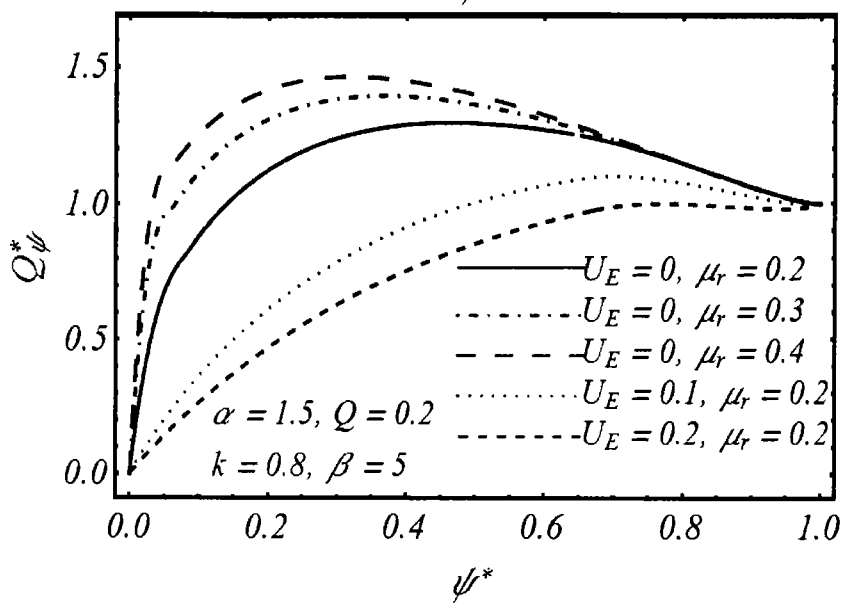

Fig. 3.13 ((a), (b)): Showing the reflux phenomena for Newtonian fluid and U_E, μ_r.

(c)

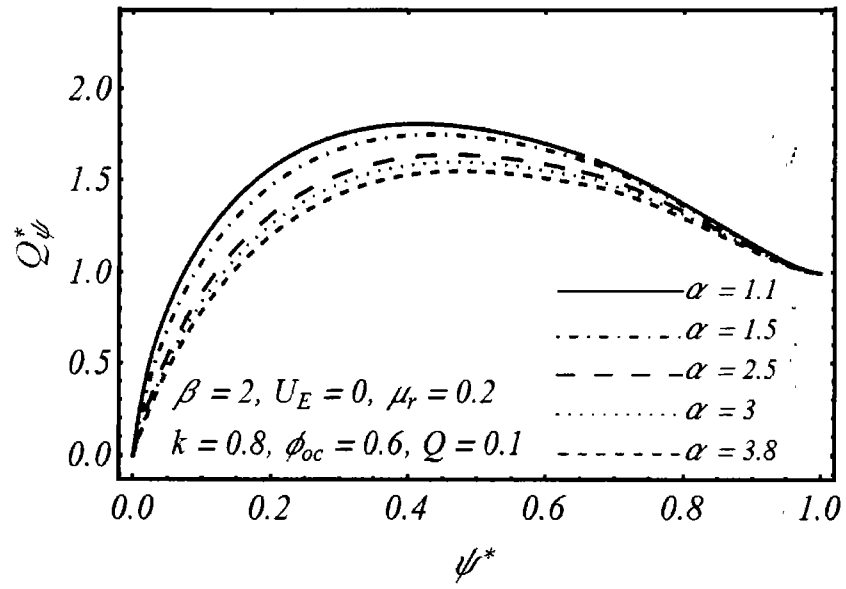

(d)

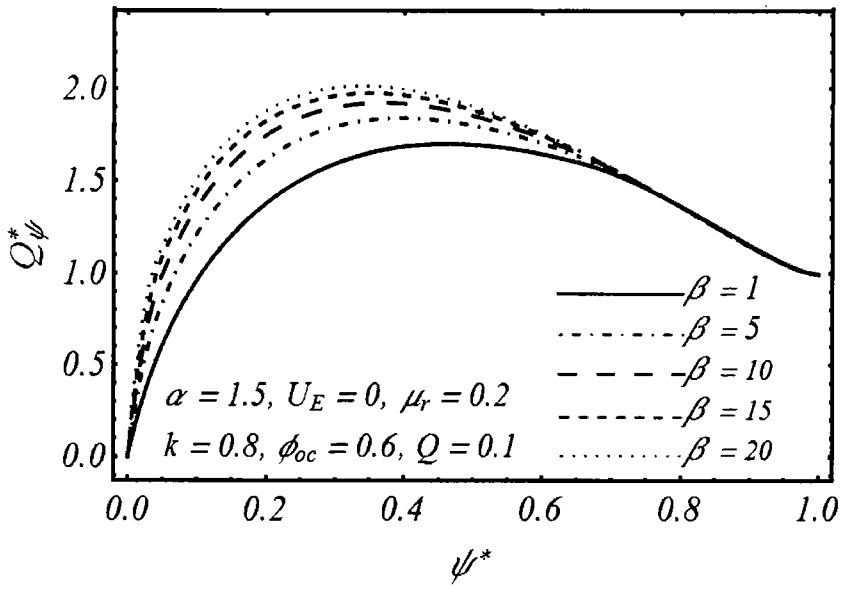

Fig. 3.13 ((c), (d)): Showing the reflux phenomena for different values of parameters α and β.

Chapter 4

Peristaltic flow of Phan-Thien-Tanner fluid: Effects of peripheral layer and electro-osmotic force

In chapter 4, we investigate the two-layer electro-osmotic peristaltic flow of Phan-Thien-Tanner (PTT) fluid in a flexible cylindrical tube. The core (inner) layer fluid satisfies the constitutive equation of PTT fluid model and peripheral (outer) layer is characterized as a Newtonian fluid. For each region, the two-dimensional conservation equations for mass and momentum with electro-osmotic body forces are transformed from the fixed frame to the moving frame of reference. These equations are further modified by invoking the constraints of long wavelength and low Reynolds number. Closed form expressions for velocity and stream function are derived and then employed to investigate the pressure variations, trapping, interface region and reflux for a variety of the involved parameters. The analysis reveals that the trapping and reflux can be restrained by appropriately tuning the electro-kinetic slip parameter and Deborah number. Further, the pumping efficacy can also been improved by adjusting the rheological and the electro-kinetic effects. These results may be helpful for improving the performance of the microfluidic peristaltic pump.

4.1 Basic equations

The constitutive equations for the Phan-Thien-Tanner (PTT) fluid model are (Oliveira and Pinho (1999), Hayat et al. (2010) and Ferras et al. (2012)):

$$\begin{cases} \mathbf{T} = -p\mathbf{I} + \mathbf{S}, \\ f\left(tr(\mathbf{S})\right)\mathbf{S} + \kappa \mathbf{S}^{\nabla} = 2\mu \mathbf{D}, \\ \mathbf{S}^{\nabla} = \dfrac{\partial \mathbf{S}}{\partial t} + (\mathbf{V}.\nabla)\mathbf{S} - \mathbf{S}(\nabla \mathbf{V})^{\mathrm{T}} - (\nabla \mathbf{V})\mathbf{S}. \end{cases} \tag{4.1}$$

where p be the pressure, κ is the relaxation time, $\mathbf{S}$ is an extra-stress tensor, $\mathbf{D}$ is the deformation rate tensor, tr is the trace, $\mathbf{I}$ is the identity tensor, $\mathbf{S}^{\nabla}$ is the Oldroyd's upper-convected derivative, $\mathbf{T}$ is the Cauchy stress tensor and μ is the dynamic viscosity. The function f is defined as

Linearized PTT (LPTT): $$f(tr(\mathbf{S}))\mathbf{S} = 1 + \frac{\varepsilon\kappa}{\mu}(\mathrm{tr}(\mathbf{S})), \tag{4.2}$$

Exponential PTT (EPTT): $$f(tr(\mathbf{S}))\mathbf{S} = \exp\left(\frac{\varepsilon\kappa}{\mu}(\mathrm{tr}(\mathbf{S}))\right). \tag{4.3}$$

4.2 Problem formulation and its solution

The physical sketch of the problem under consideration is shown in **Fig. (4.1).** It describes the flow of a bio-fluid due to combined action of the electro-osmotic force and the peristaltic movement of the tube wall. Two distinct regions can be identified inside the tube; the region adjacent to the wall of tube is outer or peripheral region and the central core is inner or core region. The charged surface of the tube is neutralized through equal and opposite ions in the polar liquid inside the tube. The charged surface attracts the opposite ion in the polar fluid and form a layer near the wall and at the same time repels the co-ions. "The thin layer of immobile counter-ion covering the inner side of the wall is known as Stern layer". A thicker layer of moving counter-ions, known as a diffuse layer, is formed next to the Stern layer. The combination of both "Stern layer and thicker layer is known as electric double layer (EDL)". Now, when a DC potential difference is applied along the axis at the inlet and outlet, an electric field is produced that exerts a body force on the opposite ions of the EDL and as a result of which EDL moves along the channel dragging the neutral core. In the next to come, our aim is to compute the flow fluid generated by both electro-kinetic body force and peristaltic movement of the wall.

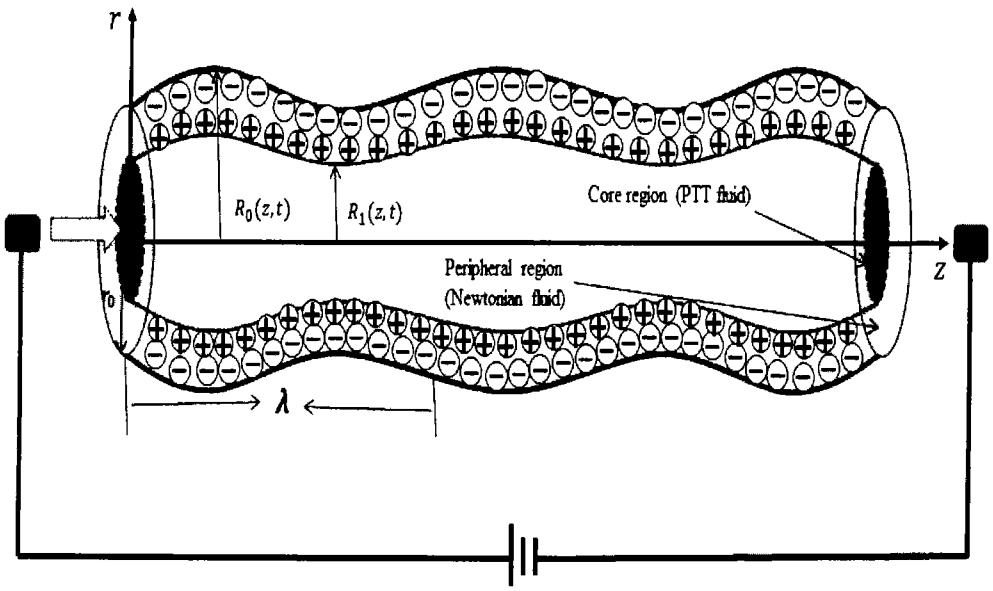

Fig. 4.1: Geometry of the flow problem.

The basic equations necessary to formulate the flow problem are same as the Eq. (3.1) and Eq. (3.2). For axisymmetric incompressible flow in the tube, it is appropriate to define the velocity vector as Eq. (3.5). The transformations of the frames from fixed to wave frames are given as Eq. (3.12) and the dimensionless quantities are defined as Eq. (3.13). To simplify the electro-osmotic body force term we follow the same line of action is adopted as provided in the chapter 3. The components forms of the governing equations in two different regions (core and peripheral regions) after the dimensionless treatment are given as:

Core region:

$$\frac{1}{r}\frac{\partial(ru_c)}{\partial r}+\frac{\partial w_c}{\partial z}=0, \tag{4.4}$$

$$\delta^2\left[\delta Re\left(u_c\frac{\partial u_c}{\partial r}+w_c\frac{\partial u_c}{\partial z}\right)\right]=-\frac{\partial p}{\partial r}+\delta\left[\left(\frac{1}{r}\frac{\partial(rS_{rr})}{\partial r}+\frac{\delta\partial S_{rz}}{\partial z}\right)-\frac{S_{\theta\theta}}{r}\right], \tag{4.5}$$

$$\delta^2\left[\delta Re\left(u_c\frac{\partial w_c}{\partial r}+w_c\frac{\partial w_c}{\partial z}\right)\right]=-\frac{\partial p}{\partial z}+\left[\left(\frac{1}{r}\frac{\partial(rS_{rz})}{\partial r}\right)\right]+\frac{\epsilon_N\mu_r U_E}{\epsilon_c}\rho_{ec}, \tag{4.6}$$

$$f(tr(S))\mu_1 S_{rr}+De\left\{\begin{array}{l}\left(\delta u_c\frac{\partial}{\partial r}+\delta w_c\frac{\partial}{\partial z}\right)\mu_1 S_{rr}-\\ 2\left[\delta\frac{\partial}{\partial r}(u_c)\mu_1 S_{rr}+\delta^2\frac{\partial}{\partial z}(u_c)\mu_1 S_{rz}\right]\end{array}\right\}=2\mu_1\delta\frac{\partial}{\partial r}(u_c), \tag{4.7}$$

$$f(tr(S))\mu_1 S_{rz}+De\left\{\begin{array}{l}\left(\delta u_c\frac{\partial}{\partial r}+\delta w_c\frac{\partial}{\partial z}\right)\mu_1 S_{rz}-\mu_1\frac{\partial w_c}{\partial r}S_{rr}\\ -\left(\delta\frac{\partial w_c}{\partial z}+\delta\frac{\partial u_c}{\partial r}\right)\mu_1 S_{rz}-\delta\mu_1\frac{\partial u_c}{\partial z}S_{zz}\end{array}\right\}=\mu_1\left(\delta^2\frac{\partial u_c}{\partial z}+\frac{\partial w_c}{\partial r}\right), \tag{4.8}$$

$$f(tr(S))\mu_1 S_{r\theta}+De\left\{\begin{array}{l}\left(\delta u_c\frac{\partial}{\partial r}+\delta w_c\frac{\partial}{\partial z}\right)\mu_1 S_{r\theta}-\delta(u_c)\mu_1 S_{r\theta}-\\ \delta u_c\frac{\partial u_c}{\partial r}S_{r\theta}-\overset{3}{\delta}u_c\frac{\partial u_c}{\partial z}\mu_1 S_{z\theta}\end{array}\right\}=0, \tag{4.9}$$

$$f(tr(S))\mu_1 S_{\theta\theta}+De\left\{\left(\delta u_c\frac{\partial}{\partial r}+\delta w_c\frac{\partial}{\partial z}\right)\mu_1 S_{\theta\theta}-2\delta(u_c U)\mu_1 S_{\theta\theta}\right\}=2\mu_1\delta u_c, \tag{4.10}$$

$$f\left(tr\left(S\right)\right)\mu_1 S_{zz} + De\begin{Bmatrix}\left(\delta u_c \dfrac{\partial}{\partial r} + \delta w_c \dfrac{\partial}{\partial z}\right)\mu_1 S_{zz} - 2\mu_1 S_{rz}\left(\dfrac{\partial w_c}{\partial r}\right) \\ -2\mu_1 \delta S_{zz}\left(\dfrac{\partial w_c}{\partial z}\right)\end{Bmatrix} = \mu_1 \delta \frac{\partial w_c}{\partial z}, \quad (4.11)$$

$$\begin{cases} Linearized\ PTT: f\left(tr\left(S\right)\right) = 1 + b\left(S_{zz}\right), \\ Exponential\ PTT: f\left(tr\left(S\right)\right) = \exp\left(b\left(S_{zz}\right)\right). \end{cases} \quad (4.12)$$

Peripheral region:

$$\frac{1}{r}\frac{\partial\left(ru_N\right)}{\partial r} + \frac{\partial w_N}{\partial z} = 0, \quad (4.13)$$

$$\delta^2\left[\delta Re\left(u_N \frac{\partial u_N}{\partial r} + w_N \frac{\partial u_N}{\partial z}\right)\right] = -\frac{\partial p}{\partial r} + \delta\left[\left(\frac{1}{r}\frac{\partial\left(r\, S_{rr}\right)}{\partial r} + \delta\delta S_{rz}\right) - \frac{S_{\theta\theta}}{r}\right], \quad (4.14)$$

$$\delta^2\left[\delta Re\left(u_N \frac{\partial w_N}{\partial r} + w_N \frac{\partial w_N}{\partial z}\right)\right] = -\frac{\partial p}{\partial z} + \left[\left(\frac{1}{r}\frac{\partial\left(r S_{rz}\right)}{\partial r}\right)\right] + \frac{\epsilon_N \mu_r U_E}{\epsilon_c}\rho_{ec}, \quad (4.15)$$

$$S_{rr} = 2\mu_r \delta \frac{\partial u_N}{\partial r}, S_{rz} = S_{zr} = \mu_r\left(\delta^2 \frac{\partial u_N}{\partial z} + \frac{\partial w_N}{\partial r}\right), S_{\theta\theta} = \mu_r \delta \frac{u_N}{r}, S_{zz} = 2\mu_r \delta \frac{\partial w_N}{\partial z},$$

$$S_{r\theta} = S_{\theta r} = S_{\theta z} = S_{z\theta} = 0. \quad (4.16)$$

The subscripts *c, N* are used to differentiate between the core and peripheral region. $\mu_r = \mu_2/\mu_1$ is the viscosity ratio between two-regions. The parameter *De* is the Deborah number and is a measure of the elasticity in the fluid. On the other hand the parameter ϵ is the measure of the extensional property of the fluid. It is evident that variations of *De* have stronger impact than similar variations of ϵ because of the manner in which both parameters appear in the analysis. The combine effects of ϵ and *De* can be felt via a single parameter $b = \varepsilon^{1/2}\, De$ which gives a measure of both elastic and extensional properties of the fluid. At this stage, we make use of long wavelength ($\delta \ll 1$) and low Reynolds number ($Re \ll 1$) constraints to get the following equations for each region.

Core region:

$$\begin{cases} 0 = -\dfrac{\partial p}{\partial z} + \left[\left(\dfrac{1}{r}\dfrac{\partial (r S_{rz})}{\partial r}\right)\right] + \dfrac{\mu_r U_E}{\epsilon_i}\rho_{ec}, \\ 0 = -\dfrac{\partial p}{\partial r}. \end{cases} \tag{4.17}$$

$$\textit{Linearized PTT:} \begin{cases} (1 + bS_{zz})S_{rz} = \left(\dfrac{\partial w_c}{\partial r}\right), \\ (1 + bS_{zz})S_{zz} = 2De\left(\dfrac{\partial w_c}{\partial r}\right)S_{rz}, \\ S_{rr} = S_{\theta\theta} = S_{z\theta} = S_{r\theta} = 0, \end{cases} \tag{4.18}$$

$$\textit{Exponential PTT:} \begin{cases} \exp(2bS_{zz})S_{rz} = \left(\dfrac{\partial w_c}{\partial r}\right), \\ \exp(2bS_{zz})S_{zz} = 2De\left(\dfrac{\partial w_c}{\partial r}\right)S_{rz}, \\ S_{rr} = S_{\theta\theta} = S_{z\theta} = S_{r\theta} = 0, \end{cases} \tag{4.19}$$

where $U_E = -\epsilon_N \xi E_z / \mu_2 U$ is the electro-kinetic slip velocity, ϵ_c and ϵ_N stand for dielectric constants corresponding to inner and outer regions, respectively.

Peripheral region:

$$\begin{cases} 0 = -\dfrac{\partial p}{\partial z} + \left[\left(\dfrac{1}{r}\dfrac{\partial (r S_{rz})}{\partial r}\right)\right] + U_E \dfrac{\mu_r}{\epsilon_N}\rho_{eN}, \\ 0 = -\dfrac{\partial p}{\partial r}, \\ S_{rz} = \mu_r\left(\dfrac{\partial w_N}{\partial r}\right). \end{cases} \tag{4.20}$$

From set of equations (4.18) and (4.19), a simple manipulation gives

$$\begin{cases} \textit{Linearized PTT}: (1 + bS^2{}_{rz})S_{rz} = \dfrac{\partial w_c}{\partial r}, \\ \textit{Exponential PTT}: \exp(2bS^2{}_{rz})S_{rz} = \dfrac{\partial w_c}{\partial r}. \end{cases} \tag{4.21}$$

The appropriate dimensionless boundary conditions for the model under consideration are:

$$\frac{\partial w_c}{\partial r} = 0, \text{at } r = 0; \text{ (symmetry at the centerline)} \tag{4.22}$$

$w_c = w_N$ and $(S_{rz})_N = (S_{rz})_c$ at $r = R_1$; (continuity of shear stress and velocity of the fluid at the interface) (4.23)

$w_N = -1$ at $r = R_0$; (no-slip condition at the wall) (4.24)

From the equations (4.17) and (4.20), we drop the electro-osmotic body force term by incorporating the well-known artifice from the electro-kinetic literature. Through this artifice the plug velocity of electro-osmotic flow can be equivalently achieved either by taking into account the body force term in the momentum equation or observing the effects of this term in the boundary in the form of slip condition based on electro-osmotic slip velocity. In our problem, we shall drop the electro-osmotic body force term from the momentum equation with an appropriate simplification of no-slip boundary condition at the wall. This process is already used by Goswami et al. (2016). In this way, our problem is now governed by the following equations and boundary conditions.

From here onward, we shall follow the approach of Goswami et al. (2016) and drop the electro-osmotic body force term form the momentum in favor of suitable modification of no-slip boundary condition at the wall. In this way, our problem is now governed by the following equations and boundary conditions.

Core region:

$$\begin{cases} 0 = -\dfrac{\partial p}{\partial z} + \left[\left(\dfrac{1}{r}\dfrac{\partial (r S_{rz})}{\partial r}\right)\right], \\ 0 = -\dfrac{\partial p}{\partial r}. \end{cases} \tag{4.25}$$

$$\begin{cases} Linearized\ PTT : \left(1 + bS^2{}_{rz}\right) S_{rz} = \dfrac{\partial w_c}{\partial r}, \\ Exponential\ PTT : \exp\left(2bS^2{}_{rz}\right) S_{rz} = \dfrac{\partial w_c}{\partial r}, \end{cases} \tag{4.26}$$

$$\frac{\partial w_c}{\partial r} = 0, \text{at } r = 0. \tag{4.27}$$

Peripheral region:

$$\begin{cases} 0 = -\dfrac{\partial p}{\partial z} + \left[\left(\dfrac{1}{r}\dfrac{\partial (r S_{rz})}{\partial r}\right)\right], \\ 0 = -\dfrac{\partial p}{\partial r}, \\ S_{rz} = \mu_r \left(\dfrac{\partial w_N}{\partial r}\right). \end{cases} \tag{4.28}$$

$$\begin{aligned} &\frac{\partial w_N}{\partial r} = 0, \text{at } r = 0, \\ &\mathrm{w}_N = U_E - 1, \text{at } r = R_0. \end{aligned} \tag{4.29}$$

In order to adopt stream function formulation, it is appropriate to define

$$u = -\frac{\partial \psi^*}{\partial z}, w = -\frac{1}{r}\frac{\partial \psi^*}{\partial r}, \tag{4.30}$$

where ψ^* is the stream function in the moving frame and it is associated to its counterpart in the fixed frame according to the relation $\psi = \psi^* - \frac{r^2}{2}$. Employing the definition of stream function, equations and boundary condition governing the flow read

$$\textit{Linearized PTT: } \frac{\partial}{\partial r}\left(\frac{1}{r}\frac{\partial \psi}{\partial r}\right) = \frac{r}{2}\frac{\partial p}{\partial z} + \frac{b}{4}\left(\frac{\partial p}{\partial z}\right)^3 r^3 \quad , 0 \le r \le R_1 \tag{4.31}$$

$$\textit{Exponential PTT: } \frac{\partial}{\partial r}\left(\frac{1}{r}\frac{\partial \psi}{\partial r}\right) = \exp\left(\frac{b}{2}\left(\frac{\partial p}{\partial z}\right)^2 r^2\right)\frac{r}{2}\frac{\partial p}{\partial r} \quad , 0 \le r \le R_1 \tag{4.32}$$

$$\frac{\partial p}{\partial z} = \frac{1}{r}\frac{\partial}{\partial r}\left[\left(r\mu_r \frac{\partial}{\partial r}\left(\frac{1}{r}\frac{\partial \psi}{\partial r}\right)\right)\right] \quad , R_1 \le r \le R_0 \tag{4.33}$$

$$\psi = 0, \frac{\partial}{\partial r}\left(\frac{1}{r}\frac{\partial \psi}{\partial r}\right) = 0 \text{ at } r = 0, \tag{4.34}$$

$$\psi = \frac{q}{2}, \frac{\partial \psi}{\partial r} = (U_E - 1) R_0 \text{ at } r = R_0, \tag{4.35}$$

$$\psi = \frac{q_1}{2}, \text{ at } r = R_1. \tag{4.36}$$

In above equations q and q_1 stand for volume flow rate over the outer and the inner cross-section, respectively. Solving Eqs. (4.31) - (4.33) subject to the boundary conditions (4.34) and (4.35), the stream function for each region appears as

For linearized PTT model:

$$\psi = \begin{cases} \dfrac{r^2}{2}\left\{\left(U_E - 1\right) + \dfrac{b}{48}\left(\dfrac{\partial p}{\partial z}\right)^3\left[r^4 - 3R_1^4\right] + \dfrac{1}{8}\dfrac{\partial p}{\partial z}\left(\left\{r^2 - 2R_1^2\right\} + \dfrac{2}{\mu_r}\left\{R_1^2 - R_0^2\right\}\right)\right\}, 0 \le r < R_1 \\ \dfrac{r^2}{2}\left(U_E - 1\right) + \left(\dfrac{q}{2} - \left(U_E - 1\right)\dfrac{R_0^2}{2}\right) + \dfrac{1}{4\mu_r}\dfrac{\partial p}{\partial z}\left(r^2 - R_0^2\right)^2 . R_1 \le r \le R_0 \end{cases} \tag{4.37}$$

For exponential PTT model:

$$\psi = \begin{cases} \dfrac{1}{b\left(\dfrac{\partial p}{\partial z}\right)^2}\dfrac{\partial p}{\partial z}\left[\exp\left(b\left(\dfrac{\partial p}{\partial z}\right)^2\dfrac{r^2}{2} - 1\right)\right] + \dfrac{r^2}{2}\left(\begin{array}{l}\left(U_E - 1\right) + \dfrac{1}{4\mu_r}\dfrac{\partial p}{\partial z}\left(R_1^2 - R_0^2\right) \\ - \dfrac{1}{2b\left(\dfrac{\partial p}{\partial z}\right)^2}\dfrac{\partial p}{\partial z}\exp\left(b\left(\dfrac{\partial p}{\partial z}\right)^2\dfrac{R_1^2}{2}\right)\end{array}\right), 0 \le r < R_1 \\ \dfrac{r^2}{2}\left(U_E - 1\right) + \left(\dfrac{q}{2} - \left(U_E - 1\right)\dfrac{R_0^2}{2}\right) + \dfrac{1}{4\mu_r}\dfrac{\partial p}{\partial z}\left(r^2 - R_0^2\right)^2 . R_1 \le r \le R_0 \end{cases} \tag{4.38}$$

From the above expressions and Eq. (4.30), the axial velocity corresponding to inner and outer region for both linearized and exponential PTT fluid models becomes

For linearized PTT model:

$$w(r,z) = \begin{cases} \left(U_E - 1\right) + \dfrac{b}{16}\left(\dfrac{\partial p}{\partial z}\right)^3\left[r^4 - R_1^4\right] + \dfrac{1}{4}\dfrac{\partial p}{\partial z}\left(\left\{r^2 - R_1^2\right\} + \dfrac{1}{\mu_r}\left\{R_1^2 - R_0^2\right\}\right), 0 \le r \le R_1 \\ \left(U_E - 1\right) + \dfrac{1}{4\mu_r}\dfrac{\partial p}{\partial z}\left(r^2 - R_0^2\right) . R_1 \le r \le R_0 \end{cases} \tag{4.39}$$

For exponential PTT model:

$$w(r,z)=\begin{cases}\dfrac{1}{b\left(\dfrac{\partial p}{\partial z}\right)^2}\dfrac{\partial p}{\partial z}\left[\exp\left(\exp\left(b\left(\dfrac{\partial p}{\partial z}\right)^2\dfrac{r^2}{2}-\exp b\left(\dfrac{\partial p}{\partial z}\right)^2\dfrac{R_1^2}{2}\right)\right)\right] \\ +(U_E-1)+\dfrac{1}{4\mu_r}\dfrac{\partial p}{\partial z}\left\{R_1^2-R_0^2\right\}, 0\le r\le R_1 \\ (U_E-1)+\dfrac{1}{4\mu_r}\dfrac{\partial p}{\partial z}\left(r^2-R_0^2\right). R_1\le r\le R_0\end{cases} \tag{4.40}$$

The function characterizing wall deformation in dimensionless is

$$R_o(z)=1+\phi_{oc}\sin(2\pi z), \tag{4.41}$$

where ϕ_{oc} is the occlusion parameter.

The solution of the considered problem is still incomplete because of two unknowns R_1 and $\partial p/\partial z$ appearing in the Eq. (4.37) and (4.38). In order to obtain these unknowns, a semi-analytical approach Goswami et al. (2016) is used. Invoking the boundary condition (4. 36) yields

$$\frac{q_1}{2}=\frac{R_1^2}{2}(U_E-1)+\left(\frac{q}{2}-(U_E-1)\frac{R_0^2}{2}\right)+\frac{1}{16\mu_r}\frac{\partial p}{\partial z}\left(R_1^2-R_0^2\right)^2. \tag{4.42}$$

In order to eliminate the q_1, we set $R_0=1$ and $R_1=k$ at $z=0$ in Eq. (4.42), to get

$$\frac{q_1}{2}=\frac{k^2}{2}(U_E-1)+\left(\frac{q}{2}-(U_E-1)\frac{1}{2}\right)+\frac{1}{16\mu_r}P_0\left(k^2-1\right)^2. \tag{4.43}$$

Eliminating q_1 from Eqs. (4.42) and (4.43), we get

$$\begin{aligned}&\frac{k^2}{2}(U_E-1)+\left(\frac{q}{2}-(U_E-1)\frac{1}{2}\right)+\frac{1}{16\mu_r}P_0\left(k^2-1\right)^2=\frac{R_1^2}{2}(U_E-1)+ \\ &\left(\left(\frac{q}{2}-(U_E-1)\frac{R_0^2}{2}\right)+\frac{1}{16\mu_r}\frac{\partial p}{\partial z}\left(R_1^2-R_0^2\right)^2\right),\end{aligned} \tag{4.44}$$

where k is the inner layer thickness measured at $z = 0$ from the boundary wall and $P_0 = (\partial p/\partial z)|_{z=0}$. In this way, q_1 is replaced by another unknown P_0. Now, there are

three unknown to be determined i.e., P_0, R_1 and $\partial p/\partial z$. However, there is only one condition available, i.e., Eq. (4.44). The other two conditions can be furnished as follow: Since the stream function given by the Eqs. (4.37) and (4.38) for both regions, must be same at the interface, therefore, the following equation emerges.

Linearized PTT:

$$b\left(\frac{\partial p}{\partial z}\right)^3 R_1^6+\frac{1}{16}\frac{\partial p}{\partial z}R_1^4+\frac{1}{16\mu_r}\frac{\partial p}{\partial z}\left(R_0^4-R_1^4\right)+\frac{q}{2}-\left(U_E-1\right)\frac{R_0^2}{2}=0, \tag{4.45}$$

Exponential PTT:

$$\frac{1}{b\left(\partial p/\partial z\right)^2}\partial p/\partial z\left[\exp\left(b\left(\partial p/\partial z\right)^2\frac{R_1^2}{2}-1/b\left(\partial p/\partial z\right)^2\right)\right]+\frac{q}{2}-\left(U_E-1\right)\frac{R_0^2}{2}+$$
$$\frac{1}{16\mu_r}\frac{\partial p}{\partial z}\left(R_0^4-R_1^4\right)=0, \tag{4.46}$$

Setting $R_0=1$ and $R_1=k$ at $z=0$, the above expressions become

Linearized PTT: $$\frac{b}{48}P_0^3k^6+\frac{1}{16}P_0k^4+\frac{1}{16\mu_r}P_0\left(1-\mathrm{k}^4\right)+\frac{q}{2}-\left(U_E-1\right)\frac{1}{2}=0. \tag{4.47}$$

Exponential PTT:
$$\frac{1}{b\left(P_0\right)^2}P_0\left[\exp\left(b\left(P_0\right)^2\frac{R_1^2}{2}-1/b\left(P_0\right)^2\right)\right]$$
$$+\frac{q}{2}-\left(U_E-1\right)\frac{1}{2}+\frac{1}{16\mu_r}P_0\left\{1-\mathrm{k}^4\right\}=0, \tag{4.48}$$

Eqs. (4.44) - (4.48) are solved numerically using the bisection technique at each axial station z to obtain the values of $P_0, R_1, \partial p/\partial z$ for both linearized and exponential PTT fluid models. Mathematica 8.1 has been used for producing the numerical results. It is mentioned that analytic treatment of Eqs. (4.45) and (4.47) is possible for LPTT model and one has to deal numerically only with Eq. (4.44). In contrast no such liberty is available for EPTT model and therefore all three Eqs. (4.44), (4.46) and (4. 44) must be solved numerically.

The interface polynomial for limiting case, that is, the fluids in the both regions are Newtonian, can be obtained by taking $b = 0$ in above expressions as:

4.3 Results and discussions

4.3.1 Analysis of interface region

The parameter b is the measure of non-Newtonian shear-thinning behavior of the core region fluid. Greater values of this parameter correspond to the enhanced shear-thinning effects of the inner (core) region fluid. The parameter μ_r is the ratio of the viscosity of the outer (peripheral) region and the core region. Three cases arise depending on the values of μ_r. The situation when the viscosity of the inner (core) region exceeds the viscosity of the outer (peripheral) region is represented by taking $\mu_r < 1$. When both regions have equal viscosities then $\mu_r = 1$. Similarly, $\mu_r > 1$ corresponds to the situation when the viscosity of the outer (peripheral) region exceeds the viscosity of the inner (core) region. The remaining important parameter in the problem is denoted by U_E and is known as electro-kinetic slip velocity. Naturally, each of the above mentioned parameters affect the interface shape, pumping characteristics, trapping and reflux. In order to quantify such effects, **Figs. (4.2(a - c))** are prepared. **Fig. (4.2(a - c))** shows that an increase in the viscosity ratio leads to an increase in the vertical force experienced by the peripheral fluid in upper level or (wave crest) region. Further, the peripheral fluid in the trough region experience is an increased vertically downward force with increasing the viscosity ratio. In such an arrangement the interface curves for $\mu_r < 1$ and $\mu_r = 1$ lies in between the interface curves for $\mu_r < 1$ and $\mu_r > 1$. In contrast, the peripheral fluid in the crest region experience is an increased vertically downward force with increasing the electro-kinetic slip velocity. While the peripheral fluid in the trough region is acted upon an increased upward force with increasing the electro-kinetic slip velocity. A similar variation in the interface is noted with increasing the parameter b as observed with raising the parameter μ_r. However, the peripheral fluid in the crest region is less sensitive to an increase in the parameter b in comparison to the peripheral fluid in the trough region for which the effects of b are much prounced. As a result the interface curves for $b = 4$ shows larger deviation from the corresponding interfacial curves for $b = 0.1$. Such a deviation is attributed to enhance shear-thinning in viscosity for larger values of the parameter b and the greater deformation gradients in the trough region.

A comparison between the predictions of the linear PTT model and the exponential PTT model is presented in **Fig. (4.3(a - c)).** It is observed that the results of both

models are in excellent correlation for smaller values of the parameter b. However, the deviation between the results of both models amplifies as the parameter b increases. Therefore, we have presented the subsequent results only for EPTT model.

4.3.2 Pressure expression and graphical discussion

From Eq. (3.44), the expression of pressure gradient $\partial p/\partial z$ in the tube is given by

$$\frac{\partial p}{\partial z}=\frac{16\mu_r}{\left(R_1^2-R_0^2\right)^2}\left\{\frac{1}{2}\left(U_E-1\right)\left(k^2-R_1^2+R_0^2\right)+\frac{1}{16\mu_r}P_0\left(k^2-1\right)^2\right\}. \tag{4.49}$$

The change in pressure rise across one wavelength is obtained by integrating the above expression as follows

$$\Delta p=16\mu_r\int_0^{\lambda}\left\{\frac{\left(\frac{1}{2}\left(U_E-1\right)\left(k^2-R_1^2+R_0^2\right)+\frac{1}{16\mu_r}P_0\left(k^2-1\right)^2\right)}{\left(R_1^2-R_0^2\right)^2}\right\}dz. \tag{4.50}$$

The volume flux in moving and fixed frame of references are linked through with the following expression

$$Q_S=2\int_0^{R_0}\left(w+1\right)r\,dr=q+R_0^2. \tag{4.51}$$

The above expression after time-averaging over a complete period gives

$$Q=\frac{1}{T_P}\int_0^{T_P}Q_S\,dt=q+\left(1+\frac{\phi^2}{2}\right), \tag{4.52}$$

where T_P is a complete period.

The integration in Eq. (4.50) is performed numerically and the profiles of pressure rise per wavelength at zero volumetric flow rate, i.e., $\Delta P_0=\Delta P\big|_{Q=0}$ against the occlusion parameter are demonstrated in **Fig. (4.4(a, b)).** Special attention is given to seek the influence of the key parameters such as electro-kinetic slip velocity U_E, viscosity ratio μ_r, and the rheological parameter b on the pressure rise at zero volume flow rate. It is observed that both electro-kinetic slip velocity (U_E) and viscosity ratio (μ_r) amplify the pressure rise at zero volume flow rate. The amplification with raising U_E is maximum at lower occlusion values and least when occlusion parameter approaches unity. On the other hand, increase in ΔP_0 with increasing μ_r is observed over the entire range of occlusion parameter. Contrary to effects of U_E and μ_r, an

increase in the fluid rheological parameter b causes a decrement in the pressure required to evolve zero volume flow rate. Again, this decrease is a consequence of enhanced shear-thinning in viscosity of fluid in the core region for larger values of b.

4.3.3 Trapping phenomenon

Trapping corresponds to the formation of eddying regions in the flow domain. Such regions enclose a volume of fluid which is usually known bolus in the literature .The bolus is transported along the tube via the peristaltic activity with the speed of wave. Its formation is linked with the bulk momentum of the flow. The zones of low bulk momentum are more vulnerable to the bolus formation in comparison to the region where bulk movement is high. **Figs. (4.5(a - d) - 4.9(a, b))** illustrates the effects of electro-kinetic slip velocity on the trapped bolus in both core and peripheral region. It is evident that trapped bolus reduces in size and eventually vanishes with raising the electro-kinetic slip velocity. In contrast, raising the parameter b results in an increase in size and circulation of the trapped bolus. Similar results are obtained with increasing the viscosity ratio μ_r. Another important aspect is to find the trapping limit on the normalized volume flow rate for a given set of the involved parameters. To do so, we have plotted the normalized volume flow rate $Q/Q_{\Delta p=0}$ against the occlusion parameter for several values of b and U_E. In fact, the values of stream function lies between 0 and Q where $\psi = 0$ is the center streamline while $\psi = Q$ represents the boundary wall. In order to obtain the pair $\left(\phi_{oc}, Q/Q_{\Delta p=0}\right)$, the first step is to locate a sub-region in the flow domain $\left\{0 \le \phi_{oc} \le 1 : 0 \le Q/Q_{\Delta p=0} \le 1\right\}$ where the stream function ψ changes its sign from negative to positive. In the next step, a suitable iterative technique is used to evaluate the exact value of the pair $\left(\phi_{oc}, Q/Q_{\Delta p=0}\right)$ at which the transition occurs. The region above a specific curve in each figure is the region of trapping. It is observed that trapping region expands with increasing the parameter b while it narrows down with enhancing the electro-kinetic slip velocity.

4.3.4 Reflux

The phenomenon which estimates the net flow of fluid in a complete wave cycle is known as reflux. It happens due to an unfavorable pressure gradient across the tube or backward motion of the fluid elements within the tube. The reflux phenomena in both regions is strongly dependent on the involved parameters, such as, electro-kinetic slip

velocity, viscosity ratio and b. In the earlier analyses Brasseur et al. (1987) estimated the amount of reflux through the quantity $(Q-Q_\psi)/Q$ during a wave cycle, where Q_ψ is given by the relation Rao and Mishra (2004)

$$Q_\psi = 2\psi + \int_0^1 r^2 dz. \tag{4.53}$$

Expression (4.53) arises as a consequence of transforming the expression $Q_{\psi'} = 2\int_0^{r(\psi' z)} rwdr$ from the fixed frame to the wave frame and then averaging over one period of wave. The quantity $Q_{\psi'}$ is the average volumetric flow rate between the axis of the tube and a streamline $\psi' = \text{constant}$ in the fixed frame. The quantity $(Q-Q_\psi)/Q$ is such that $1<(Q-Q_\psi)/Q<0$ because $0<Q_\psi/Q<1$. However, it may happen that Q_ψ/Q takes values greater than unity from some values of ψ' thereby indicating that there is some sort of backward motion or reflux in the flow domain. **Fig. (4.10(a, b))** shows that reflux is enhanced by increasing the parameter b while it reduces with the increase in electro-kinetic slip velocity.

4.4 Deductions

In this chapter, we study the electro-osmotic peristaltic flow of PTT fluid model in contact with the Newtonian in a tube. The governing equations are simplified by using well known approximations of long wave length and low Reynolds number. The main focus of this study is to highlight the effects of electro-kinetic slip velocity and PTT model parameters on pressure rise per wavelength, interface region, trapping and reflux phenomena. The information about these phenomena is important for both physiological and industrial application of peristaltic transport. Our study reveals that both trapping and reflux can be controlled either by increasing the strength of the applied electric field or by exploiting the viscoelastic and extensional characteristics of the core region fluid. In fact, it turns out that in order avoid trapping and reflux the non-dimensional number b which provides a measure of both the extensional (measured by ϵ) and the elastic (measured by De) characteristics of the core fluid must be kept small. This observation also advocates carrying out a complete rheological characterization of the material in the core region. In contrast, the efficiency of the pumping can be improved by taking the lower values of the non-

dimensional group b associated with the core region fluid or by regulating the strength of the applied electric field.

(a)

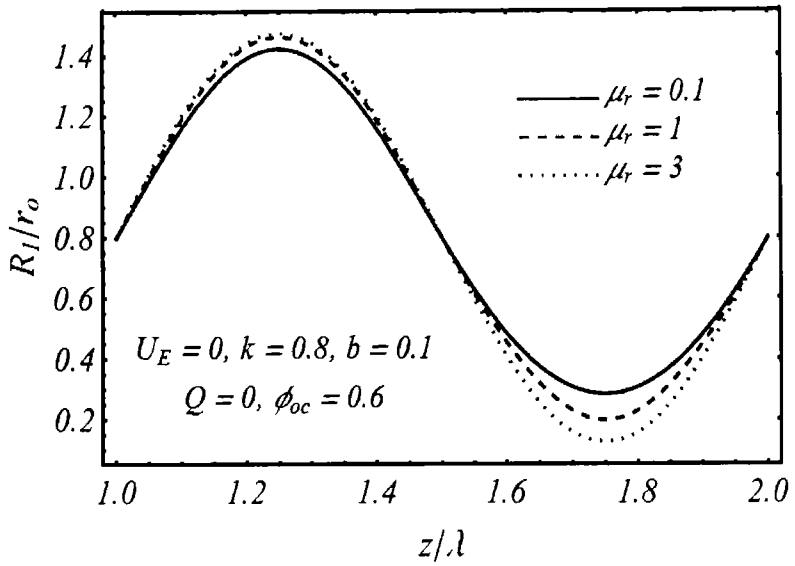

(b)

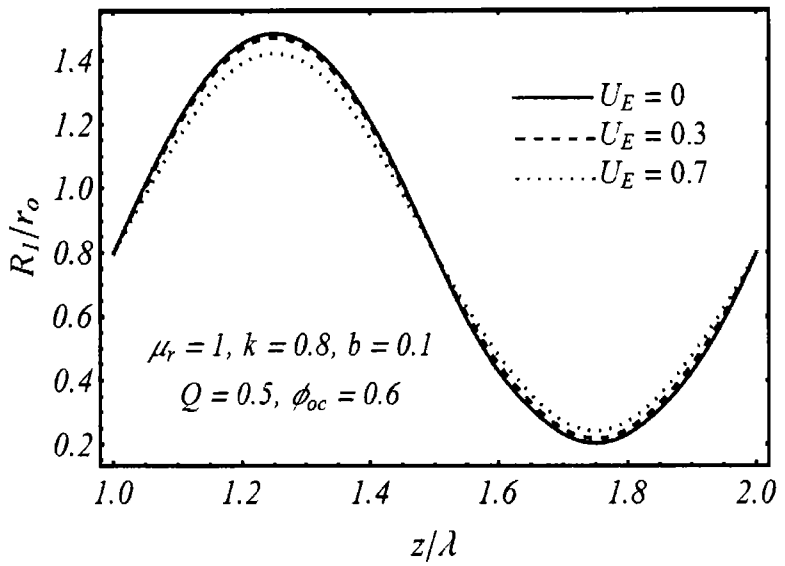

(c)

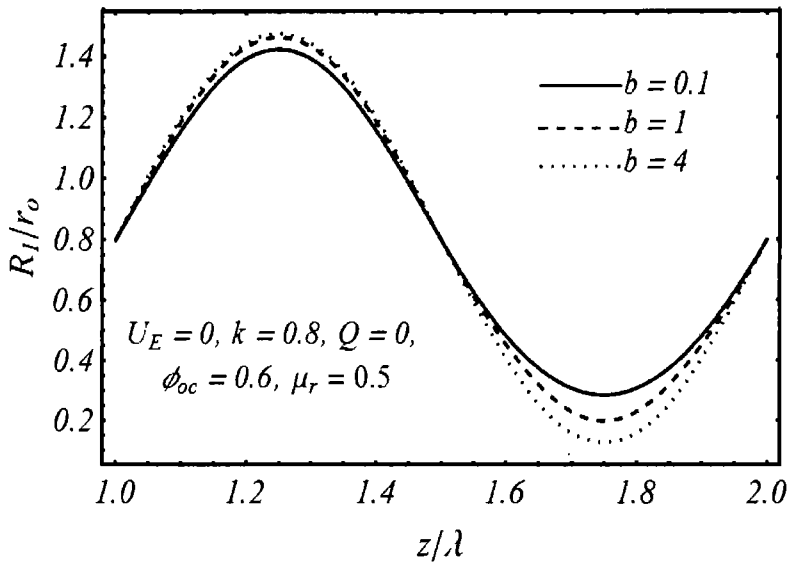

Fig. 4.2 ((a) – (c)): The behavior of interface region with respect to μ_r, U_E and b.

(a)

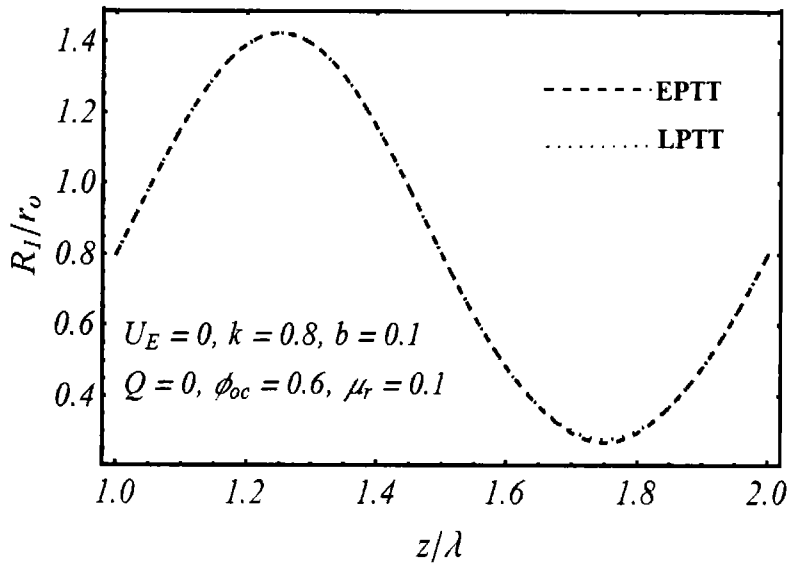

(b)

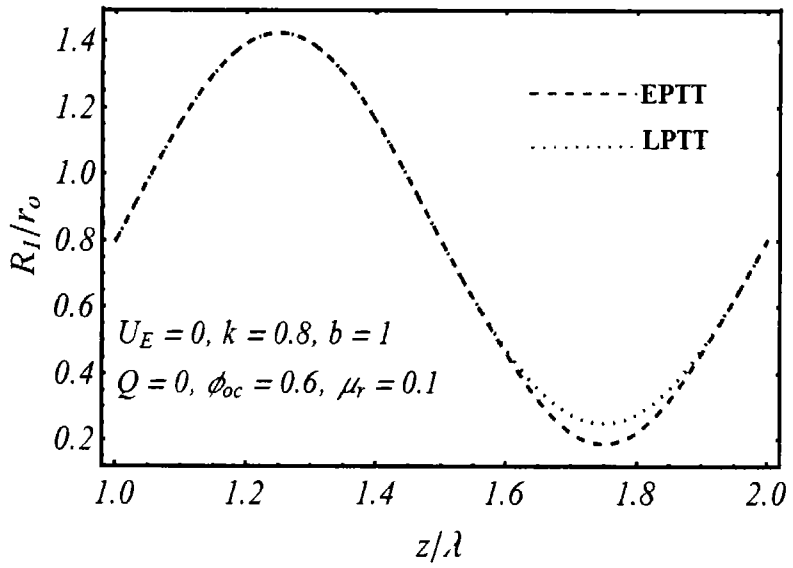

(c)

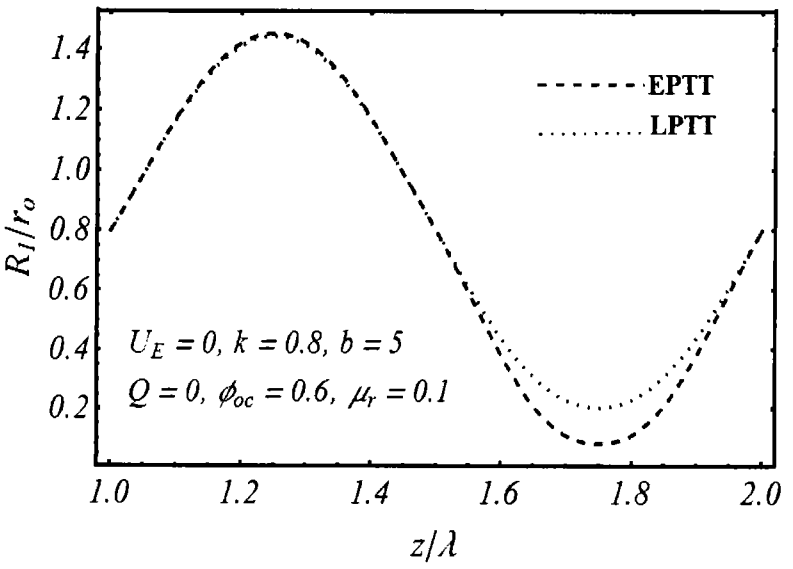

Fig. 4.3 ((a) - (c)): Comparison between the results of linear and exponential PTT models.

(a)

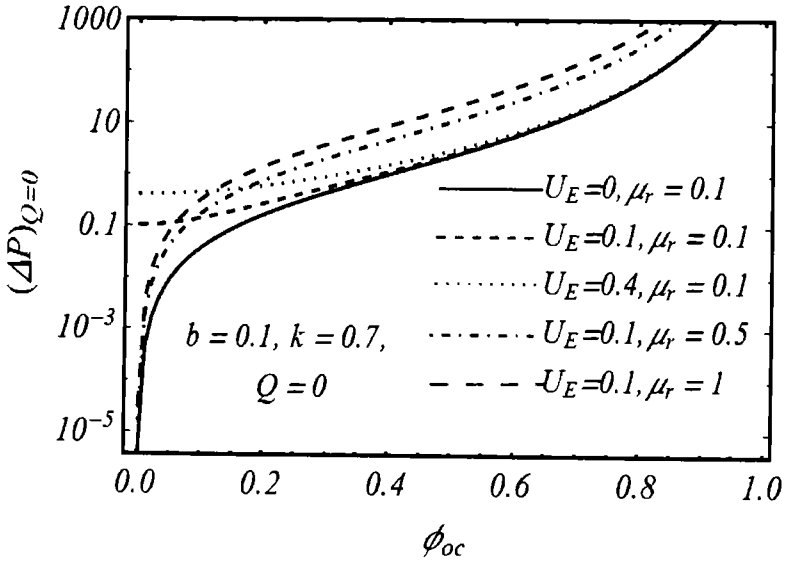

(b)

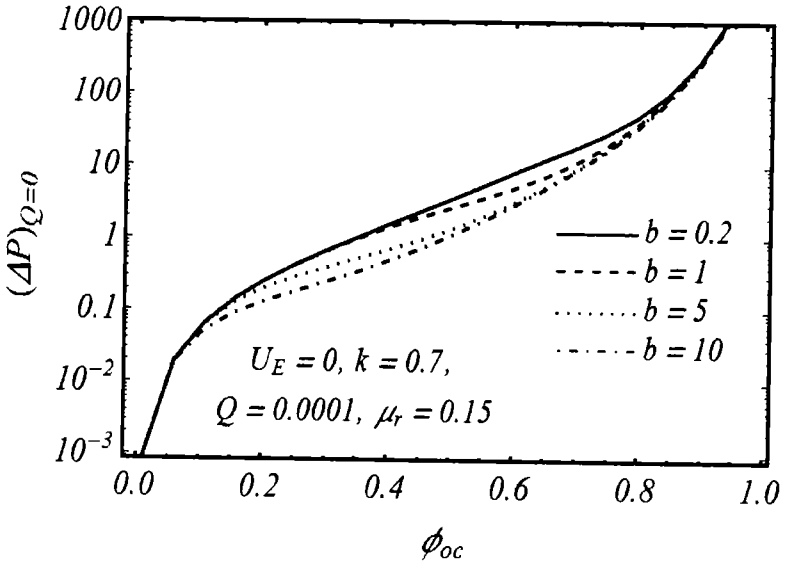

Fig. 4.4 ((a), (b)): The variation in pumping characteristic with respect to U_E, μ_r and b.

(a)

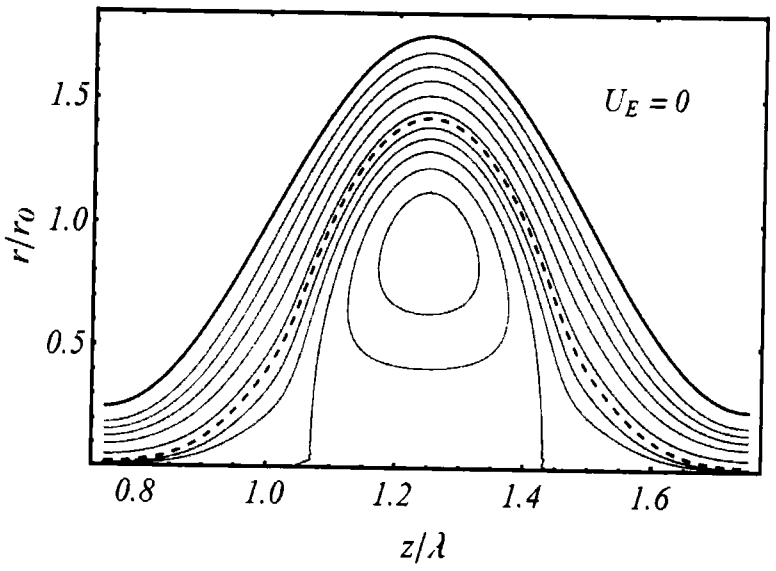

Fig. 4.5 (a): The streamline behavior in the core region when k = 0.4, b = 0.1, μ_r = 10, ϕ_{oc} = 0.75, Q = 0.

(b)

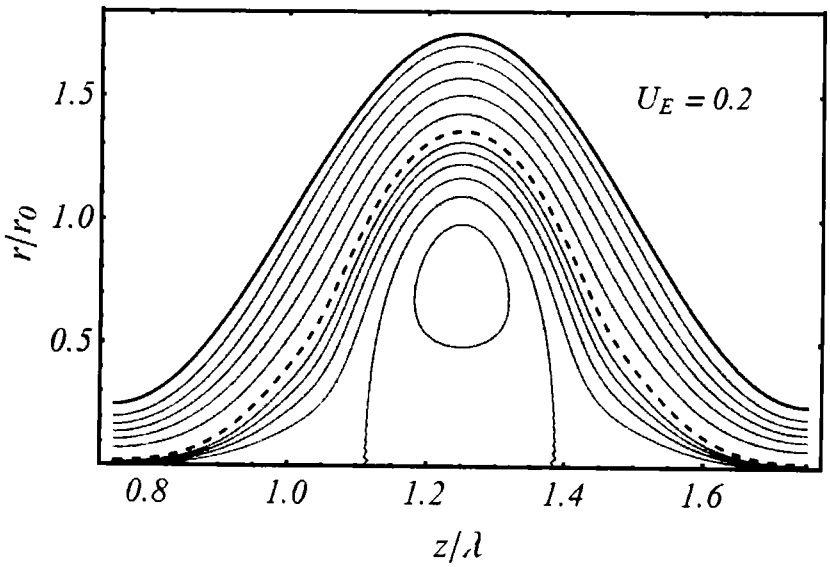

(c)

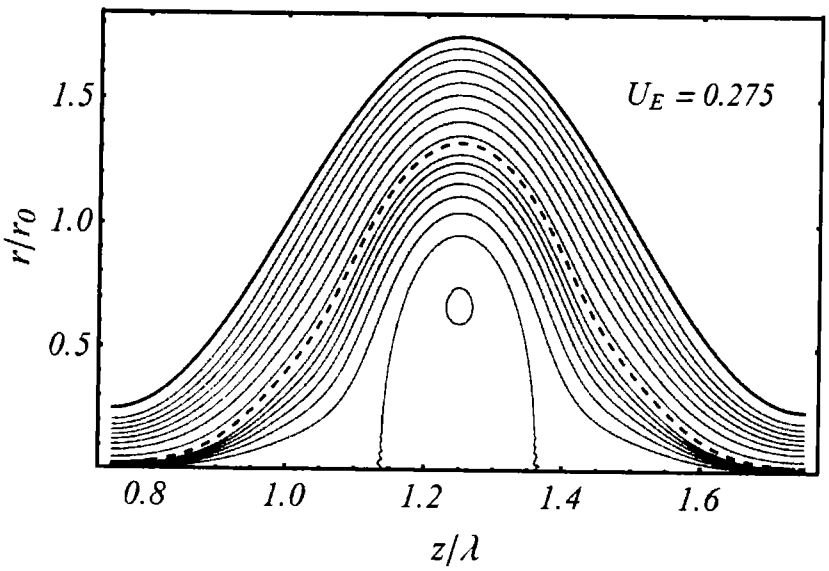

(d)

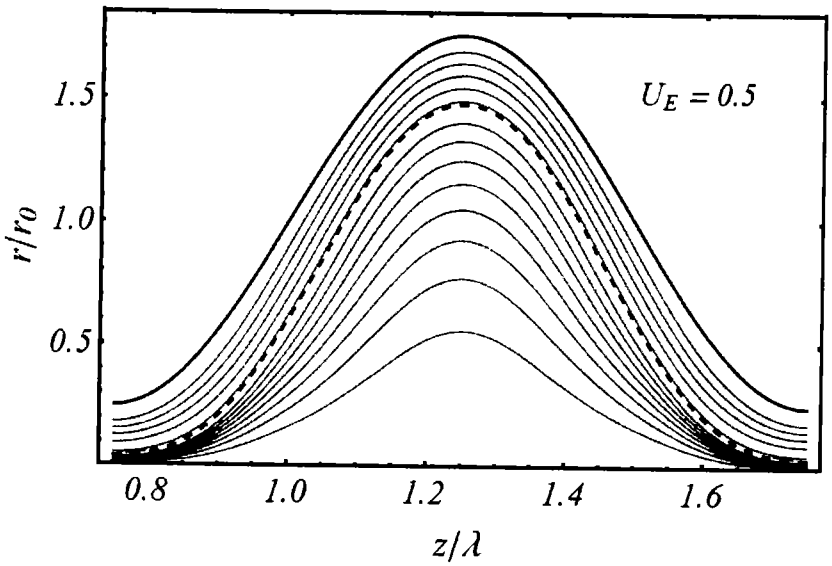

Fig. 4.5 ((b) – (d)): The streamline behavior in the core region when k = 0.4, b = 0.1, $\mu_r = 10, \phi_{oc} = 0.75, Q = 0$.

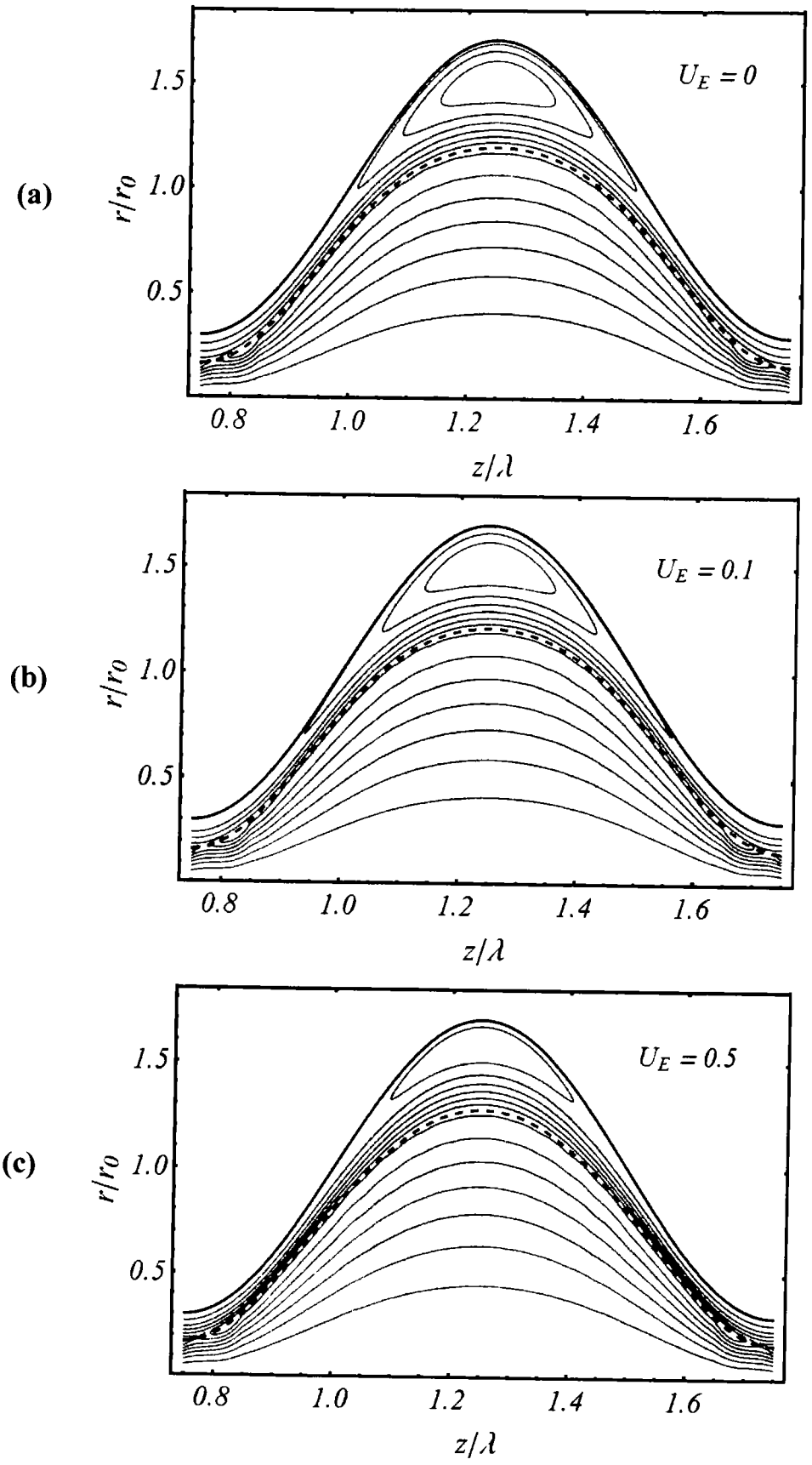

Fig. 4.6 ((a) – (c)): The streamline behavior in the peripheral region when $k = 0.8, b = 0.1, \mu_r = 1, \phi_{oc} = 0.75, Q = 4$.

(d)

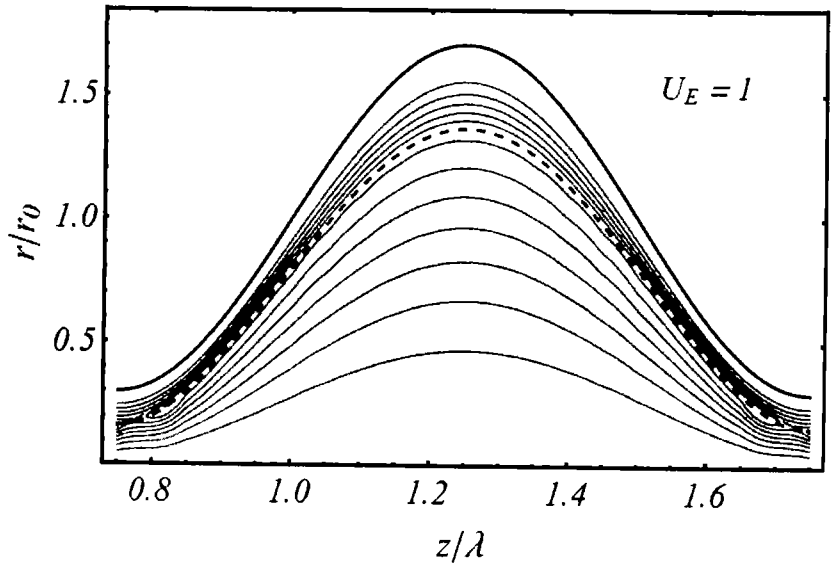

Fig. 4.6 (d): The streamline behavior in the peripheral region when $k = 0.8, b = 0.1, \mu_r = 1, \phi_{oc} = 0.75, Q = 4$.

(a)

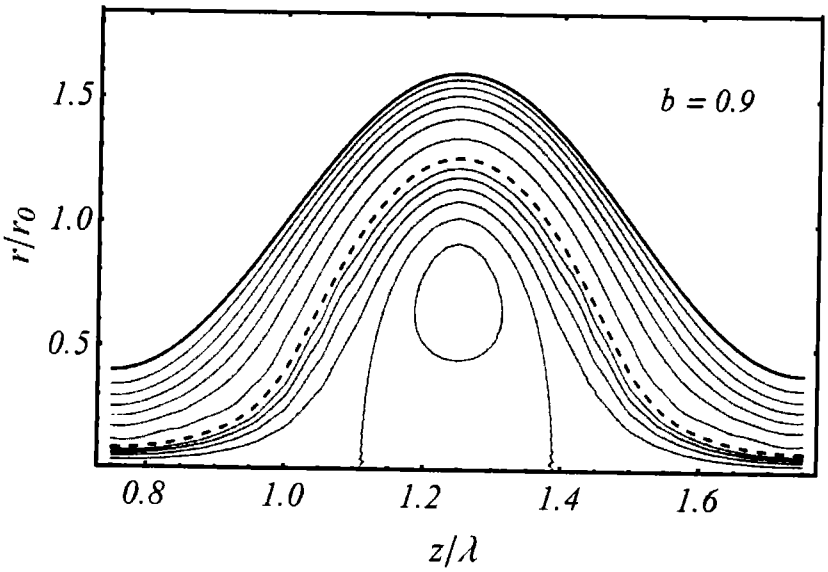

(b)

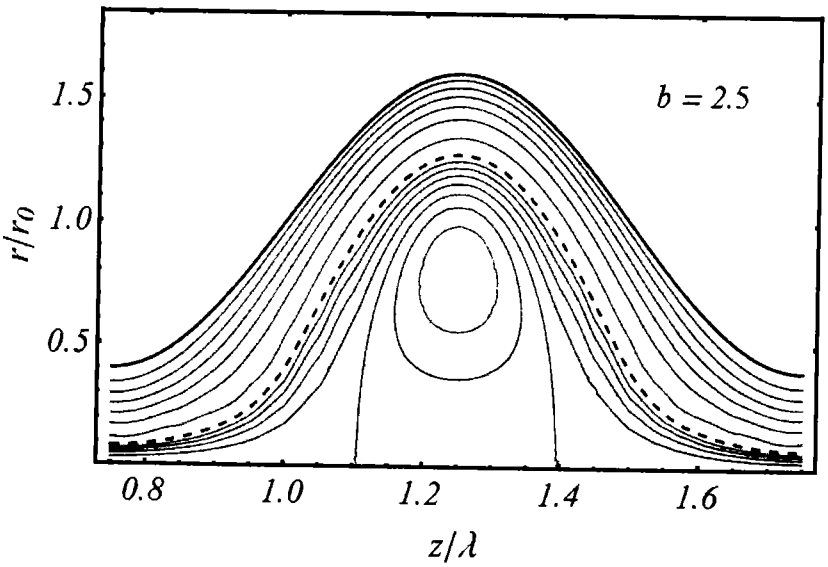

Fig. 4.7 ((a), (b)): Effect of b on trapping when $k = 0.4, \mu_r = 0.1, \phi_{oc} = 0.6, Q = 0.6, U_E = 0$.

(c)

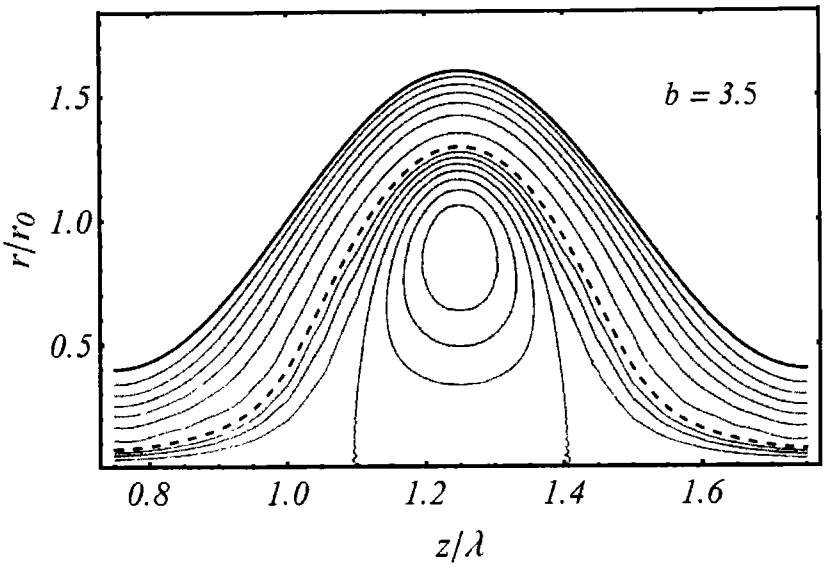

(d)

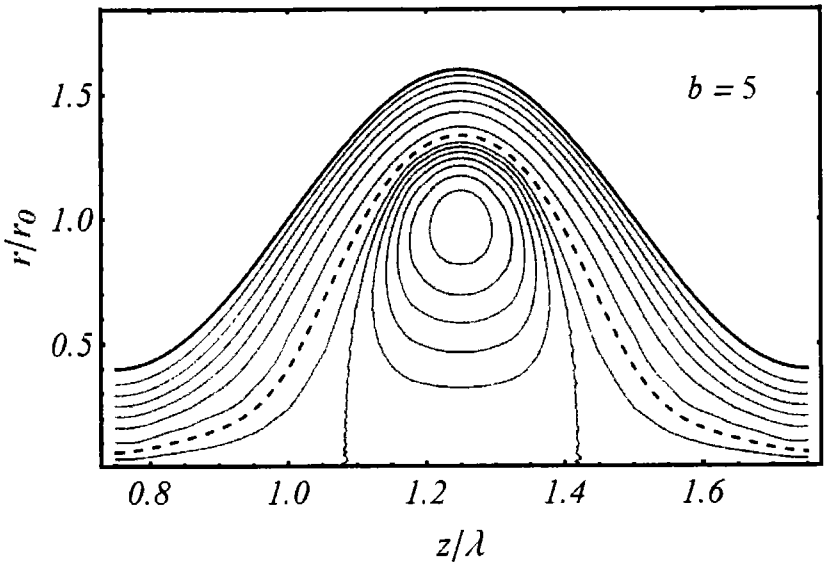

Fig. 4.7 ((c), (d)): Effect of b on trapping when $k = 0.4, \mu_r = 0.1, \phi_{oc} = 0.6, Q = 0.6, U_E = 0$.

(a)

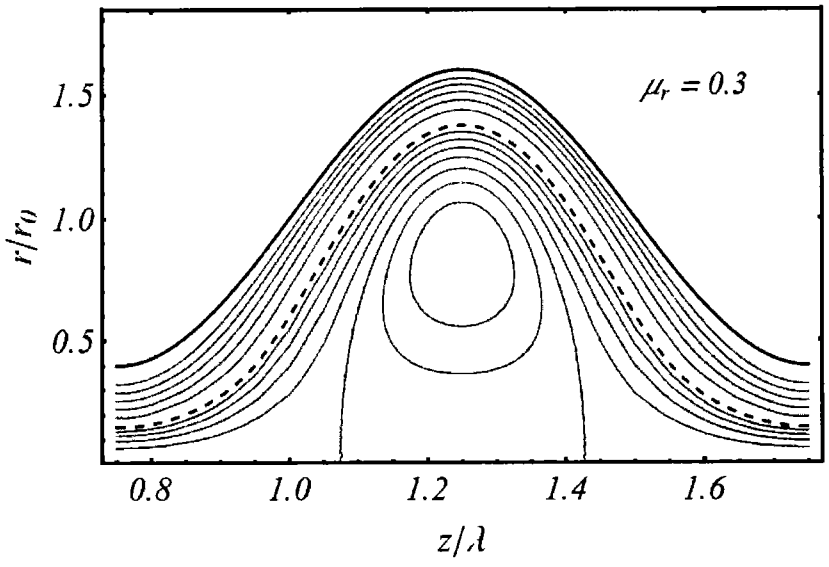

Fig. 4.8 (a): The trapping phenomenon for viscosity ratio when $\boldsymbol{k = 0.4, b = 0.1, \phi_{oc} = 0.75, Q = 0.1, U_E = 0}$.

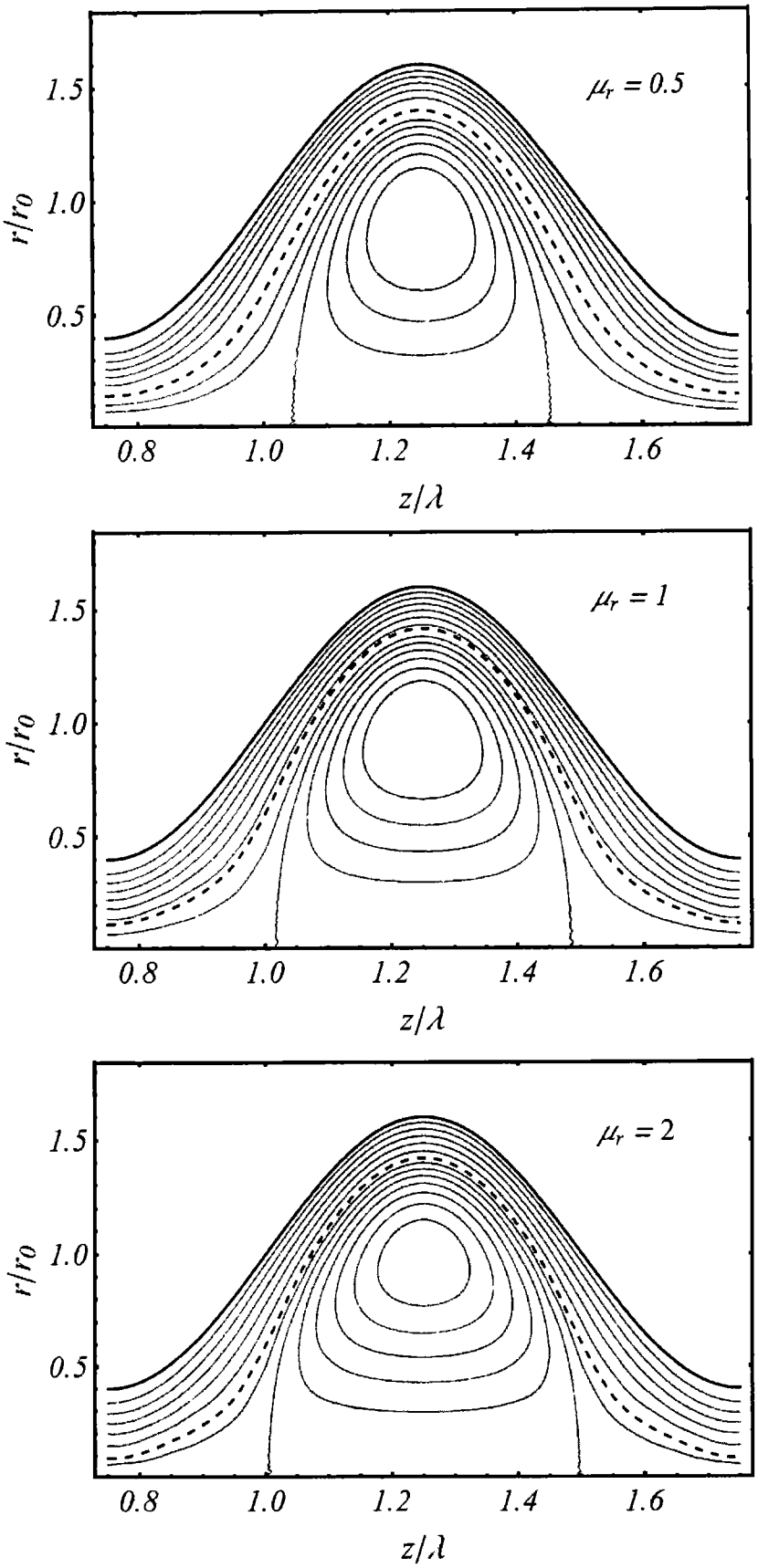

Fig. 4.8 ((b) – (d)): The trapping phenomenon for viscosity ratio when $k = 0.4, b = 0.1$, $\phi_{oc} = 0.75, Q = 0.1, U_E = 0$.

(a)

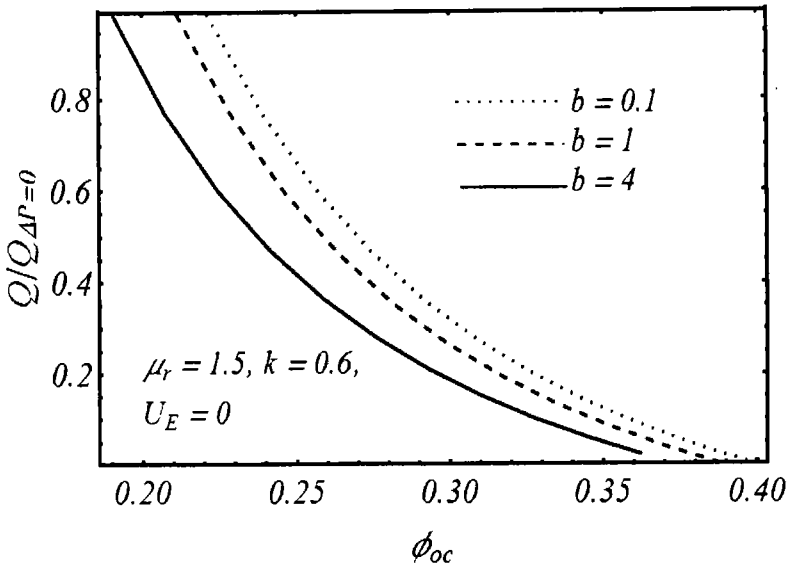

(b)

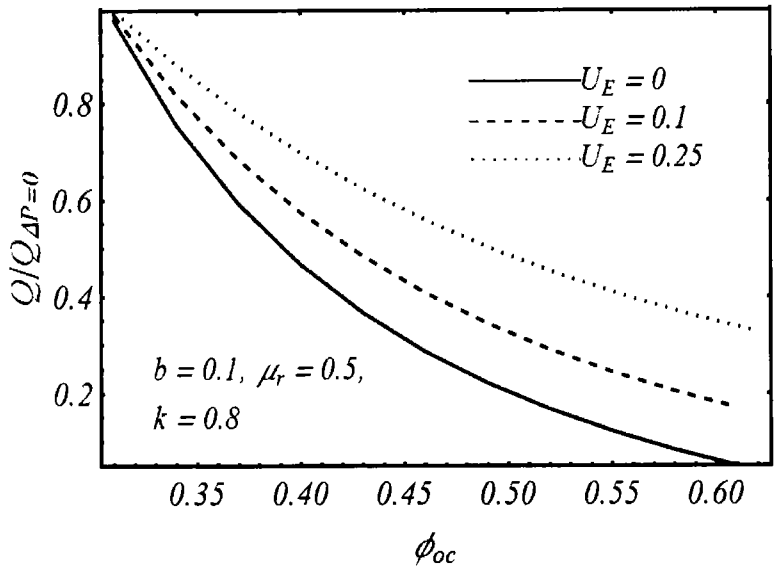

Fig. 4.9 ((a), (b)): Variation in the trapping limit for different values of b and U_E.

(a)

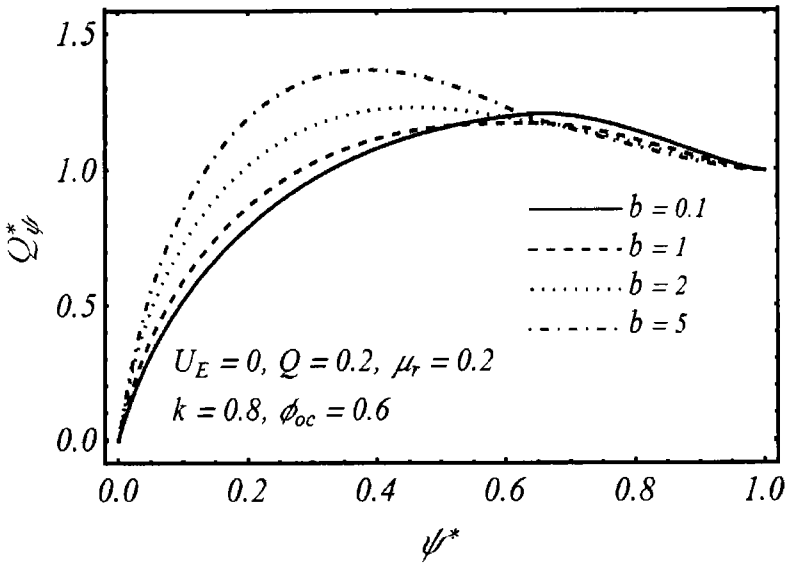

Fig. 4.10 (a): The reflux phenomenon against different values of the parameter b.

(b)

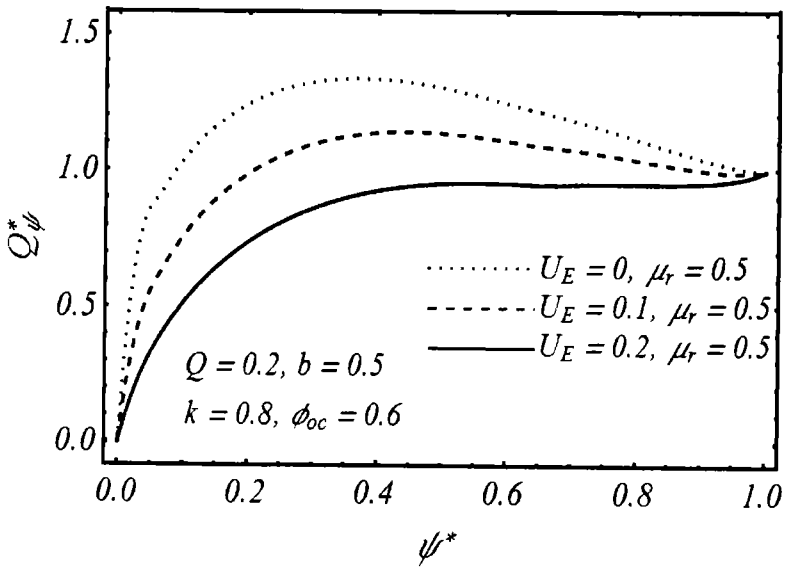

Fig. 4.10 ((a) – (b)): The reflux phenomenon against different combinations of viscosity ratio, electrokinetic slip velocity.

Chapter 5

An analysis of two-layered electro-osmotic peristaltic flow of FENE-P fluid in an axisymmetric tube

In this chapter 5 we presented the theoretical analysis of two-dimensional peristaltic transport of two-fluids in a flexible tube under the influence of electro-osmotic force. The flow domain is composed of two regions, namely, the core region and the peripheral region. The Newtonian and the FENE-P models are used to describe the rheology of fluids in the peripheral and the core regions, respectively. Governing flow equations corresponding to each region are developed under the assumption of long wavelength and low-Reynolds number. The interface between the two regions is computed numerically by employing a system of non-linear algebraic equations. Influence of relevant controlling parameters on pressure gradient, interface, trapping and reflux are highlighted graphically and explained in detail. Special consideration is given to estimate the influence of viscoelastic parameter of the core region fluid in the presence of electro-osmotic environment. Our investigation indicates an augmentation in the pressure loss at zero volumetric flow rate with growing the viscoelastic and occlusion parameters. Moreover, trapping, reflux and pumping efficiency are found to increase with raising the electro-osmotic and viscoelastic parameters. The analysis presented here may be helpful in controlling the micro-vascular transport through the fractionation of blood into plasma and erythrocytes. This study may also have potential applications in areas like electrophoresis, hematology, design and improvement of bio-mimetic electro-osmotic pumps.

5.1 Problem description

Consider the flow of an incompressible FENE-P fluid through a flexible tube of un-deformed radius r_0 due to combined action of the peristaltic wall movement and electro-osmotic force **(see Fig. 5. 1).** The region within the tube is categorized as core and peripheral regions. Fluid present in the central region is described by the FENE-P model while the peripheral region fluid is assumed as a Newtonian fluid. The electro-

osmotic mechanism work in the following manner. The negatively charged surface of the tube wall attracts the opposite ions (cations) from the ionized solution in the peripheral region and at the same time repels the same charge ions (co-ions). Due to this repulsion and attraction two types of layers generated are Stern layer and diffusion layer and the combination of both these layers is called electric double layer (EDL). The motion of the counter-ions of the EDL is achieved through the application of the DC potential difference between the two electrodes at inlet and outlet of the tube. This motion results in the dragging of the remaining fluid in the tube. Apart from that the superimposed peristaltic wall movement is also present and described by the equation

$$R_0(z,t) = r_0 + a_0 sin\left(\frac{2\pi}{\lambda}(z - Ut)\right) \tag{5.1}$$

where λ, r_0, a_0 and U are the wavelength, undeform radius, amplitude and speed of the wave. In the next section, we present mathematical modeling of the flow produced by both electro-osmotic and peristaltic mechanisms.

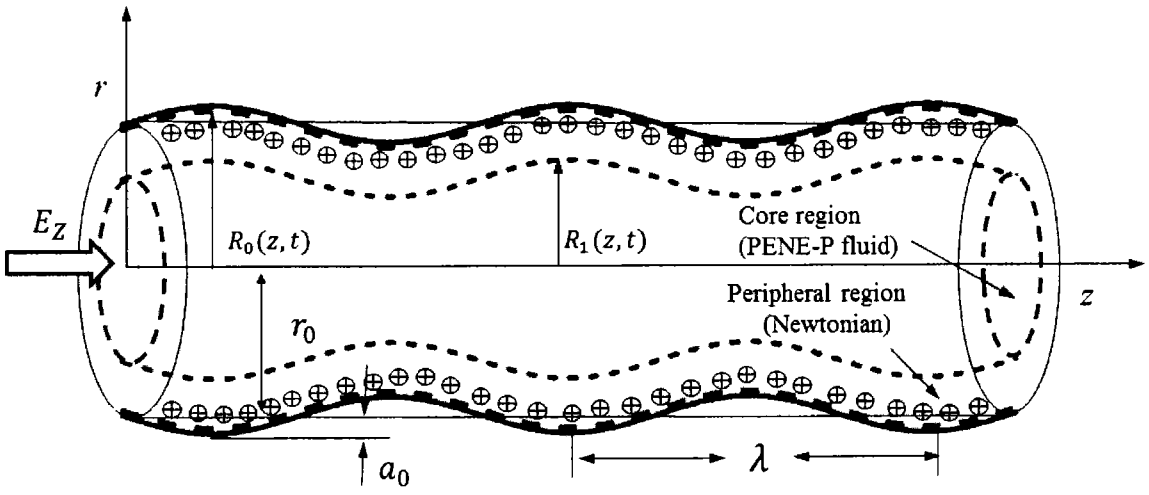

Fig. 5. 1: Geometry of the problem and coordinate system.

5.2 Mathematical formulation

The vectorial form of the continuity and momentum equations are same as Eq. (3.1) and Eq. (3.2). Basic constitutive equations of the FENE-P fluid model are Ali and Asghar (2014)

$$\mathbf{T} = -p\mathbf{I} + \mathbf{S}, \tag{5.2}$$

$$Y_1\left(tr(\mathbf{S})\right)\mathbf{S} + \lambda_p \overset{\nabla}{\mathbf{S}} = 2a\mu_1\mathbf{D}, \tag{5.3}$$

$$\overset{\nabla}{\mathbf{S}} = \frac{\partial \mathbf{S}}{\partial t} + (\mathbf{V}.\nabla)\mathbf{S} - \mathbf{S}(\nabla \mathbf{V})^{\mathrm{T}} - (\nabla \mathbf{V})\mathbf{S},\ 0 \le r \le R_1(z,t),$$

where λ_p be the relaxation time, **D** be the rate of strain tensor and S is the deviatoric stress of FENE-P fluid. The function Y_1 is defined as

$$Y_1(tr(\mathbf{S})) = 1 + \frac{3a + \frac{\lambda_p}{\mu}(\mathrm{tr}(\mathbf{S}))}{L^2}, \tag{5.4}$$

where a is the model parameter defined in terms of the extensibility parameter L as $a = \frac{1}{1-3/L^2}$.

The expression of stress tensor for the peripheral region $(R_1(z,t) \le r \le R_0(z,t))$, is

$$\mathbf{T} = -p\mathbf{I} + \mathbf{S}, \tag{5.5}$$

where $\mathbf{S} = 2\mu_2 \mathbf{D}$. (5.6)

The velocity profile for an incompressible flow in an axisymmetric tube is given as in Eq. (3.5). We perform our analysis in the wave frame of reference, which is related to the laboratory frame of reference via relations as Eq. (3.12).

The continuity and momentum equations in moving frame of reference can be written as:

$$\frac{1}{\bar{r}}\frac{\partial(\bar{r}\bar{u})}{\partial \bar{r}} + \frac{\partial \bar{w}}{\partial \bar{z}} = 0, \tag{5.7}$$

$$\rho\left(\bar{u}\frac{\partial \bar{u}}{\partial \bar{r}} + \bar{w}\frac{\partial \bar{u}}{\partial \bar{z}}\right) = -\frac{\partial \bar{p}}{\partial \bar{r}} + \left[\frac{1}{\bar{r}}\frac{\partial(\bar{r}\bar{S}_{rr})}{\partial \bar{r}} + \frac{\partial \bar{S}_{rz}}{\partial \bar{z}} - \frac{\bar{S}_{\theta\theta}}{\bar{r}}\right], \tag{5.8}$$

$$\rho\left(\bar{u}\frac{\partial \bar{w}}{\partial \bar{r}} + \bar{w}\frac{\partial \bar{w}}{\partial \bar{z}}\right) = -\frac{\partial \bar{p}}{\partial \bar{z}} + \left[\frac{1}{\bar{r}}\frac{\partial(\bar{r}\bar{S}_{rz})}{\partial \bar{r}} + \frac{\partial \bar{S}_{zz}}{\partial \bar{z}}\right] + \bar{F}_e. \tag{5.9}$$

Under the action of external axial electric field $\mathbf{E} = (0,0,E_z)$, the fluid undergoes a body force given as Hunter (1981).

$$\bar{F}_e = \bar{\rho}_e E_z \mathbf{k}, \tag{5.10}$$

where **k** is the unit vector in the axial direction and $\bar{\rho}_e$ be the total ionic charge density, which is associated to the electric potential $\bar{\phi}$ through the equation

$$\nabla^2 \bar{\phi} = -\bar{\rho}_e/\varepsilon, \tag{5.11}$$

in which ε is the permittivity of the medium. For symmetric electrolyte solution, the total ionic distribution $\bar{\rho}_e$ is defined as $\bar{\rho}_e = ez(\bar{n}^+ - \bar{n}^-)$. Further, the order pairs $(\bar{\rho}_{eN}, \varepsilon_N)$ and $(\bar{\rho}_{ec}, \varepsilon_c)$ respectively denote the ionic charge density and permittivity of

the fluid in peripheral and core regions. To simplify the Eq. (5.11) for electric potential, the rest of the subsequent analysis is same as mention in the chapter 3.

Now introducing the dimensionless variables

$$\left.\begin{aligned} &r^* = \frac{\bar{r}}{r_0},\ z^* = \frac{\delta \bar{z}}{r_0},\ u^* = \frac{\bar{u}}{(\delta U)}, w^* = \frac{\bar{w}}{U}, t^* = \frac{\delta U}{r_0}\bar{t}, \delta = \frac{r_0}{\lambda}, \\ &p^* = \frac{\delta r_0}{\mu_1 U}\bar{p},\ Re = \frac{\rho U r_0}{\mu_1},\ De = \frac{\lambda_p U}{r_0}, \phi^* = \frac{ez\bar{\phi}}{k_B T}, S^* = \frac{r_0}{\mu_1 U}\bar{S}, \\ &n^* = \frac{\bar{n}}{n_0}, \phi_{oc} = \frac{a_0}{r_0}, \rho_e^* = \frac{r_0^2 k_B T \bar{\rho}_e}{ez\varepsilon_N}. \end{aligned}\right\} \tag{5.12}$$

where Re is the Reynold number, De be the Deborah number and δ is the wave number.

Applying the long wavelength ($\delta \ll 1$) and low Reynolds number ($Re \ll 1$) approximations, Eqs. (5.7) – (5.9) for both regions (core and peripheral) become (dropping asterisk)

Core region

$$\begin{cases} 0 = -\dfrac{\partial p}{\partial z} + \left[\left(\dfrac{1}{r}\dfrac{\partial (r S_{rz})}{\partial r}\right)\right] + U_E \dfrac{\mu_r}{\varepsilon_r}\rho_{ec}, \\ 0 = -\dfrac{\partial p}{\partial r}, \end{cases} \tag{5.13}$$

$$\begin{cases} Y_1\left(tr(s)\right) S_{zz} = 2De \dfrac{\partial w_c}{\partial r} S_{rz}, \\ Y_1\left(tr(s)\right)_1 S_{rz} = a\dfrac{\partial w_c}{\partial r}, \\ S_{rr} = S_{\theta\theta} = S_{r\theta} = S_{\theta z} = 0. \end{cases} \tag{5.14}$$

Peripheral region

$$\begin{cases} 0 = -\dfrac{\partial p}{\partial z} + \left[\left(\dfrac{1}{r}\dfrac{\partial (r S_{rz})}{\partial r}\right)\right] + U_E \mu_r \rho_{eN}, \\ 0 = -\dfrac{\partial p}{\partial r}, \\ S_{rz} = \mu_r\left(\dfrac{\partial w_N}{\partial r}\right), \end{cases} \tag{5.15}$$

where, $U_E = -\varepsilon_N k_B T E_z / Uez\mu_2$ is the electro-kinetic slip velocity, $\varepsilon_r (= \varepsilon_N / \varepsilon_c)$ is the permittivity ratio and $\mu_r (= \mu_2 / \mu_1)$ is the ratio of viscosities.

Solving and simplifying the system (5.17) gives

$$\left(1 + \frac{2De^2 \left(S_{rz}^{\ 2}\right)}{a^2 L^2}\right) S_{rz} = \frac{\partial w_c}{\partial r}. \tag{5.16}$$

The dimensionless boundary conditions are defined as

$\frac{\partial w_c}{\partial r} = 0, \text{at } r = 0$; (central line symmetry)

$w_c = w_N$ and $\left(S_{rz}\right)_N = \left(S_{rz}\right)_c$ at $r = R_1$; (continuity of velocity and shear stresses at the interface)

$w_N = -1$ at $r = R_0$; (no-slip condition) .

From now onward, we omit the body force term from the governing equations by invoking a well-established assumption from the electro-osmotic studies. According to this assumption, the velocity of the plug-core region in electro-kinetic transport may be equivalently obtained either by considering the body force term in the equation of motion or shifting its contribution in the boundary at the wall. Therefore, we drop the electro-kinetic term from the equation of motion by properly modifying the no-slip condition at the boundary. This approach is already used by Goswami et al (2016). There the authors have thoroughly discussed the validity of this assumption. According to their discussion, which is supported by several previous studies from electro-osmotic flows, this assumption is valid under thin Debye-layer and weak electric field limit. Thus, our flow problem is governed as:

In core region

$$\begin{cases} 0 = -\frac{\partial p}{\partial z} + \left[\left(\frac{1}{r}\frac{\partial \left(r S_{rz}\right)}{\partial r}\right)\right], \\ 0 = -\frac{\partial p}{\partial r}, \end{cases} \tag{5.17}$$

$$\left(1 + \frac{2De^2 \left(S_{rz}^{\ 2}\right)}{a^2 L^2}\right) S_{rz} = \frac{\partial w_c}{\partial r}, \tag{5.18}$$

$$\frac{\partial w_c}{\partial r} = 0, \text{at } r = 0; \tag{5.19}$$

In peripheral region

$$\begin{cases} 0 = -\dfrac{\partial p}{\partial z} + \left[\left(\dfrac{1}{r}\dfrac{\partial (r S_{rz})}{\partial r}\right)\right], \\ 0 = -\dfrac{\partial p}{\partial r}, \\ S_{rz} = \mu_r \left(\dfrac{\partial w_N}{\partial r}\right). \end{cases} \tag{5.20}$$

$$\begin{aligned} &\frac{\partial w_N}{\partial r} = 0, \text{at } r = 0; \\ &\mathrm{w}_N = U_E - 1, \text{at } r = R_0. \end{aligned} \tag{5.21}$$

The velocity components in term of stream function are defined by the Cauchy-Riemann equations as Eq. (3.40). In the presence of the relation of the stream function as Eq. (3.40) the momentum equations in the core and peripheral regions become and boundary condition are emerge as:

$$\frac{\partial}{\partial r}\left(\frac{1}{r}\frac{\partial \psi}{\partial r}\right) = \frac{r}{2}\frac{\partial p}{\partial z} + \frac{De^2}{4a^2 L^2}\left(\frac{\partial p}{\partial z}\right)^3 r^3 \quad , 0 \le r \le R_1 \tag{5.22}$$

$$\frac{\partial p}{\partial z} = \frac{1}{r}\frac{\partial}{\partial r}\left[\left(r\mu_r \frac{\partial}{\partial r}\left(\frac{1}{r}\frac{\partial \psi}{\partial r}\right)\right)\right] \quad , R_1 \le r \le R_0 \tag{5.23}$$

$$\psi = 0, \frac{\partial}{\partial r}\left(\frac{1}{r}\frac{\partial \psi}{\partial r}\right) = 0, \text{at } r = 0, \tag{5.24}$$

$$\psi = \frac{q}{2}, \frac{\partial \psi}{\partial r} = (U_E - 1) R_0, \text{at } r = R_0, \tag{5.25}$$

$$\psi = \frac{q_1}{2}, \text{at } r = \mathrm{R}_1. \tag{5.26}$$

Integrating Eqs. (5.22) and (5.23) and invoking the boundary conditions (5.24) and (5.25) yield

$$\psi=\begin{cases}\dfrac{r^2}{2}\left\{\left(U_E-1\right)+\dfrac{\beta}{3}\left(\dfrac{\partial p}{\partial z}\right)^3\left[r^4-3R_1^4\right]+\dfrac{1}{8}\dfrac{\partial p}{\partial z}\left(\left\{r^2-2R_1^2\right\}+\dfrac{2}{\mu_r}\left\{R_1^2-R_0^2\right\}\right)\right\}, 0\le r<R_1\\ \dfrac{r^2}{2}\left(U_E-1\right)+\left(\dfrac{q}{2}-\left(U_E-1\right)\dfrac{R_0^2}{2}\right)+\dfrac{1}{16\mu_r}\dfrac{\partial p}{\partial z}\left(r^2-R_0^2\right)^2, R_1\le r\le R_0\end{cases} \tag{5.27}$$

where $\beta=De^2/16a^2L^2$ is the viscoelastic parameter which is affected by extensibility of fluid and relaxation time. From Eq. (5.27), the velocity components for inner $\left(0\le r\le R_1\right)$ and outer $\left(R_1\le r\le R_0\right)$ regions become

$$w(r,z)=\begin{cases}\left(U_E-1\right)+\beta\left(\dfrac{\partial p}{\partial z}\right)^3\left[r^4-R_1^4\right]+\dfrac{1}{4}\dfrac{\partial p}{\partial z}\left(\left\{r^2-R_1^2\right\}+\dfrac{1}{\mu_r}\left\{R_1^2-R_0^2\right\}\right), 0\le r\le R_1\\ \left(U_E-1\right)+\dfrac{1}{4\mu_r}\dfrac{\partial p}{\partial z}\left(r^2-R_0^2\right). R_1\le r\le R_0\end{cases}$$

(5.28)

The dimensionless equation describing the wall deformation is

$$R_o(z)=1+\phi_{oc}\sin(2\pi z). \tag{5.29}$$

In order to evaluate R_1 and $\partial p/\partial z$, a semi-analytical technique is considered Goswami et al. (2016). Using the boundary condition (5.26), the second equation in (5.27) gives

$$\frac{q_1}{2}=\frac{R_1^2}{2}\left(U_E-1\right)+\left(\frac{q}{2}-\left(U_E-1\right)\frac{R_0^2}{2}\right)+\frac{1}{16\mu_r}\frac{\partial p}{\partial z}\left(R_1^2-R_0^2\right)^2. \tag{5.30}$$

In order to find q_1, we set $R_1=k$ and $R_0=1$ at $z=0$. Thus, Eq. (5.30) becomes

$$\frac{q_1}{2}=\frac{k^2}{2}\left(U_E-1\right)+\left(\frac{q}{2}-\left(U_E-1\right)\frac{1}{2}\right)+\frac{1}{16\mu_r}P_0\left(k^2-1\right)^2. \tag{5.31}$$

where, $P_0=(\partial p/\partial z)|_{z=0}$. Then eliminating q_1 from Eqs. (5.30) and (5.31) yields

$$\left(\begin{matrix}\dfrac{k^2}{2}\left(U_E-1\right)+\\ \left(\dfrac{q}{2}-\left(U_E-1\right)\dfrac{1}{2}\right)\end{matrix}\right)+\frac{1}{16\mu_r}P_0\left(k^2-1\right)^2=\left(\begin{matrix}\dfrac{R_1^2}{2}\left(U_E-1\right)+\\ \left(\dfrac{q}{2}-\left(U_E-1\right)\dfrac{R_0^2}{2}\right)\end{matrix}\right)+\frac{1}{16\mu_r}\frac{\partial p}{\partial z}\left(R_1^2-R_0^2\right)^2. \tag{5.32}$$

Now, there are three unknown in Eq. (5.32) i.e., P_0, R_1 and $\partial p/\partial z$. For a unique solution there must be three equations connecting these unknowns. The other two

equations can be easily developed since the stream function specified by the expression (5.27) for both regions must be same at the interface. Employing this continuity condition yields

$$\frac{\beta}{3}\left(\frac{\partial p}{\partial z}\right)^3 R_1^6+\frac{1}{16}\frac{\partial p}{\partial z}R_1^4+\frac{1}{16\mu_r}\frac{\partial p}{\partial z}\left(R_0^4-R_1^4\right)+\frac{q}{2}-\left(U_E-1\right)\frac{R_0^2}{2}=0. \tag{5.33}$$

Setting $R_1=k$ and $R_0=1$ at $z=0$, the above expression becomes

$$\frac{\beta}{3}P_0^3k^6+\frac{1}{16}P_0k^4+\frac{1}{16\mu_r}P_0\left(1-\mathrm{k}^4\right)+\frac{q}{2}-\left(U_E-1\right)\frac{1}{2}=0. \tag{5.34}$$

From Eq. (5.35), we get

$$\frac{\partial p}{\partial z}=\frac{16\mu_r}{\left(R_1^2-R_0^2\right)^2}\left\{\frac{1}{2}\left(U_E-1\right)\left(k^2-R_1^2+R_0^2\right)+\frac{1}{16\mu_r}P_0\left(k^2-1\right)^2\right\}, \tag{5.35}$$

substituting $\partial p/\partial z$ from (5.34) into (5.33) gives

$$\begin{aligned}&\frac{\beta}{3}\left(\frac{16\mu_r}{\left(R_1^2+R_0^2\right)^2}\left\{\frac{1}{2}\left(U_E-1\right)\left(k^2-R_1^2+R_0^2\right)+\frac{1}{16\mu_r}P_0\left(k^2-1\right)^2\right\}\right)^3 R_1^6\\&+\left(\frac{\mu_r}{\left(R_1^2-R_0^2\right)^2}\left\{\frac{1}{2}\left(U_E-1\right)\left(k^2-R_1^2+R_0^2\right)+\frac{1}{16\mu_r}P_0\left(k^2-1\right)^2\right\}\right)R_1^4\\&+\left(\frac{1}{\left(R_1^2-R_0^2\right)^2}\left\{\frac{1}{2}\left(U_E-1\right)\left(k^2-R_1^2+R_0^2\right)+\frac{1}{16\mu_r}P_0\left(k^2-1\right)^2\right\}\right)\left(R_0^4-R_1^4\right)+\\&\frac{q}{2}-\left(U_E-1\right)\frac{R_0^2}{2}=0.\end{aligned} \tag{5.36}$$

Eqs. (5.34) and (5.36) are solved numerically by employing bisection method to obtain the values of P_0, R_1. The numerical value of pressure gradient follows from Eq. (5.36).

5.3 Results and graphical discussions

5.3.1 Analysis of interface

The numerical calculations for P_0, R_1 and $\partial p/\partial z$ based on bisection technique are carried out by using symbolic software **Mathematica 8.1** at each axial position z. The physical interpretation of our results is facilitated through graphs which show the variations of interface with respect to the emerging parameters β, μ_r, U_E in **Fig. (5.2(a**

- d)). The parameter β characterizes the effect of viscoelastic nature of the core region fluid whereas U_E estimates the effect of electro-kinetic slip velocity. Larger values of β correspond to enhanced viscoelastic effects manifested by the core region fluid while higher values of U_E (larger slip velocity) represent the situation of intense movement of counter-ions in the EDL. The parameter μ_r which the ratio of viscosities corresponding to the core and peripheral regions can be used to identify three scenarios: $\mu_r = 1$ represents the scenario in which fluid viscosities in both regions are equal, $\mu_r < 1$ is the case in which the viscosity of central region fluid is greater than the outer layer fluid and $\mu_r > 1$ corresponds to situation in which a lower viscosity fluid is surrounded by a higher viscosity fluid. In most of the real physiological flows, the fluid in peripheral region has smaller viscosity than that of the core region. But for the sake of completeness, both situations are highlighted in **Fig. (5.2(a))**. Generally, the core layer fluid in the crest portion pushes the peripheral layer fluid with normal force acting in the upward direction while the outer layer fluid pushes the inner layer fluid with a normal force in downward direction. This situation resembles with that a couple to some extent. However, the magnitude of upward normal force is not equal to the magnitude of downward normal force. Hence, the interface though similar in shape to that of boundary wall is not symmetric for all three situations. These results are in accordance with the results of Brasseur et al. (1987) and Rao and Usha (1995). It is necessary to highlight that the present analysis is not performed for a presumed interface shape as done by Shukla et al. (1980). In fact, Shukla et al. (1980) assumed the interface shape according to the relation $R_1 \propto R_0$ which clearly indicates that R_1 is symmetric and known as a priori. However, this assumption was subject to criticism by Brasseur et al. (1980). They argued that such a deduction of the interface shape leads to violation of condition that mass must be independently conserved in the peripheral layer and the core layer. Further, they explicitly showed that the interface shape $R_1 \propto R_0$ of Shukla et al. (1980) is never achieved for any choice of the involved parameters. **Fig. (5.2(a))** further reveals that the interface in the crest region for $\mu_r < 1$ lies above the interface for $\mu_r = 1$ and vice versa. In contrast, a completely opposite trend prevails for $\mu_r > 1$. **Fig. (5.2(b))** highlights the variations of interface with respect to electro-kinetic slip parameter U_E. It is observed that the interface in the crest region slightly shift downward with raising U_E. However a reverse trend is noted in the trough region. The variations of

interface against viscoelastic parameter β, which is the ratio of the Deborah number De and the extensibility parameter L, are shown through **Fig. (5.2(c)).** Clearly, the effects of the β is similar to the effect of μ_r. **Fig. (5.2(d))** illustrates the variations in interfaces for several parametric values of μ_r by setting $\beta = 0, U_E = 0$. This corresponds to the situation, in which the core and peripheral regions are occupied by Newtonian fluids of different viscosities and flow is purely peristaltic. The computations for this scenario have been already reported by Rao and Usha (1995). In order to validate present analysis, we have reproduce **Fig. 2** of their paper in **Fig. (5.2(d))** through our numerical procedure and found that there is an excellent match between both figures. This clearly testifies that our numerical procedure and all the subsequent extended results are correct.

5.3.2 Pressure expression and results discussion

The solution of Eq. (5.38) gives us following expression for pressure gradient $\partial p/\partial z$ in the tube

$$\frac{\partial p}{\partial z} = \frac{16\mu_r}{\left(R_1^2 - R_0^2\right)^2}\left\{\frac{1}{2}\left(U_E - 1\right)\left(k^2 - R_1^2 + R_0^2\right) + \frac{1}{16\mu_r}P_0\left(k^2 - 1\right)^2\right\}. \qquad (5.37)$$

By integrating the above equation over z from $z = 0$ to $z = \lambda$, gives

$$\Delta P = \int_0^{\lambda}\left\{\frac{\left(8\mu_r\left(U_E - 1\right)\left(k^2 - R_1^2 + R_0^2\right) + P_0\left(k^2 - 1\right)^2\right)}{\left(R_1^2 - R_0^2\right)^2}\right\}dz. \qquad (5.38)$$

However, due to unavailability of analytical expression of P_0 and R_1, the above expression do not give the analytical expression for $\partial p/\partial z$. Infact, the numerical values of P_0 and R_1 obtained from Eqs. (5.34) and (5.36) are used to obtain the numerical values of $\partial p/\partial z$ from Eq. (5.37) at each cross section z. The numerical values of ΔP follows through numerical integration as indicated in Eq. (5.38).

The relation between volume fluxes in wave and laboratory frame of references is given by following equation

$$Q_S = 2\int_0^{R_0}(w+1)r\,dr = q + R_0^2. \qquad (5.39)$$

Time-averaging yields

$$Q = \frac{1}{T_P}\int_0^{T_P} Q_S\,dt = q + \left(1 + \frac{\phi^2}{2}\right), \qquad (5.40)$$

where, $T_p = \lambda/U$ is a complete period.

Graphically, we visualize the pressure growth $\Delta P_1 = \Delta P\big|_{Q=0}$ against the ϕ_{oc} in **Fig. (5.3(a, b))** for distinct values of U_E, μ_r, and the FENE-P fluid model parameter. **Fig. (5.3(a))** depicts the combined effects of viscoelastic parameter and viscosity ratio on ΔP_1. A progressive increase in ΔP_1 is noted with raising the occlusion parameter ϕ_{oc}. In fact, with an increase in the value of occlusion parameter, the fluid is squeezed through the trough region with greater velocity. To retain a zero volume flow rate over one wavelength of the cylindrical tube, the fluid under crest impedes the motion of the fluid in the trough portion by evolving a pressure gradient, which rises by increasing the occlusion parameter. It is further observed that for a fixed value of occlusion parameter, the pressure rise at zero flow rate increases with increasing the viscosity ratio while a reverse trend prevails with increasing viscoelastic parameter. **Fig. (5.3(b))** demonstrates variations of pressure growth ΔP_1 for several values of electro-kinetic slip velocity U_E. The corresponding curve for $U_E = 0$ depicts the situations when the pressure rise ΔP_1 is only due to peristaltic activity. Further, an increase in U_E results in an increase in ΔP_1 at smaller occlusions. However, opposite trend is observed at larger occlusions. Thus, synchronization in peristaltic activity and electro-osmotic phenomenon is observed at smaller occlusions.

5.3.3 Velocity profile

In this section, velocity distribution (5.33) is analyzed graphically for different U_E, μ_r, and β. **Fig. (5.4(a))** demonstrates the impact of electro-kinetic slip velocity on the velocity profile. It is found that the velocity of fluid in the inner (core) region increases for large values of the electro-kinetic slip velocity U_E. The same trend is noted by varying the viscosity ratio **Fig. (5.4(b)).** The changes in the behavior of velocity profile due to the variations of Deborah number and extensibility parameter are depicted in **Fig. (5.4(c)).** An increment in the velocity of fluid at the center of the tube is observed by increasing the Deborah number. While the flow accelerates with a decrement in the extensibility parameter. The plug-flow situation is also visible at the center of the tube (core region) for non-zero β only. For $\beta = 0$ there is no indication of any such region which clearly shows that plug-flow situation is a typical characteristic of FENE-P fluid.

5.3.4 Mechanical efficiency

The machenical efficiency of pumping is defined as Rao and Usha (1995)

$$E = \frac{Q\Delta P}{\frac{1}{T}\int_0^T \int_0^\lambda 2R_0 p \frac{dR_0}{dt} dz dt} = \frac{Q\Delta P}{\Delta P\left(1+\frac{\phi^2}{2}\right) - l_1}, \tag{5.41}$$

where

$$l_1 = \int_0^1 \frac{dp}{dz} {R_0}^2 \, dz.$$

Physically it is defined as the ratio between average rate per wavelength at which work is carried out by the movement of the fluid against a pressure rise and average rate at which the peristaltic walls motion do work on the fluid Rao and Usha (1995). Profiles of the mechanical efficiency (E) against ratio of time-averaged flow rate and maximum average flow rate are shown in **Fig. (5.5(a-d))** to highlight the impact of emerging parameters at $\phi_{oc} = 0.4$. The change in mechanical efficiency with viscosity ratio is illustrated in **Fig. (5.5(a)).** The mechanical efficiency grows by increasing the viscosity ratio and this growth eventually becomes slower after a certain value of μ_r. The influence of electro-kinetic slip velocity on mechanical efficiency is demonstrated in **Fig. (5.5(b))** wherein it is noted that the mechanical efficiency increases with rise the value slip parameter. The variation in mechanical efficiency with respect to viscoelastic parameter is illustrated in **Fig. (5.5(c)).** Here a progressive growth in mechanical efficiency is observed with augmenting the viscoelastic parameter. **Fig. (5.5(d))** demonstrates the variations in mechanical efficiency for several values of μ_r by setting $\beta = 0, U_E = 0$. Physically, this corresponds to the situation in which both core and peripheral regions are occupied by Newtonian fluids and there is not any electrokinetic body force. This scenario is already dealt by Rao and Usha (1995). The values of μ_r assumed in **Fig. (5.5(d))** are similar to those as considered by Rao and Usha. It is clearly observed that our results agree well with the results of Rao and Usha (1995). This trend again strongly supports the authenticity of our analysis.

5.3.5 Trapping phenomenon

Streamlines play a vital role in fluid flow investigations. In peristaltic transport, the phenomenon when closed streamlines are perceived, at certain values of embedded parameters, is known as trapping. These closed streamlines enclose a quantity of fluid that is termed as trapped bolus in the peristaltic literature. The size/area of such bolus

is largely affected by the involved parameters. In order to have a better understanding of this claim, **Figs. (5.6(a - h) - 5.8(a - d))** are plotted to see the variations in streamlines for several values of electro-kinetic slip parameter, viscosity ratio and viscoelastic parameter. **Fig. (5.6((a) – (h))** depicts the variation of electro-kinetic slip parameter on the area of trapped bolus of fluid in both inner (core) and outer (peripheral) regions of tube. It is noted that the area of trapped bolus reduces with increasing the electro-kinetic slip velocity and the bolus finally disappears in both outer (peripheral) and inner (core) regions for large slip velocities. In fact, increasing the electro-kinetic slip velocity reduces the resistance within the fluid that opposes the fluid flow. This ensures the transport of fluid with greater bulk momentum in the axial directions and disappearing of the trapped bolus. **Fig. (5.7(a - d))** reveals the variations in the trapped bolus for different values of viscoelastic parameter. Here it is noticed that the trapped bolus increases in size with increasing the viscoelastic parameter. **Fig. (5.8(a - d))** illustrates the influence of μ_r on the trapping region. A prominent growth in the trapped bolus is observed with increasing the viscosity ratio. For further understanding of trapping mechanism, we calculate the limits of the involved parameter and point out the region where tapping phenomenon occurs. In this context, we determine the sub-region in the domain $\left(0 \le \phi_{oc} \le 1; 0 \le Q/Q_{\Delta p=0} \le 1\right)$ in which the transition occurs in the values of ψ from negative to positive and then use a suitable iterative scheme to locate the values of $Q/Q_{\Delta p=0}$ and ϕ_{oc} at which this change in sign appears Goswami et al. (2016). Finally, we plot $Q/Q_{\Delta p=0}$ verses ϕ_{oc} for several values of the emerging parameters. The region above a specific curve corresponds to the trapping region. **Fig. (5.9(a))** illustrates variations in the trapping region for electro-osmotic slip velocity. A contraction in trapping region is observed with growing values of electro-kinetic parameter. **Fig. (5.9(b))** demonstrates the variations in the trapping region for several values of viscoelastic parameter. It is found that trapping region expands with growing the value of viscoelastic parameter.

5.3.6 Reflux

Reflux is important phenomenon in the peristaltic transport mechanism which occurs due to movement of fluid particles against the flow direction or backward movement of fluid particles inside the tube. The reflux phenomenon in peripheral and core regions strongly depend on the emerging parameters such as viscoelastic parameter,

viscosity ratio and electro-osmotic parameter. Following Brasseur et al. (1987), are approximate the quantity of backward fluid or reflux from the ratio $(Q-Q_\psi)/Q$ throughout a wave cycle. Where Q_ψ is obtained as

$$Q_\psi = 2\psi + \int_0^1 r^2 dz. \tag{5.42}$$

The above equation is obtained by converting the following relation from wave frame to fixed frame and averaging over one time period.

$$Q_{\psi'} = 2\int_0^{r(\psi',z)} rwdr. \tag{5.43}$$

In (5. 43), $Q_{\psi'}$ represents average volumetric flow rate between the axis of tube and the ψ' streamlines in the moving frame. Naturally, the ratio $Q_\psi^* = Q_\psi/Q$ lies between 0 and 1 and hence the quantity $(Q-Q_\psi)/Q$ must vary from 1 to 0. However, it may happen that Q_ψ^* exceeds unity for some specific cases thereby indicating that there is some kind of backflow or reflux in the tube. **Fig. (5.10(a))** depicts the variations in Q_ψ^* for different values of the viscoelastic parameters. This figure indicates that for large extensibility parameter or for small of Deborah number, the reflux reduces. **Fig. (5.10(b))** presents the variations in Q_ψ^* for μ_r and electro-kinetic slip velocity. It is noted that reflux is increased with increasing the viscosity ratio while an opposite trend is observed when electro-kinetic slip velocity is increased.

5.4 Deductions

In the present study, we investigated the electro-osmotically modulated peristaltic movement in an axisymmetric tube containing a two-fluid system. The governing flow problem is simplified by incorporating the well-known assumptions of low Reynolds number and long wavelength. Prime focus of this analysis is to study the influence of electro-osmotic parameter and viscoelastic behavior of the fluid on pressure, trapping, interface region, and reflux phenomena. Results are suggestive of adjusting the emerging controlling parameters for avoiding the trapping and reflux. Physiologically, trapping is undesirable because it causes thrombosis in blood vessels. Further it can also cause undesirable chemical reactions in reactive fluids. In context of biological fluids, the reflux is also unfavorable phenomenon because of its role in

the migration of micro-organism against the direction of peristaltic movement. Our findings show that it is possible to avoid both trapping and reflux by augmenting the electro-kinetic slip velocity. The situation where it is required to enhance the trapping and to avoid the reflux, one can use the other option i.e. the excitation of the viscoelastic effects of the core region fluid.

(a)

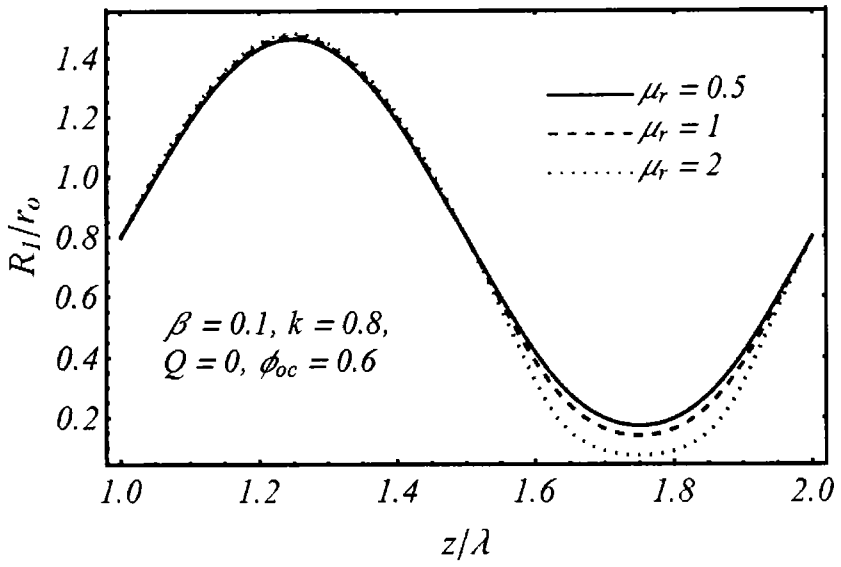

(b)

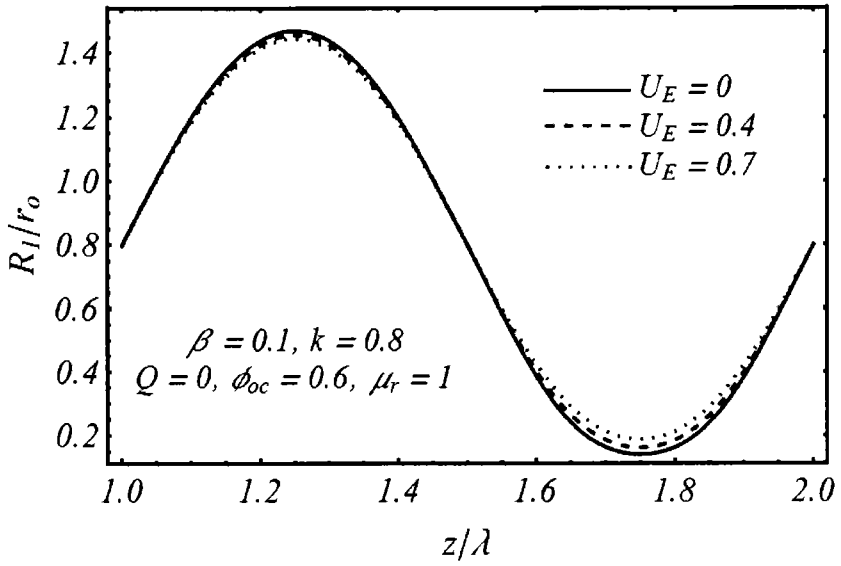

(c)

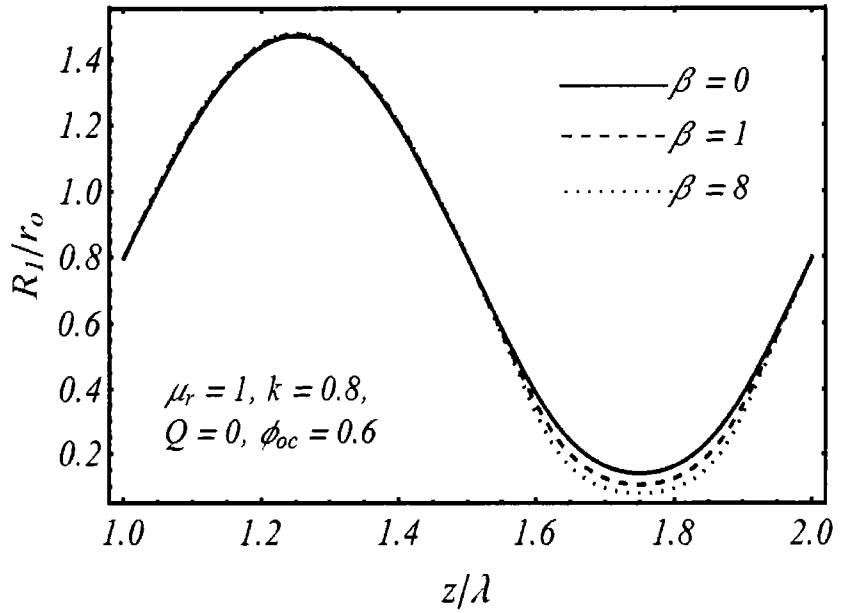

Fig. 5.2 ((a) – (c)): Interface region behavior for several values of μ_r, U_E and β.

(d)

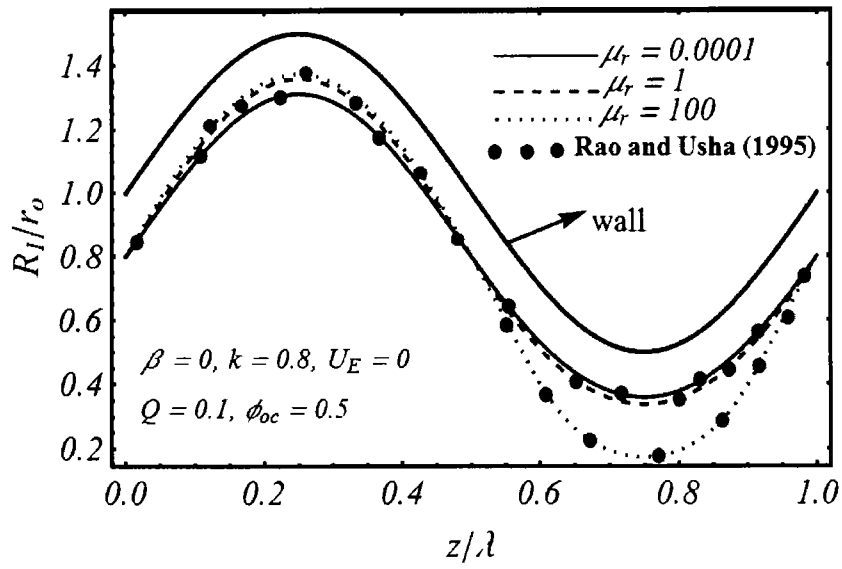

Fig. 5.2 (d): Comparison with the study of Rao and Usha (1995).

(a)

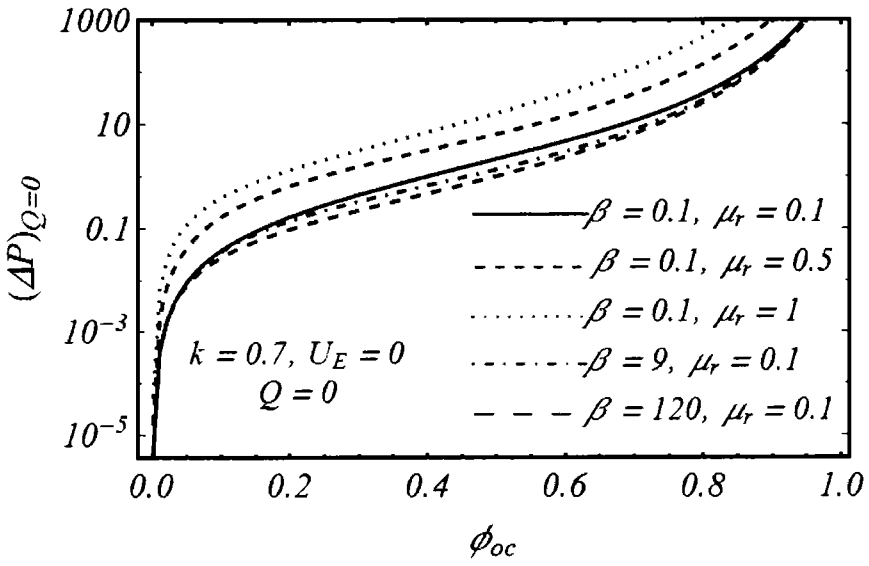

(b)

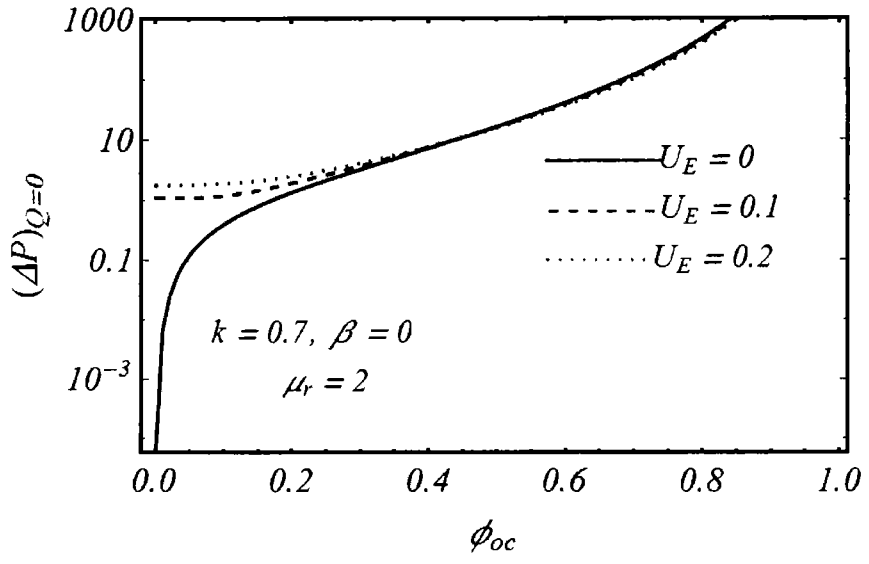

Fig. 5.3 ((a), (b)): The pumping characteristics with respect to the β, μ_r and U_E.

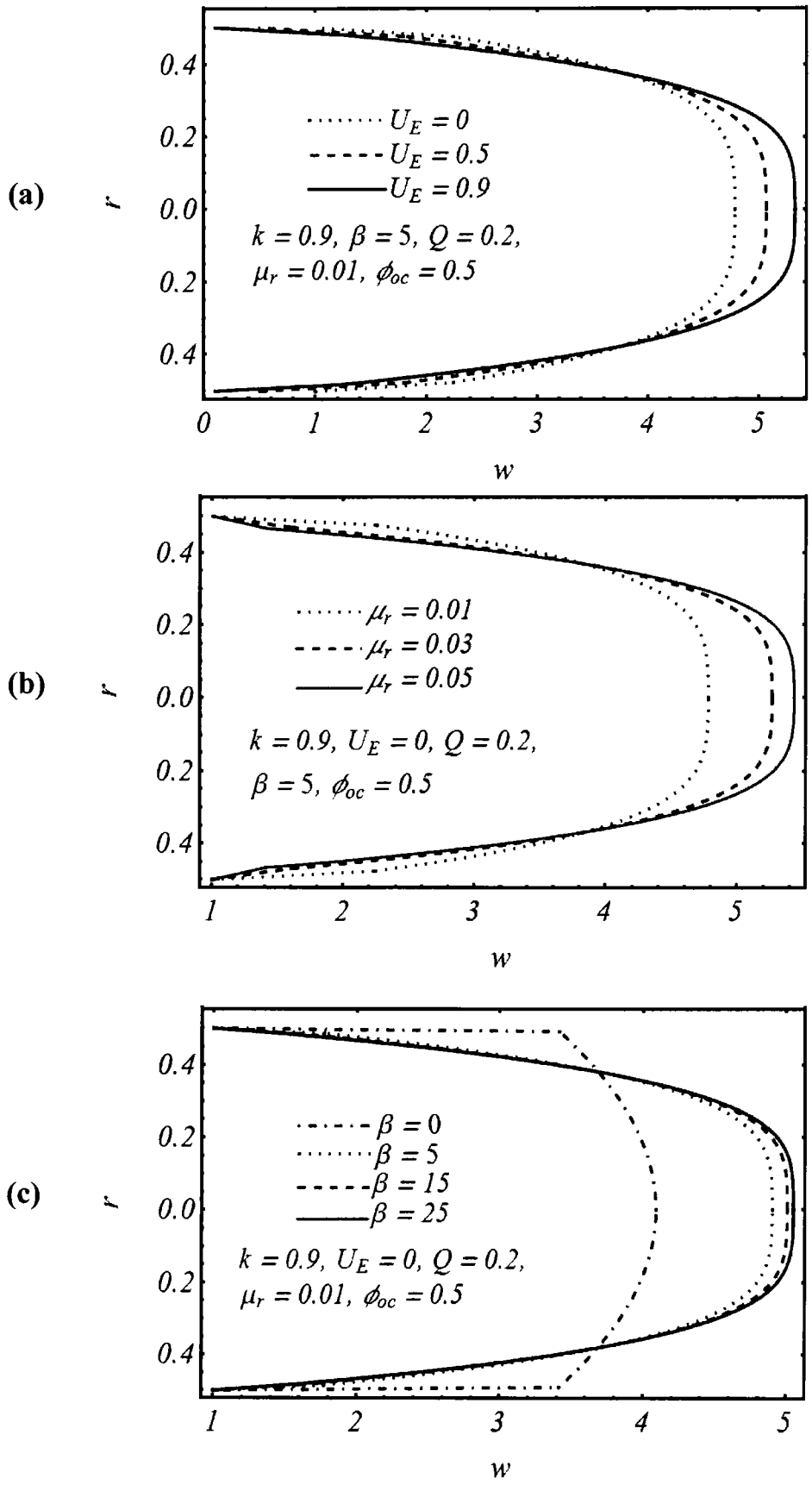

Fig. 5.4 ((a) – (c)): Velocity variations against different parameters U_E, μ_r and β.

(a)

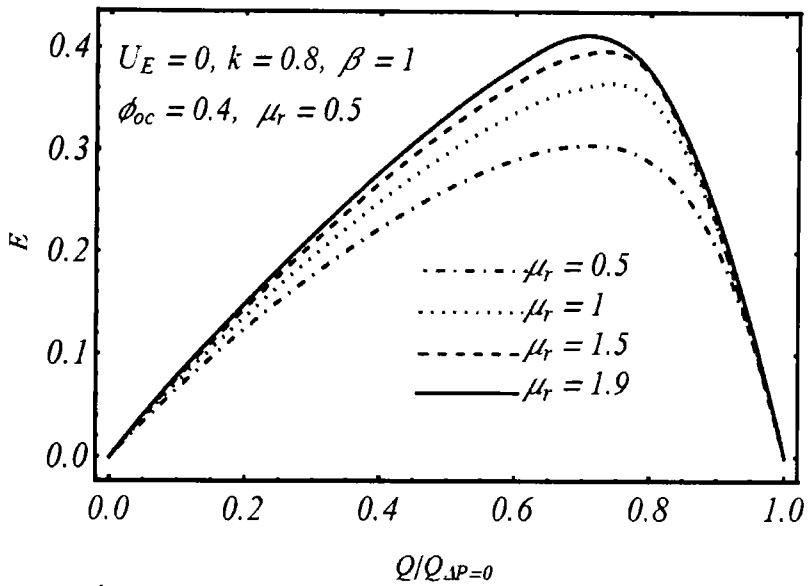

(b)

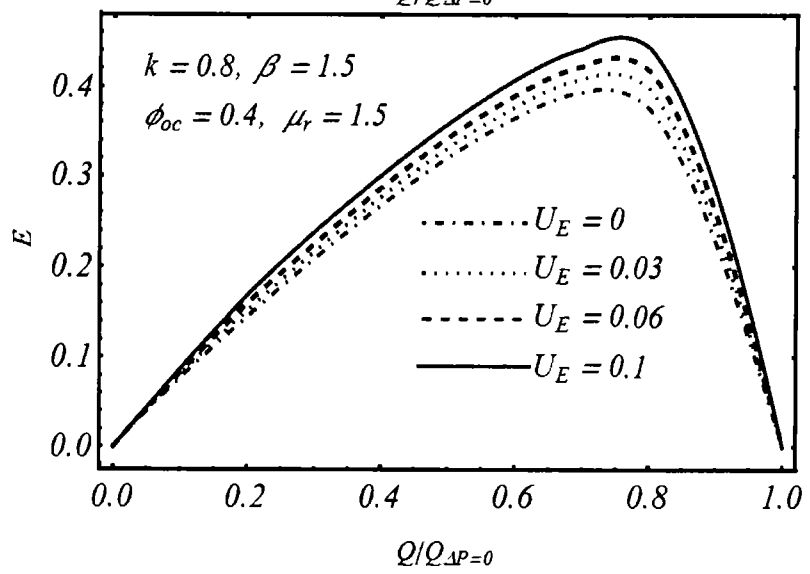

(c)

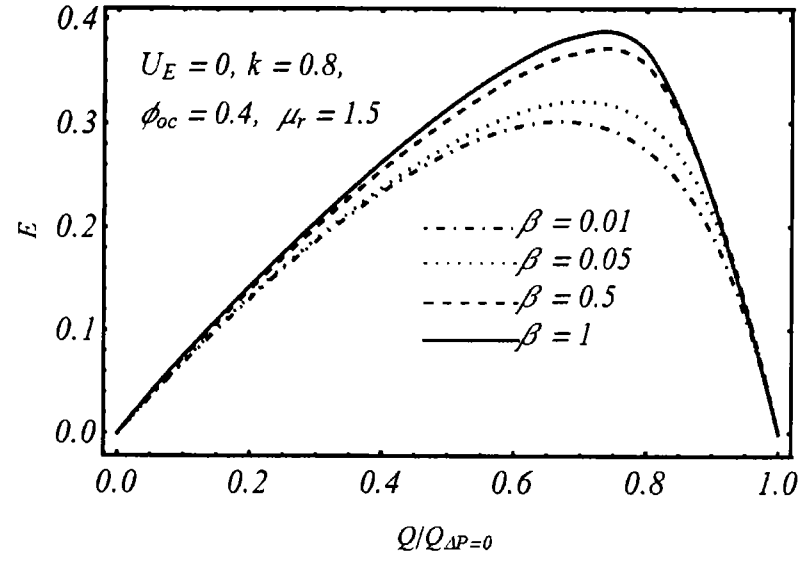

Fig. 5.5 ((a) – (c)): Efficiency variations against different parameters μ_r, U_E and β.

(d)

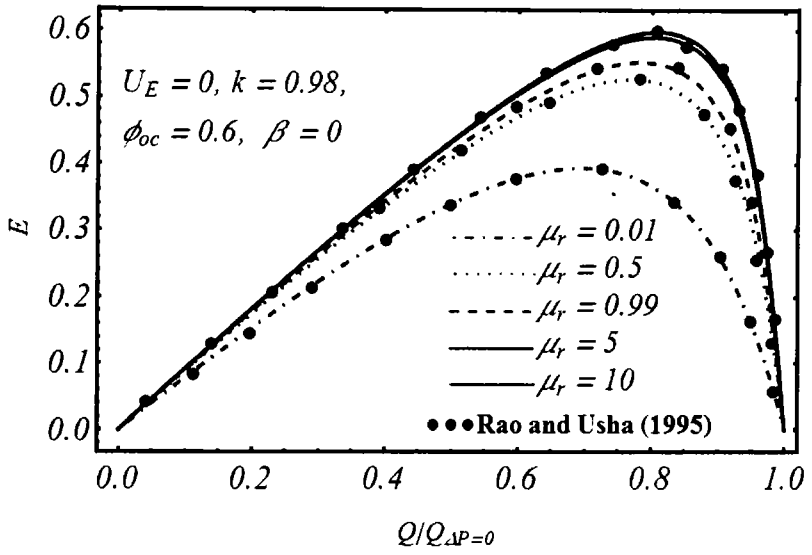

Fig. 5.5 (d): Efficiency variations against different values of μ_r and the comparison with the study of Rao and Usha (1995).

(a)

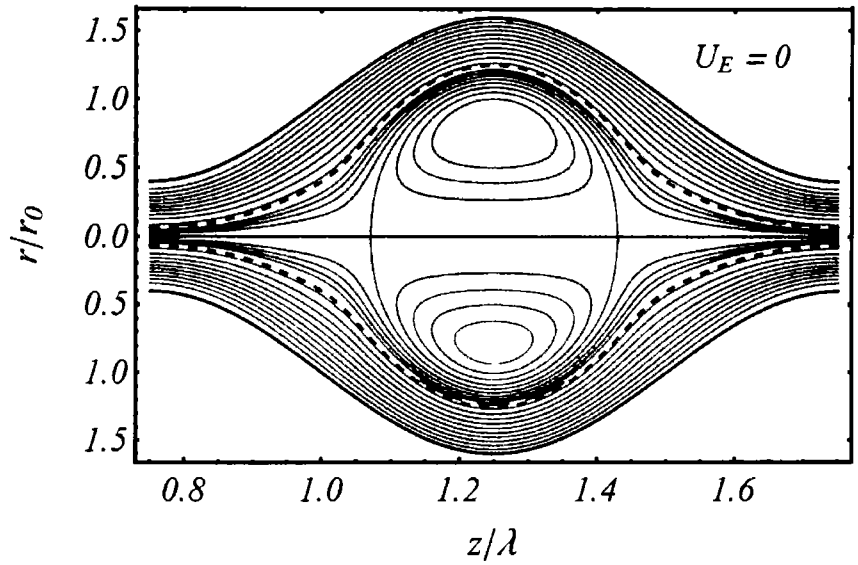

(b)

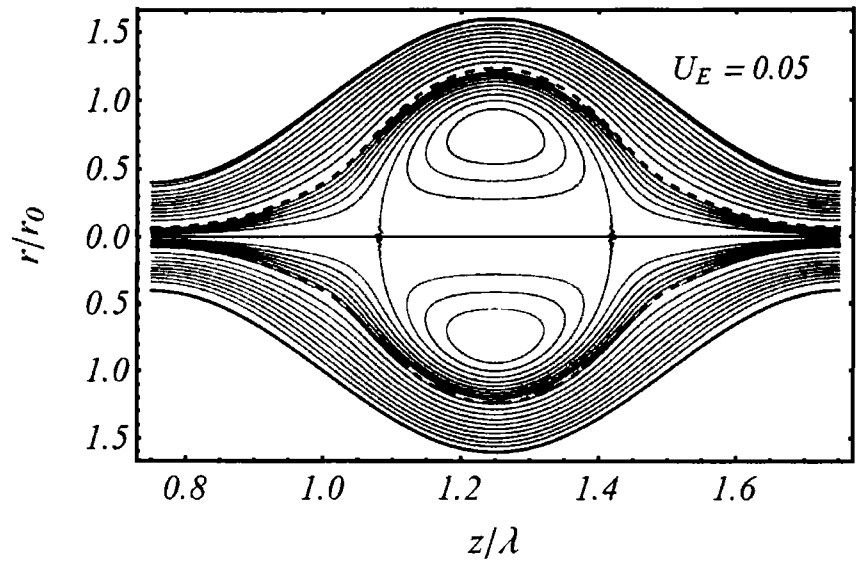

Fig. 5.6 ((a), (b)): The streamlines variation in the core region for U_E when $\beta = 0.0001, Q = 0, \mathrm{k} = 0.4, \phi_{oc} = 0.75, \mu_r = 10.$

(c)

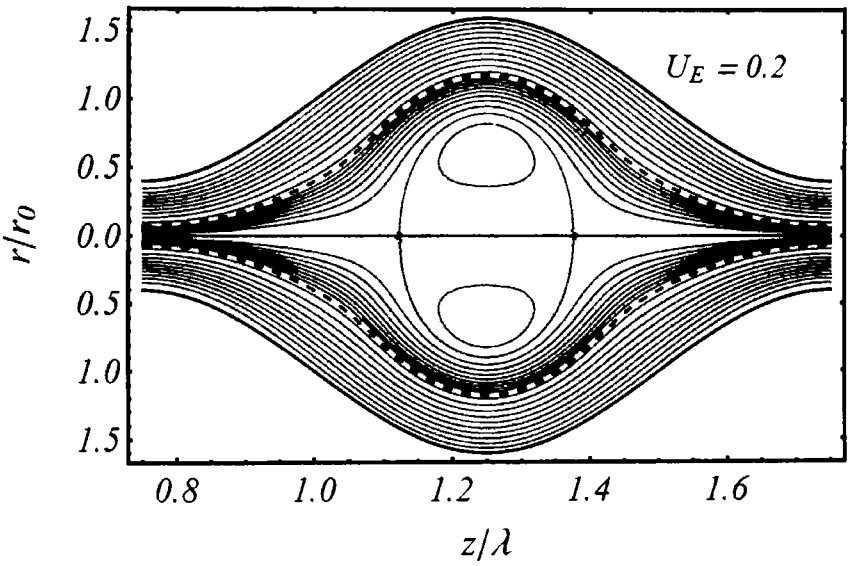

(d)

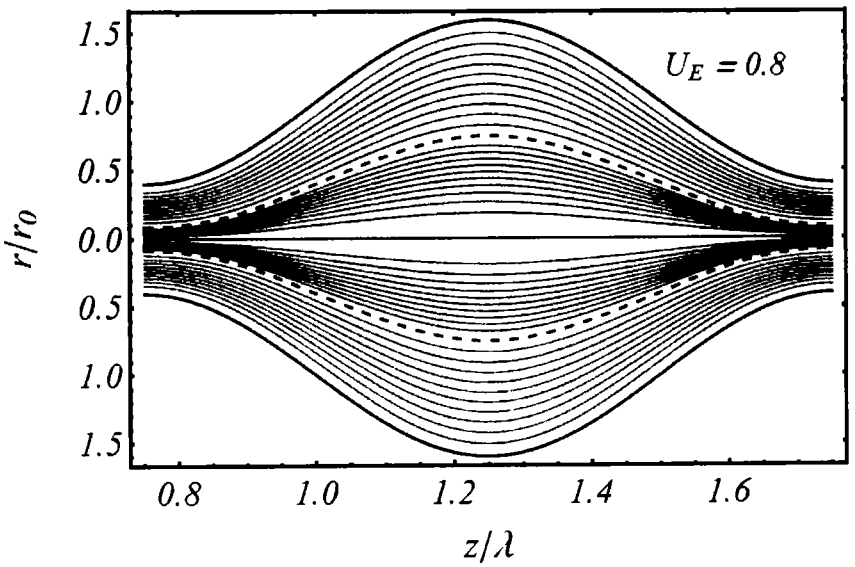

Fig. 5.6 ((c), (d)): The streamlines variation in the core region for U_E when $\beta = 0.0001, Q = 0, \mathrm{k} = 0.4, \phi_{oc} = 0.75, \mu_r = 10.$

(e)

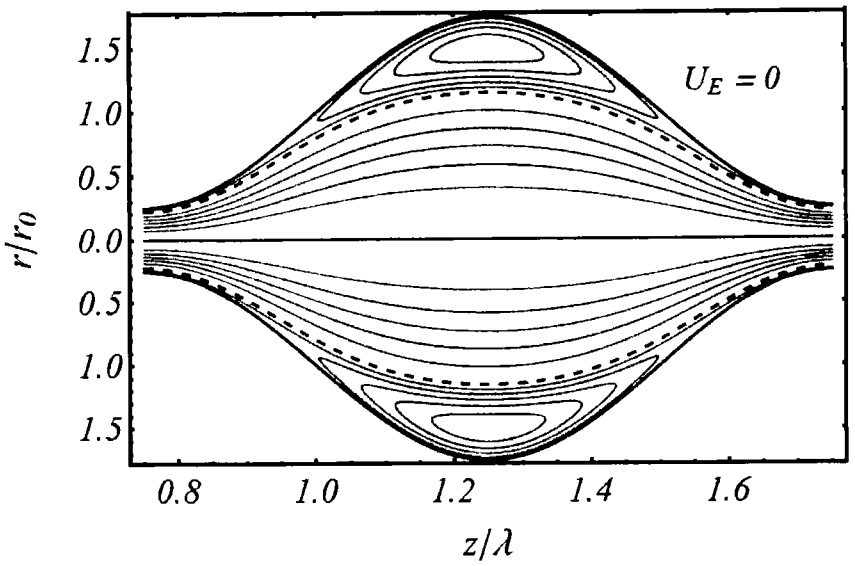

Fig. 5.6 (e). The streamlines variation in the peripheral region when $\phi_{oc} = 0.75, Q = 4, \beta = 0.0001, \mu_r = 1, k = 0.8.$

(f)

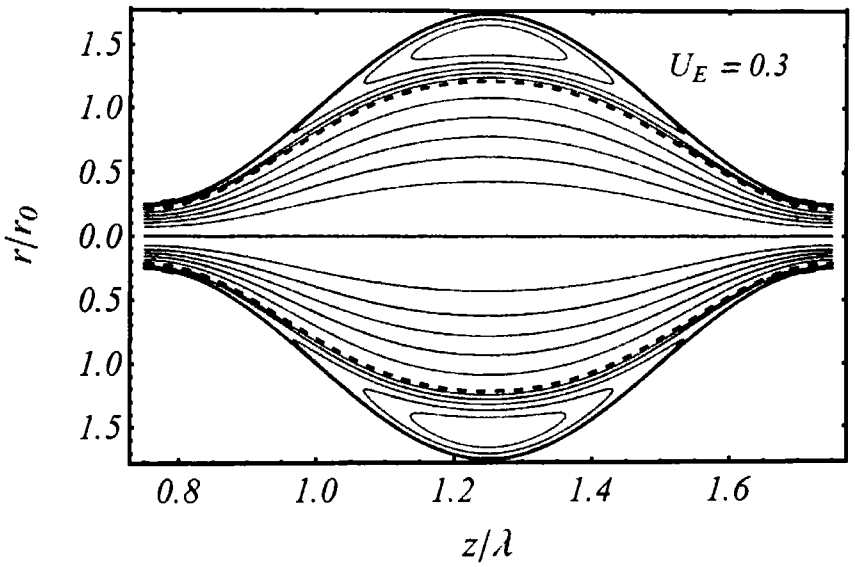

(g)

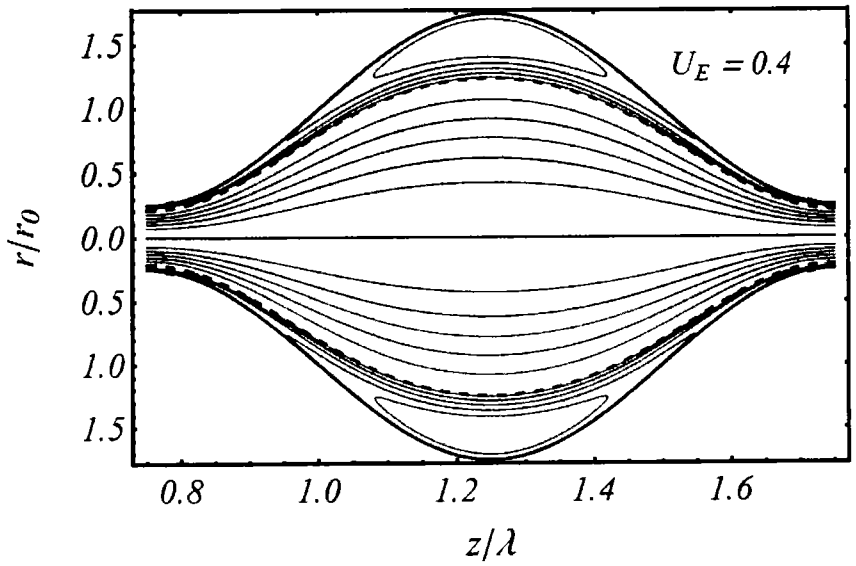

(h)

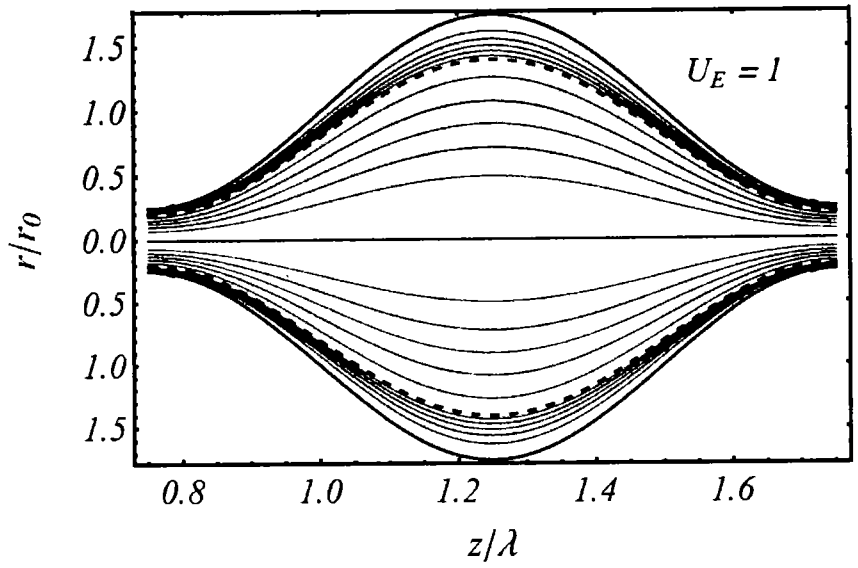

Fig. 5.6 ((f) – (h)). The streamlines variation in the peripheral region when $\phi_{oc} = 0.75, Q = 4, \beta = 0.0001, \mu_r = 1, k = 0.8$.

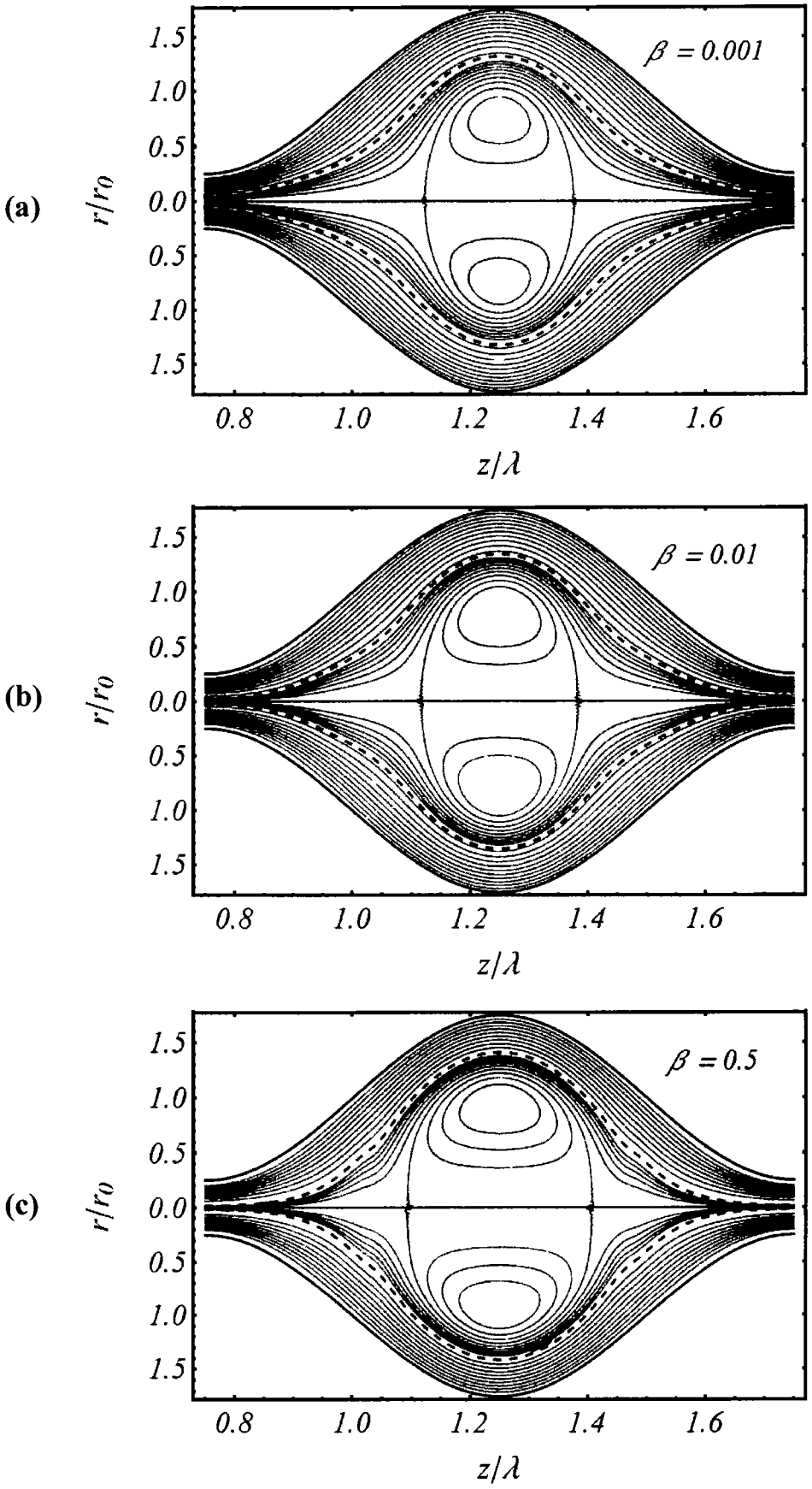

Fig. 5.7 ((a) – (c)): Variations in trapped bolus with respect to the viscoelastic parameter β for $U_E = 0, k = 0.4, \phi_{oc} = 0.75, \mu_r = 1.5, Q = 0$.

(d)

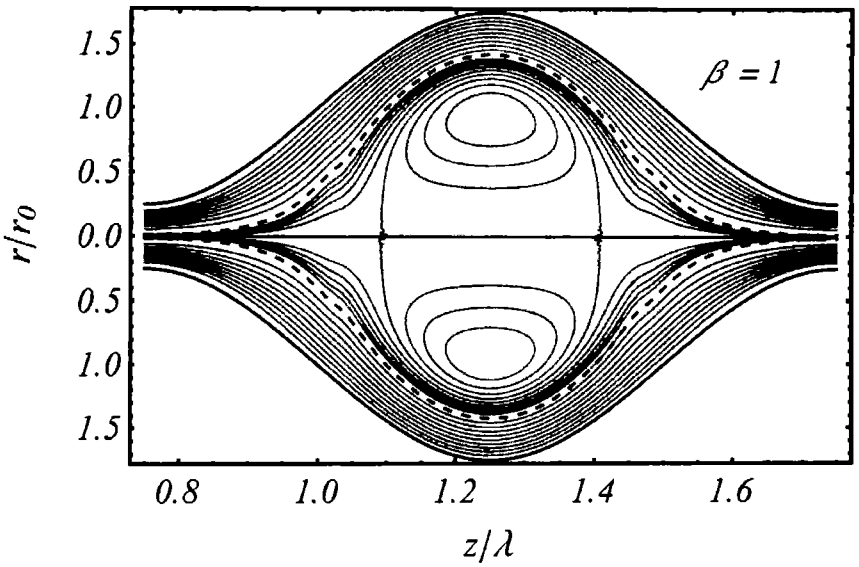

Fig. 5.7 (d): Variations in trapped bolus with respect to the viscoelastic parameter β for $U_E = 0, k = 0.4, \phi_{oc} = 0.75, \mu_r = 1.5, Q = 0$.

(a)

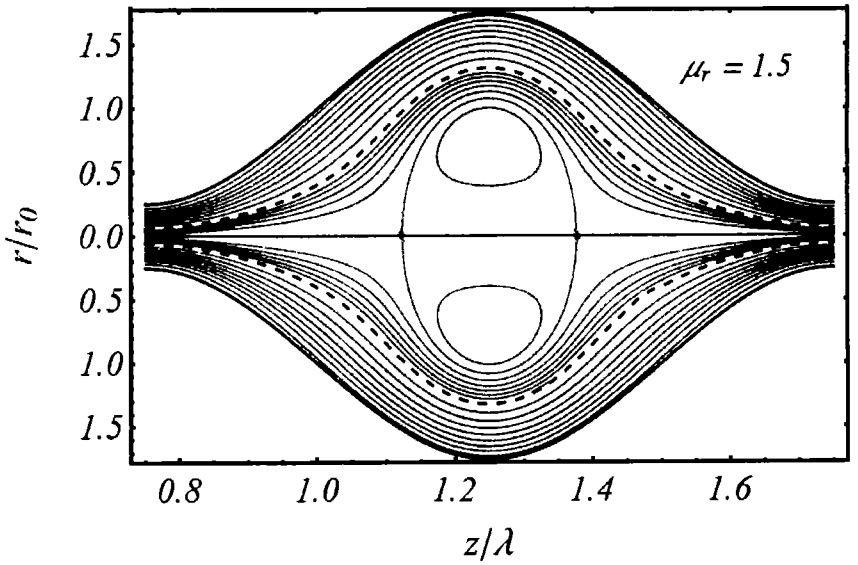

(b)

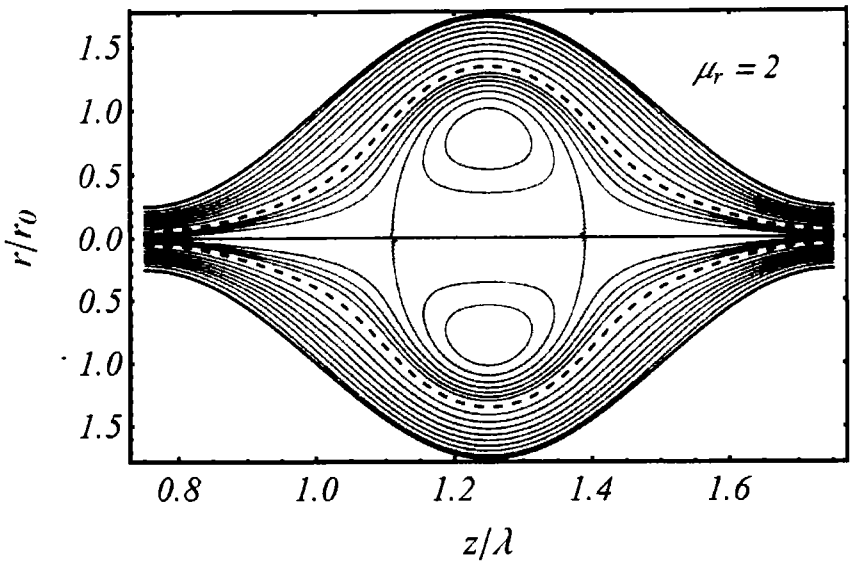

Fig. 5.8 ((a), (b)). Variations in trapped bolus with respect to the viscosity ratio for $k = 0.4, Q = 0, U_E = 0, \beta = 0.0001, \mu_r = 1, \phi_{oc} = 0.75$.

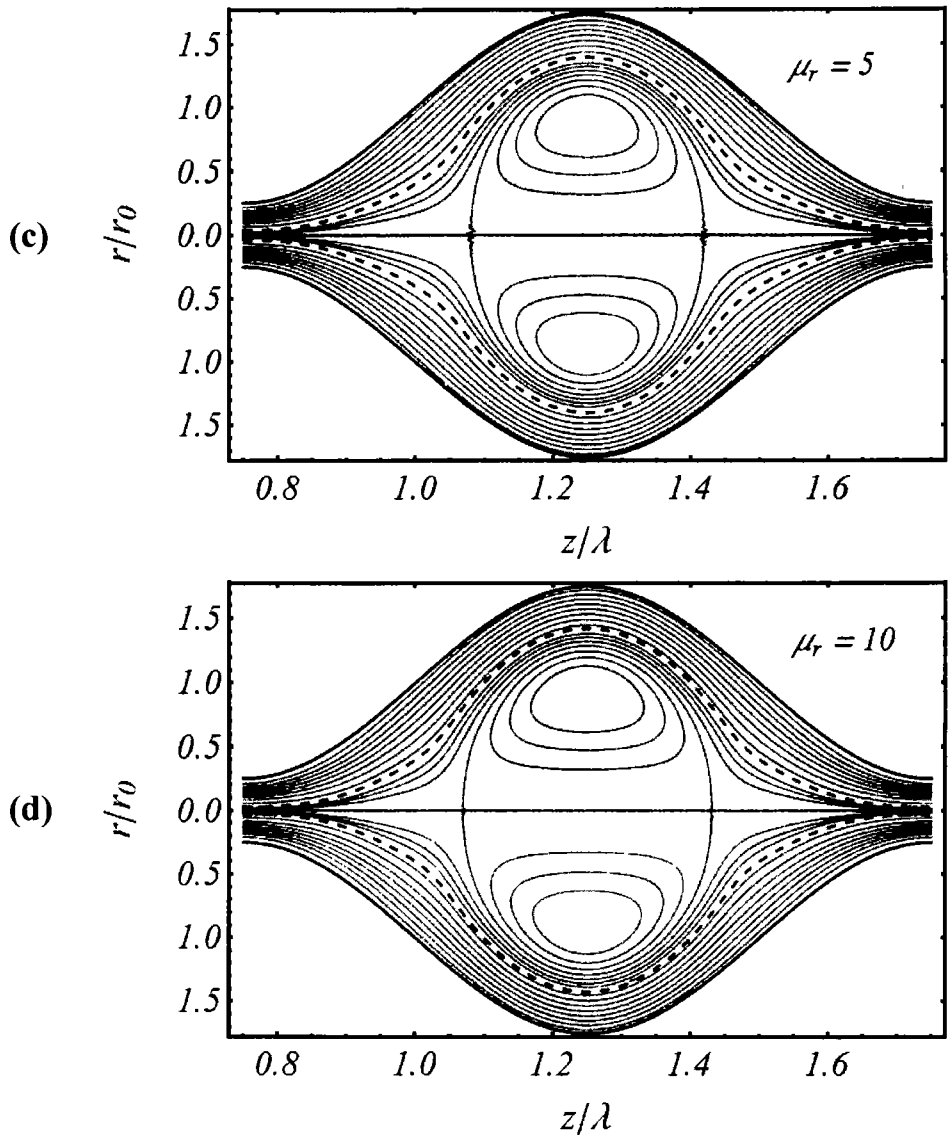

Fig. 5.8 ((c), (d)): Variations in trapped bolus with respect to the viscosity ratio for $k = 0.4, Q = 0, U_E = 0, \beta = 0.0001, \mu_r = 1, \phi_{oc} = 0.75$.

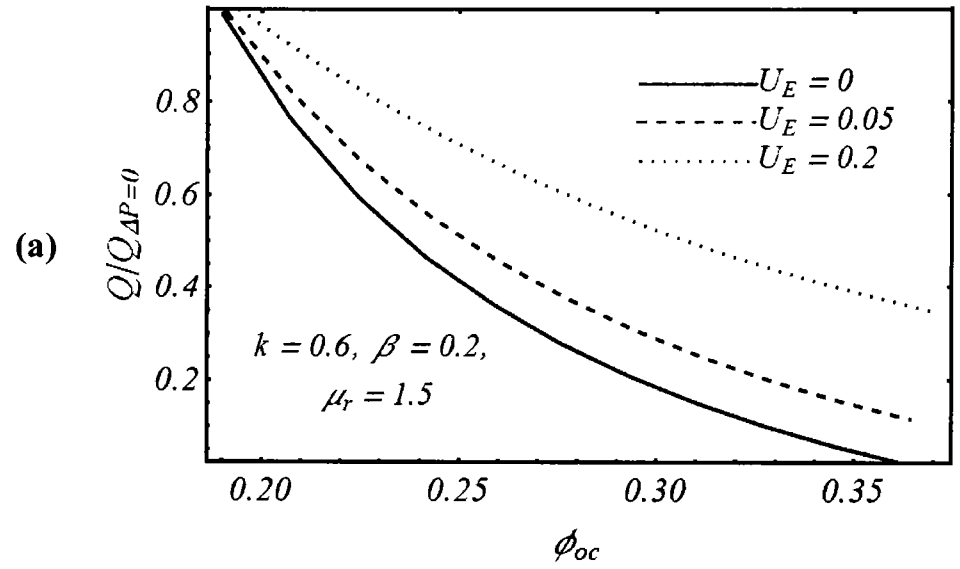

Fig. 5.9 (a): Trapping limit against different parameter U_E.

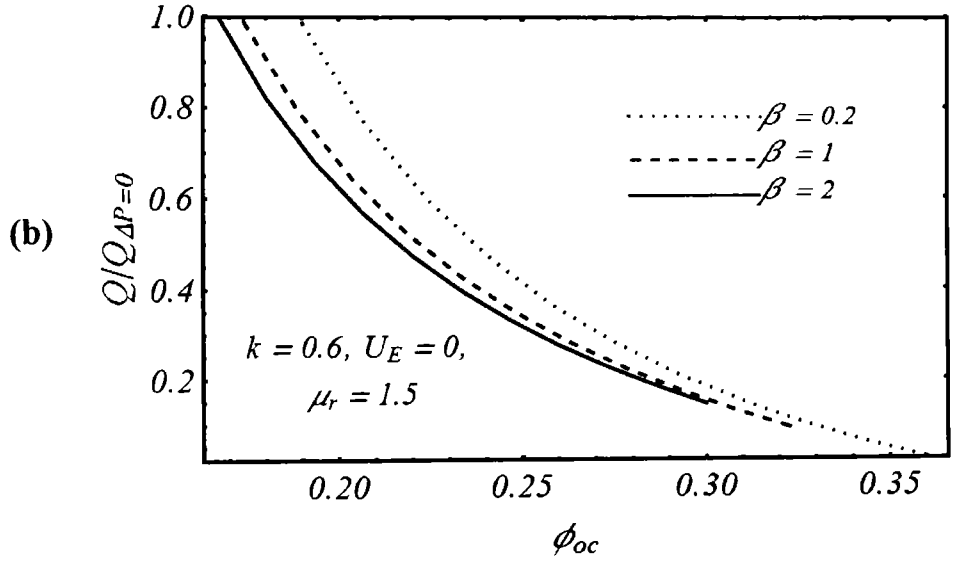

Fig. 5.9 (b): Trapping limit against different parameter β.

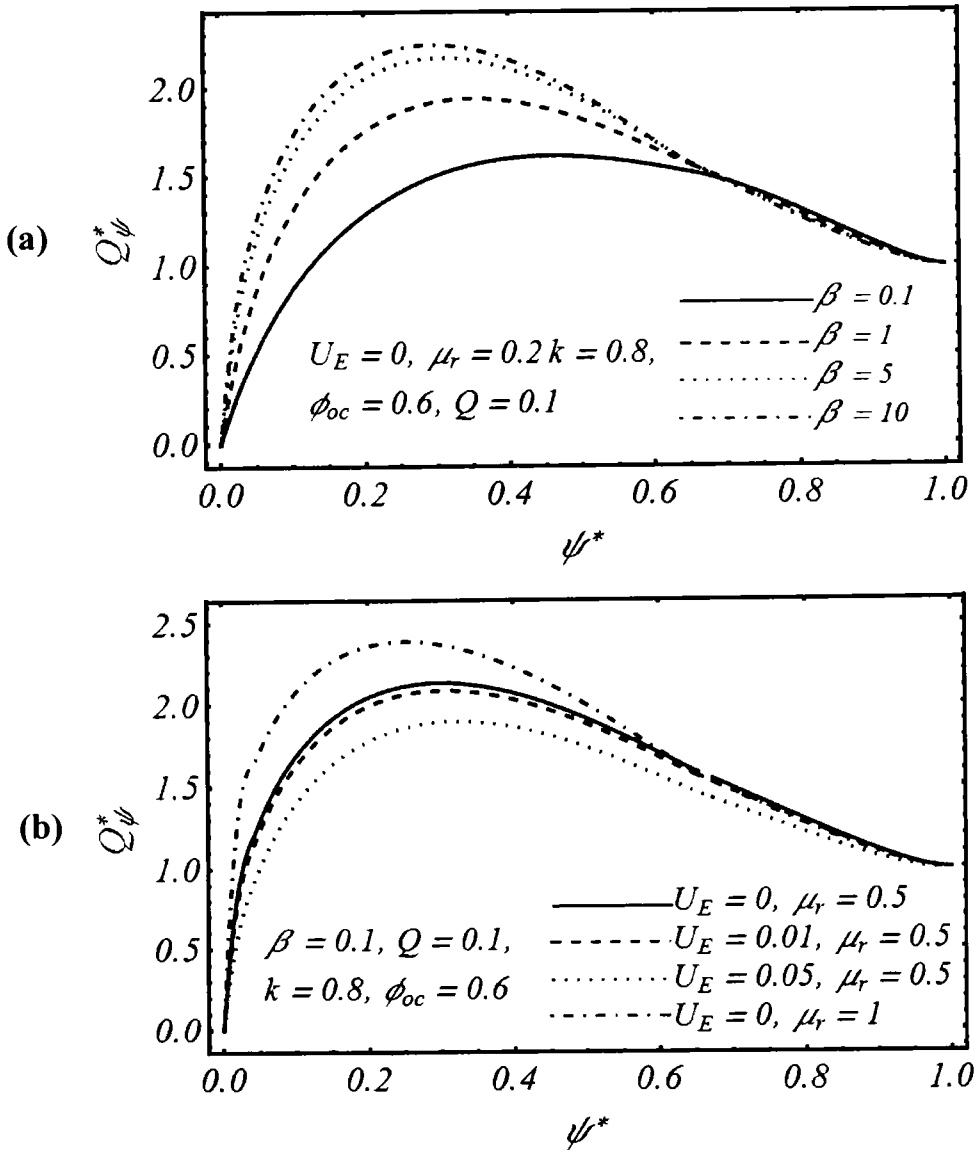

Fig. 5.10 ((a), (b)): Effects of different values of the parameter β, U_E and μ_r on reflux.

Chapter 6

Peristaltic flow of Rabinowitsch fluid in an axisymmetric tube under the influence of electro-osmotic force

This chapter, provides the theoretical study of electro-osmotic peristaltic transport of Rabinowitsch fluid in a cylindrical tube. We highlight the characteristics of the Newtonian fluid in contact with non-Newtonian fluid under the effects of external electric field. The fluid in the peripheral layer is taken as Newtonian while, the non-Newtonian fluid located at the center region (core layer) of the tube is modeled as Rabinowitsch model. Some physical restrictions such as approximations of long wavelength and low Reynolds number, have been adopted to simplify the governing equations in each region. The stream function expression for both peripheral and core layers are obtained. The computations for interface, pressure rise, trapping and reflux are carried out using Mathematica 8.1. Visual illustrations for trapping, pressure rise, velocity, pumping efficiency and reflux are presented. A detail interpretation of the obtained results accompanied with physical significance is provided. This study finds potential applications in bio-medical devices and drug delivery instruments.

6.1 Mathematical treatment of the flow problem

We consider an incompressible fluid in a cylindrical elastic tube having uniform radius r_0. The movement of the fluid is due to the motion of tube wall and electro-osmotic body force as shown in **Fig. (6.1)**. Two different layers are manifested in the flow field. The region adjacent to the wall is peripheral layer while the region at the center of the tube is referred as core layer. Electro-osmotic phenomenon appears due to the solid-fluid interaction. The charged surface of tube wall attracts the oppositely charged ions from the ionized solution within the tube and repels the ions having same charge. This phenomenon generates two types of layers, Stern layer and diffusion layer, whose combination is called EDL. When the system is subjected the electric field, a body force arises (particularly in the diffusion layer) which drag the fluid from positive to negative terminal.

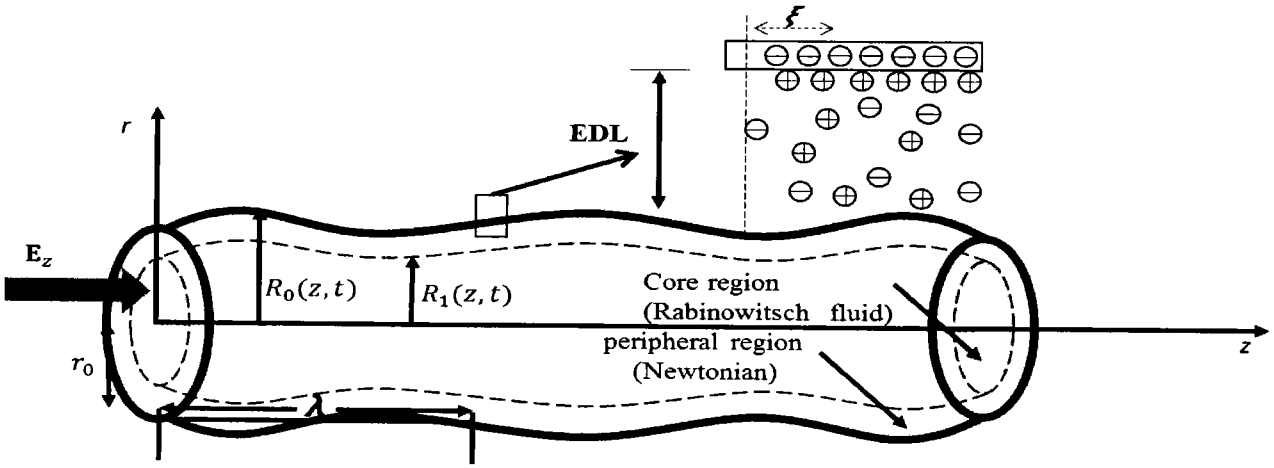

Fig. 6. 1: Geometry

6.2 Governing equations and its solution

The fundamental equations of continuity and momentum are same as given by Eq. (3.1) and Eq. (3.2). In the core region $0 \le r \le R_0(z,t)$, basic constitutive equations of the Rabinowitsch fluid model are reported by Singh and Singh (2014) and Naduvinamani et al. (2014). According to this model, empirical stress–strain relations in components form are given by (Asghar et al. (2017))

$$S_{rz} + \gamma (S_{rz})^3 = \mu_1 \frac{\partial w}{\partial r}, S_{rr} = 2\mu_1 \frac{\partial u}{\partial r}, S_{zz} = 2\mu_1 \frac{\partial w}{\partial z}. \tag{6.1}$$

In the peripheral region $R_1(z,t) \le r \le R_0(z,t)$, the stress will be governed by the equation

$$\mathbf{T} = -p\mathbf{I} + \mathbf{S}, \tag{6.2}$$

where,

$$\mathbf{S} = 2\mu_2 \mathbf{D}. \tag{6.3}$$

Assuming the velocity profile given in Eq. (3.5) and using the transformations reported in Eq. (3.12), the governing equations and stress components along with body force term F_e in the wave frame of reference are:

$$\frac{1}{\bar{r}} \frac{\partial (\bar{r}\bar{u})}{\partial \bar{r}} + \frac{\partial \bar{w}}{\partial \bar{z}} = 0, \tag{6.4}$$

$$\rho\left(\bar{u}\frac{\partial\bar{u}}{\partial\bar{r}}+\bar{w}\frac{\partial\bar{u}}{\partial\bar{z}}\right)=-\frac{\partial\bar{p}}{\partial\bar{z}}+\left[\frac{1}{\bar{r}}\frac{\partial\left(\bar{r}\bar{S}_{rr}\right)}{\partial\bar{r}}+\frac{\partial\bar{S}_{rz}}{\partial\bar{z}}-\frac{\bar{S}_{\theta\theta}}{\bar{r}}\right], \tag{6.5}$$

$$\rho\left(\bar{u}\frac{\partial\bar{w}}{\partial\bar{r}}+\bar{w}\frac{\partial\bar{w}}{\partial\bar{z}}\right)=-\frac{\partial\bar{p}}{\partial\bar{z}}+\left[\frac{1}{\bar{r}}\frac{\partial\left(\bar{r}\bar{S}_{rz}\right)}{\partial\bar{r}}+\frac{\partial\bar{S}_{zz}}{\partial\bar{z}}\right]+\bar{F}_e. \tag{6.6}$$

Stress components for inner region:

$$\bar{S}_{rz}+\gamma\left(\bar{S}_{rz}\right)^3=\mu_1\frac{\partial\bar{w}}{\partial\bar{r}},\bar{S}_{rr}=2\mu_1\frac{\partial\bar{u}}{\partial\bar{r}},\bar{S}_{zz}=2\mu_1\frac{\partial\bar{w}}{\partial\bar{z}}. \tag{6.7}$$

Stress components for outer region:

$$\bar{S}_{rr}=2\mu_2\frac{\partial\bar{u}}{\partial\bar{r}},\bar{S}_{rz}=\bar{S}_{zr}=\mu_2\left(\frac{\partial\bar{u}}{\partial\bar{z}}+\frac{\partial\bar{w}}{\partial\bar{r}}\right),\bar{S}_{\theta\theta}=\mu_2\frac{\bar{u}}{\bar{r}},\bar{S}_{zz}=2\mu_2\frac{\partial\bar{w}}{\partial\bar{z}},$$

$$\bar{S}_{r\theta}=\bar{S}_{\theta r}=\bar{S}_{\theta z}=\bar{S}_{z\theta}=0. \tag{6.8}$$

The subsequently analysis is based on the simplification of electro-kinetic body force term $\bar{F}_e=\bar{\rho}_e E_z$ for which the detail are provided in the chapter 3. Thus, the body force term in the momentum equation is treated according to the same argument. After using the dimensionless variables as given by Eq. (3.15) and the physical restriction such as long wavelength ($\delta \ll 1$) and low Reynolds number($Re \ll 1$) approximation, Eqs (6.4) – (6.8) in the both regions reduce to

Core region:

$$\begin{cases}0=-\dfrac{\partial p}{\partial z}+\left[\left(\dfrac{1}{r}\dfrac{\partial\left(rS_{rz}\right)}{\partial r}\right)\right]+U_E\dfrac{\mu_r}{\epsilon_r}\rho_{ec},\\ 0=-\dfrac{\partial p}{\partial r},\end{cases} \tag{6.9}$$

$$S_{rz}+\alpha_1\left(S_{rz}\right)^3=\frac{\partial w_c}{\partial r}, \tag{6.10}$$

where $\alpha_1=\gamma\mu_1^2U^2/r_0^2$ is called the model parameter of Rabinowitsch constitutive equation.

Peripheral region:

$$\begin{cases} 0 = -\dfrac{\partial p}{\partial z} + \left[\left(\dfrac{1}{r}\dfrac{\partial (r S_{rz})}{\partial r}\right)\right] + U_E \dfrac{\mu_{\mathrm{r}}}{\epsilon_r}\rho_{ec}, \\ 0 = -\dfrac{\partial p}{\partial r}, \end{cases} \tag{6.11}$$

$$S_{rz} = \mu_r\left(\frac{\partial w_N}{\partial r}\right). \tag{6.12}$$

where, $U_E = -\epsilon_N \xi E_z / \mu_2 U$ is the electro-kinetic slip velocity. The dimensionless boundary conditions linked with Eqs. (6.9) - (6.12) are given Eqs. (3.28) - (3.30). Here, we have two choices to analyze the problem; first, we can solve the problem by considering the electro-kinetic term in the momentum equation and second one is to include the influence of electro-kinetic term in a boundary condition. The output yielded from both ways will always be the same (Goswami et al. (2016)). The present fluid problem is figured out by taking body force term in the boundary condition. Therefore, the following problem emerges.

In core region:

$$\begin{cases} 0 = -\dfrac{\partial p}{\partial z} + \left[\left(\dfrac{1}{r}\dfrac{\partial (r S_{rz})}{\partial r}\right)\right], \\ 0 = -\dfrac{\partial p}{\partial r}, \end{cases} \tag{6.13}$$

$$S_{rz} + \alpha_1 \left(S_{rz}\right)^3 = \frac{\partial w_c}{\partial r}, \tag{6.14}$$

$$\frac{\partial w_c}{\partial r} = 0, \text{at } r = 0; \tag{6.15}$$

In peripheral region:

$$\begin{cases} 0 = -\dfrac{\partial p}{\partial z} + \left[\left(\dfrac{1}{r}\dfrac{\partial (r S_{rz})}{\partial r}\right)\right], \\ 0 = -\dfrac{\partial p}{\partial r}, \end{cases}, \tag{6.16}$$

$$S_{rz} = \mu_r\left(\frac{\partial w_N}{\partial r}\right). \tag{6.17}$$

$$\begin{aligned} &\frac{\partial w_N}{\partial r} = 0, \text{at } r = 0; \\ &w_N = U_E - 1, \text{at } r = R_0. \end{aligned} \tag{6.18}$$

The above equations after adopting stream function formulation take the form

$$\frac{\partial}{\partial r}\left(\frac{1}{r}\frac{\partial \psi}{\partial r}\right)=\frac{r}{2}\frac{\partial p}{\partial z}+\frac{\alpha_1}{8}\left(\frac{\partial p}{\partial z}\right)^3 r^3 \quad ,0\le r\le R_1 \tag{6.19}$$

$$\frac{\partial p}{\partial z}=\frac{1}{r}\frac{\partial}{\partial r}\left[\left(r\mu_r\frac{\partial}{\partial r}\left(\frac{1}{r}\frac{\partial \psi}{\partial r}\right)\right)\right] \quad ,R_1\le r\le R_0 \tag{6.20}$$

$$\psi=0,\ \frac{\partial}{\partial r}\left(\frac{1}{r}\frac{\partial \psi}{\partial r}\right)=0, \text{at } r=0, \tag{6.21}$$

$$\psi=\frac{q}{2},\ \frac{\partial \psi}{\partial r}=\left(U_E-1\right)R_0, \text{at } r=R_0, \tag{6.22}$$

$$\psi=\frac{q_1}{2}, \text{at } r=\mathrm{R}_1. \tag{6.23}$$

Solving Eq. (6.19) and (6.20) subject to the boundary conditions (6.21) and (6.22), the stream functions are given by

$$\psi=\begin{cases}\dfrac{r^2}{2}\left\{\left(U_E-1\right)+\dfrac{\alpha_1}{96}\left(\dfrac{\partial p}{\partial z}\right)^3\left[r^4-3R_1^{\,4}\right]+\dfrac{1}{8}\dfrac{\partial p}{\partial z}\left(\left\{r^2-2R_1^{\,2}\right\}+\dfrac{2}{\mu_r}\left\{R_1^{\,2}-R_0^{\,2}\right\}\right)\right\}, 0\le r<R_1\\ \dfrac{r^2}{2}\left(U_E-1\right)+\left(\dfrac{q}{2}-\left(U_E-1\right)\dfrac{R_0^{\,2}}{2}\right)+\dfrac{1}{16\mu_r}\dfrac{\partial p}{\partial z}\left(r^2-R_0^{\,2}\right)^2 . R_1\le r\le R_0\end{cases} \tag{6.24}$$

From Eq. (6.24), the velocity components for inner $\left(0\le r\le R_1\right)$ and outer $\left(R_1\le r\le R_0\right)$ regions are:

$$w(r,z)=\begin{cases}\left(U_E-1\right)+\dfrac{\alpha_1}{32}\left(\dfrac{\partial p}{\partial z}\right)^3\left[r^4-R_1^{\,4}\right]+\dfrac{1}{4}\dfrac{\partial p}{\partial z}\left(\left\{r^2-R_1^{\,2}\right\}+\dfrac{1}{\mu_r}\left\{R_1^{\,2}-R_0^{\,2}\right\}\right), 0\le r\le R_1\\ \left(U_E-1\right)+\dfrac{1}{4\mu_r}\dfrac{\partial p}{\partial z}\left(r^2-R_0^{\,2}\right). R_1\le r\le R_0\end{cases} \tag{6.25}$$

The dimensionless wall equation of the tube is $R_o(z)=1+\phi_{oc}\sin(2\pi z)$

Employing the semi-analytical approach outlined by Goswami et al. (2016), the following expression for computation of interface emerges.

$$\frac{q_1}{2}=\frac{R_1^2}{2}(U_E-1)+\left(\frac{q}{2}-(U_E-1)\frac{R_0^2}{2}\right)+\frac{1}{16\mu_r}\frac{\partial p}{\partial z}\left(R_1^2-R_0^2\right)^2. \tag{6.26}$$

For eliminating q_1, we set $R_0=1$ and $R_1=k$ at $z=0$, so that Eq. (6.26) becomes

$$\frac{q_1}{2}=\frac{k^2}{2}(U_E-1)+\left(\frac{q}{2}-(U_E-1)\frac{1}{2}\right)+\frac{1}{16\mu_r}P_0\left(k^2-1\right)^2. \tag{6.27}$$

Eliminating q_1 from Eq. (6.26) and (6.27), we get

$$\begin{aligned}&\left(\frac{k^2}{2}(U_E-1)+\left(\frac{q}{2}-(U_E-1)\frac{1}{2}\right)\right)+\frac{1}{16\mu_r}P_0\left(k^2-1\right)^2-\\&\left(\frac{R_1^2}{2}(U_E-1)+\left(\frac{q}{2}-(U_E-1)\frac{R_0^2}{2}\right)\right)-\frac{1}{16\mu_r}\frac{\partial p}{\partial z}\left(R_1^2-R_0^2\right)^2=0.\end{aligned} \tag{6.28}$$

Solving Eq. (6.28) yields the following expression for pressure gradient,

$$\frac{\partial p}{\partial z}=\frac{16\mu_r}{\left(R_1^2-R_0^2\right)^2}\left\{\frac{1}{2}(U_E-1)\left(k^2-R_1^2+R_0^2\right)+\frac{1}{16\mu_r}P_0\left(k^2-1\right)^2\right\}. \tag{6.29}$$

Integrating Eq. (6.29) over one wavelength gives

$$\Delta p=\int_0^{\lambda}\left\{\frac{\left(8\mu_r(U_E-1)\left(k^2-R_1^2+R_0^2\right)+P_0\left(k^2-1\right)^2\right)}{\left(R_1^2-R_0^2\right)^2}\right\}dz. \tag{6.30}$$

The conversion of the volume flux from fixed to moving frame of reference is obtained through the equation

$$Q_S=2\int_0^{R_0}(u+1)r\,dr=q+R_0^2. \tag{6.31}$$

On simplification, Eq. (6.31) will give

$$Q=\frac{1}{T_P}Q_S\,dt=q+\left(1+\frac{\phi^2}{2}\right), \tag{6.32}$$

Using Eq. (6.29) in Eq. (6.28) yields

$$\frac{\alpha_1}{96}\left(\frac{16\mu_r}{\left(R_1^2-R_0^2\right)^2}\left\{\frac{1}{2}\left(U_E-1\right)\left(k^2-R_1^2+R_0^2\right)+\frac{1}{16\mu_r}P_0\left(k^2-1\right)^2\right\}\right)^3 R_1^6$$
$$+\frac{1}{16}\left(\frac{\mu_r}{\left(R_1^2-R_0^2\right)^2}\left\{\frac{1}{2}\left(U_E-1\right)\left(k^2-R_1^2+R_0^2\right)+\frac{1}{16\mu_r}P_0\left(k^2-1\right)^2\right\}\right)R_1^4 \qquad (6.33)$$
$$+\frac{1}{16\mu_r}\left(\frac{1}{\left(R_1^2-R_0^2\right)^2}\left\{\frac{1}{2}\left(U_E-1\right)\left(k^2-R_1^2+R_0^2\right)+\frac{1}{16\mu_r}P_0\left(k^2-1\right)^2\right\}\right)\left(R_0^4-R_1^4\right)+$$
$$\frac{q}{2}-\left(U_E-1\right)\frac{R_0^2}{2}=0.$$

Now, we have two unknown in Eq. (6.33) i.e., P_0 and R_1. For attaining the complete solution, the only available equation is Eq. (6.28). Other conditions are developed by using the fact that stream functions given by the expression (6.24) for both regions must be same at the interface. Thus, we get

$$\frac{\alpha_1}{96}\left(\frac{\partial p}{\partial z}\right)^3 R_1^6+\frac{1}{16}\frac{\partial p}{\partial z}R_1^4+\frac{1}{16\mu_r}\frac{\partial p}{\partial z}\left(R_0^4-R_1^4\right)+\frac{q}{2}-\left(U_E-1\right)\frac{R_0^2}{2}=0, \qquad (6.34)$$

setting $R_0=1$ and $R_1=k$ at $z=0$, above equation becomes

$$\frac{\alpha_1}{96}P_0^3k^6+\frac{1}{16}P_0k^4+\frac{1}{16\mu_r}P_0\left(1-k^4\right)+\frac{q}{2}-\left(U_E-1\right)\frac{1}{2}=0. \qquad (6.35)$$

The system in now consistent i.e. three known ($P_0, R_1, \partial p/\partial z$) with three equations (6.33 – 6.35). It is important to note that these equations are difficult to solve analytically. Therefore, we shall solve them numerically using Mathematica 8.1. The obtained results are highlighted through graphs with comprehensive discussion in the next section.

6.3 Results and discussions

In this section, we will perform a detailed parametric analysis to study the effects of emerging parameter on the two-layered electro-osmotic peristaltic bio-fluid flow. The salient results of our simulation can be observed from **Figs. (6.2 - 6.9).** These graphical results highlight the influences of various involved parameters on important flow features such as velocity profile, fluid-fluid interface, pressure difference and mechanical efficiency. Moreover, the effects of emerging parameters on trapping and reflux in both the core and the peripheral layers have also been considered. **Fig. (6.2a)**

interprets behavior or the interface against the viscoelastic parameter. In this model, α_1 indicates three different responses, that is, $\alpha_1 > 0\ (shear - thinning), \alpha_1 < 0 (shear - thickening)$ and $\alpha_1 = 0\ (Newtonian)$. when $\alpha_1 < 0$, the fluid in the crest region experiences a reduced normal force due to large viscosity in the core region and the interface curve will remain below the interface curve for $\alpha_1 = 0$. But in the trough region, this trend is reversed and interface curve will appear above the interface curve for $\alpha_1 = 0$. For $\alpha_1 > 0$, interface curve shows an opposite behavior in both regions. A similar behavior of interface curve at crest and trough regions for different viscosity ratio, $\mu_r < 1, \mu_r > 1$ and $\mu_r = 1$, are observed in the **Fig. (6.2b).** In the wave crest region, the fluid experiences an upward normal force while in the trough region this force appears to be in the downward direction. **Fig. (6.2c)** illustrates the interfacial behavior for several values of the electro-osmotic slip velocity. Actually, increment in the electro-osmotic slip velocity decreases the viscous resistance within the fluid domain. In response to that the fluid experiences a reduced upward normal force in the crest region and thus the interfacial curve for positive value of U_E remains below the curve for $U_E = 0$. In contrast, a reverse trend prevails for positive electro-osmotic slip velocity in the trough region.

The pressure variations in pressure with respect to the involved parameters are shown in **Fig. (6.3(a - d)). Fig. (6.3a)** depicts pressure difference at zero flow rate for several values of the electro-kinetic slip velocity and viscosity ratio. The fluid propagates with high velocity at the trough region as compared to the crest region. An enlargement in the pressure rise is observed for large electrokinetic slip velocity at moderate occlusion parameter. But at the higher values of the occlusion parameter, the influence of the electro-kinetic slip velocity becomes negligible. **Figs. (6.3(b-d))** demonstrate the pressure difference against the volumetric flow rate for different values of the parameters k, α_1 and U_E. It is observed that the pressure rise increases by increasing the values of the electro-kinetic slip velocity but decreasing trend is noted for k and α_1. The mechanical efficiency against the time-averaged volumetric rate is shown in the **Figs. (6.4(a, b))**. We observe an increment in the mechanical efficiency for increasing values of the electro-kinetic slip velocity. This ensures the maximum fluid transmission from the conduit. We may conclude that the increase in the intensity of external potential efficiency leads to the improvement of the system. On

the other hand, the opposite trend observed when the value of Rabinowitsch parameter is increased.

Velocity distribution (6.25) is visualized in the **Fig. 6.5(a - c)** for several values of the emerging parameters μ_r, α_1 and U_E. **Fig. (6.5a)** demonstrates the behavior of the velocity profile for the fluid in the central region at different values of the Rabinowitsch model parameter. It is observed that the velocity in the center region decreases by increasing the values of α_1. **Figs. (6.5(b, c))** illustrate the variations of the velocity for different parametric values of viscosity ratio and electro-osmotic parameter. It is noted that the velocity of the fluid in the central region increases for large values of the electro-kinetic slip velocity. A similar trend in velocity prevails for different values of the viscosity ratio μ_r.

The streamline topologies play a significant role to understand the fluid flow phenomenon. At some certain values of the volume flow rate and occlusion parameter some closed streamlines are found in the flow. These closed streamlines originate the phenomenon called as trapping. Trapping has a significant role in many physiological and industrial systems. Sometimes, it creates many disorders in human body in the form of thrombosis in the blood circulation. Further, it can also cause undesirable chemical reactions in reactive fluids. The trapping phenomenon for different values of involved parameters is depicted in **Figs. (6.6(a - c)) – (6.8(a - c)). Fig. (6.6(a - c))** highlights the trapping mechanism for several values of the Rabinowitsch parameter. It is found that the size of the trapped bolus increases with an increment in the parameter α_1. **Figs. (6.7(a - c))** and **(6.8(a - c))** illustrate the behavior of the trapped fluid in the flow domain for both core and peripheral region. Trapped boluses are observed at small values of electro-kinetic slip velocity in both core and peripheral regions. One can observe a gradual reduction in the size of trapped bolus with eventual disappearance with increasing electro-osmotic slip velocity. **Fig. (6.9)** explores the reflux phenomenon for different values of parameters α_1 and U_E. It is found that the reflux phenomenon reduces by increasing the values of U_E and an opposite trend is noted for α_1.

6.4 Conclusion

In this chapter, we presented theoretical analysis of two-layered electro-osmotic peristaltic flow of Rabinowitsch fluid in a cylindrical tube. Appropriate electro-kinetic

suppositions are considered to model a problem. We also considered the creeping flow along with long wavelength approximation. The momentum equations for each region are solved analytically to get the closed form expressions for stream function and axial velocity. Mechanical efficiency, pressure difference, trapping and reflux are evaluated numerically. Interface between the two-fluids is also computed using Mathematica software. The computational results have been presented graphically. Following conclusions are made from the present study:

- The mechanical efficiency increases by increasing the electro-kinetic slip velocity at low volumetric flow rate, whereas follows a decreasing trend with respect to the Rabinowitsch parameter.
- An increment in the pressure rise is found for large values of the involved parameters
- Velocity increases in the center region for higher electro-kinetic slip velocities.
- Trapping phenomenon is observed in the core and peripheral regions at certain values of electro-kinetic slip velocity. The trapped boluses are only prominent in both regions for smaller electro-kinetic slip velocities while increasingly higher velocities make them disappear from the flow field.
- The size of the trapped bolus increases and becomes prominent in the core region when the viscosity of the core region fluid is greater than the fluid of peripheral region.
- The reflux reduces by increasing the values of the electro-kinetic slip velocity.
- The volume of the trapped boluses increases for higher values of the Rabinowitsch parameter. Similarly, reflux grows for increasing Rabinowitsch parameter.

(a)

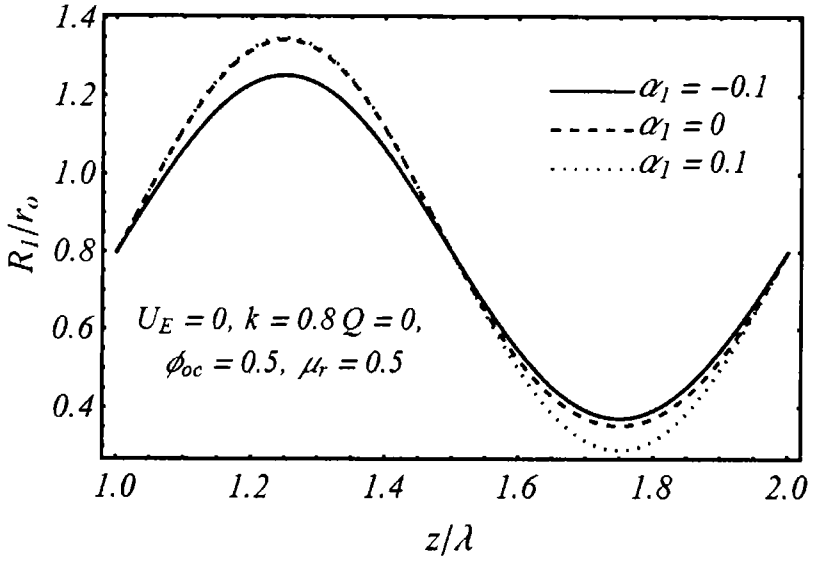

(b)

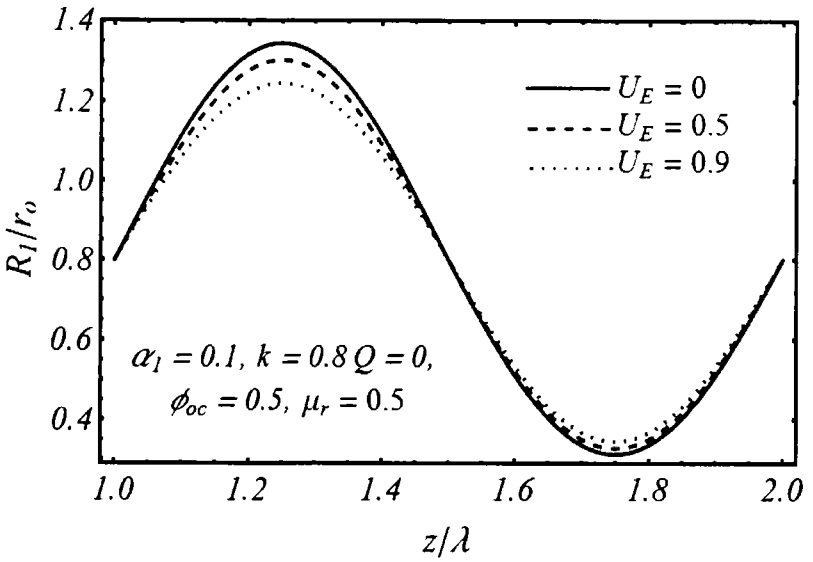

(c)

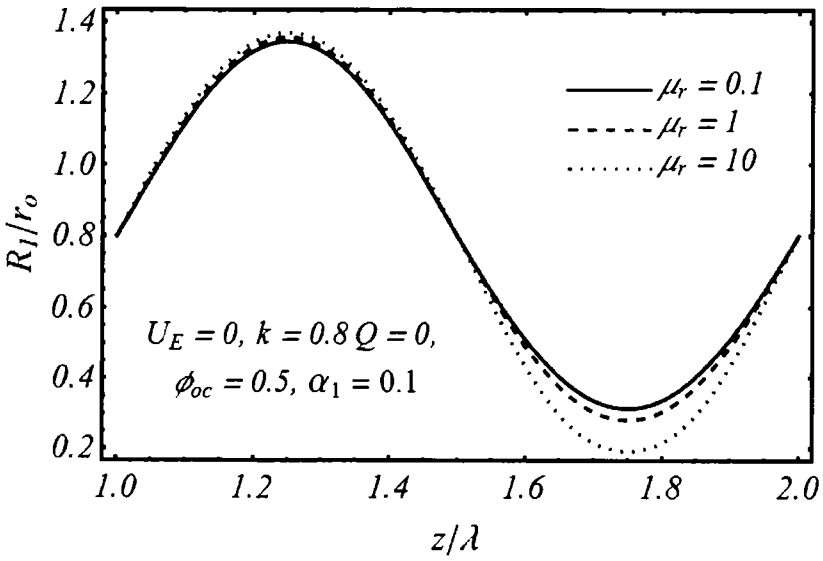

Fig. 6.2 ((a) – (c)): The behavior of the interface for different values of parameters α_1, U_E, μ_r.

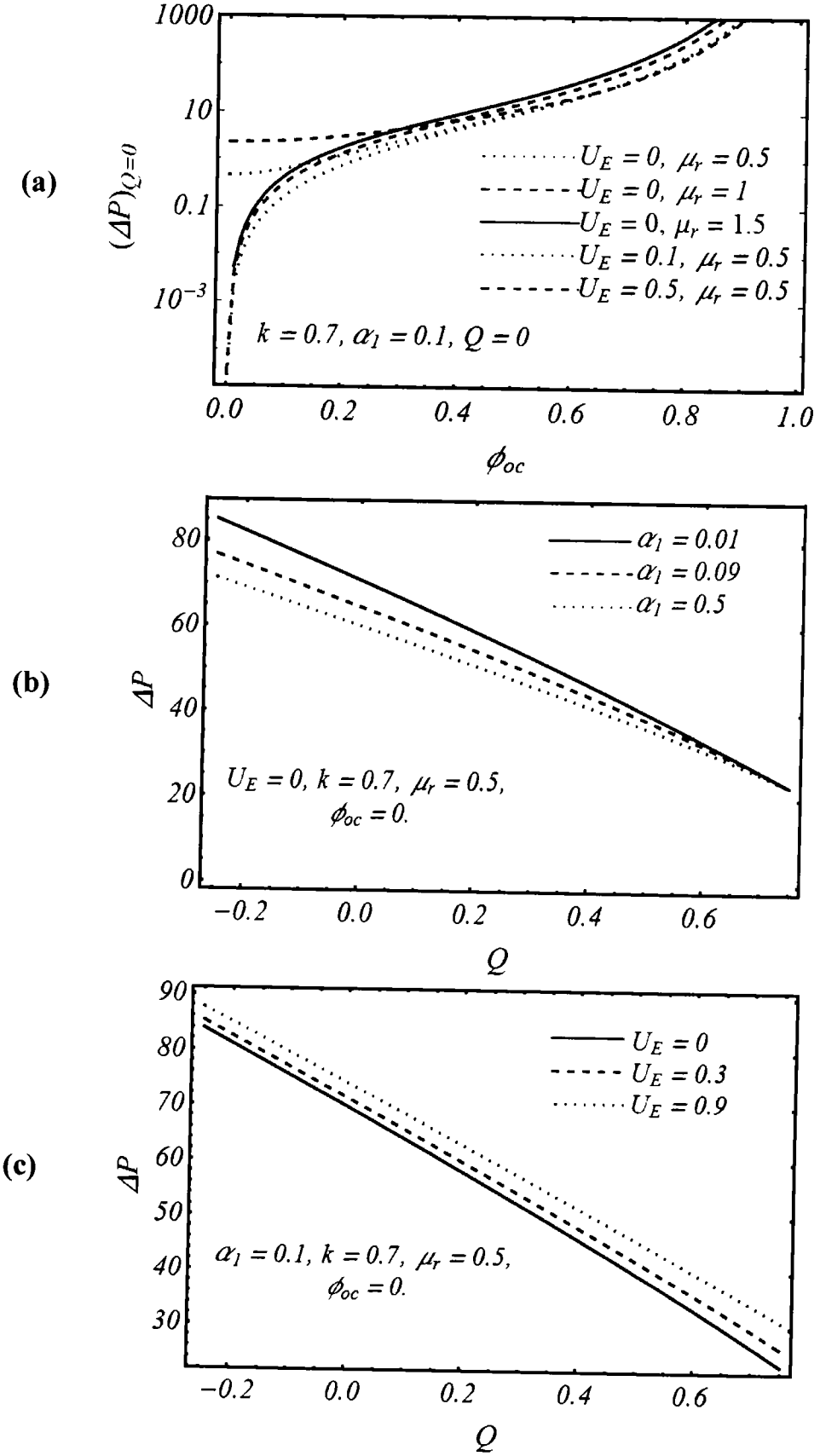

Fig. 6.3 ((a) – (c)): Displays the pumping characteristics for different values of viscosity ratio α_1, U_E.

(d)

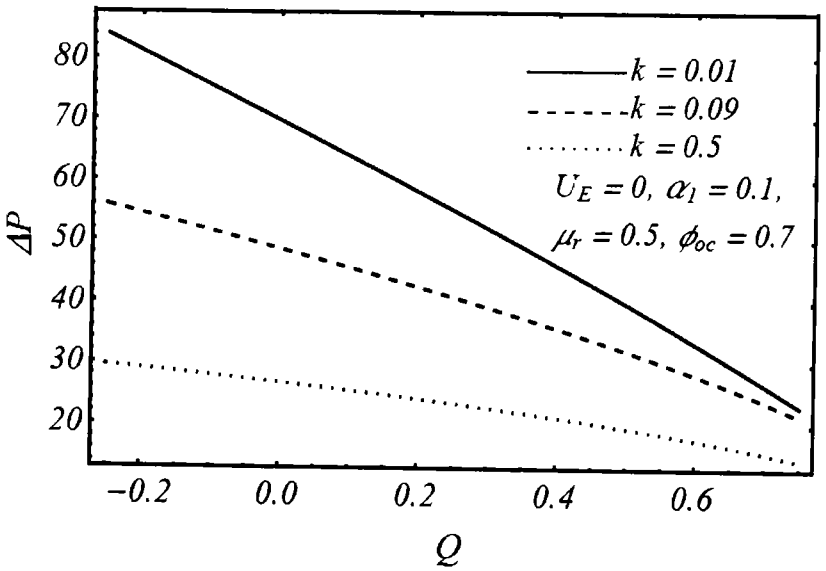

Fig. 6.3 (d): Displays the pumping characteristics for different values of k.

(a)

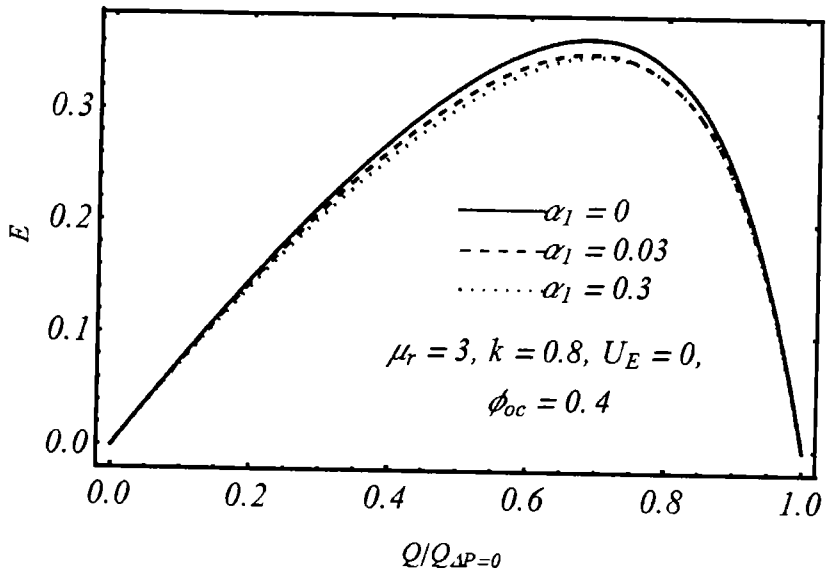

(b)

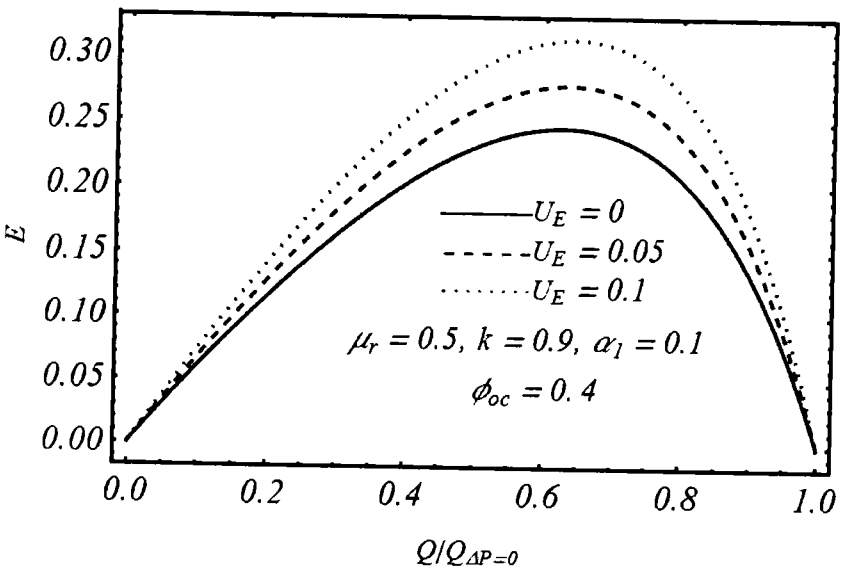

Fig. 6.4 ((a), (b)): Pumping efficiency with respect to parameters α_1 and the electro-kinetic parameter U_E.

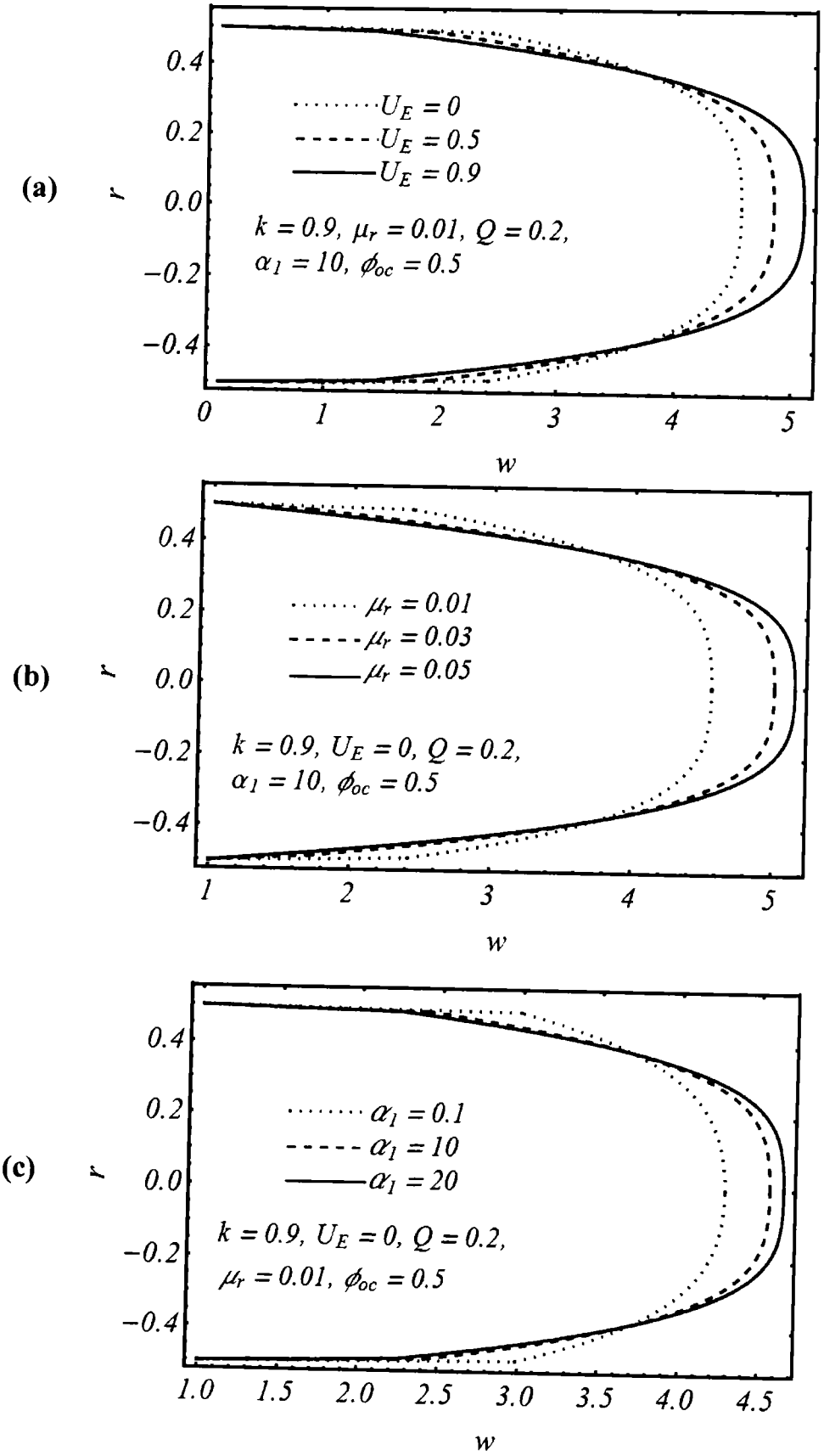

Fig. 6.5 ((a) – (c)): Velocity variations against different parameters U_E, μ_r and α_1.

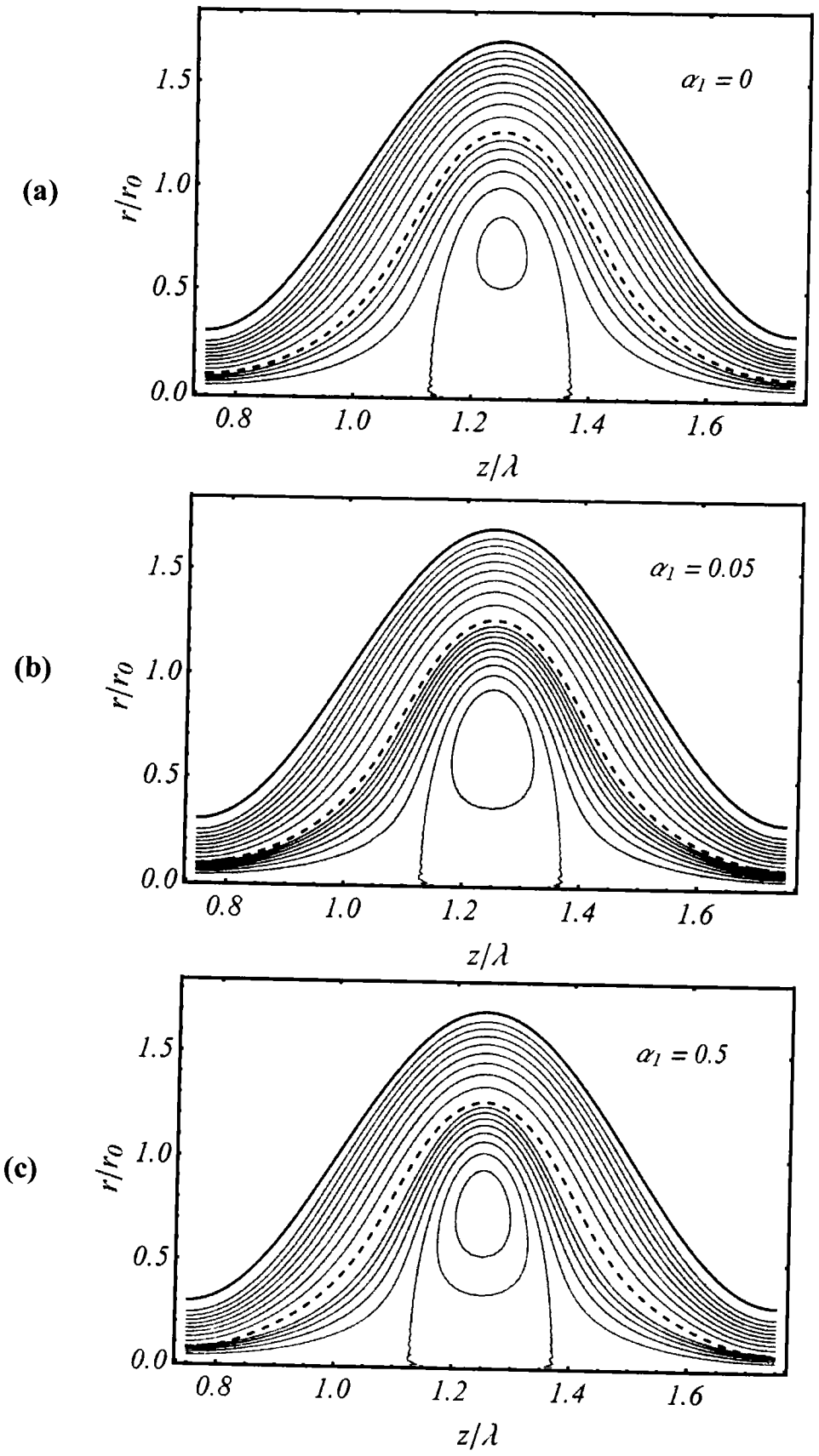

Fig. 6.6 ((a) – (c)): The streamlines variation in the core region for different values of α_1 when $U_E = 0.05, Q = 0, k = 0.4, \phi_{oc} = 0.75, \mu_r = 10$.

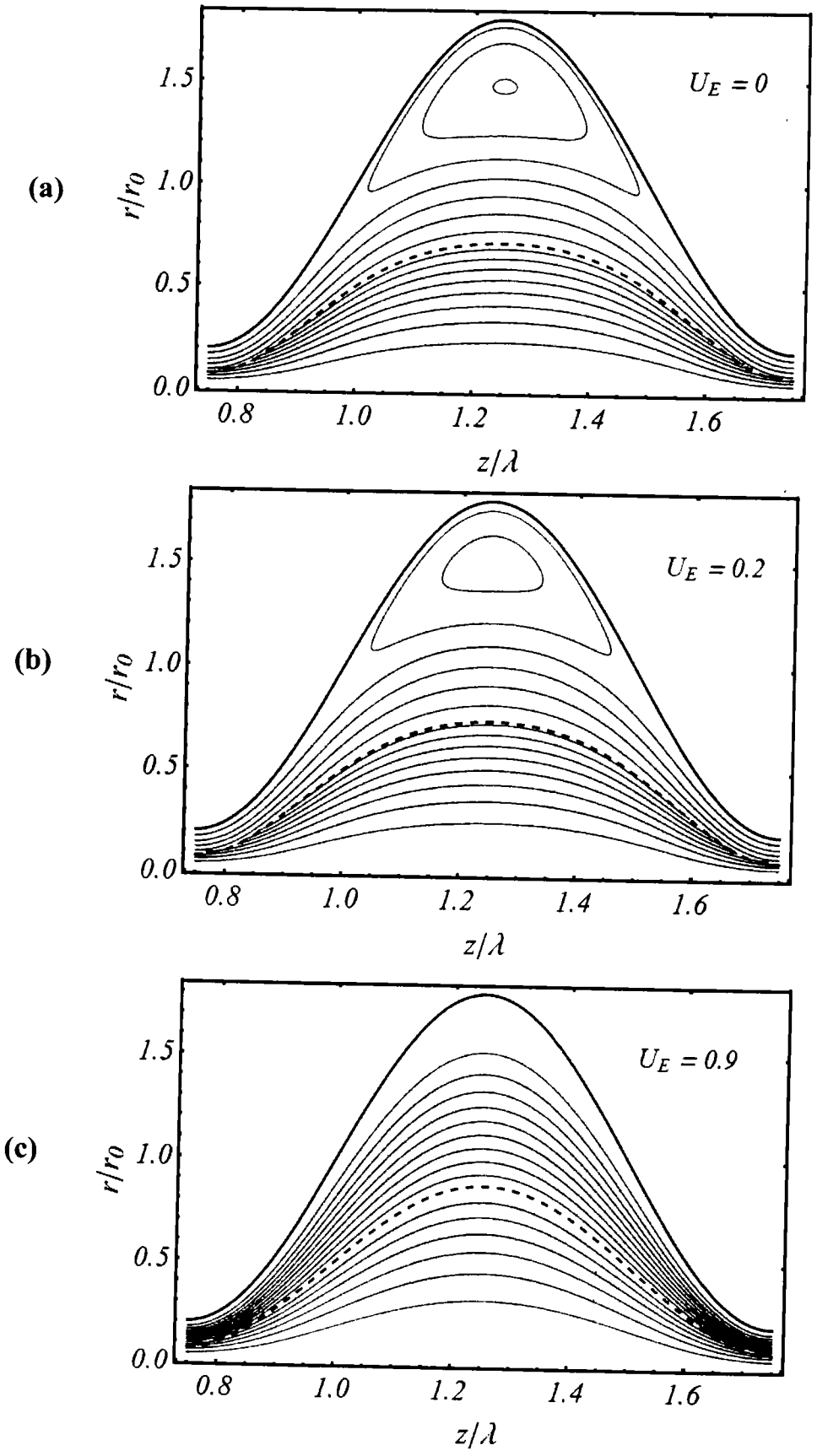

Fig. 6.7 ((a) – (c)): The streamlines variation in the peripheral region for U_E when $\alpha_1 = 0.1, Q = 0, \mathrm{k} = 0.4, \phi_{oc} = 0.75, \mu_r = 1$.

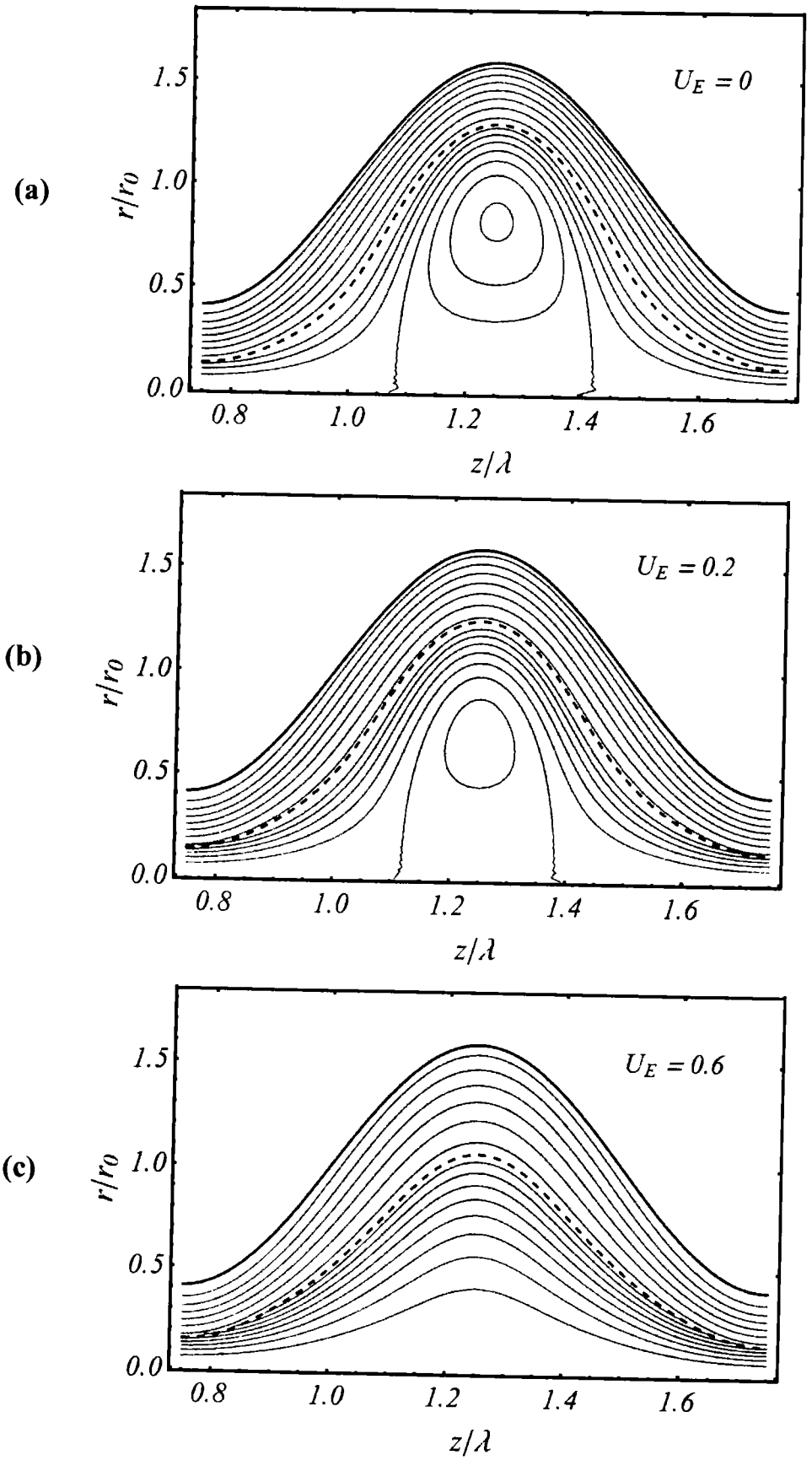

Fig. 6.8 ((a) – (c)): The streamlines variation in the core region for U_E when $\alpha_1 = 0.1, Q = 0, \mathrm{k} = 0.4, \phi_{oc} = 0.75, \mu_r = 10.$

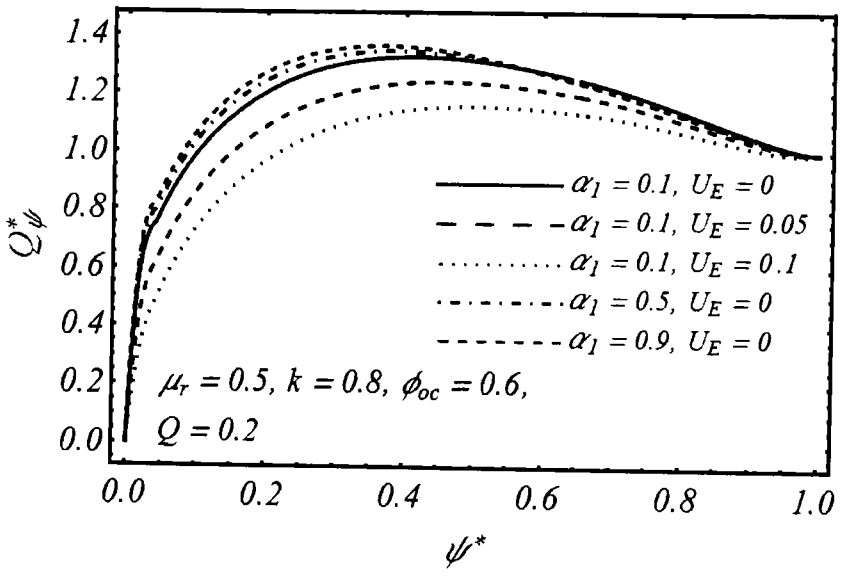

Fig. 6.9: Display the reflux variation against the different values of the α_1 and U_E.

Chapter 7

Electro-kinetically modulated peristaltic transport of multi-layered power-law fluid in an axisymmetric tube

The objective of this chapter is to investigate three-layered flow of power-law fluid driven by peristaltic activity and electro-osmotic phenomenon. The flow problem is modeled by invoking long wavelength and low Reynolds number constraints. Closed form expressions of stream function are obtained for each region. The interfaces between core and intermediate and intermediate and peripheral regions are computed by solving a system of nonlinear equations numerically and displayed graphically. Pressure rise, mechanical efficiency and trapping phenomena are also evaluated by varying the involved parameters. The present study generalizes many of the available studies on multi-phase peristaltic transport.

7.1 Mathematical formulation and solution of the problem

Consider three-layered electro-osmotic peristaltic transport of an incompressible power-law fluid in an axisymmetric flexible tube (**Fig. 7.1**). The movement of the fluid inside the tube is due to peristaltic motion of the tube wall and the electro-osmotic force. The electro-osmosis is a process in which the solid boundary of the ducts remains stationary and the motion of the liquid is due to an applied external electric potential. It occurs due to solid-fluid interaction. The solid is in the form of a capillary or a porous plug which is filled with liquid. Consider solid has a negatively charged surface and assume bio-fluid as an aqueous ionic solution. The negatively charged surface attracts the counter-ions forming layers of positively charged liquid near the wall. The thin layers in the immediate neighborhood of wall consisting of immobile counter-ions are called the Stern layers. The Stern layers are followed by layers of mobile counter-ions. The two-layers formed in this way constitute the so called electric-double layer (EDL). Now in response to an externally applied electric field the counter-ions move along the channel dragging the neutral liquid core. In addition to the electro-osmotic phenomena, the tube wall is deformed as a result of the peristaltic movement according to law

$$R_0(z^*,t^*) = r_0\left(1+\phi_0 \sin\left(\frac{2\pi}{\lambda}(z^*-Ut^*)\right)\right). \tag{7.1}$$

In above expression, r_0 is the radius of the undeformed tube, c is the wave speed, occlusion ϕ_0 is the occlusion, λ is the wavelength and t is the time. Moreover, this expression is valid in the fixed frame of reference (r^*, z^*).

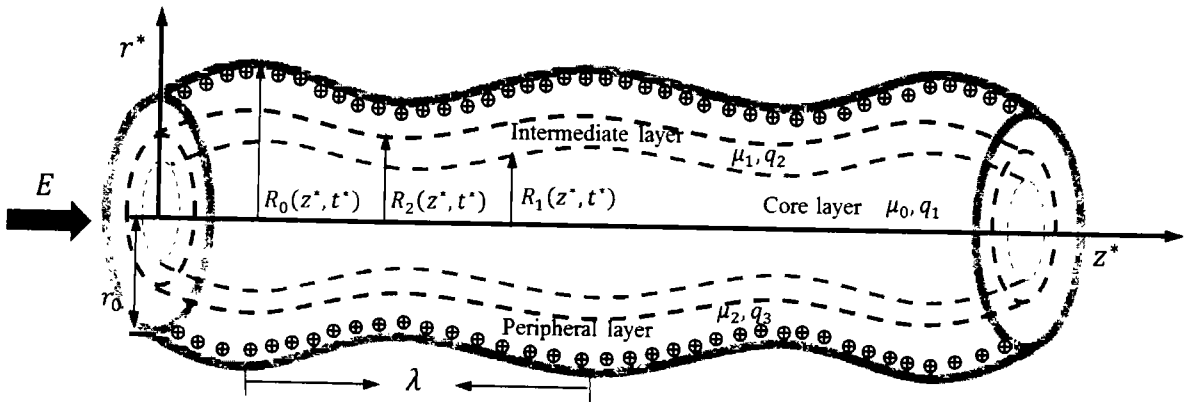

Fig. 7. 1: Flow geometry and coordinate system

The continuity and momentum equations for the flow under consideration are

$$\frac{\partial \rho}{\partial t^*} + \nabla.(\rho \mathbf{V}^*) = 0, \tag{7.2}$$

$$\rho\left(\frac{D\mathbf{V}^*}{Dt^*}\right) = -\nabla p^* + \nabla.\mathbf{S}^* + \mathbf{F}_e^*, \tag{7.3}$$

where ρ is the density, p^* is the pressure, $\mathbf{S}^*$ is the stress tensor, $\mathbf{F}_e^*$ is the body force and $\mathbf{V}^*$ is the velocity. The constitutive equation for power-law model is given by

$$\boldsymbol{\tau}^* = \left\{\mu^*\left[\sqrt{\tfrac{1}{2}(\mathbf{B}_1^* : \mathbf{B}_1^*)}\right]^{n-1}\right\}\mathbf{B}_1^*, \tag{7.4}$$

where $\mathbf{B}_1^*$ is related to the velocity gradient tensor $\mathbf{L}^*$ as

$$\mathbf{B}_1^* = \mathbf{L}^* + \mathbf{L}^{*T} \quad \text{and} \quad \mathbf{L}^* = \nabla \mathbf{V}^*,$$

The quantity $\mu^*\left[\sqrt{\frac{1}{2}(\mathbf{B}_1^* : \mathbf{B}_1^*)}\right]^{n-1}$ in (7.4) is termed as the apparent viscosity. μ^* and n refer to consistency and fluid behavior index, respectively. The cases, $n < 1$,

$n > 1$and $n = 1$ in Eq. (7.4) correspond to shear-thinning, shear-thickening and Newtonian fluid, respectively. The velocity profile for an axisymmetric tube flow is

$$\mathbf{V}^* = [u^*(r^*, z^*, t^*),\ 0\ , w^*(r^*, z^*, t^*)]. \tag{7.5}$$

The magnitude of the body force in the present scenario is given by Hunter (1981)

$$\mathbf{F}_e^* = \rho_e^*\, E, \tag{7.6}$$

in which ρ_e^* is the total ionic charge distribution and E is the constant axial electric field.

The viscosity function is assumed as follows

$$\mu^* = \begin{cases} \mu_0 & 0 \le r \le R_1 \\ \mu_1 & R_1 \le r \le R_2 \\ \mu_2 & R_2 \le r \le R_0, \end{cases} \tag{7.7}$$

where μ_0, μ_1 and μ_2 are defined as the viscosity of the core, intermediate and peripheral regions, respectively.

If we invoke the transformations relating the frames (r^*, z^*) and $(\bar{r}, \bar{z})$ in the form

$$\bar{z} = z^* - Ut^*,\ \bar{r} = r^*,\ \bar{w} = w^* - U,\quad \bar{u} = u^*, \bar{p} = p^*\ and\ \bar{\rho}_e = \rho_e^*, \tag{7.8}$$

then the flow in the new frame $(\bar{r}, \bar{z})$ can be treated as steady. The frame $(\bar{r}, \bar{z})$ is called the wave frame. In this frame the equations of continuity and momentum (7.2), (7.3) take the form

$$\frac{1}{\bar{r}}\frac{\partial(\bar{r}\bar{u})}{\partial \bar{r}} + \frac{\partial \bar{w}}{\partial \bar{z}} = 0, \tag{7.9}$$

$$\rho\left(\bar{u}\,\frac{\partial \bar{u}}{\partial \bar{r}} + \bar{w}\,\frac{\partial \bar{u}}{\partial \bar{z}}\right) = -\frac{\partial \bar{p}}{\partial \bar{r}} + \frac{1}{\bar{r}}\frac{\partial(\bar{r}\,\bar{S}_{\bar{r}\bar{r}})}{\partial \bar{r}} + \frac{\partial \bar{S}_{\bar{r}\bar{z}}}{\partial \bar{z}}, \tag{7.10}$$

$$\rho\left(\bar{u}\,\frac{\partial \bar{w}}{\partial \bar{r}} + \bar{w}\,\frac{\partial \bar{w}}{\partial \bar{z}}\right) = -\frac{\partial \bar{p}}{\partial \bar{z}} + \frac{1}{\bar{r}}\frac{\partial(\bar{r}\,\bar{S}_{\bar{r}\bar{z}})}{\partial \bar{r}} + \frac{\partial \bar{S}_{\bar{z}\bar{z}}}{\partial \bar{z}} + \bar{F}_e, \tag{7.11}$$

where, $\bar{S}_{\bar{r}\bar{r}} = 2\phi_1\frac{\partial \bar{u}}{\partial \bar{r}}$, $\bar{S}_{\bar{r}\bar{z}} = \bar{S}_{\bar{z}\bar{r}} = \phi_1\left(\frac{\partial \bar{w}}{\partial \bar{r}} + \frac{\partial \bar{u}}{\partial \bar{z}}\right)$, $\bar{S}_{\bar{z}\bar{z}} = 2\phi_1\frac{\partial \bar{u}}{\partial \bar{z}}$, (7.12)

$$\phi_1 = \bar{\mu}\left[2\left\{\left(\frac{\partial \bar{w}}{\partial \bar{z}}\right)^2 + \left(\frac{\bar{u}}{\bar{r}}\right)^2 + \left(\frac{\partial \bar{u}}{\partial \bar{r}}\right)^2\right\} + \left(\frac{\partial \bar{w}}{\partial \bar{r}} + \frac{\partial \bar{u}}{\partial \bar{z}}\right)^2\right]^{\frac{n-1}{2}}, \bar{F}_e = \bar{\rho}_e E. \tag{7.13}$$

Under the action of external axial electric field $\mathbf{E} = (0, 0, E_z)$, the fluid undergoes a body force given as Hunter (1981).

$$\bar{F}_e = \bar{\rho}_e E_z \mathbf{k}, \tag{7.14}$$

where $\mathbf{k}$ is the unit vector in the axial direction and $\bar{\rho}_e$ be the total ionic charge density, which is associated to the electric potential $\bar{\phi}$ through the equation

$$\nabla^2\bar{\phi} = -\bar{\rho}_e/\varepsilon, \tag{7.15}$$

in which ε is the permittivity of the medium. For symmetric electrolyte solution, the total ionic distribution $\bar{\rho}_e$ is defined as $\bar{\rho}_e = ez(\bar{n}^+ - \bar{n}^-)$. e, z, $\bar{n}^+$, $\bar{n}^-$elementary

charge, charge valance, number density of cations, number density of anions, respectively. The ionic number distributions of single species are obtained through Nernst-Planck equation for each species. That is,

$$\frac{\partial \bar{n}_{\pm}}{\partial \bar{t}}+\bar{u}\frac{\partial \bar{n}_{\pm}}{\partial \bar{r}}+\bar{w}\frac{\partial \bar{n}_{\pm}}{\partial \bar{z}}=D_0\left(\frac{\partial^2 \bar{n}_{\pm}}{\partial \bar{z}^2}+\frac{1}{\bar{r}}\frac{\partial}{\partial \bar{r}}\left(\bar{r}\frac{\partial \bar{n}_{\pm}}{\partial \bar{r}}\right)\right)\pm\frac{D_0 ze}{k_B T}\left(\frac{\partial}{\partial \bar{z}}\left(\bar{n}_{\pm}\frac{\partial \bar{\phi}}{\partial \bar{z}}\right)+\frac{1}{\bar{r}}\frac{\partial}{\partial \bar{r}}\left(\bar{r}\bar{n}_{\pm}\frac{\partial \bar{\phi}}{\partial \bar{r}}\right)\right). \tag{7.16}$$

It is assumed that coefficients of ionic diffusions for both species are equal and the transport of the species is evaluated through Einstein formula.

Now introducing the dimensionless variables

$$\left.\begin{aligned} &r^*=\frac{\bar{r}}{r_0},\ z^*=\frac{\delta \bar{z}}{r_0},\ u^*=\frac{\bar{u}}{(\delta U)},\ w^*=\frac{\bar{w}}{U},\ t^*=\frac{\delta U}{r_0}\bar{t},\ \delta=\frac{r_0}{\lambda},\\ &p^*=\frac{\delta r_0}{\mu_0 U}\bar{p},\ Re=\frac{\rho U r_0}{\mu_0},\ De=\frac{\lambda_p U}{r_0},\ \phi^*=\frac{ez\bar{\phi}}{k_B T},\ S^*=\frac{r_0}{\mu_0 U}\bar{S},\\ &n^*=\frac{\bar{n}}{n_0},\ \phi_{oc}=\frac{a_0}{r_0},\ \rho_e^*=\frac{r_0^2 k_B T\bar{\rho}_e}{ez\varepsilon_N}. \end{aligned}\right\} \tag{7.17}$$

where Re is the Reynold number, De be the Deborah number and δ is the wave number. After applying the dimensionless quantities (7.17) and the approximations that $\delta, Pe, Re \ll 1$, where $Pe = ReSc, Sc = \mu_0/\rho D_0$ represents the ionic Peclet number and Schmidt number, respectively. Under these assumptions, the Poisson and Nernst Planck equations reduce to (dropping asterisk)

$$\frac{1}{r}\frac{\partial}{\partial r}\left(r\frac{\partial \phi}{\partial r}\right)=-\kappa^2\left(\frac{n_+-n_-}{2}\right), \tag{7.18}$$

$$0=\frac{1}{r}\frac{\partial}{\partial r}\left(\frac{1}{r}\frac{\partial n_{\pm}}{\partial r}\right)\pm\frac{1}{r}\frac{\partial}{\partial r}\left(rn_{\pm}\frac{\partial \phi}{\partial r}\right), \tag{7.19}$$

where $\kappa = r_0 ez\sqrt{2n_0/\varepsilon K_B T} = r_0/\lambda_d$, is the electro-osmotic parameter. Eqs. (7.18) and (7.19) subject to appropriate boundary conditions may give the potential distribution for both regions. Based on these potentials the explicit form of body force term can be derived Tripathi et al. (2017). However, we shall not follow this line of action in the subsequent analysis. The details about alternative course of action shall be provided in the later part of this section.

The dimensionless equation of wall reads:

$$R_0(z) = 1 + \phi_0\, sin2\pi(z). \tag{7.20}$$

Applying the long wavelength ($\delta \ll 1$) and low Reynolds number ($Re \ll 1$) approximations, Eqs. (7.9) – (7.11) become (dropping asterisk)

$$\frac{\partial p}{\partial z} = \frac{1}{r}\frac{\partial}{\partial r}\left\{r\mu \frac{\partial w}{\partial r}\left|\frac{\partial w}{\partial r}\right|^{n-1}\right\} + U_E \frac{\mu}{\varepsilon}\rho_e \quad , \qquad \frac{\partial p}{\partial r} = 0, \tag{7.21}$$

where $U_E = -\frac{\varepsilon \zeta E}{\mu U}$ is the electro-kinetic slip parameter.

The boundary conditions applicable to present flow problem are:

$$\frac{\partial w}{\partial r} = 0 \qquad at \quad r = 0, \tag{7.22}$$

$$w = -1 \qquad at \quad r = R_0. \tag{7.23}$$

Here, we have two choices: we can either solve the problem by considering the electro-kinetic term in the momentum equation or shift its contribution in the boundary condition at the wall through the inclusion of electrokinetic slip parameter. The output yielded via both the approaches will always be the same. The subsequent analysis of the present fluid problem is figured out by taking the contribution of body force term in the boundary condition at the wall. A detailed explanation about this approach is given by Goswami et al.(2016). After this treatment the governing equation and boundary condition are reduce to:

$$\frac{\partial p}{\partial z} = \frac{1}{r}\frac{\partial}{\partial r}\left\{r\mu \frac{\partial w}{\partial r}\left|\frac{\partial w}{\partial r}\right|^{n-1}\right\}, \qquad \frac{\partial p}{\partial r} = 0, \tag{7.24}$$

$$w = U_E - 1 \qquad at \quad r = R_0, \tag{7.25}$$

$$\frac{\partial w}{\partial r} = 0 \qquad at \quad r = 0. \tag{7.26}$$

Now, introducing the relations, $w = 1/r\,(\partial\psi/\partial r)$and $u = w = -1/r\,(\partial\psi/\partial z)$, the governing equations in term of stream function become

$$\frac{\partial p}{\partial z} = \frac{1}{r}\frac{\partial}{\partial r}\left\{r\mu \frac{\partial}{\partial r}\left(\left(\frac{1}{r}\right)\left(\frac{\partial \psi}{\partial r}\right)\right)\left|\frac{\partial}{\partial r}\left(\left(\frac{1}{r}\right)\left(\frac{\partial \psi}{\partial r}\right)\right)\right|^{n-1}\right\}, \qquad \frac{\partial p}{\partial r} = 0. \tag{7.27}$$

The dimensionless viscosity function appearing in the above equation is defined as follow:

$$\mu = \begin{cases} 1 & 0 \le r \le R_1, \\ \mu_1 & R_1 \le r \le R_2, \\ \mu_2 & R_2 \le r \le R_0. \end{cases} \tag{7.28}$$

The volume flow rate in the wave frame of reference q is related to the time-averaged flow rate $\bar{Q}$ in the laboratory frame of reference via the equation

$$q = \bar{Q} - \left(1 + \frac{\phi^2}{2}\right) = q_1 + q_2 + q_3. \tag{7.29}$$

In the above equation q_1, q_2 and q_3 are the volume flow rates in wave frame corresponding to core, intermediate and peripheral regions, respectively (see **Fig. 7.1** for more clarification) and $\bar{Q} = \int_0^1 Q dt$, where Q is the volume flow rate in the laboratory frame. The volume flow rates q_1, q_2 are related to their respective counterparts $\bar{Q}_1$ and $\bar{Q}_2$ by the expressions

$$\begin{aligned} \dot{q}_1 &= \bar{Q}_1 - \int_0^1 {R^2}_1 dz = q_1, \\ \dot{q}_2 &= \bar{Q}_2 - \int_0^1 {R^2}_2 dz = q_1 + q_2, \end{aligned} \tag{7.30}$$

where the parameters $\dot{q}_1$and $\dot{q}_2$ are used to relate flow rates between the wave and fixed frames.

The boundary conditions in term of stream function are:

$$\begin{aligned} &\psi = 0, \quad \left(\frac{\partial}{\partial r}\left(\frac{1}{r}\frac{\partial \psi}{\partial r}\right)\right) = 0, \qquad at \quad r = 0, \\ &\frac{1}{r}\frac{\partial \psi}{\partial r} = U_E - 1 \qquad at\, r = R_0, \\ &\psi = \frac{q}{2} = constant \qquad at\, r = R_0, \\ &\psi = \frac{\dot{q}_1}{2} = constant \qquad at\, r = R_1, \\ &\psi = \frac{\dot{q}_2}{2} = constant \qquad at\, r = R_2. \end{aligned} \tag{7.31}$$

The first boundary condition represents the symmetry of flow with respect to the central plane $r = 0$, the second is the condition is the adherence condition at the fluid-solid interface and the remaining conditions arise as a consequences of the mass conservation in the three regions.

7.2 Problem description

Eliminating of pressure from two equations of (7.27) yields

$$\frac{\partial}{\partial r}\left[\frac{1}{r}\frac{\partial}{\partial r}\left(r\mu \frac{\partial}{\partial r}\left(\frac{1}{r}\frac{\partial \psi}{\partial r}\right)\left|\frac{\partial}{\partial r}\left(\frac{1}{r}\frac{\partial \psi}{\partial r}\right)\right|^{n-1}\right)\right] = 0. \tag{7.32}$$

Now, integrating the Eq. (7.32) and invoking the first four boundary conditions in (7.31), we get the following expression of stream function

$$\psi = \frac{(U_E - 1)r^2}{2} - \frac{((U_E - 1){R_0}^2 - q)}{2}\frac{I_1}{I_2}, \tag{7.33}$$

where

$$I_1 = \int_0^r s \int_s^{R_0} \left(\frac{s_0}{\bar{\mu}}\right)^{\frac{1}{n}} ds_0 ds, \qquad (7.34)$$

$$I_2 = \int_0^{R_0} r \int_r^{R_0} \left(\frac{s}{\bar{\mu}}\right)^{\frac{1}{n}} ds dr.$$

In view of the Eq. (7.28), the stream function for three regions is computed as:

Core region $0 \leq r \leq R_1$:

$$\psi = \frac{(U_E-1)r^2}{2} + \frac{\frac{1}{2}r^2(q-(U_E-1)R_0{}^2)\left(\frac{3n+1}{n+1}\right)\left[\left(1-\frac{1}{\mu_1{}^{\frac{1}{n}}}\right)R_1{}^{\frac{(n+1)}{n}} + \left(\frac{1}{\mu_1{}^{\frac{1}{n}}} - \frac{1}{\mu_2{}^{\frac{1}{n}}}\right)R_2{}^{\frac{(n+1)}{n}} + \frac{1}{\mu_2{}^{\frac{1}{n}}}R_0{}^{\frac{(n+1)}{n}} - \left(\frac{2n}{3n+1}\right)r^{\frac{(n+1)}{n}}\right]}{\left(1-\frac{1}{\mu_1{}^{\frac{1}{n}}}\right)R_1{}^{\frac{(3n+1)}{n}} + \left(\frac{1}{\mu_1{}^{\frac{1}{n}}} - \frac{1}{\mu_2{}^{\frac{1}{n}}}\right)R_2{}^{\frac{(3n+1)}{n}} + \frac{1}{\mu_2{}^{\frac{1}{n}}}R_0{}^{\frac{(3n+1)}{n}}}, \qquad (7.35)$$

Intermediate region $R_1 \leq r \leq R_2$:

$$\psi = \frac{(U_E-1)}{2}r^2 + \frac{\frac{1}{2}(q-(U_E-1)R_0{}^2)\left[\left(1-\frac{1}{\mu_1{}^{\frac{1}{n}}}\right)R_1{}^{\frac{(n+1)}{n}} + \left(\frac{3n+1}{n+1}\right)r^2\left\{\left(\frac{1}{\mu_1{}^{\frac{1}{n}}} - \frac{1}{\mu_2{}^{\frac{1}{n}}}\right)R_2{}^{\frac{(n+1)}{n}} + \frac{1}{\mu_2{}^{\frac{1}{n}}}R_0{}^{\frac{(n+1)}{n}} - \left(\frac{2n}{3n+1}\right)\frac{1}{\mu_1{}^{\frac{1}{n}}}r^{\frac{(n+1)}{n}}\right\}\right]}{\left(1-\frac{1}{\mu_1{}^{\frac{1}{n}}}\right)R_1{}^{\frac{(3n+1)}{n}} + \left(\frac{1}{\mu_1{}^{\frac{1}{n}}} - \frac{1}{\mu_2{}^{\frac{1}{n}}}\right)R_2{}^{\frac{(3n+1)}{n}} + \frac{1}{\mu_2{}^{\frac{1}{n}}}R_0{}^{\frac{(3n+1)}{n}}}, \qquad (7.36)$$

Peripheral region $R_2 \leq r \leq R_0$:

$$\psi = \frac{(U_E-1)}{2}r^2 + \frac{\frac{1}{2}(q-(U_E-1)R_0{}^2)\left[\left(1-\frac{1}{\mu_1{}^{\frac{1}{n}}}\right)R_1{}^{\frac{(n+1)}{n}} + \left(\frac{1}{\mu_1{}^{\frac{1}{n}}} - \frac{1}{\mu_2{}^{\frac{1}{n}}}\right)R_2{}^{\frac{(n+1)}{n}} + \left(\frac{3n+1}{n+1}\right)\frac{1}{\mu_2{}^{\frac{1}{n}}}r^2\left\{R_0{}^{\frac{(n+1)}{n}} - \left(\frac{2n}{3n+1}\right)r^{\frac{(n+1)}{n}}\right\}\right]}{\left(1-\frac{1}{\mu_1{}^{\frac{1}{n}}}\right)R_1{}^{\frac{(3n+1)}{n}} + \left(\frac{1}{\mu_1{}^{\frac{1}{n}}} - \frac{1}{\mu_2{}^{\frac{1}{n}}}\right)R_2{}^{\frac{(3n+1)}{n}} + \frac{1}{\mu_2{}^{\frac{1}{n}}}R_0{}^{\frac{(3n+1)}{n}}}, \qquad (7.37)$$

From Eqs. (7.35) - (7.37), it is noted that the solution of the problem is still incomplete due to presence of the unknowns R_1 and R_2. In order of obtain, R_1 and R_2 we proceed as follows.

7.2.1 Determinations fluid-fluid interface

In the present three-layer problem, there exist two interfaces. The first interface lies between core and intermediate regions while the second one exists between intermediate and peripheral regions. To find these interfaces, we use Eqs. (7.35) and (7.36) and remaining boundary conditions in Eq. (7.31) to get

$$\frac{(\dot{q_1}-(U_E-1)R_1{}^2)}{(q-(U_E-1)R_0{}^2)} = \frac{\left[\left(1-\left(\frac{3n+1}{n+1}\right)\frac{1}{\mu_1{}^{\frac{1}{n}}}\right)R_1{}^{\frac{(3n+1)}{n}}+\left(\frac{3n+1}{n+1}\right)\left(\frac{1}{\mu_1{}^{\frac{1}{n}}}-\frac{1}{\mu_2{}^{\frac{1}{n}}}\right)R_2{}^{\frac{(n+1)}{n}}R_1{}^2+\left(\frac{3n+1}{n+1}\right)\frac{1}{\mu_2{}^{\frac{1}{n}}}R_0{}^{\frac{(n+1)}{n}}R_1{}^2\right]}{\left(1-\frac{1}{\mu_1{}^{\frac{1}{n}}}\right)R_1{}^{\frac{(3n+1)}{n}}+\left(\frac{1}{\mu_1{}^{\frac{1}{n}}}-\frac{1}{\mu_2{}^{\frac{1}{n}}}\right)R_2{}^{\frac{(3n+1)}{n}}+\frac{1}{\mu_2{}^{\frac{1}{n}}}R_0{}^{\frac{(3n+1)}{n}}}, \tag{7.38}$$

$$\frac{(\dot{q_2}-(U_E-1)R_2{}^2)}{(q-(U_E-1)R_0{}^2)} = \frac{\left[\left(1-\frac{1}{\mu_1{}^{\frac{1}{n}}}\right)R_1{}^{\frac{(3n+1)}{n}}+\left(\frac{1}{\mu_1{}^{\frac{1}{n}}}-\left(\frac{3n+1}{n+1}\right)\frac{1}{\mu_2{}^{\frac{1}{n}}}\right)R_2{}^{\frac{(3n+1)}{n}}+\left(\frac{3n+1}{n+1}\right)\frac{1}{\mu_2{}^{\frac{1}{n}}}R_0{}^{\frac{(n+1)}{n}}R_2{}^2\right]}{\left(1-\frac{1}{\mu_1{}^{\frac{1}{n}}}\right)R_1{}^{\frac{(3n+1)}{n}}+\left(\frac{1}{\mu_1{}^{\frac{1}{n}}}-\frac{1}{\mu_2{}^{\frac{1}{n}}}\right)R_2{}^{\frac{(3n+1)}{n}}+\frac{1}{\mu_2{}^{\frac{1}{n}}}R_0{}^{\frac{(3n+1)}{n}}}, \tag{7.39}$$

From the above equations, Eqs. (7.38) and (7.39), we obtain a system of non-linear equations for interfaces as

$$A_1R_1{}^{(5n+1)/n}+B_1R_1{}^{(3n+1)/n}+C_1(R_2)\,R_1{}^2+D_1(R_2)=0, \tag{7.40}$$

$$A_2R_2{}^{(5n+1)/n}+B_2R_2{}^{(3n+1)/n}+C_2(R_1)\,R_2{}^2+D_2(R_1)=0, \tag{7.41}$$

where

$$A_1=-(U_E-1)\left(1-\frac{1}{\mu_1{}^{\frac{1}{n}}}\right),$$

$$A_2=-(U_E-1)\left(\frac{1}{\mu_1{}^{\frac{1}{n}}}-\frac{1}{\mu_2{}^{\frac{1}{n}}}\right),$$

$$B_1=\left[\dot{q_1}\left(1-\frac{1}{\mu_1{}^{\frac{1}{n}}}\right)-(q-(U_E-1)R_0{}^2)\left(1-\left(\frac{3n+1}{n+1}\right)\frac{1}{\mu_1{}^{\frac{1}{n}}}\right)\right],$$

$$B_2=\left[\dot{q_2}\left(\frac{1}{\mu_1{}^{\frac{1}{n}}}-\frac{1}{\mu_2{}^{\frac{1}{n}}}\right)-(q-(U_E-1)R_0{}^2)\left(\frac{1}{\mu_1{}^{\frac{1}{n}}}-\left(\frac{3n+1}{n+1}\right)\frac{1}{\mu_2{}^{\frac{1}{n}}}\right)\right],$$

$$C_1(R_2)=\left[-(U_E-1)\left(\frac{1}{\mu_1{}^{\frac{1}{n}}}-\frac{1}{\mu_2{}^{\frac{1}{n}}}\right)R_2{}^{\frac{(3n+1)}{n}}-\frac{(U_E-1)}{\mu_2{}^{\frac{1}{n}}}R_0{}^{\frac{(3n+1)}{n}}-\left(\frac{3n+1}{n+1}\right)(q-(U_E-1)R_0{}^2)\left(\left(\frac{1}{\mu_1{}^{\frac{1}{n}}}-\frac{1}{\mu_2{}^{\frac{1}{n}}}\right)R_2{}^{\frac{(n+1)}{n}}+\frac{1}{\mu_2{}^{\frac{1}{n}}}R_0{}^{\frac{(n+1)}{n}}\right)\right],$$

$$C_2(R_1) = \left[-(U_E-1)\left(1-\frac{1}{\mu_1^{\frac{1}{n}}}\right)R_1^{\frac{(3n+1)}{n}} - \frac{(U_E-1)}{\mu_2^{\frac{1}{n}}}R_0^{\frac{(3n+1)}{n}} - \left(\frac{3n+1}{n+1}\right)\left(q-(U_E-1)R_0^{\,2}\right)\left(\frac{1}{\mu_2^{\frac{1}{n}}}R_0^{\frac{(n+1)}{n}}\right)\right],$$

$$D_1(R_2) = \dot{q_1}\left[\left(\frac{1}{\mu_1^{\frac{1}{n}}} - \frac{1}{\mu_2^{\frac{1}{n}}}\right)R_2^{\frac{(3n+1)}{n}} + \frac{1}{\mu_2^{\frac{1}{n}}}R_0^{\frac{(3n+1)}{n}}\right],$$

$$D_2(R_1) = \left[\left(\dot{q_2} - (q-(U_E-1)R_0^{\,2})\right)\left(1-\frac{1}{\mu_1^{\frac{1}{n}}}\right)R_1^{\frac{(3n+1)}{n}} + \dot{q_2}\frac{1}{\mu_2^{\frac{1}{n}}}R_0^{\frac{(3n+1)}{n}}\right].$$

Assuming that $R_1(0) = \alpha$, $R_1(0) = \beta$, one can relate $\dot{q_1}$and $\dot{q_2}$ with α and β in the following manner:

$$\dot{q_1} = (U_E-1)\alpha^2 + \frac{q-(U_E-1)\left[\left(1-\left(\frac{3n+1}{n+1}\right)\frac{1}{\mu_1^{\frac{1}{n}}}\right)\alpha^{\frac{(3n+1)}{n}} + \left(\frac{3n+1}{n+1}\right)\left(\frac{1}{\mu_1^{\frac{1}{n}}} - \frac{1}{\mu_2^{\frac{1}{n}}}\right)\beta^{\frac{(n+1)}{n}}\alpha^2 + \left(\frac{3n+1}{n+1}\right)\frac{\alpha^2}{\mu_2^{\frac{1}{n}}}\right]}{\left(1-\frac{1}{\mu_1^{\frac{1}{n}}}\right)\alpha^{\frac{(3n+1)}{n}} + \left(\frac{1}{\mu_1^{\frac{1}{n}}} - \frac{1}{\mu_2^{\frac{1}{n}}}\right)\beta^{\frac{(3n+1)}{n}} + \frac{1}{\mu_2^{\frac{1}{n}}}}, \quad (7.42)$$

$$\dot{q_2} = (U_E-1)\beta^2 + \frac{q-(U_E-1)\left[\left(1-\left(\frac{3n+1}{n+1}\right)\frac{1}{\mu_1^{\frac{1}{n}}}\right)\alpha^{\frac{(3n+1)}{n}} + \left(\frac{1}{\mu_1^{\frac{1}{n}}} - \left(\frac{3n+1}{n+1}\right)\frac{1}{\mu_2^{\frac{1}{n}}}\right)\beta^{\frac{(n+1)}{n}} + \left(\frac{3n+1}{n+1}\right)\frac{\beta^2}{\mu_2^{\frac{1}{n}}}\right]}{\left(1-\frac{1}{\mu_1^{\frac{1}{n}}}\right)\alpha^{\frac{(3n+1)}{n}} + \left(\frac{1}{\mu_1^{\frac{1}{n}}} - \frac{1}{\mu_2^{\frac{1}{n}}}\right)\beta^{\frac{(3n+1)}{n}} + \frac{1}{\mu_2^{\frac{1}{n}}}}. \quad (7.43)$$

Substituting the values of $\dot{q_1}$and $\dot{q_2}$ from above equation in equations (7.38) and (7.39) leads to the equations for R_1 and R_2 which are then solved by Newton's method for each z. The graphical results for interfaces along with the outermost boundary $R_0(z)$ are shown for several values of involved parameters in **Figs. (7.2 - 7.5)**. **Fig. (7.2(a))** presents the variations in the interfaces R_1 and R_2 over one wavelength with respect to the parameter U_E (electro-osmotic slip velocity) for five different situations. In **Fig. (7.2(a))** it is assumed that $\mu_1 > \mu_2$ and $n = 1.5$ i.e the fluid in all three regions is shear-thickening and the vicosity of the intermadiate region is greater than the viscosity of the periphral region. In this situation, both interfaces experience a downward force in the crest region and an upward force in the trough region with increasing U_E. As a result, both interfaces drops down in the crest region whilst they elevates in the trough region with rasing U_E. However, the drop down effect is much more stornger than that of elevation effect. A similar trend

is noted form **Fig. (7.2(b))** where it is assumed that $\mu_1 < \mu_2$. A comparison of both figures reveals that variation in R_1 with respect to U_E is more intense for the case $\mu_1 < \mu_2$ than that of the case $\mu_1 > \mu_2$. Further, a flattening trend is also identified in both interfaces in the trough region for later situation i.e. $\mu_1 > \mu_2$ and this trend is found to diminish with raising U_E. **Figs. (7.2(c - e))** display the variations in interfaces with respect to U_E for shear-thinning, Newtonian and shear-thickening fluids by assuming equal viscosites in both intermediate and peripheral regions. Again, it is observed that both interfaces drop down in the crest region and elevate in the trough region with raising U_E irrespective of the rheological nature of the fluid. However, changing the rheological nature from shear-thinning to shear thickening intensifies the variation in both interfaces with respect to U_E. **Figs. (7.3(a - d))** highlight the effects of viscosity ratio μ_1 on both interfaces for $n < 1, n = 1$ and $n > 1$, respectively. In all three cases, an elevation of both interfaces in the trough region and a drop down in the crest region is noted with increasing μ_1. Morever, variations in both interfaces with respect to μ_1 is intense for shear-thinning fluid and mild for shear-thickening fluid. **Figs. (7.4(a - c))** show the impact of vicosity ratio μ_2 on both interfaces for $n < 1, n = 1$ and $n > 1$, respectively. It is evident that the effect of μ_2 is quite opposite to the effects of μ_1. Here, instead in the trough region an elevation of both interfaces are observed in the crest region with raising the parameter μ_2. Again, the effect of increasing μ_2 is much pronounced in shear-thinning fluid than that of Newtonian and shear-thickening fluids. The influence of fluid rheology on both interfaces is demonstrated for three cases, namely, $\mu_1 > \mu_2$, $\mu_1 < \mu_2$ and $\mu_1 = \mu_2$ in **Fig. (7.5(a - c))**, respectively. For $\mu_1 > \mu_2$, both interfaces elevate in the crest region and drop down in the trough region with enhancing n from 0.5 to 1.5. A similar trend prevails for $\mu_1 = \mu_2$. In contrast, a reverse trend is noted for $\mu_1 < \mu_2$. It is further observed that both interfaces are more vulnerable to changes with respect to n in the crest region for $\mu_1 > \mu_2$. In contrast, pronounced changes in both interfaces are identified with respect to n in the trough region for $\mu_1 < \mu_2$ and $\mu_1 = \mu_2$.

7.2.2 Pumping characteristics

Invoking Eqs. (7.32) - (7.34) in Eq. (7.29), the expression of the pressure gradient is obtained as:

$$\frac{\partial p}{\partial z} =$$

$$-2\left(\frac{3n+1}{n}\right)^n \left[\frac{(q-(U_E-1)R_0{}^2)}{\left[\left(1-\frac{1}{\mu_1{}^{\frac{1}{n}}}\right)R_1{}^{\frac{(3n+1)}{n}}+\left(\frac{1}{\mu_1{}^{\frac{1}{n}}}-\frac{1}{\mu_2{}^{\frac{1}{n}}}\right)R_2{}^{\frac{(3n+1)}{n}}+\frac{1}{\mu_2{}^{\frac{1}{n}}}R_0{}^{\frac{(3n+1)}{n}}\right]}\right] \left|-\frac{(q-(U_E-1)R_0{}^2)}{\left[\left(1-\frac{1}{\mu_1{}^{\frac{1}{n}}}\right)R_1{}^{\frac{(3n+1)}{n}}+\left(\frac{1}{\mu_1{}^{\frac{1}{n}}}-\frac{1}{\mu_2{}^{\frac{1}{n}}}\right)R_2{}^{\frac{(3n+1)}{n}}+\frac{1}{\mu_2{}^{\frac{1}{n}}}R_0{}^{\frac{(3n+1)}{n}}\right]}\right|^{(n-1)} \quad (7.44)$$

Integrating the above expression with respect to z from 0 to 1 yields the following expression of pressure rise per wavelength.

$$\Delta p = -2\left(\frac{3n+1}{n}\right)^n \int_0^1 \left\{M(z)\frac{(q-(U_E-1)R_0{}^2)}{R_0{}^{\frac{(3n+1)}{n}}}\right\}\left|-M(z)\frac{(q-(U_E-1)R_0{}^2)}{R_0{}^{\frac{(3n+1)}{n}}}\right|^{n-1} dz, \quad (7.45)$$

where

$$M(z) = \left[\left(1-\frac{1}{\mu_1{}^{\frac{1}{n}}}\right)\frac{R_1{}^{\frac{(3n+1)}{n}}}{R_0{}^{\frac{(3n+1)}{n}}}+\left(\frac{1}{\mu_1{}^{\frac{1}{n}}}-\frac{1}{\mu_2{}^{\frac{1}{n}}}\right)\frac{R_0{}^{\frac{(3n+1)}{n}}}{R_0{}^{\frac{(3n+1)}{n}}}+\frac{1}{\mu_2{}^{\frac{1}{n}}}\right]^{-1}.$$

From Eq. (7.42), one can obtain the maximum flow rate $\bar{Q}_0$ and the maximum pressure rise per wavelength Δp_0. Δp achieves the maximum values Δp_0 for $\bar{Q} = 0$ and similarly, flow rate achieves its maximum $\bar{Q}_0$ for $\Delta p = 0$. The explicit expression for computation of Δp_0 is

$$\Delta p_0 =$$

$$-2\left(\frac{3n+1}{n}\right)^n \int_0^1 \left\{M(z)\frac{(-(U_E-1)R_0{}^2-1-\phi^2/2)}{R_0{}^{\frac{(3n+1)}{n}}}\right\}\left|-M(z)\frac{-(U_E-1)R_0{}^2-1-\phi^2/2}{R_0{}^{\frac{(3n+1)}{n}}}\right|^{n-1} dz. \quad (7.46)$$

However, such an explicit expression is not achievable for $\bar{Q}_0$. For obtaining $\bar{Q}_0$ one has to solve the following nonlinear equation.

$$\int_0^1 \left\{M(z)\frac{(\bar{Q}_0-(U_E-1)R_0{}^2-1-\phi^2/2)}{R_0{}^{\frac{(3n+1)}{n}}}\right\}\left|-M(z)\frac{(\bar{Q}_0-(U_E-1)R_0{}^2-1-\phi^2/2)}{R_0{}^{\frac{(3n+1)}{n}}}\right|^{n-1} dz = 0. \quad (7.47)$$

The profiles of Δp with respect to $\bar{Q}$ for numerous values of n, U_E, μ_1 and μ_2 are shown in **Figs. (7.6(a - d))**, respectively. **Fig. 7.6(a)** shows that the maximum pressure raises Δp_0 increase with raising the power-law index from 0.5 to 1.5. In contrast, the maximum flow rate $\bar{Q}_0$ decreases with enhancement in the power-law index. **Fig. 7.6(b)** illustrates that both maximum pressure Δp_0 and maximum flow rate $\bar{Q}_0$ increase with an increase in the electro-kinetic slip velocity U_E. **Fig. 7.6(c)** depicts that the impact of viscosity ratio μ_1 and μ_2 on Δp is similar to the impact of

n. From above observations it is evident that a reduction in the maximum pressure rise Δp_0 and enhancement in the maximum flow rate $\overline{Q}_0$ can be achieved at the same time either by taking the power-law index below unity or decreasing the viscosity of the intermediate region. Further, the enhancement in maximum flow rate can also be achieved by raising the electro-osmotic slip velocity but this may happen at the cost of increase in the maximum pressure.

7.2.3 Pumping efficiency

Following the definition of mechanical efficiency (E) as provided by Shapiro et al. (1969) it turn out that

$$E = \bar{Q}\left(\frac{\int_0^1\left\{M(z)\frac{\left(q-(U_E-1)R_0{}^2\right)}{R_0\ \frac{(3n+1)}{n}}\right\}\left|-M(z)\frac{\left(q-(U_E-1)R_0{}^2\right)}{R_0\ \frac{(3n+1)}{n}}\right|^{n-1} dz}{\int_0^1\left\{M(z)\frac{\left(q-(U_E-1)R_0{}^2\right)}{R_0\ \frac{(3n+1)}{n}}\right\}\left|-M(z)\frac{\left(q-(U_E-1)R_0{}^2\right)}{R_0\ \frac{(3n+1)}{n}}\right|^{n-1} (R_0{}^2-1)dz}\right). \tag{7.48}$$

The integrals appearing in above expression are evaluated numerically. Further, variations in mechanical efficiency E with respect to normalized flow rate $\bar{Q}/\bar{Q}_{\Delta p=0}$ for different values of n, μ_1, μ_2 and U_E are shown in **Figs. (7.7(a - d)).**

It is observed that the mechanical efficiency increases by increasing electro-osmotic slip velocity, power-law index and viscosity of the peripheral region. In contrast, mechanical efficiency reduces with enhancing the viscosity of the intermediate layer. Thus, reasonable pumping efficiencies can be achieved over a wider range of flow rate by increasing the viscosity of the peripheral region or by increasing the electro-osmotic slip velocity.

7.2.4 Trapping phenomenon

Trapping is another important characteristic of the peristaltic flow in which an internally circulating bolus of fluid is developed by closed streamlines and this trapped bolus is transported along with the peristaltic wave Shapiro et al. (1969). This phenomenon occurs for certain values of the time-averaged flow rate and the occlusion parameter. Moreover, depending on the flow rate trapped bolus may appear in the core, intermediate and peripheral regions. In order to obtain the range of the flow rate for which trapping appears in the core region, we equate ψ for the core region (Eq. (7.32)) to zero to get

$$r^{\frac{n+1}{n}} = \frac{1}{2n(q-(U_E-1)R_0{}^2)}\left[\left(1-\frac{1}{\mu_1{}^{\frac{1}{n}}}\right)R_1{}^{\frac{(n+1)}{n}}\{(3n+1)(q-(U_E-1)R_0{}^2)-(n+1)R_1{}^2\}+\left(\frac{1}{\mu_1{}^{\frac{1}{n}}}-\frac{1}{\mu_2{}^{\frac{1}{n}}}\right)R_0{}^{\frac{(n+1)}{n}}\{(3n+1)(q-(U_E-1)R_0{}^2)-(n+1)R_2{}^2\}+\frac{1}{\mu_2{}^{\frac{1}{n}}}R_0{}^{\frac{(n+1)}{n}}\{(3n+1)(q-(U_E-1)R_0{}^2)-(n+1)R_0{}^2\}\right]. \quad (7.49)$$

Eq. (7.46) represents an implicit relation for the curve at which $\psi = 0$. It is also evident from Eq. (7.32) that the trivial solution $r = 0$ is the other curve at which $\psi = 0$. Now, for trapping to exist in the core region, one must have $r^{\frac{n+1}{n}} > 0$ for some z. This requirement is fulfilled only when both numerator and denominator on right hand side of (7.46) have same signs. For a given z, it turns out that $r^{\frac{n+1}{n}} > 0$ when

$$\bar{Q}^- < \bar{Q} < \bar{Q}^+, \quad (7.50)$$

where

$$\bar{Q}^- = \left(\frac{3n+1}{n+1}\right)\left(-\frac{(U_E-1)\left[\left(1-\frac{1}{\mu_1{}^{\frac{1}{n}}}\right)R_{1\,max}{}^{\frac{(3n+1)}{n}}+\left(\frac{1}{\mu_1{}^{\frac{1}{n}}}-\frac{1}{\mu_2{}^{\frac{1}{n}}}\right)R_{2\,max}{}^{\frac{(3n+1)}{n}}+\frac{1}{\mu_2{}^{\frac{1}{n}}}(1+\phi)^{\frac{(n+1)}{n}}\right]}{\left[\left(1-\frac{1}{\mu_1{}^{\frac{1}{n}}}\right)R_{1\,max}{}^{\frac{(n+1)}{n}}+\left(\frac{1}{\mu_1{}^{\frac{1}{n}}}-\frac{1}{\mu_2{}^{\frac{1}{n}}}\right)R_{2\,max}{}^{\frac{(n+1)}{n}}+\frac{1}{\mu_2{}^{\frac{1}{n}}}(1+\phi)^{\frac{(n+1)}{n}}\right]}\right)-2\phi-\frac{\phi^2}{2},$$

$$\bar{Q}^+ = \left(\frac{n+1}{3n+1}\right)\left(-\frac{(U_E-1)\left[\left(1-\frac{1}{\mu_1{}^{\frac{1}{n}}}\right)R_{1\,min}{}^{\frac{(3n+1)}{n}}+\left(\frac{1}{\mu_1{}^{\frac{1}{n}}}-\frac{1}{\mu_2{}^{\frac{1}{n}}}\right)R_{2\,min}{}^{\frac{(3n+1)}{n}}+\frac{1}{\mu_2{}^{\frac{1}{n}}}(1+\phi)^{\frac{(n+1)}{n}}\right]}{\left[\left(1-\frac{1}{\mu_1{}^{\frac{1}{n}}}\right)R_{1\,min}{}^{\frac{(n+1)}{n}}+\left(\frac{1}{\mu_1{}^{\frac{1}{n}}}-\frac{1}{\mu_2{}^{\frac{1}{n}}}\right)R_{2\,min}{}^{\frac{(n+1)}{n}}+\frac{1}{\mu_2{}^{\frac{1}{n}}}(1+\phi)^{\frac{(n+1)}{n}}\right]}\right)+2\phi-\frac{\phi^2}{2}.$$

and $R_{1\,max} = R_1|_{z=1/4}$, $R_{2max} = R_2|_{z=1/4}$, $R_{1\,mim} = R_1|_{z=3/4}$, $R_{2\,mim} = R_2|_{z=3/4}$. Inequality (7.47) gives the range of $\bar{Q}$ for trapping in the core region. Such analytic expressions for $\bar{Q}^-$ and $\bar{Q}^+$ are not available for intermediate and peripheral regions. Therefore, one has to relay on numerical procedure to get $\bar{Q}^-$ and $\bar{Q}^+$ corresponding to intermediate and peripheral regions. The trapping limit provided in (7.47) is a generalization of the limits provided by Pandey et al. (2015), Tripathi et al. (2017) and Elshehawey and Gharseldien (2004).

The graphical results illustrating the effects of various involved parameters on trapped bolus in the core region are shown in **Figs. (7.8(a - c) - 7.11(a - c)). Fig. (7.8(a - c))** shows the effects of the μ_2 on trapped bolus. This figure clearly predicts an increase in the area of the trapping region with increasing μ_2. Similarly, **Fig. (7.9(a - c))** depicts an expansion in the area of the trapping region with increasing μ_1. Similar trend is observed by raising the power-law index n from 0.8 to 1.5. In contrast, the area of the trapping region diminishes with increasing the electro-osmotic slip parameter.

7.3 Conclusion

A theoretical analysis is obtained for multilayered electro-osmotic peristaltic tube transport of power-law fluid. By using appropriate transformation, the flow problem is transformed from fixed frame to moving frame. Long wavelength and low Reynolds number assumption are employed to simplify the problem. In order to obtain the closed form expressions of stream functions valid for three regions, the simplified momentum equation is integrated subject to the appropriate boundary conditions. Moreover, the expression of stream function is used to derive the expression of the pressure gradient, mechanical efficiency, time-averaged flow rate and trapping limits. The non-linear equations for interfaces are also obtained and solved numerically. The main outcomes of the present analysis are:

- The area of the trapped bolus in the core region expands with raising the viscosities of the intermediate and peripheral regions.
- Trapped bolus appears at lower flow rate for shear-thickening fluids as compared to shear-thinning fluids.
- The area of the trapped bolus in the core region reduces with rise in electro-osmotic slip parameter. The trapped bolus completely disappears at higher electro-osmotic slip velocities.
- Mechanical efficiency can be increased by raising all emerging parametric except the viscosity of the intermediate layer.
- Growth in maximum pressure rise owes to the high values of the involved parameters.
- A linear decay in pressure rise is observed with increasing the volumetric flow rate.

- Intense variations in both interfaces are observable either by varying the viscosity ratios corresponding to the intermediate and peripheral regions or by varying the electro-osmotic slip velocity.

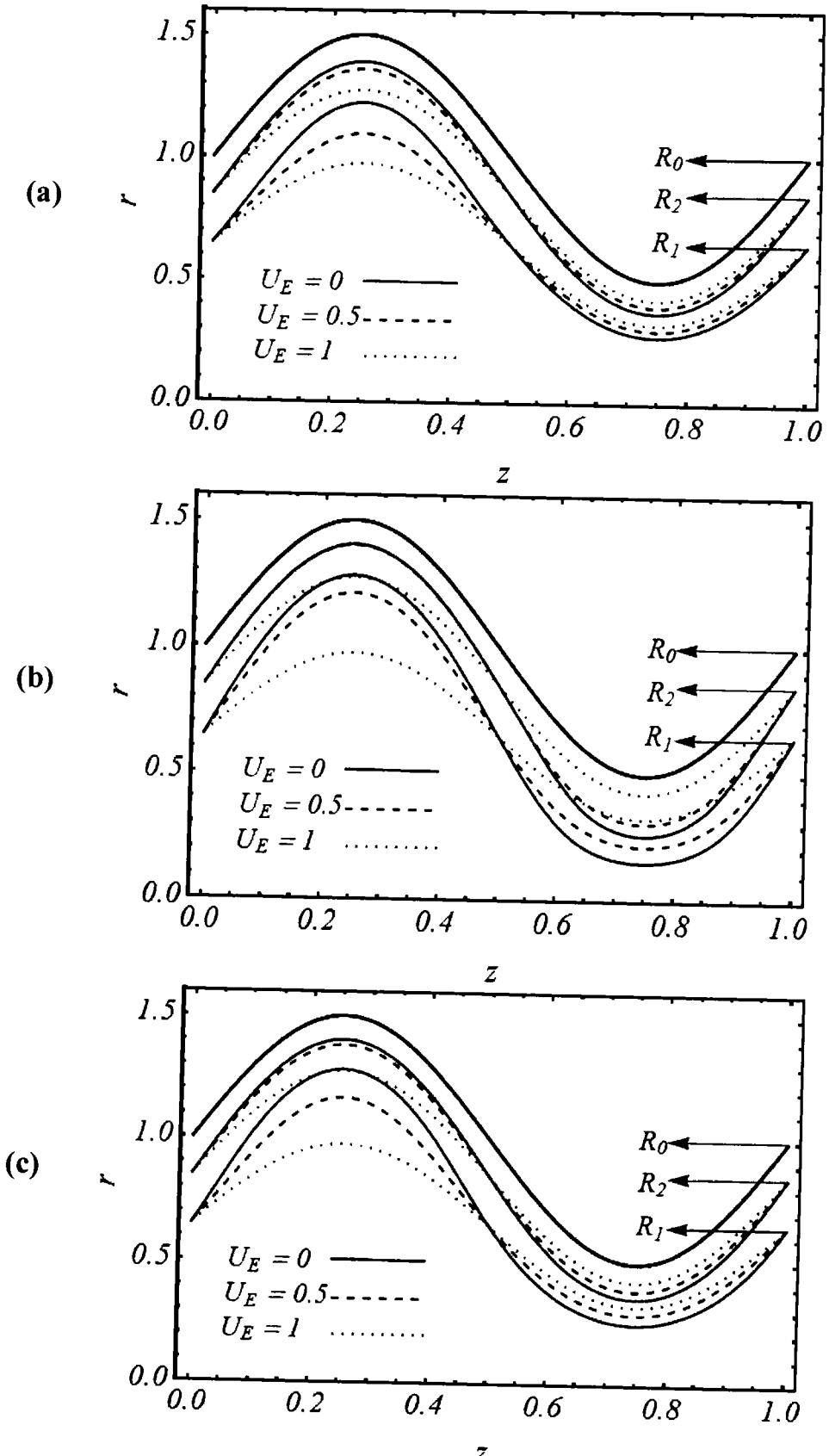

Fig. 7.2 ((a) – (c)): Variation in the interfaces $R_1$and R_2 for different values of the involved parameters (a) $\mu_1 = 10,\ \mu_2 = 0.1, \phi = 0.5, Q = 0.4, n = 1.5, \alpha = 0.65, \beta = 0.85$ (b) $\mu_1 = 0.1, \mu_2 = 10, \phi = 0.5, Q = 0.4, n = 1.5, \alpha = 0.65, \beta = 0.85$ (c) $\mu_1 = 1, \mu_2 = 1, \phi = 0.5, Q = 0.4, n = 0.5, \alpha = 0.65, \beta = 0.85.$

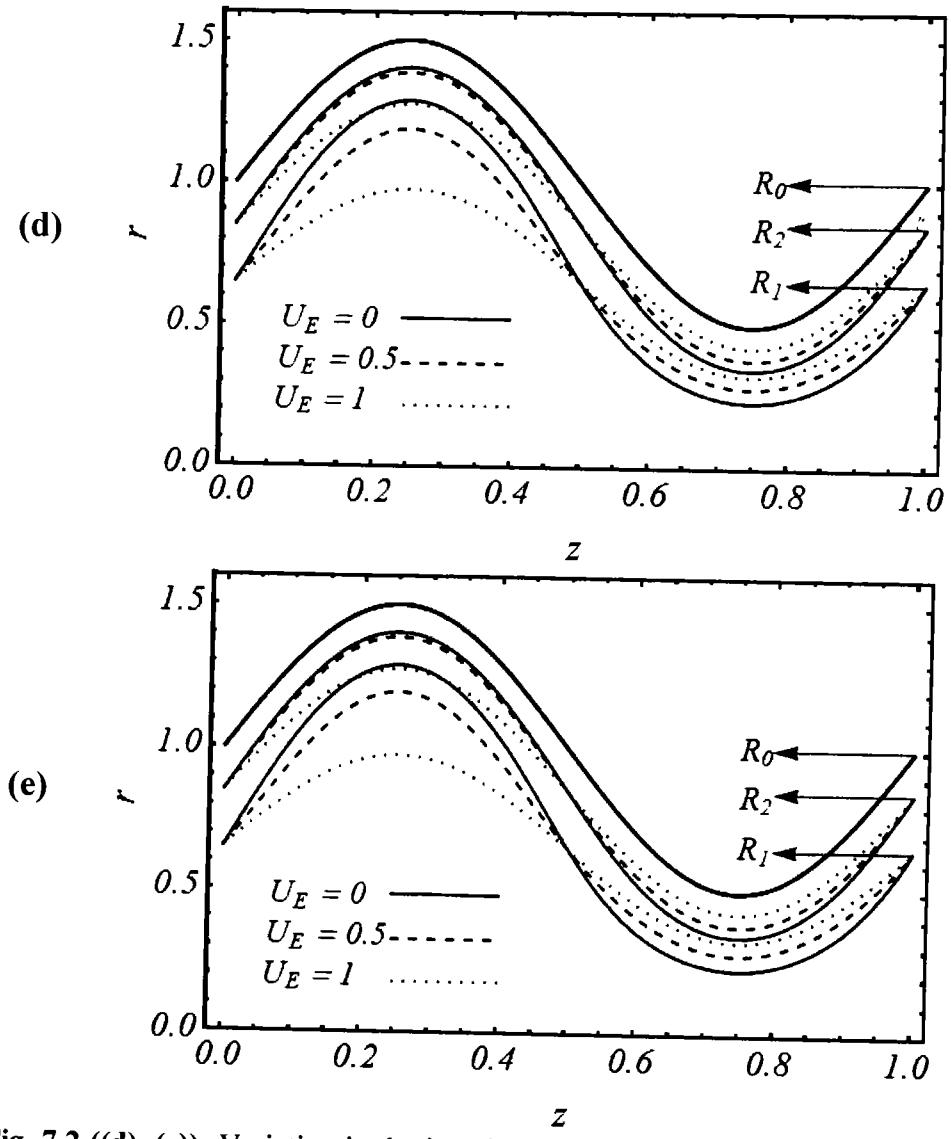

Fig. 7.2 ((d), (e)): Variation in the interfaces $R_1$and R_2 for different values of the U_E when the other parameters (d)$\mu_1 = 1, \mu_2 = 1, \phi = 0.5, Q = 0.4, n = 1, \alpha = 0.65, \beta = 0.85$ (e) $\mu_1 = 1, \mu_2 = 1, \phi = 0.5, Q = 0.4, n = 1.5, \alpha = 0.65, \beta = 0.85$.

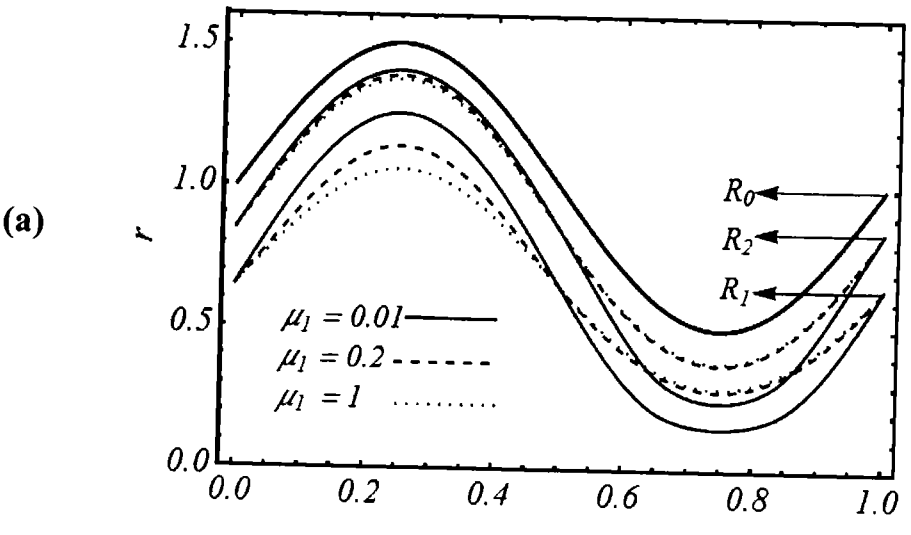

Fig. 7.3 (a): Variation in the interfaces $R_1$and R_2 for different values of the μ_1 the other parameters (a) $\mu_2 = 0.1, \phi = 0.5, Q = 0.4, n = 0.5, \alpha = 0.65, \beta = 0.85$.

(b)

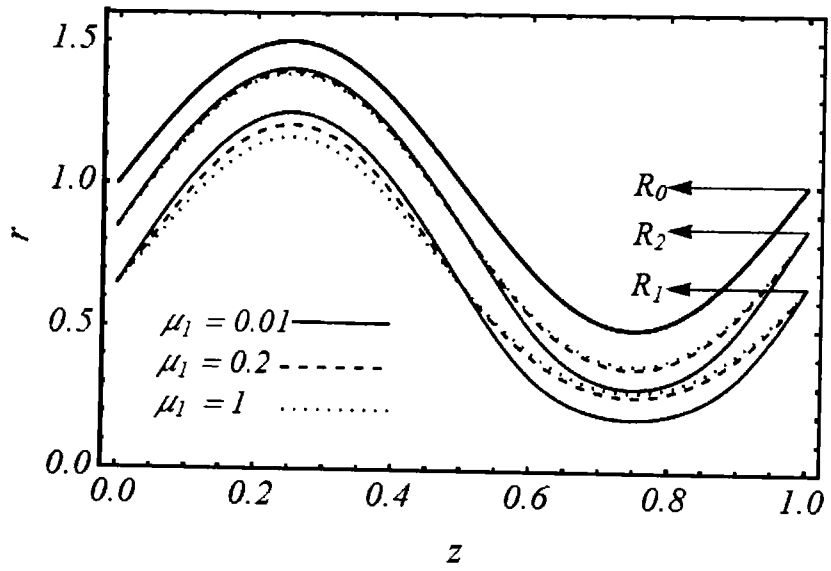

(c)

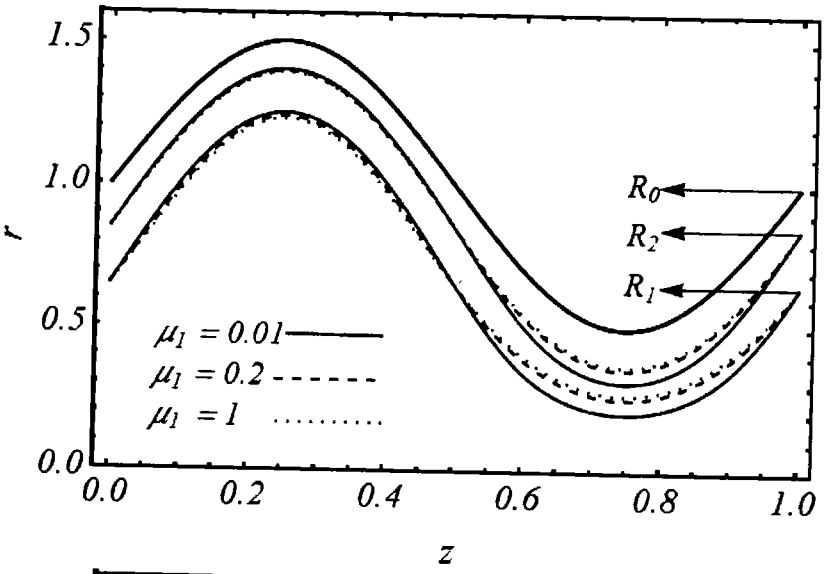

(d)

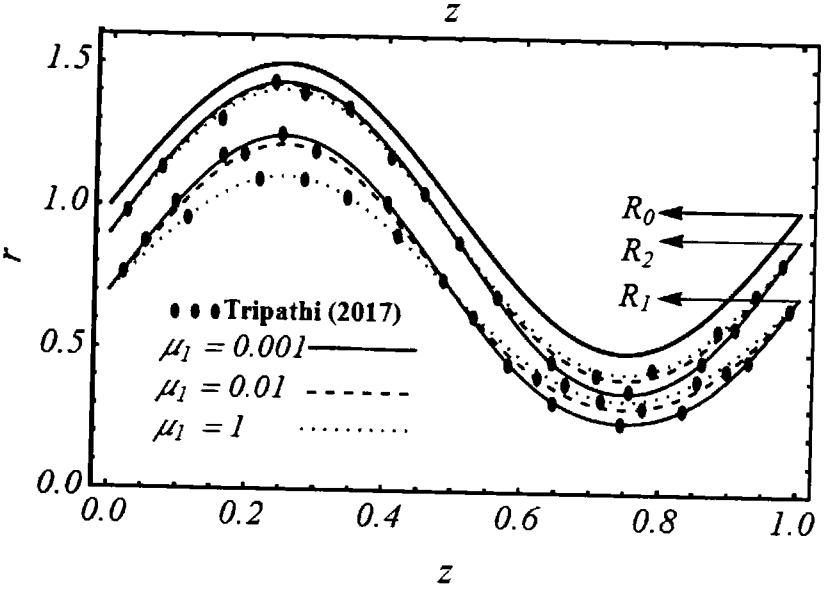

Fig. 7.3 ((b) – (d)): Variation in the interfaces $R_1$and R_2 for different values of the different values of the μ_1 other parameters (b) $\mu_2 = 0.1, U_E = 0, \phi = 0.5, Q = 0.4, n = 1, \alpha = 0.65, \beta = 0.85$ (c) $\mu_2 = 0.1, U_E = 0, \phi = 0.5, Q = 0.4,\ n = 1.5, \alpha = 0.65, \beta = 0.85$ and (d) the compasion with Tripathi results (2017).

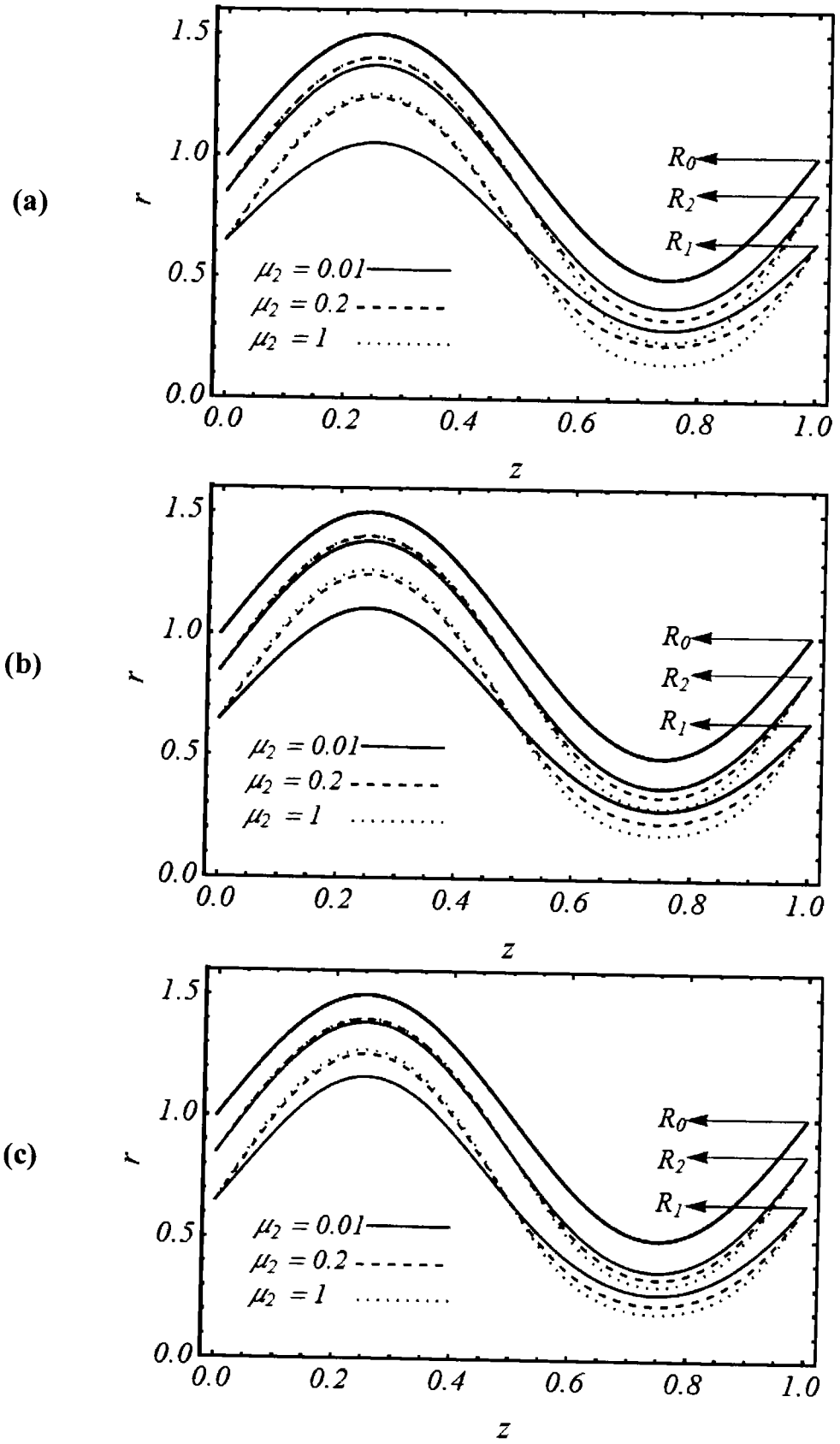

Fig. 7.4 ((a) – (c)): Variation in the interfaces $R_1$and R_2 for different values of the μ_1 the other parameters (a) $\mu_1 = 0.1, U_E = 0, \phi = 0.5, Q = 0.4, n = 0.5, \alpha = 0.65, \beta = 0.8$ (b) $\mu_1 = 0.1, U_E = 0, \phi = 0.5, Q = 0.4, n = 1, \alpha = 0.65, \beta = 0.85$ $(c)\mu_1 = 0.1, U_E = 0, \phi = 0.5, Q = 0.4,\ n = 1.5, \alpha = 0.65, \beta = 0.85.$

(a)

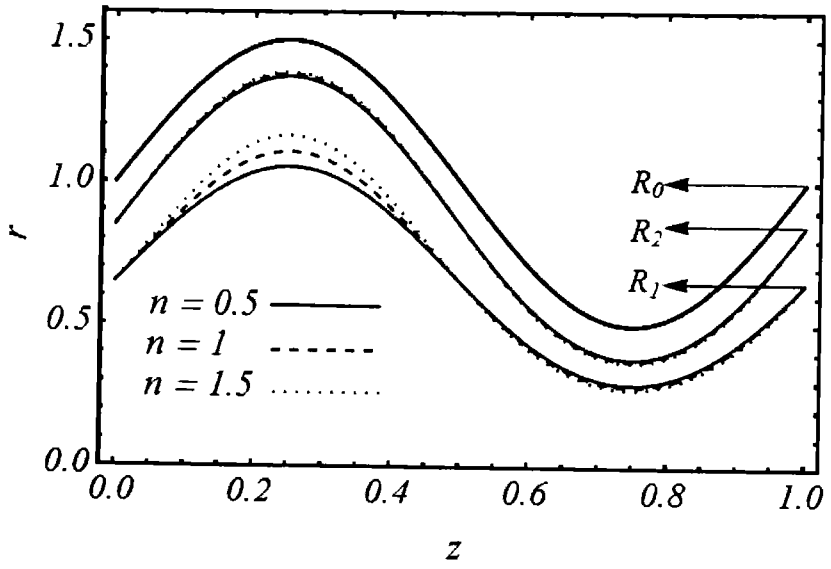

(b)

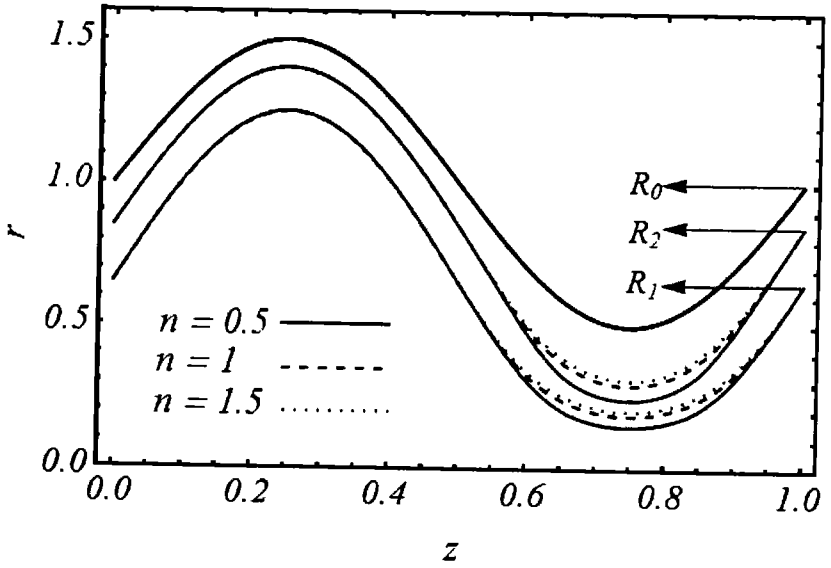

(c)

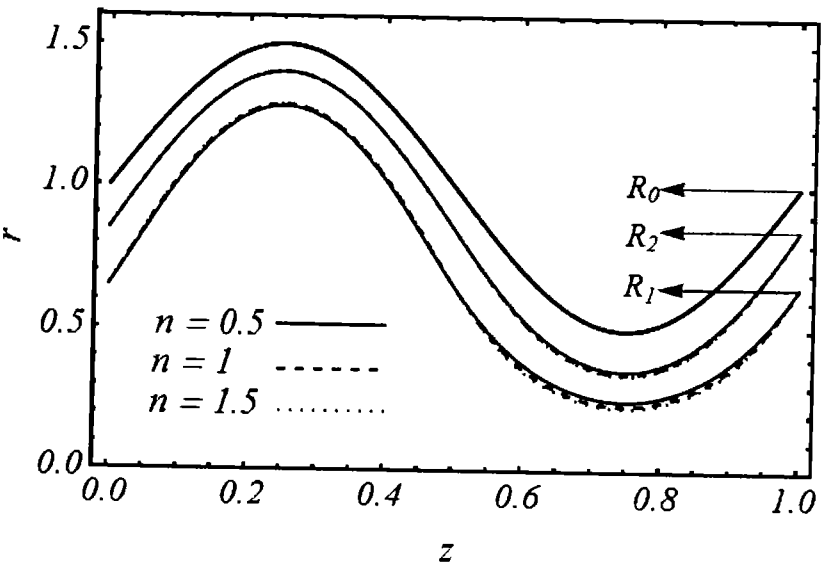

Fig. 7.5 ((a) – (c)): Variation in the interfaces $R_1$and R_2 for different values of n other parameters (a) $\mu_1 = 0.1, U_E = 0, \phi = 0.5, Q = 0.4, \mu_2 = 0.01, \alpha = 0.65, \beta = 0.85$ (b) $\mu_2 = 0.1, U_E = 0, \phi = 0.5, Q = 0.4, \mu_1 = 0.01, \alpha = 0.65, \beta$ 0.85 (c) $\mu_1 = 1, U_E = 0, \phi = 0.5, Q = 0.4, \mu_2 = 1, \alpha = 0.65, \beta = 0.85$.

(a)

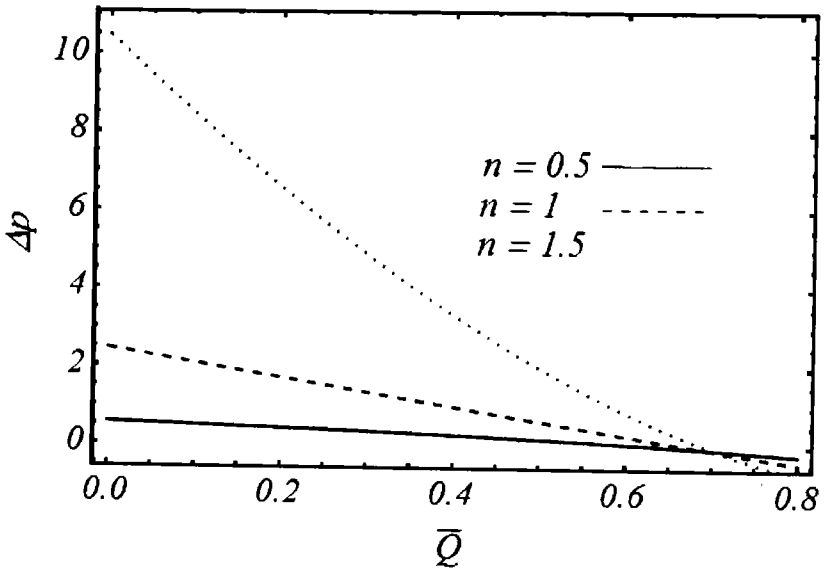

(b)

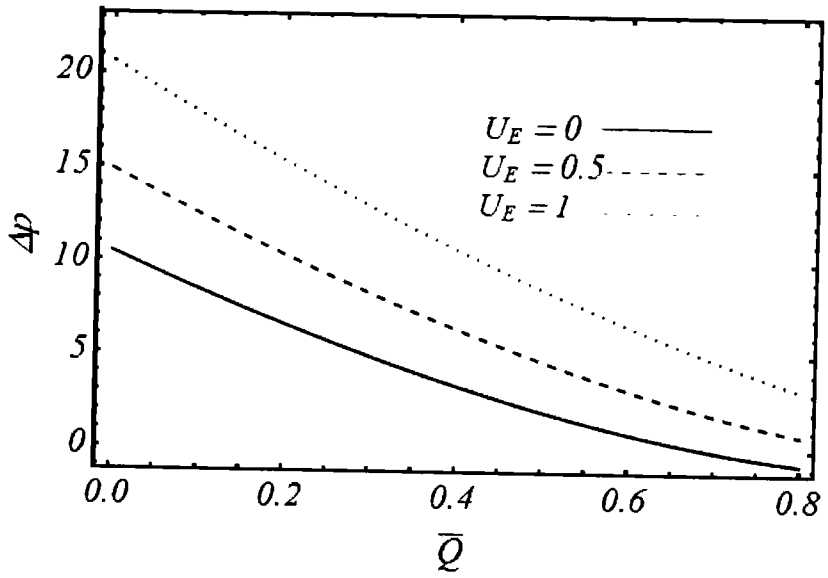

(c)

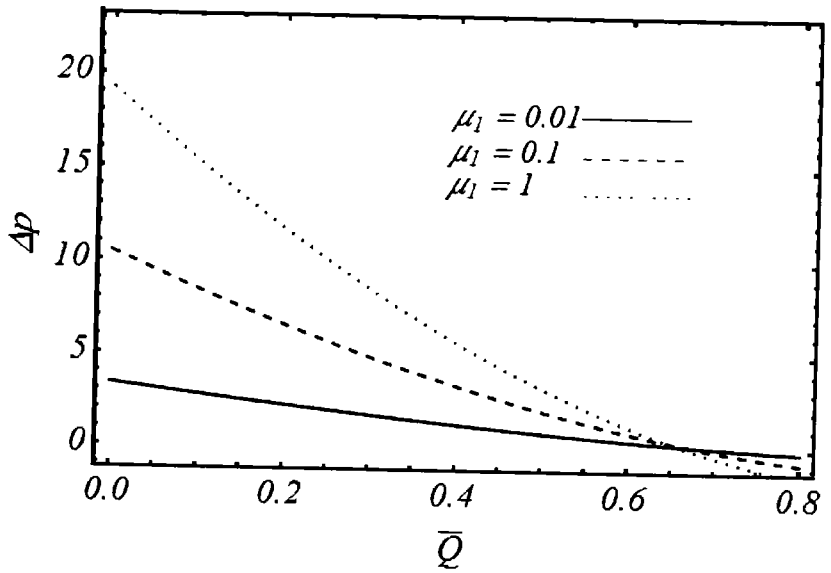

Fig. 7.6 ((a) – (c)): Pumping variations for different values of n, U_E and μ_1 the other parameters (a) $\mu_1 = 0.1, U_E = 0, \phi = 0.5, Q = 0.4, \mu_2 = 0.1, \alpha = 0.7, \beta = 0.9$ (b) $\mu_2 = 0.1, n = 1.5, \phi = 0.5, Q = 0.4, \mu_1 = 0.1, \alpha = 0.7, \beta = 0.9$ (c) $\mu_2 = 0.1, U_E = 0, \phi = 0.5, Q = 0.4, n = 1.5, \alpha = 0.7, \beta = 0.9$.

(d)

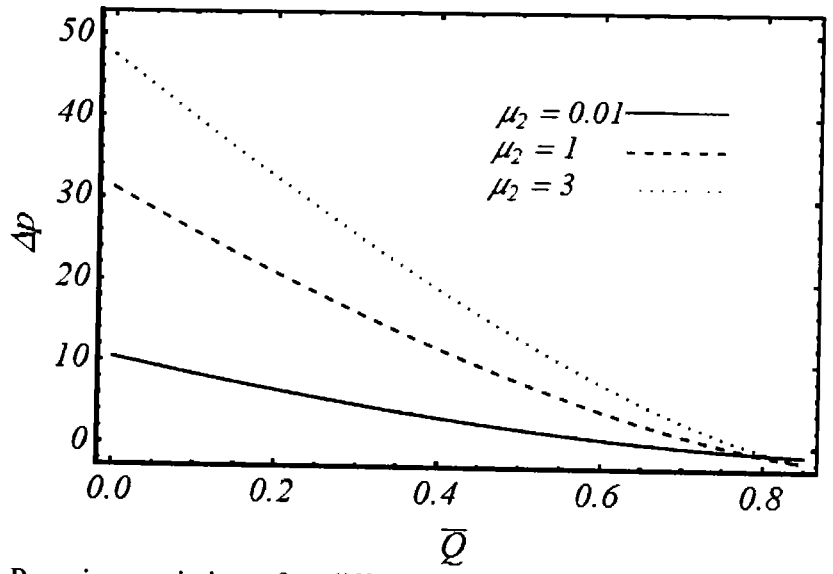

Fig. 7.6 (d): Pumping variations for different values of μ_2 the other parameters $(d)\ \mu_1 = 0.1, U_E = 0, \phi = 0.5, Q = 0.4, n = 1.5, \alpha = 0.7, \beta = 0.9.$

(a)

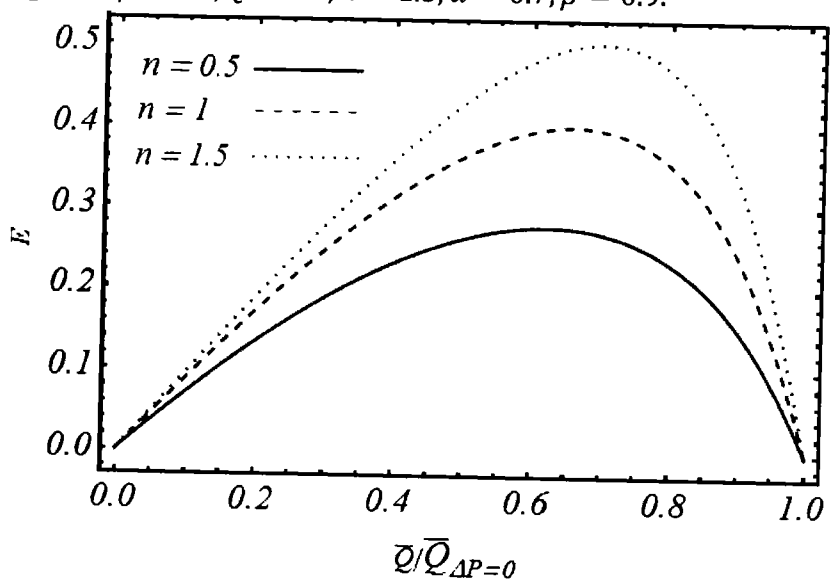

(b)

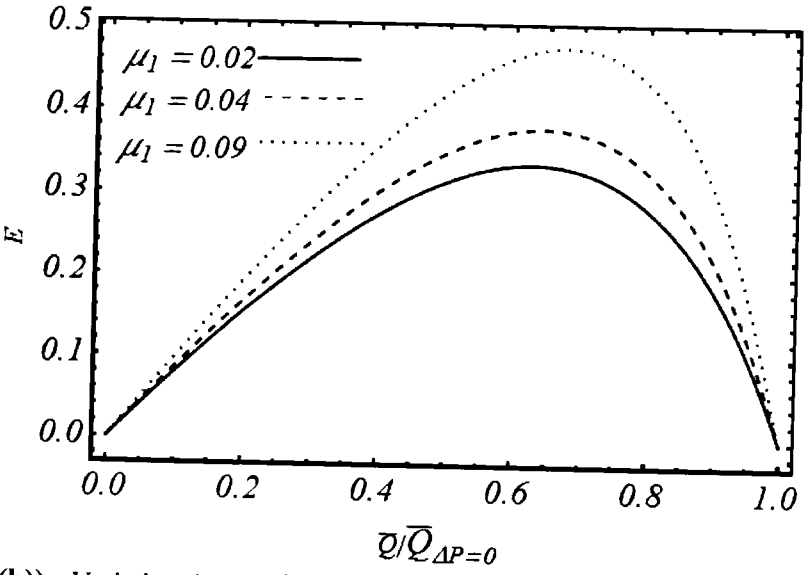

Fig. 7.7 ((a), (b)): Variation in mechanical efficiency for n and μ_1 when (a) $\mu_1 = 1, U_E = 0, \phi = 0.5, \mu_2 = 1, \alpha = 0.7, \beta = 0.9$ (b) $\mu_2 = 0.1, n = 1.5, \phi = 0.5, U_E = 0, \alpha = 0.7, \beta = 0.9.$

(c)

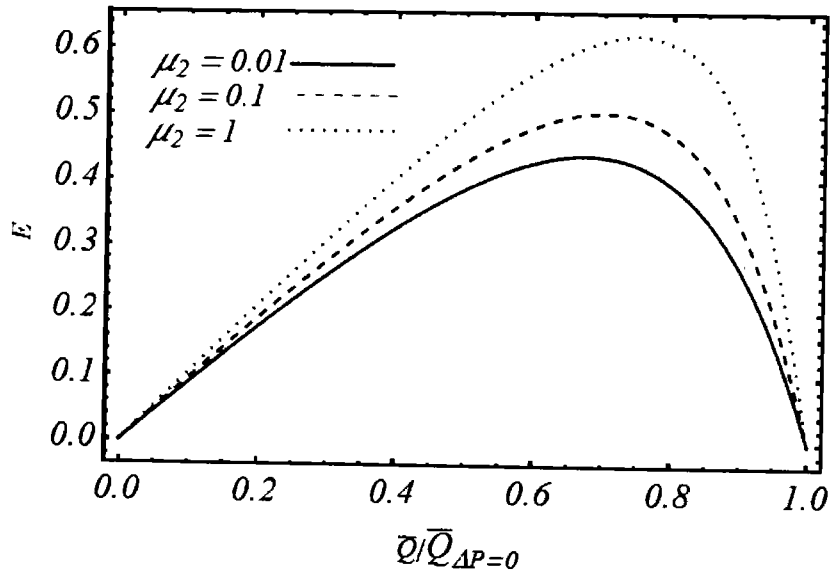

(d)

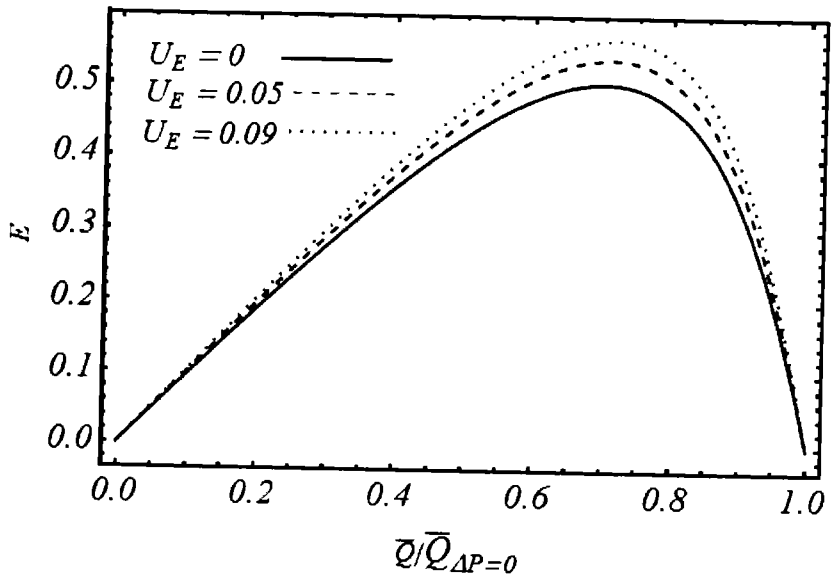

Fig. 7.7 ((c), (d)): Variation in mechanical efficiency for μ_2 and U_E when $(c)\ \mu_1 = 0.1, U_E = 0, \phi = 0.5, Q = 0.4, n = 1.5, \alpha = 0.7, \beta = 0.9$ $(d)\ \mu_1 = 0.1, \mu_2 = 0.1, \phi = 0.5, n = 1.5, \alpha = 0.7, \beta = 0.9$.

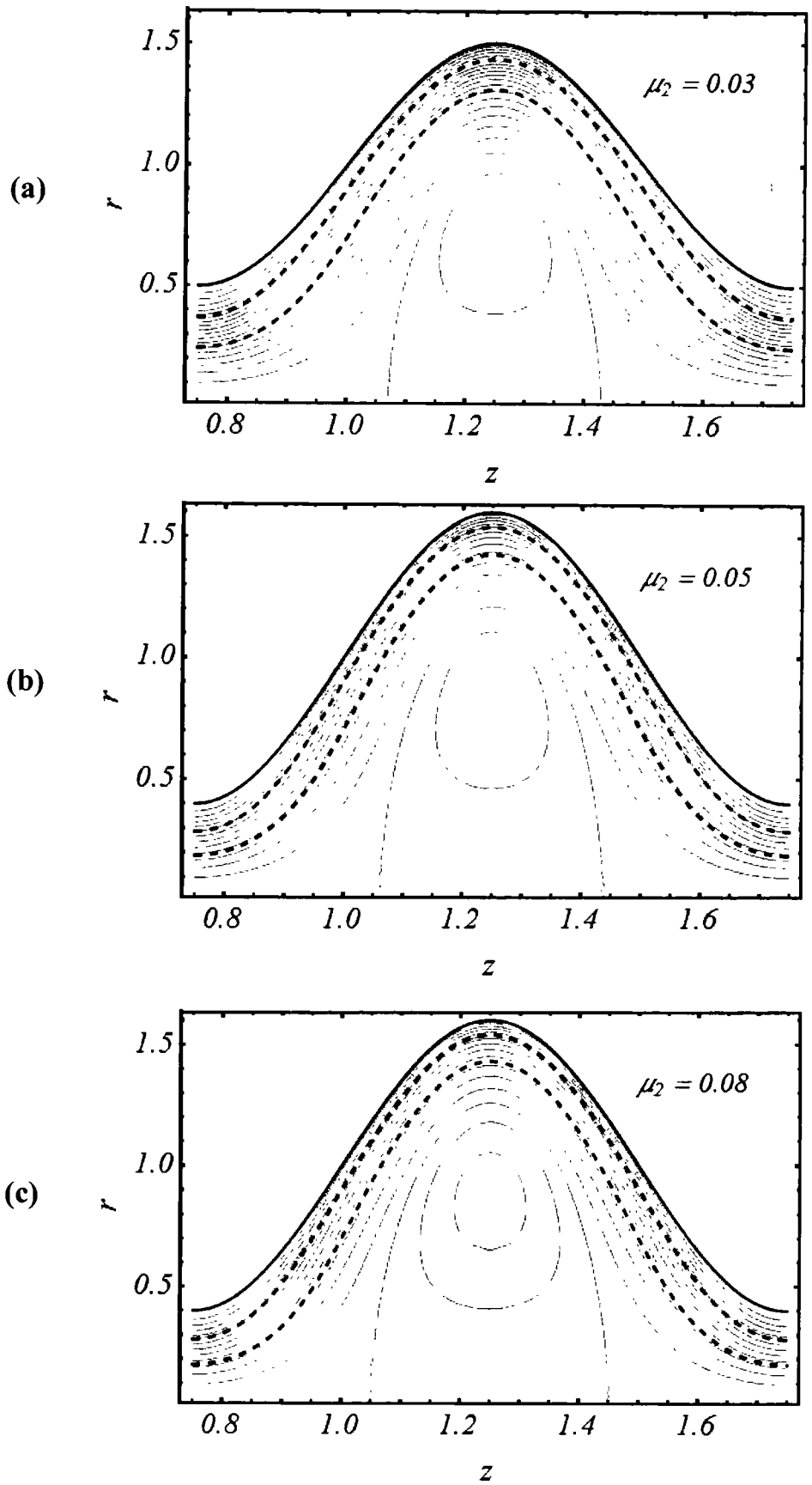

Fig. 7.8 ((a) – (c)): Variation in trapped bolus for different values of μ_2 when $\mu_1 = 0.1, U_E = 0, \phi = 0.6, Q = 0.7, \alpha = 0.7, \beta = 0.9, n = 1.5$.

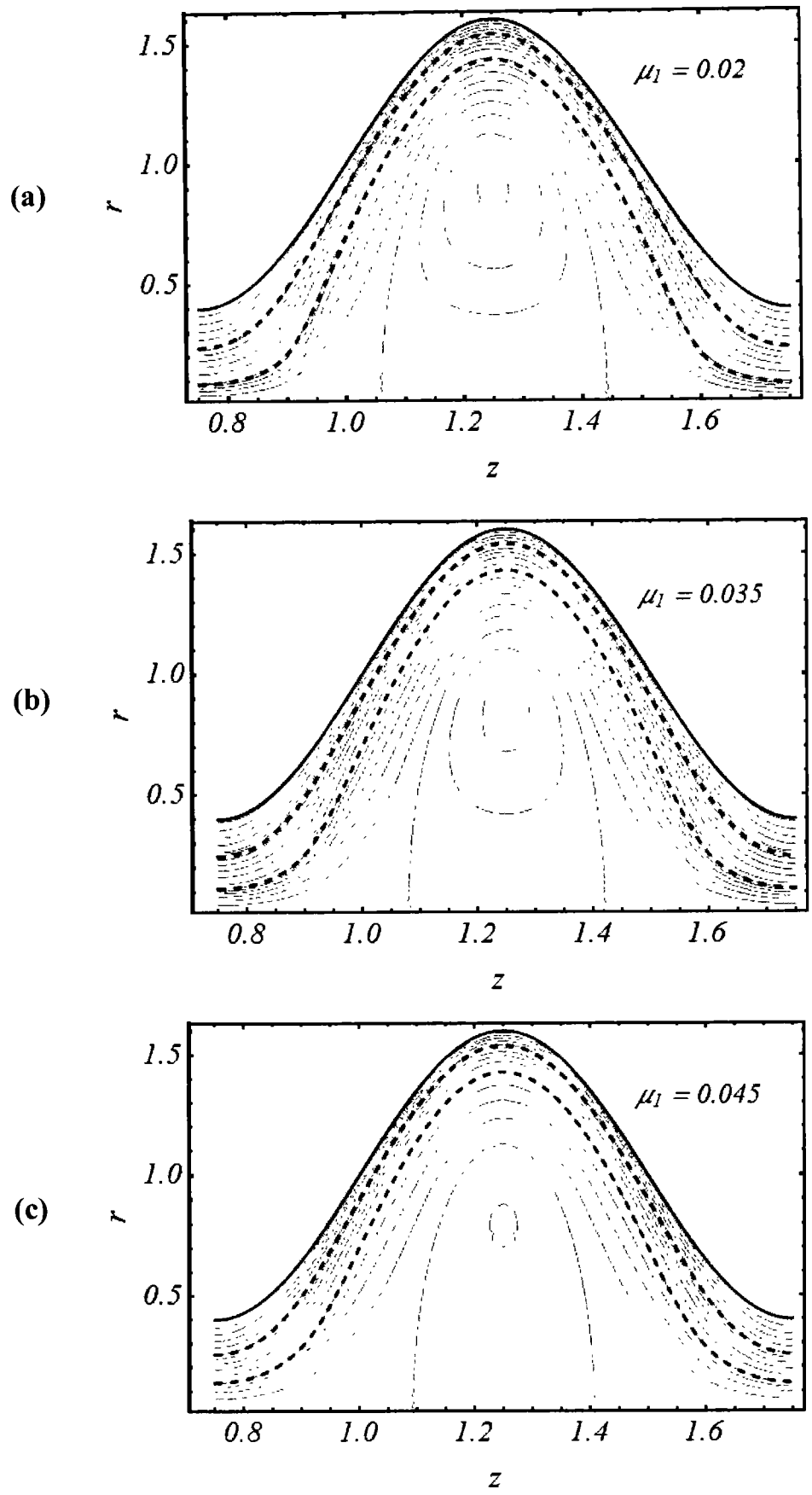

Fig. 7.9 ((a) – (c)): Variation in trapped bolus for different values of μ_1 when $\mu_2 = 0.1$, $U_E = 0, \phi = 0.6, Q = 0.7, \alpha = 0.7, \beta = 0.9, n = 1.5$.

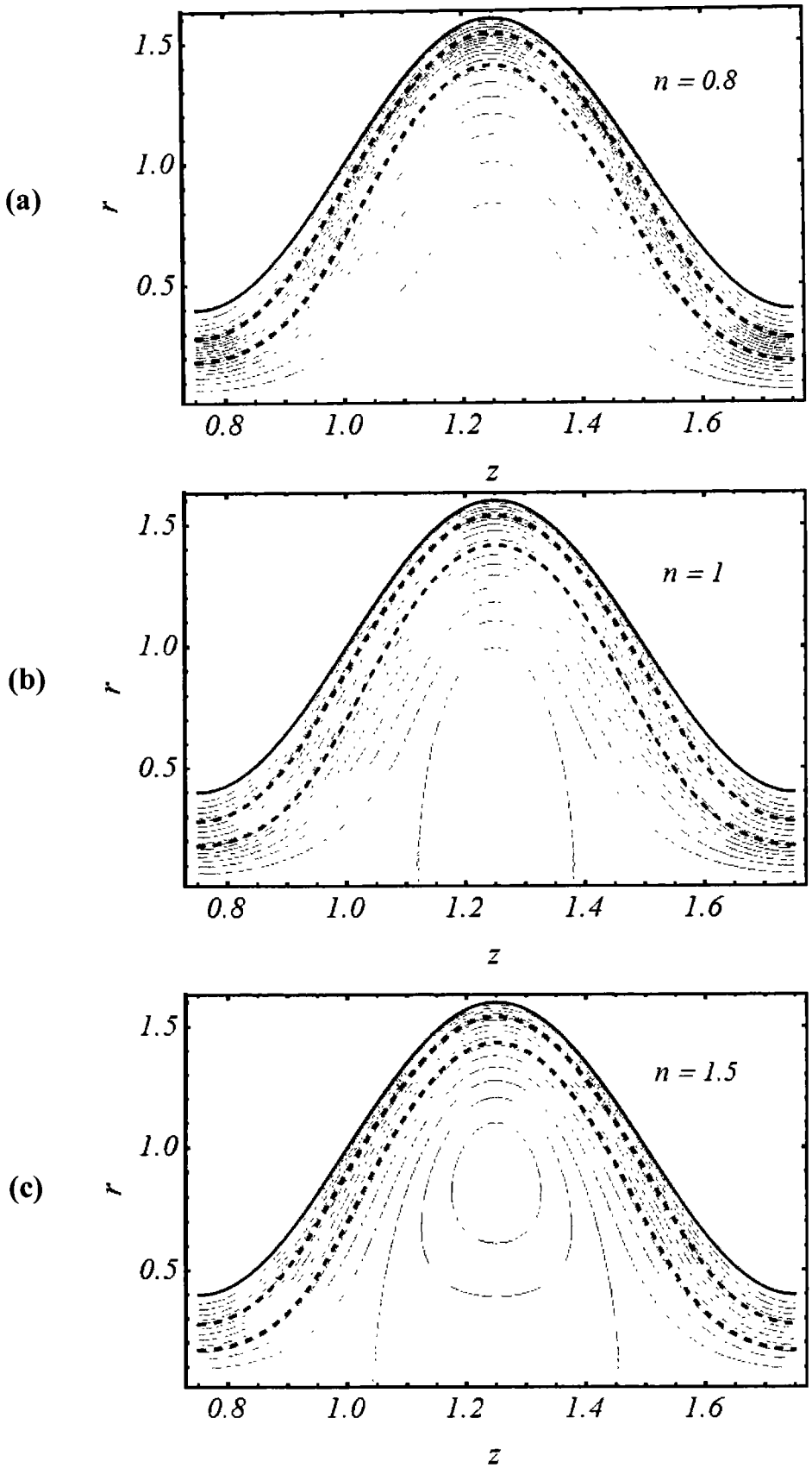

Fig. 7.10 ((a) – (c)): Variation in trapped bolus for different values of n when $\mu_2 = 0.1$, $U_E = 0, \phi = 0.6, Q = 0.7, \alpha = 0.7, \beta = 0.9$, $\mu_1 = 0.1$.

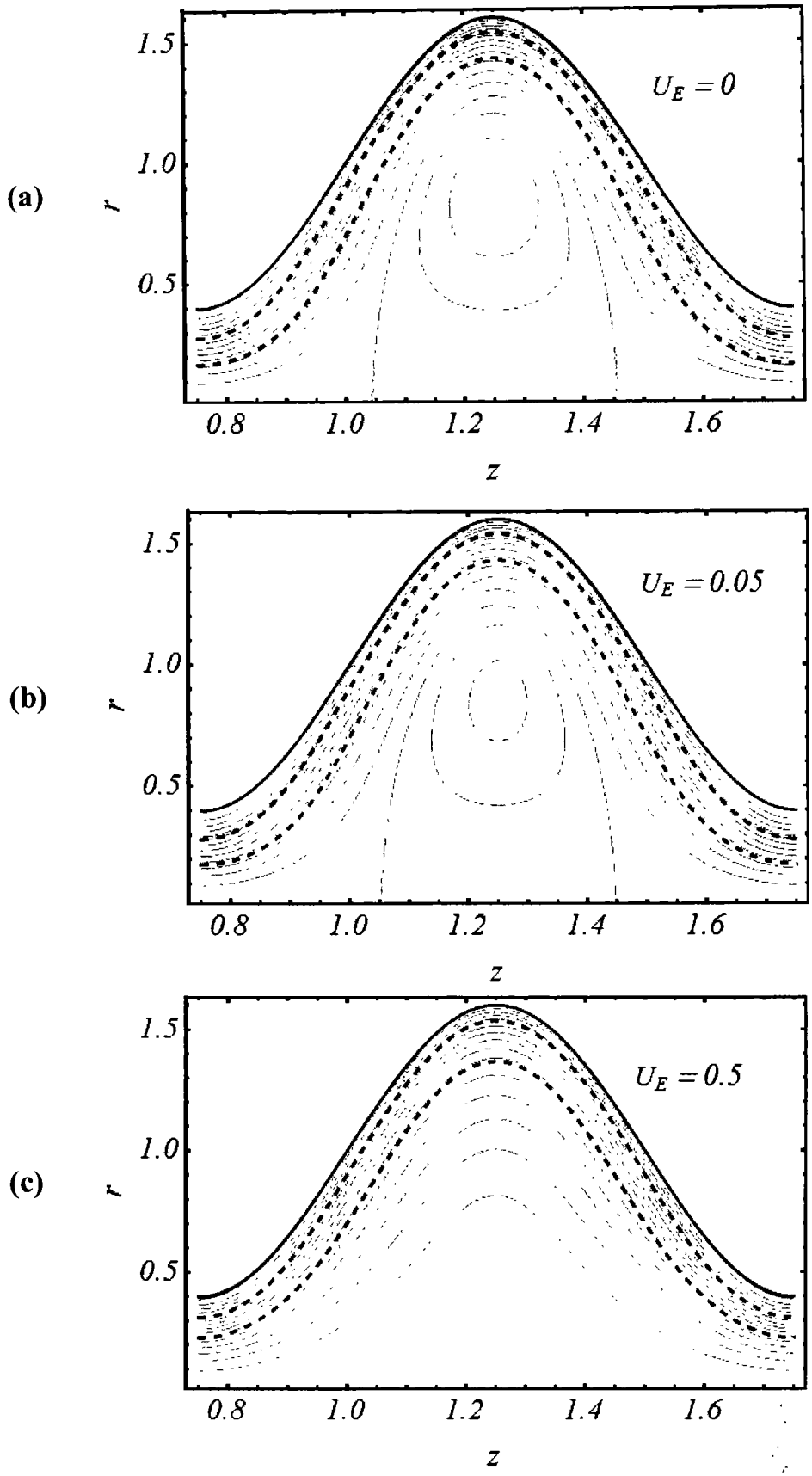

Fig. 7.11 ((a) – (c)): Variation in trapped bolus for different values of U_E when $\mu_2 = 0.1, \mu_1 = 0.1, \phi = 0.6, Q = 0.7, \alpha = 0.7, \beta = 0.9, n = 1.5$.

Summary and future research directions

In this thesis, we investigated electro-osmotic peristaltic transport of single-layer and multi-layered fluids by taking into account various complex non-Newtonian fluid models such as, third grade, Ellis, PTT, FENE-P, Rabinowitsch and power-law models. The governing equations are derived by using the appropriate suppositions of "long wavelength and low Reynolds number". The differential equations thus obtained involve geometries, rheological and electro-osmotic parameters. A detailed investigation is carried out to quantify the influence of these model parameters on different features of electro-osmotic peristaltic transport phenomenon. In particular, flow features like, velocity, interface behaviors, pumping efficiency, mechanical efficiency, trapping and reflux are thoroughly scrutinized by varying parameters. It is observed that the dynamics of peristaltic flow can be controlling by proper tuning of these parameters. Specially, the role electro-osmotic slip velocity in controlling the flow dynamics is highly significant and potentially useful in various applications. In fact, electro-osmotic slip velocity offers an alternative mechanism to control the transport properties in addition to geometric and rheological solutions. Thus, for a predefined peristaltic wave the liquid transport in the conduit can be modulated via electro-kinetic activity without actually changing the mechanical properties of the liquid. The multi-layered flow structure is also found to be assistive factor in modulating the transport properties. These observations are made in the frame work that does not incorporate the effect of geometric curvature, streamline curvature, inertia and Reynolds number. Further, the effects of variable fluid properties magnetic field, porous medium, different wave shapes and advanced constitutive relations cannot be visualized in this frame work. Therefore, the mathematical model analyzed in this thesis could be extended to include:

- More complex rheological fluid models in multi-layered peristaltic transport processes
- Curvature of the conduit
- The effects of heat transfer, magnetic field, variable viscosity and porous medium
- Inertia and streamline coverture effects by using appropriate numerical techniques
- The effect of different types of waves shapes propagating along the ducts walls

References

Afonso, A. M., Alves, M. A., & Pinho, F. T. (2009). Analytical solution of mixed electro-osmotic/pressure driven flows of viscoelastic fluids in microchannels. Journal of Non-Newtonian Fluid Mechanics, 159(1-3), 50-63.

Afonso, A. M., Alves, M. A., & Pinho, F. T. (2013). Analytical solution of two-fluid electro-osmotic flows of viscoelastic fluids. Journal of Colloid and Interface Science, 395, 277-286.

Ali, N., & Asghar, Z. (2014). An analysis of peristaltic flow of finitely extendable nonlinear elastic-Peterlin fluid in two-dimensional planar channel and axisymmetric tube. Zeitschrift für Naturforschung A, 69(8-9), 462-472.

Ali, N., & Hayat, T. (2008). Peristaltic flow of a micropolar fluid in an asymmetric channel. Computers & Mathematics with Applications, 55(4), 589-608.

Ali, N., Abbasi, A., & Ahmad, I. (2015). Channel flow of Ellis fluid due to peristalsis. AIP Advances, 5(9), 097214.

Ali, N., Javid, K., & Sajid, M. (2016). Simulations of peristaltic slip-flow of hydromagnetic bio-fluid in a curved channel. AIP Advances, 6(2), 025111.

Ali, N., Javid, K., Sajid, M., Zaman, A., & Hayat, T. (2016). Numerical simulations of Oldroyd 8-constant fluid flow and heat transfer in a curved channel. International Journal of Heat and Mass Transfer, 94, 500-508.

Ali, N., Sajid, M., Abbas, Z., & Javed, T. (2010). Non-Newtonian fluid flow induced by peristaltic waves in a curved channel. European Journal of Mechanics-B/Fluids, 29(5), 387-394.

Ali, N., Sajid, M., Javed, T., & Abbas, Z. (2010). Heat transfer analysis of peristaltic flow in a curved channel. International Journal of Heat and Mass Transfer, 53(15-16), 3319-3325.

Ali, N., Sajid, M., Javed, T., & Abbas, Z. (2011). An analysis of peristaltic flow of a micropolar fluid in a curved channel. Chinese Physics Letters, 28(1), 014704.

Alokaily, S., Feigl, K., & Tanner, F. X. (2019). Characterization of peristaltic flow during the mixing process in a model human stomach. Physics of Fluids, 31(10), 103105.

Barz, D. P., & Ehrhard, P. (2005). Model and verification of electrokinetic flow and transport in a micro-electrophoresis device. Lab on a Chip, 5(9), 949-958.

Batra, S. K. (1974). Sperm transport through vas deferens: review of hypotheses and suggestions for a quantitative model. Fertility and Sterility, 25(2), 186-202.

Berli, C. L., & Olivares, M. L. (2008). Electrokinetic flow of non-Newtonian fluids in microchannels. Journal of Colloid and Interface Science, 320(2), 582-589.

Blanchette, F. (2014). The influence of suspended drops on peristaltic pumping. Physics of Fluids, 26(6), 061902.

Böhme, G., & Friedrich, R. (1983). Peristaltic flow of viscoelastic liquids. Journal of Fluid Mechanics, 128, 109-122.

Brasseur, J. G., & Corrsin, S. (1987). The influence of a peripheral layer of different viscosity on peristaltic pumping with. Journal of Fluid Mechanics, 174, 495-519.

Chakraborty, S. (2006). Augmentation of peristaltic microflows through electro-osmotic mechanisms. Journal of Physics D: Applied Physics, 39(24), 5356.

Chang, J. S., & Watson, A. (1994). Electromagnetic hydrodynamics. IEEE Transactions on Dielectrics and Electrical Insulation, 1(5), 871-895.

Chaube, M. K., Yadav, A., & Tripathi, D. (2018). Electroosmotically induced alterations in peristaltic microflows of power law fluids through physiological vessels. Journal of the Brazilian Society of Mechanical Sciences and Engineering, 40(9), 423.

Das, S., & Chakraborty, S. (2006). Analytical solutions for velocity, temperature and concentration distribution in electroosmotic microchannel flows of a non-Newtonian bio-fluid. Analytica Chimica Acta, 559(1), 15-24.

Dhinakaran, S., Afonso, A. M., Alves, M. A., & Pinho, F. T. (2010). Steady viscoelastic fluid flow between parallel plates under electro-osmotic forces: Phan-Thien–Tanner model. Journal of Colloid and Interface Science, 344(2), 513-520.

Dobrolyubov, A. I., & Douchy, G. (2002). Peristaltic transport as the travelling deformation waves. Journal of Theoretical Biology, 219(1), 55-61.

Elshehawey, E. F., & Gharsseldien, Z. M. (2004). Peristaltic transport of three-layered flow with variable viscosity. Applied Mathematics and Computation, 153(2), 417-432.

Eytan, O., & Elad, D. (1999). Analysis of intra-uterine fluid motion induced by uterine contractions. Bulletin of Mathematical Biology, 61(2), 221-238.

Eytan, O., Jaffa, A. J., & Elad, D. (2001). Peristaltic flow in a tapered channel: application to embryo transport within the uterine cavity. Medical Engineering & Physics, 23(7), 475-484.

Ferrás, L. L., Afonso, A. M., Alves, M. A., Nóbrega, J. M., & Pinho, F. T. (2014). Analytical and numerical study of the electro-osmotic annular flow of viscoelastic fluids. Journal of Colloid and Interface Science, 420, 152-157.

Ferrás, L. L., Afonso, A. M., Alves, M. A., Nóbrega, J. M., & Pinho, F. T. (2016). Electro-osmotic and pressure-driven flow of viscoelastic fluids in microchannels: Analytical and semi-analytical solutions. Physics of Fluids, 28(9), 093102.

Ferrás, L. L., Nóbrega, J. M., & Pinho, F. T. (2012). Analytical solutions for channel flows of Phan-Thien–Tanner and Giesekus fluids under slip. Journal of Non-Newtonian Fluid Mechanics, 171, 97-105.

Fosdick, R. L., & Rajagopal, K. R. (1980). Thermodynamics and stability of fluids of third grade. Proceedings of the Royal Society of London. A. Mathematical and Physical Sciences, 369(1738), 351-377.

Fung, Y. C., & Yih, C. S. (1968). Peristaltic transport. 669-675.

Gaikwad, H. S., Basu, D. N., & Mondal, P. K. (2017). Slip driven micro-pumping of binary system with a layer of non-conducting fluid under electrical double layer phenomenon. Colloids and Surfaces A: Physicochemical and Engineering Aspects, 518, 166-172.

Gaikwad, H., Basu, D. N., & Mondal, P. K. (2016). Electroosmotic transport of immiscible binary system with a layer of non-conducting fluid under interfacial slip: The role applied pressure gradient. Electrophoresis, 37(14), 1998-2009.

Ghosh, U., & Chakraborty, S. (2016). Electro-osmosis over inhomogeneously charged surfaces in presence of non-electrostatic ion-ion interactions. Physics of Fluids, 28(6), 062007.

Goswami, P., Chakraborty, J., Bandopadhyay, A., & Chakraborty, S. (2016). Electrokinetically modulated peristaltic transport of power-law fluids. Microvascular Research, 103, 41-54.

Goud, J. S., & Reddy, R. H. (2018). Peristaltic motion of an Ellis fluid model in a vertical uniform tube with wall properties. International Journal of Civil Engineering and Technology, 9, 847-856.

Hayat, T., & Ali, N. (2006). Peristaltically induced motion of a MHD third grade fluid in a deformable tube. Physica A: Statistical Mechanics and its Applications, 370(2), 225-239.

Hayat, T., Ali, N., & Abbas, Z. (2007). Peristaltic flow of a micropolar fluid in a channel with different wave forms. Physics Letters A, 370(3-4), 331-344.

Hayat, T., Asghar, S., Tanveer, A., & Alsaedi, A. (2017). Homogeneous–heterogeneous reactions in peristaltic flow of Prandtl fluid with thermal radiation. Journal of Molecular Liquids, 240, 504-513.

Hayat, T., Farooq, S., Ahmad, B., & Alsaedi, A. (2016). Characteristics of convective heat transfer in the MHD peristalsis of Carreau fluid with Joule heating. AIP Advances, 6(4), 045302.

Hayat, T., Hussain, Q., & Ali, N. (2008). Influence of partial slip on the peristaltic flow in a porous medium. Physica A: Statistical Mechanics and its Applications, 387(14), 3399-3409.

Hayat, T., Nawaz, S., Alsaedi, A., & Rafiq, M. (2017). Influence of radial magnetic field on the peristaltic flow of Williamson fluid in a curved complaint walls channel. Results in Physics, 7, 982-990.

Hayat, T., Noreen, S., & Ali, N. (2010). Effect of an induced magnetic field on the peristaltic motion of Phan-Thien-Tanner (PTT) fluid. Zeitschrift für Naturforschung A, 65(8-9), 665-676.

Hayat, T., Noreen, S., Ali, N., & Abbasbanday, S. (2012). Peristaltic motion of Phan-Thien-Tanner fluid in a planar channel. Numerical Methods for Partial Differential Equations, 28(3), 737-748.

Hayat, T., Saleem, N., & Ali, N. (2010). Effect of induced magnetic field on peristaltic transport of a Carreau fluid. Communications in Nonlinear Science and Numerical Simulation, 15(9), 2407-2423.

Haywood, D. G., Harms, Z. D., & Jacobson, S. C. (2014). Electroosmotic flow in nanofluidic channels. Analytical Chemistry, 86(22), 11174-11180.

Herr, A. E., Molho, J. I., Santiago, J. G., Mungal, M. G., Kenny, T. W., & Garguilo, M. G. (2000). Electroosmotic capillary flow with nonuniform zeta potential. Analytical Chemistry, 72(5), 1053-1057.

Hunter, R. J. (2013). Zeta potential in colloid science: principles and application (2). Academic Press.

Jackman, W. S., Lougheed, W., Marliss, E. B., Zinman, B., & Albisser, A. M. (1980). For insulin infusion: a miniature precision peristaltic pump and silicone rubber reservoir. Diabetes Care, 3(2), 322-331.

Jayavel, P., Jhorar, R., Tripathi, D., & Azese, M. N. (2019). Electroosmotic flow of pseudoplastic nanoliquids via peristaltic pumping. Journal of the Brazilian Society of Mechanical Sciences and Engineering, 41(2), 61.

Jian, Y., Su, J., Chang, L., Liu, Q., & He, G. (2014). Transient electroosmotic flow of general Maxwell fluids through a slit microchannel. Zeitschrift für Angewandte Mathematik und Physik, 65(3), 435-447.

Jiménez, E., Escandón, J., Bautista, O., & Méndez, F. (2016). Start-up electroosmotic flow of Maxwell fluids in a rectangular microchannel with high zeta potentials. Journal of Non-Newtonian Fluid Mechanics, 227, 17-29.

Kang, Y., Yang, C., & Huang, X. (2002). Electroosmotic flow in a capillary annulus with high zeta potentials. Journal of Colloid and Interface Science, 253(2), 285-294.

Kaushik, P., & Chakraborty, S. (2017). Startup electroosmotic flow of a viscoelastic fluid characterized by Oldroyd-B model in a rectangular microchannel with symmetric and asymmetric wall zeta potentials. Journal of Non-Newtonian Fluid Mechanics, 247, 41-52.

Kavitha, A., Reddy, R. H., Saravana, R., & Sreenadh, S. (2017). Peristaltic transport of a Jeffrey fluid in contact with a Newtonian fluid in an inclined channel. Ain Shams Engineering Journal, 8(4), 683-687.

Kou, Z., & Dejam, M. (2019). Dispersion due to combined pressure-driven and electro-osmotic flows in a channel surrounded by a permeable porous medium. Physics of Fluids, 31(5), 056603.

Latham, T. W. (1966). Fluid motions in a peristaltic pump (Doctoral dissertation, Massachusetts Institute of Technology).

Lei, J. C., Chen, Y. S., Chang, C. C., & Wang, C. Y. (2017). Analysis of electro-osmotic flow over a slightly bumpy plate. Physics of Fluids, 29(12), 122005.

Macagno, E. O., & Christensen, J. (1980). Fluid mechanics of the duodenum. Annual Review of Fluid Mechanics, 12(1), 139-158.

Mekheimer, K. S. (2004). Peristaltic flow of blood under effect of a magnetic field in a non-uniform channels. Applied Mathematics and Computation, 153(3), 763-777.

Mishra, M., & Rao, A. R. (2005). Peristaltic transport in a channel with a porous peripheral layer: model of a flow in gastrointestinal tract. Journal of Biomechanics, 38(4), 779-789.

Misra, J. C., & Pandey, S. K. (1999). Peristaltic transport of a non-Newtonian fluid with a peripheral layer. International Journal of Engineering Science, 37(14), 1841-1858.

Misra, J. C., & Pandey, S. K. (2001). Peristaltic flow of a multilayered power-law fluid through a cylindrical tube. International Journal of Engineering Science, 39(4), 387-402.

Misra, J. C., & Pandey, S. K. (2002). Peristaltic transport of blood in small vessels: study of a mathematical model. Computers & Mathematics with Applications, 43(8-9), 1183-1193.

Misra, J. C., Chandra, S., Shit, G. C., & Kundu, P. K. (2014). Electroosmotic oscillatory flow of micropolar fluid in microchannels: application to dynamics of blood flow in microfluidic devices. Applied Mathematics and Mechanics, 35(6), 749-766.

Misra, J. C., Mallick, B., & Sinha, A. (2018). Heat and mass transfer in asymmetric channels during peristaltic transport of an MHD fluid having temperature-dependent properties. Alexandria Engineering Journal, 57(1), 391-406.

Mondal, P. K., DasGupta, D., & Chakraborty, S. (2015). Rheology-modulated contact line dynamics of an immiscible binary system under electrical double layer phenomena. Soft Matter, 11(33), 6692-6702.

Naduvinamani, N. B., Rajashekar, M., & Kadadi, A. K. (2014). Squeeze film lubrication between circular stepped plates: Rabinowitsch fluid model. Tribology International, 73, 78-82.

Narahari, M., & Sreenadh, S. (2010). Peristaltic transport of a Bingham fluid in contact with a Newtonian fluid. International Journal of Applied Mathematics and Mechanics, 6(11), 41-54.

Narla, V. K., & Tripathi, D. (2019). Electroosmosis modulated transient blood flow in curved microvessels: Study of a mathematical model. Microvascular Research, 123, 25-34.

Narla, V. K., Tripathi, D., & Anwar Bég, O. (2019). Electro-osmosis modulated viscoelastic embryo transport in uterine hydrodynamics: mathematical modeling. Journal of Biomechanical Engineering, 141(2).

Ng, C. O. (2013). Combined pressure-driven and electroosmotic flow of Casson fluid through a slit microchannel. Journal of Non-Newtonian Fluid Mechanics, 198, 1-9.

Ng, C. O., & Qi, C. (2014). Electroosmotic flow of a power-law fluid in a non-uniform microchannel. Journal of Non-Newtonian Fluid Mechanics, 208, 118-125.

Oliveira, P. J. (2002). An exact solution for tube and slit flow of a FENE-P fluid. Acta Mechanica, 158(3-4), 157-167.

Oliveira, P. J., & Pinho, F. T. (1999). Analytical solution for fully developed channel and pipe flow of Phan-Thien–Tanner fluids. Journal of Fluid Mechanics, 387, 271-280.

Pandey, S. K., Chaube, M. K., & Tripathi, D. (2011). Peristaltic transport of multilayered power-law fluids with distinct viscosities: a mathematical model for intestinal flows. Journal of Theoretical Biology, 278(1), 11-19.

Pandey, S. K., Chaube, M. K., & Tripathi, D. (2015). Flow characteristics of distinctly viscous multilayered intestinal fluid motion. Applied Bionics and Biomechanics, 2015.

Park, H. M., & Lee, W. M. (2008). Effect of viscoelasticity on the flow pattern and the volumetric flow rate in electroosmotic flows through a microchannel. Lab on a Chip, 8(7), 1163-1170.

Prabakaran, P. H., Reddy, R. H., Sreenadh, S., Saravana, R., & Kavitha, A. (2013). Peristaltic Pumping Of A Bingham Fluid In Contact With A Newtonian Fluid In An Inclined Channel Under Long Wavelength Approximation. Advances and Applications in Fluid Mechanics, 13(2), 127.

Prakash, J., & Tripathi, D. (2018). Electroosmotic flow of Williamson ionic nanoliquids in a tapered microfluidic channel in presence of thermal radiation and peristalsis. Journal of Molecular Liquids, 256, 352-371.

Prakash, J., Sharma, A., & Tripathi, D. (2018). Thermal radiation effects on electroosmosis modulated peristaltic transport of ionic nanoliquids in biomicrofluidics channel. Journal of Molecular Liquids, 249, 843-855.

Provost, A. M., & Schwarz, W. H. (1994). A theoretical study of viscous effects in peristaltic pumping. Journal of Fluid Mechanics, 279, 177-195.

Raju, K. K., & Devanathan, R. (1972). Peristaltic motion of a non-Newtonian fluid. Rheologica Acta, 11(2), 170-178.

Rao, A. R., & Mishra, M. (2004). Nonlinear and curvature effects on peristaltic flow of a viscous fluid in an asymmetric channel. Acta Mechanica, 168(1-2), 35-59.

Rao, A. R., & Mishra, M. (2004). Peristaltic transport of a power-law fluid in a porous tube. Journal of Non-Newtonian Fluid Mechanics, 121(2-3), 163-174.

Rao, A. R., & Usha, S. (1995). Peristaltic transport of two immiscible viscous fluids in a circular tube. Journal of Fluid Mechanics, 298, 271-285.

Reuss, F. F. (1809). Sur un nouvel effet de l'électricité galvanique. Mem. Soc. Imp. Natur. Moscou, 2, 327-337.

Rivlin, R. S., & Ericksen, J. L. (1997). Stress-deformation relations for isotropic materials. In Collected Papers of RS Rivlin (pp. 911-1013). Springer, New York, NY.

Roshani, H., Dabhoiwala, N. F., Tee, S., Dijkhuis, T., Kurth, K. H., Ongerboer de Visser, B. W., ... & Lamers, W. H. (1999). A study of ureteric peristalsis using a single catheter to record EMG, impedance, and pressure changes. Techniques in Urology, 5(1), 61-66.

Sadeghi, A., Saidi, M. H., & Mozafari, A. A. (2011). Heat transfer due to electroosmotic flow of viscoelastic fluids in a slit microchannel. International Journal of Heat and Mass Transfer, 54(17-18), 4069-4077.

Saville, D. A. (1977). Electrokinetic effects with small particles. Annual Review of Fluid Mechanics, 9(1), 321-337.

Tanveer, A., Hayat, T., Alsaadi, F., & Alsaedi, A. (2017). Mixed convection peristaltic flow of Eyring-Powell nanofluid in a curved channel with compliant walls. Computers in Biology and Medicine, 82, 71-79.

Tripathi, D. (2011). A mathematical model for the peristaltic flow of chyme movement in small intestine. Mathematical Biosciences, 233(2), 90-97.

Tripathi, D. (2012). A mathematical study on three layered oscillatory blood flow through stenosed arteries. Journal of Bionic Engineering, 9(1), 119-131.

Tripathi, D., & Bég, O. A. (2014). A study on peristaltic flow of nanofluids: Application in drug delivery systems. International Journal of Heat and Mass Transfer, 70, 61-70.

Tripathi, D., Bhushan, S., & Bég, O. A. (2016). Transverse magnetic field driven modification in unsteady peristaltic transport with electrical double layer effects. Colloids and Surfaces A: Physicochemical and Engineering Aspects, 506, 32-39.

Tripathi, D., Bhushan, S., & Bég, O. A. (2017). Analytical study of electro-osmosis modulated capillary peristaltic hemodynamics. Journal of Mechanics in Medicine and Biology, 17(03), 1750052.

Tripathi, D., Borode, A., Jhorar, R., Bég, O. A., & Tiwari, A. K. (2017). Computer modelling of electro-osmotically augmented three-layered microvascular peristaltic blood flow. Microvascular Research, 114, 65-83.

Tripathi, D., Jhorar, R., Bég, O. A., & Shaw, S. (2018). Electroosmosis modulated peristaltic biorheological flow through an asymmetric microchannel: mathematical model. Meccanica, 53(8), 2079-2090.

Tripathi, D., Jhorar, R., Borode, A., & Bég, O. A. (2018). Three-layered electro-osmosis modulated blood flow through a microchannel. European Journal of Mechanics-B/Fluids, 72, 391-402.

Tripathi, D., Sharma, A., & Bég, O. A. (2018). Joule heating and buoyancy effects in electro-osmotic peristaltic transport of aqueous nanofluids through a microchannel with complex wave propagation. Advanced Powder Technology, 29(3), 639-653.

Tripathi, D., Sharma, A., Anwar Bég, O., & Tiwari, A. (2017). Electrothermal transport in biological systems: an analytical approach for electrokinetically

modulated peristaltic flow. Journal of Thermal Science and Engineering Applications, 9(4).

Turkyilmazoglu, M. (2015). Anomalous heat transfer enhancement by slip due to nanofluids in circular concentric pipes. International Journal of Heat and Mass Transfer, 85, 609-614.

Turkyilmazoglu, M. (2017). Condensation of laminar film over curved vertical walls using single and two-phase nanofluid models. European Journal of Mechanics-B/Fluids, 65, 184-191.

Usha, S., & Rao, A. R. (2000). Effects of curvature and inertia on the peristaltic transport in a two-fluid system. International Journal of Engineering Science, 38(12), 1355-1375.

Vajravelu, K., Sreenadh, S., & Babu, V. (2006). Peristaltic transport of a Herschel-Bulkley fluid in contact with a Newtonian fluid. Quarterly of Applied Mathematics, 64(4), 593-604.

Vajravelu, K., Sreenadh, S., Reddy, R. H., & Murugesan, K. (2009). Peristaltic Transport of a Casson fluid in contact with a Newtonian Fluid in a Circular Tube with permeable wall. International Journal of Fluid Mechanics Research, 36(3).

Vasu, N., & De, S. (2010). Electroosmotic flow of power-law fluids at high zeta potentials. Colloids and Surfaces A: Physicochemical and Engineering Aspects, 368(1-3), 44-52.

Wang, Y., Hayat, T., & Hutter, K. (2007). Peristaltic flow of a Johnson-Segalman fluid through a deformable tube. Theoretical and Computational Fluid Dynamics, 21(5), 369-380.

Wang, Y., Ali, N., Hayat, T., & Oberlack, M. (2011). Peristaltic motion of a magnetohydrodynamic micropolar fluid in a tube. Applied Mathematical Modelling, 35(8), 3737-3750.

Wang, Y., Ali, N., & Hayat, T. (2011). Peristaltic motion of a magnetohydrodynamic generalized second-order fluid in an asymmetric channel. Numerical Methods for Partial Differential Equations, 27(2), 415-435.

Wang, Y., Hayat, T., Ali, N., & Oberlack, M. (2008). Magnetohydrodynamic peristaltic motion of a Sisko fluid in a symmetric or asymmetric channel. Physica A: Statistical Mechanics and its Applications, 387(2-3), 347-362.

Walker, S. W., & Shelley, M. J. (2010). Shape optimization of peristaltic pumping. Journal of Computational Physics, 229(4), 1260-1291.

Weidner, D. E., & Schwartz, L. W. (1994). Contact-line motion of shear-thinning liquids. Physics of Fluids, 6(11), 3535-3538.

Yang, R. J., Fu, L. M., & Lin, Y. C. (2001). Electroosmotic flow in microchannels. Journal of Colloid and Interface Science, 239(1), 98-105.

Yue, P., & Feng, J. J. (2012). Phase-field simulations of dynamic wetting of viscoelastic fluids. Journal of Non-Newtonian Fluid Mechanics, 189, 8-13.

Zhao, C., & Yang, C. (2013). Electroosmotic flows of non-N ewtonian power-law fluids in a cylindrical microchannel. Electrophoresis, 34(5), 662-667.

Zhao, C., Zholkovskij, E., Masliyah, J. H., & Yang, C. (2008). Analysis of electroosmotic flow of power-law fluids in a slit microchannel. Journal of Colloid and Interface Science, 326(2), 503-510.

Zhao, M., Wang, S., & Wei, S. (2013). Transient electro-osmotic flow of Oldroyd-B fluids in a straight pipe of circular cross section. Journal of Non-Newtonian Fluid Mechanics, 201, 135-139.

Zhou, C., Yue, P., Feng, J. J., Ollivier-Gooch, C. F., & Hu, H. H. (2010). 3D phase-field simulations of interfacial dynamics in Newtonian and viscoelastic fluids. Journal of Computational Physics, 229(2), 498-511.